Wavelet Quasilinearization Methods for Fractional Differential Equations

Umer Saeed

School of Natural Sciences
National University of Sciences and Technology
Pakistan

PhD Thesis

2015

Wavelet Quasilinearization Methods for Fractional Differential Equations

by

Umer Saeed

Supervised by

Dr. Mujeeb ur Rehman

School of Natural Sciences,
National University of Sciences and Technology,
Islamabad, Pakistan

A thesis submitted for the degree of
Doctor of Philosophy

Abstract

The main objective of this thesis is to develop numerical methods for solving nonlinear fractional ordinary differential equations, nonlinear fractional partial differential equations, and linear and nonlinear fractional delay differential equation. Some methods are proposed by utilizing wavelets operational matrix methods and quasilinearization technique, these methods are used for the solution of nonlinear fractional differential equations, we call these methods as wavelet quasilinearization techniques. According to the wavelet quasilinearization techniques, we convert the fractional nonlinear differential equation to fractional discretize differential equation by using quasilinearization technique and apply wavelet methods at each iteration of quasilinearization technique to get the solution.

We established a technique by utilizing both the Haar wavelet and Picard technique for solving the fractional nonlinear differential equation. While some methods based on the wavelets methods and method of steps, used for the solution of linear and nonlinear fractional delay differential equation. These techniques converts the fractional linear or nonlinear delay differential equation on a given interval to an fractional linear or nonlinear differential equation without delay over that interval, by using the function defined on previous interval, and then apply the wavelet method on the obtained fractional differential equation to find the solution on a given interval. The same procedure provides the solution on next intervals.

We also developed a method, Gegenbauer wavelet operational matrix method, by using Gegenbauer polynomials. The Gegenbauer wavelet matrix, Gegenbauer wavelet operational matrix of fractional integration and Gegenbauer wavelet operational matrix of fractional integration for boundary value problems are derived, constructed and utilized for the solution of fractional differential equations.

The convergence and supporting analysis of our methods are also investigated. The comparison analysis of methods with other existing numerical methods is also performed.

Acknowledgement

First of all, I would like to thank my supervisor Dr. Mujeeb ur Rehman for his excellent guidance and overall support during my Ph.D. Studies. His guidance helped me in all the time of research and writing of this thesis. I especially thank him for introducing me such interesting fields, fractional calculus and wavelet analysis, sharing his vast knowledge and teaching me to be a better mathematician.

Besides my supervisor, I would like to thank my GEC members, Prof. Faiz Ahmad, Prof. Azad Akhter Siddiqui and Dr. Sajid Ali for their encouragement, comments and questions during my seminar presentations and thesis writing, which let to the improvement of the presentation and thesis.

I would like to acknowledge the help and support that I have received from the faculty, staff and students in the School of Natural Sciences. I am very thankful to principle of the school, Prof. Azad Akhter Siddiqui, for providing excellent research environment.

I would like to thank National University of Sciences and Technology for providing me Mega S&T scholarship to support my study, and also for awarding me the financial assistance to support my research work.

I would also like to thank my mother and elder brother for their support, patience, kindness and encouragement during my Ph.D. studies.

Umer Saeed

List of Publications and Manuscripts

1. U. Saeed and M. Rehman, Haar wavelet-quasilinearization technique for fractional nonlinear differential equations, *Applied Mathematics and Computation*, 220 (2013) 630–648.
2. U. Saeed and M. Rehman, Wavelet-Galerkin quasilinearization method for nonlinear boundary value problems, *Abstract and Applied Analysis*, Volume 2014 (2014), Article ID 868934, 10 pages http://dx.doi.org/10.1155/2014/868934.
3. U. Saeed and M. Rehman and M. A. Iqbal, Haar wavelet-Picard technique for fractional order nonlinear initial and boundary value problems, *Scientific Research and Essays*, 9 (2014) 571–580.
4. U. Saeed and M. Rehman, Assessment of Haar wavelet-quasilinearization technique in heat convection-radiation equations, *Applied Computational Intelligence and Soft Computing*, Volume 2014 (2014), Article ID 454231, 5 pages http://dx.doi.org/10.1155/2014/454231.
5. U. Saeed and M. Rehman, Haar wavelet operational matrix method for fractional oscillation equations, *International Journal of Mathematics and Mathematical Sciences*, Volume 2014 (2014), Article ID 174819, 8 pages http://dx.doi.org/10.1155/2014/174819.
6. U. Saeed and M. Rehman, Hermite wavelet method for fractional delay differential equations, *Journal of Difference Equations*, Volume 2014 (2014), Article ID 359093, 8 pages http://dx.doi.org/10.1155/2014/359093.
7. U. Saeed, A numerical technique for solving fractional nonlinear differential equations, submitted.
8. U. Saeed and M. Rehman, Numerical solution of fractional differential equations by the non-uniform Haar wavelet, submitted.
9. U. Saeed and M. Rehman, Haar wavelet operational matrix method for fractional nonlinear partial differential equations, submitted.
10. U. Saeed and M. Rehman, Legendre wavelet method for nonlinear fractional differential equations, submitted
11. U. Saeed and M. Rehman, Radial basis function networks for delay differential equation, submitted.
12. U. Saeed and M. Rehman and M. A. Iqbal, Chebyshev wavelet method for fractional delay-type equations, submitted.

13. U. Saeed and M. Rehman, Gegenbauer wavelets operational matrix method for fractional differential equations, submitted.

Contents

Chapter 1

Introduction

1.1 Fractional Calculus

Fractional calculus is a branch of mathematics which deals with derivatives and integrals of non–integer orders. In a letter dated 30^{th} September 1695, L′Hospital wrote to Leibniz asking him about a particular notation he has used in his publication for the nth order derivative of a function $\frac{d^n}{dx^n}f(x)$, $n \in \mathbb{N}$, i.e. "*what would be the result if* $n = \frac{1}{2}$?" Leibniz′s response "*an apparent paradox from which one day useful consequences will be drawn.*" A list of mathematicians who have provided important contributions up to the middle of last century, includes Abel, Liouville, Laplace, Riemann, Fourier, Grunwald, Levy, Riesz, Erdelyi, Marchaud, and Letnikov.

A brief historical overview and exposition of the fundamental theory of fractional calculus is given by Ross [111]. Oldham and Spanier [96] wrote a book in 1974, in which they concerned with the definitions and the properties of fractional order differential and integral operators. A survey of many different applications which have emerged from fractional calculus is given by Podlubny [98]. The first application of the fractional calculus was made by Abel in 1823. He discovered that the solution of the integral equation for the tautochrone problem could be obtained via derivative of order one half. The fractional calculus has gained considerable importance during the past decades mainly due to its application in diverse fields of science and engineering such as viscoelasticity, control theory of dynamical systems, diffusion of biological population, electrical networks, signal processing, electromagnetism, fluid mechanics, electrochemistry, optics and signal processing, rheology etc. Many researchers pointed out that derivatives and integrals of non–integer order are very suitable for the description of properties of various real phenomena.

In recent years, numerous applications of fractional order ordinary and partial differential equations have appeared in many areas of physics and engineering. There have found a number of works, especially in hereditary solid mechanics and in viscoelasticity theory, where fractional order derivatives are used for a better description of material properties. This is the main advantage of fractional derivatives in comparison with classical integer order models in which such effects are neglected. The

mathematical modeling and simulation of systems and processes, based on the description of their properties in terms of fractional derivatives, naturally lead to differential equations of fractional order and to the necessity of solving such equations. For most of fractional order differential equations, exact solutions are not known. Therefore different numerical methods have been applied for providing approximate solutions. Some of these techniques include, the Adomian decomposition method (ADM) [24, 112], the homotopy perturbation method (HPM) [78, 89], the variational iteration method (VIM) [59, 90], the generalized differential transform method (DTM) [35, 95] and wavelet methods [22, 50, 54, 71–73].

We provide basic theory of some special functions of the fractional calculus which are used in the other chapters. We give some information on the gamma and the Mittag- Leffler functions. These functions play an important role in the theory of fractional differential equations.

Euler's Gamma Function

In 1729, Euler introduced the gamma function $\Gamma(x)$ while generalizing the factorial to non integer values. The Euler's gamma function is defined as

$$\Gamma(x) = \int_0^\infty t^{x-1} e^{-t} dt. \tag{1.1.1}$$

The integral (1.1.1) converges for $x \in \mathbb{R}^+$. Also $\Gamma(1) = \int_0^\infty e^{-t} dt = 1$ and for $x > 0$, an integration by parts yields

$$\begin{aligned} \Gamma(x+1) &= \int_0^\infty t^x e^{-t} dt, \\ &= [-t^x e^{-t}]_0^\infty + x \int_0^\infty t^{x-1} e^{-t} dt, \\ &= x\Gamma(x), \end{aligned} \tag{1.1.2}$$

which is an important functional equation. For integer values n, the functional equation (1.1.2) becomes $\Gamma(n+1) = n!$.

Mittag Leffler Function

A Swedish mathematician Gosta Mittag Leffler introduced the Mittag Leffler function in 1902, which is a generalization of exponential function. The one parameter Mittag Leffler function $E_\alpha(x)$ is defined by

$$E_\alpha(x) = \sum_{l=0}^{\infty} \frac{x^l}{\Gamma(\alpha l + 1)}, \ x \in \mathbb{C}, \ \alpha > 0. \tag{1.1.3}$$

The two parameter Mittag Leffler function is introduced by Wiman in 1905 and later investigated by agrawal and Humbert in 1953, which is a generalization of the one parameter Mittag Leffler function. The two parameter Mittag Leffler function $E_{\alpha,\beta}(x)$ is defined by

$$E_{\alpha,\beta}(x) = \sum_{l=0}^{\infty} \frac{x^l}{\Gamma(\alpha l+\beta)},\ x \in \mathbb{C},\ \mathbf{R}(\alpha), \mathbf{R}(\beta) > 0. \tag{1.1.4}$$

Some particular case of two parameter Mittag Leffler function are as under:

$$\begin{aligned} E_{1,1}(x) &= \sum_{l=0}^{\infty} \frac{x^l}{\Gamma(l+1} = \sum_{l=0}^{\infty} \frac{x^l}{l!} = e^x, \\ E_{2,1}(x^2) &= \sum_{l=0}^{\infty} \frac{x^{2l}}{\Gamma(2l+1} = \sum_{l=0}^{\infty} \frac{x^{2l}}{(2l)!} = \cosh(x), \\ E_{2,2}(x^2) &= \sum_{l=0}^{\infty} \frac{x^{2l}}{\Gamma(2l+2} = \frac{1}{x} \sum_{l=0}^{\infty} \frac{x^{2l+1}}{(2l+1)!} = \frac{\sinh(x)}{x}. \end{aligned} \tag{1.1.5}$$

We review most commonly used definition of fractional integration and differentiation.

Riemann-Liouville fractional integral operator of order α:

The Riemann-Liouville fractional order integral of order $\alpha \in \mathbb{R}^+$ is defined as

$$I_a^{\alpha} y(x) = \frac{1}{\Gamma(\alpha)} \int_a^x (x-t)^{\alpha-1} y(t) dt, \tag{1.1.6}$$

for $a < x \leq b$, and I_a^{α} becomes zero for $x = a$.

Riemann-Liouville fractional derivative operator of order α:

The Riemann-Liouville fractional order derivative of order $\alpha \in \mathbb{R}^+$ is defined as

$${}_R D_a^{\alpha} y(x) = \frac{1}{\Gamma(n-\alpha)} \left(\frac{d}{dx}\right)^n \int_a^x (x-t)^{n-\alpha-1} y(t) dt, \tag{1.1.7}$$

for $a < x \leq b$, where $n-1 < \alpha < n,\ n \in \mathbb{N}$ and $n = \lceil \alpha \rceil$.

Caputo fractional derivative operator of order α:

The Caputo fractional order derivative of order $\alpha \in \mathbb{R}^+$ is defined as

$${}_C D_a^{\alpha} y(x) = \frac{1}{\Gamma(n-\alpha)} \int_a^x (x-t)^{n-\alpha-1} \left(\frac{d}{dt}\right)^n y(t) dt, \tag{1.1.8}$$

for $a < x \leq b$, where $n-1 < \alpha < n,\ n \in \mathbb{N}$ and $n = \lceil \alpha \rceil$. ${}_R D_a^{\alpha}$and ${}_C D_a^{\alpha}$ becomes zero for $x = a$.

1.2 Wavelets

In 1807, a French mathematician, Joseph Fourier, discovered that complex function could be represented and approximated as a weighted sum of basic trigonometric functions. There are many advantages to such approximations and representations, as they provide valuable insight to analysis of complicated functions. Fourier used sinusoids of varying frequencies as basis functions. These representations had one major drawback due to using sinusoids as basis functions. Sinusoids have

perfect compact support in frequency domain, but not in time domain. Therefore, they cannot be used to approximate non-stationary signals. The Fourier representation only provides spectral content of the signal with no indication about the time localization of the spectral components. Therefore the analysis of non-stationary signals, whose spectral content change in time, requires a time-frequency representation, rather than just a frequency representation. Dennis Gabor was modify the Fourier transform into short time Fourier transform in 1946. The idea behind the short time Fourier transform was segmenting the signal by using a time-localized window, and the Fourier transform was computed for every windowed segment of the signal. It suffered from one major drawback that the fixed width of the window function for the analysis of the entire signal lead to the resolution fixed.

Jean Morlet, a geophysical engineer, was faced problem while analyzing signals which had very high frequency components with short time spans, and low frequency components with long time spans. STFT was not able to analyze both at the same time. In 1982, Jean Morlet [97] first introduced the idea of using a different window function for analyzing different frequency bands. These windows were all generated by dilation or compression of a single window function. These window functions had compact support both in time and frequency. The nature of these window functions are small and oscillatory, Morlet named his basis functions as wavelets of constant shape. In 1985, Yves Meyer, a French mathematician, he constructed orthogonal wavelet basis functions with very good time and frequency localization. The first entrant in the wavelet theory was a Hungarian mathematician named Alfred Haar, who introduced in 1909 the functions that are now called Haar wavelets. These functions consist simply of a short positive pulse followed by a short negative pulse. Inspired by the work of Meyer, Ingrid Daubechies, a former graduate student of Grossman at the Free University of Brussels, developed the wavelet frames for discretization of time and scale parameters of the wavelet transform. In 1986 Mallat, a graduate student at Upenn, developed the idea of multiresolution analysis (MRA) for discrete wavelet transform (DWT) with Meyer. In 1988, Ingrid Daubechies constructed families of compactly supported orthonormal wavelets with some degree of smoothness, which laid the foundations of the modern wavelet theory. For more detail about the development of wavelet theory, we refer the readers to [26, 97].

Wavelet analysis is a new development in the area of applied mathematics. Wavelets are a special kind of functions which exhibits oscillatory behavior for a short period of time and then die out. In wavelets, we use a single function and its dilations and translations to generate a set of orthonormal basis functions to represent a signal. We define wavelet (mother wavelet) by [100]:

$$\psi_{a,b}(x) = \frac{1}{\sqrt{|a|}}\psi(\tfrac{x-b}{a}),\ a, b \in \mathbf{R},\ a \neq 0, \tag{1.2.1}$$

where a and b are called scaling and translation parameter respectively. If $|a| < 1$, the wavelet (1.2.1) is the compressed version (smaller support in time-domain) of the mother wavelet and corresponds to mainly higher frequencies. On the other hand, when $|a| > 1$, the wavelet (1.2.1) has larger support

in time-domain and corresponds to lower frequencies.

A wavelet is a function ψ which satisfies the condition, known as the wavelet admissibility condition:

$$C_\psi = \int_{-\infty}^{\infty} \frac{|\hat{\psi}(\omega)|^2}{|\omega|} d\omega < \infty, \tag{1.2.2}$$

where $\hat{\psi}(\omega)$ is the Fourier transform of $\psi(x)$. This condition ensures that $\hat{\psi}(\omega)$ goes to zero quickly as $\omega \to 0$, it is required that

$$\hat{\psi}(0) = \int_{-\infty}^{\infty} \psi(x) dx = 0.$$

Another condition impose on wavelet function is finite energy, that is

$$\int_{-\infty}^{\infty} |\psi(x)|^2 dx < \infty.$$

Continuous Wavelet Transform

Continuous wavelet transform is defined by the inner product of the function $f(x) \in L^2(\mathbf{R})$ and the basis wavelet $\psi_{a,b}(x) \in L^2(\mathbf{R})$,

$$CWT_f(a,b) = (f, \psi_{a,b}) = \frac{1}{\sqrt{|a|}} \int_{-\infty}^{\infty} f(x)\psi(\tfrac{x-b}{a}) dx. \tag{1.2.3}$$

Inverse Continuous Wavelet Transform

$$f(x) = \frac{1}{C_\psi} \int_{-\infty}^{\infty} \int_{-\infty}^{\infty} CWT_f(a,b)\psi_{a,b}(x) \frac{dadb}{a^2}.$$

Continuous Wavelet Transform (CWT) is not of a greater practical use, because the correlation of the function and the wavelet is calculated during the wavelet being continuously translated and continuously scaled that is, the parameters a and b are continuous variables. Most of the coefficients thus calculated are redundant and there are infinitely many of them. For that reason discretization is performed. From a mathematical point of view, a continuous representation of a function of two continuous parameters a, b in equation (1.2.3) can be converted into a discrete one by assuming that a and b take only integer values. Discretizing the CWT parameters via $a = 2^{-j}$ and $b = k2^{-j}$, we get

$$\psi_{j,k}(x) = 2^{\frac{j}{2}} \psi(2^j x - k). \tag{1.2.4}$$

These wavelets for all integers j and k produce an orthogonal basis and it is called mother wavelet. Other wavelets are produced by translation and dilation of the mother wavelet.

Daubechies' constructed a family of orthonormal bases of compactly supported wavelets for the space of square-integrable functions, $L^2(\mathbf{R})$. Due to the fact that they possess several useful properties, such as orthogonality, compact support, exact representation of polynomials to a certain degree, and ability to represent functions at different levels of resolution. The Daubechies' wavelet

discretization of differential equations is based on the Galerkin approach. The wavelet-Galerkin scheme involves the evaluation of connection coefficients [25] to approximate derivatives as well as non-linear terms. Since Daubechies' wavelet do not have an explicit expression, therefore analytical differentiation or integration is not possible. This complicates the solution of differential equations. The connection coefficients are integrals with integrands being products of wavelet bases and their derivatives. Due to the derivatives of compactly supported wavelets being highly oscillatory, it is difficult and unstable to compute the connection coefficients by the numerical evaluation of integral. In order to overcome this problem, algorithms have been given in chapter 7 for the exact evaluation of connection coefficients. The detail analysis of Daubechies' wavelet, multi-resolution analysis and wavelet-Galerkin scheme are given in chapter 7.

There are many kinds of wavelets. The most simplest orthonormal wavelet with compact support is the Haar wavelet. Haar wavelet is a rectangular function. In the 1980s, it turned out that the Haar function was in fact the Daubechies' wavelet of order 1. A good feature of the Haar wavelets is the possibility to integrate them analytically arbitrary times. A drawback of the Haar wavelets is their discontinuity. Since the derivatives do not exist in the points of discontinuity, it is not possible to apply the Haar wavelets for solving differential equation directly. There are two possibilities to handle this situation. One way is to regularize the Haar wavelets with interpolating splines. This approach has been introduced by Cattani [15]. But this approach complicates the solution process and lost the simplicity of the Haar wavelets. The other way is to make use of the integral method, which was proposed by Chen and Hsiao [16]. They expand the highest derivative in the differential equation into Haar series, and lower derivatives are obtained through integrations. The Haar wavelet algorithm for solving differential equations is based on the collocation method. A detail study of Haar wavelet is given in [52].

1.3 Quasilinearization

Linearization is carried out by considering the first two terms in the Taylor′s series expansion of the original nonlinear differential equation. This technique is a generalized Newton-Raphson method for functional equations. It is also known as the quasilinearization method. The quasilinearization technique not only linearizes the nonlinear equation but also provides a sequence of functions which in general converges rather rapidly to the solution of the original nonlinear equation. The main advantage of this technique is that the procedure converges quadratically to the solution of the original equation, if there is convergence at all. Quadratic convergence implies that the error in every succeeding iteration tends to be proportional to the square of the error in its immediately preceding iteration. The method of quasilinearization developed by Bellman [5, 6] and was first used to obtain a representation for the solution of the initial value problem for the Riccati equation. Bellman and Kalaba [7] generalized these results and obtained a solution formula for a wide class of nonlinear

first order differential equations. Garg and Rajagopal [51] used the method of quasilinearization and the orthonormalization technique to solve nonlinear boundary value problems arising in non-Newtonian fluid flow. Mohapatra et al. [91] established the existence, uniqueness, and convergence results for general second order nonlinear boundary value problems by using quasilinearization and monotone iterative methods. Devi et al. [32] developed the method of quasilinearization for fractional differential equations. Existence and uniqueness result for an initial value problem of fractional differential equations using generalized quasilinearization technique is obtained in [33]. Wang et al. [129] constructed the two monotone sequences of upper and lower solutions for the initial value problems of the system of fractional differential equations.

1.4 Picard Method

1.5 Overview

In Chapter 2, we have constructed Haar matrix, Haar wavelet operational matrix of fractional integration and operational matrix of fractional integration for boundary value problems. These matrices are utilized for the solution of fractional initial and boundary value problems over non-uniform grids. The purpose of considering the non-uniform grids is to deal with those differential equation whose solution have abrupt behavior on some part of the domain. Comparison of uniform and non-uniform Haar wavelet method is also performed.

We proposed a method for fractional nonlinear differential equations by utilizing Haar wavelet operational matrix method and quasilinearization technique, as given in Chapter 3. Implementation of the method for both initial and boundary value problems are described. Convergence analysis for Haar wavelet quasilinearization method is derived and given in subsection 3.2.3. In section 3.3, Haar wavelet quasilinearization method is applied on nonlinear fractional initial and boundary value problems by utilizing both uniform and non-uniform grids. Comparison of uniform and non-uniform Haar wavelet quasilinearization method is also given.

The main aim of the Chapter 4 is to develop the Haar wavelet quasilinearization technique for the solution of heat convection radiation equations, because when some numerical method applied for the solution of heat convection radiation equations they becomes unstable when we increase the value of parameter epsilon, which appears in heat convection radiation equations, while Haar wavelet quasilinearization technique gives stable and accurate results. We also introduce Haar wavelet quasilinearization method for fractional nonlinear oscillation equations, in which we consider the forced and forced free duffing Van der Pol oscillation equation and higher order oscillation equation.

The purpose of Chapter 5 is to extend the Haar wavelet quasilinearization method for the solution of fractional nonlinear partial differential equations. The procedure of implementation of method is described in section 5.2. Convergence of the method is derived and given in section 5.3. We

considered fractional generalized Berger-Fisher equation, fractional Klein-Gordon equations and fractional Bergers equation as a test problems.

Solution of nonlinear fractional initial and boundary value problems is concerned in Chapter 6 by introducing a numerical method, which is a combination of Haar wavelet operational matrix method and Picard technique. Convergence of the proposed method is also considered. We described the procedure of implementation of the method while solving nonlinear fractional differential equations.

In Chapter 7, we introduced another numerical method for solving nonlinear differential equations. The developed method is the combination of wavelet Galerkin and quasilinearization technique. We derived an expression for computing the two term connection coefficients, which are used for the solution of nonlinear differential equation. The method is implemented on different nonlinear differential equations to show the applicability of the wavelet Galerkin quasilinearization method.

Two numerical techniques are proposed in Chapter 8. First technique is the combination of Chebyshev wavelet operational matrix method and quasilinearization technique while other utilizes the Legendre wavelet operational matrix method and quasilinearization technique. The operational matrices for these two methods are derived and utilized for the solution of fractional nonlinear differential equations. The procedure of implementation of methods for fractional nonlinear ordinary and partial differential equation are given. Convergence analysis for both the methods is also provided.

In Chapter 9, we introduced a new wavelet method, Gegenbauer wavelets operational matrices method, for solving fractional differential equations. The Gegenbauer matrix, operational matrix of fractional integration and operational matrix of fractional integration for boundary value problems are derived and constructed. The convergence analysis and implementation of method is also provided.

Chapter 10 is used to introduce the three numerical methods for the solution of delay differential equations. First method is proposed by utilizing radial basis function networks and method of steps. The procedure of implementation of radial basis function collocation method and proposed technique for delay differential equation are given. The second method is the combination of Chebyshev wavelet method and method of steps. Convergence analysis of the Chebyshev wavelet method is provided. The procedure of implementation of Chebyshev wavelet method and proposed method are developed and implemented on fractional linear and nonlinear delay differential equations. Comparison of Chebyshev wavelet method and proposed method is also concerned. The third method is obtained by combining Hermite wavelet method and method of step. We compared the obtained method and Hermite wavelet method to check the efficiency of the proposed method.

Chapter 2

Numerical Solution of Linear Fractional Differential Equation by Non–uniform Haar Wavelet Method

The Haar wavelet technique for solving linear homogeneous/inhomogeneous, constant and variable coefficients differential equations has been discussed for uniform grids in [21, 49, 69]. We utilize uniform grids for those differential equation which have sufficiently smooth behavior of solution i.e., there is no abrupt behavior of solution over the given domain and uniform grids are used for better results and accuracy.

The differential equation arising from locally disturbed vibrations is solved by Lepik [72] by using non-uniform grids because solution has abrupt behavior. We solved the fractional differential equation of locally fractionally disturbed vibrations and showed that the results are converging to the locally disturbed vibrations over the same domain and nonuniform grids. The non-uniform Haar wavelets are used by Fazal-i-Haq et al. [55] for the solution of singularly perturbed boundary value problem with different value of epsilon, we considered the fractionally singularly perturbed boundary value problem and showed that it converged to the singularly perturbed boundary value problem for different epsilon. We used the different non-uniform grid structures for better approximations.

2.1 The Uniform Haar Wavelets

The Haar functions contains just one wavelet during some subinterval of time, and remains zero elsewhere and are orthogonal. The uniform Haar wavelets are useful for the treatment of solution of differential equations which has no abrupt behavior. The lth uniform Haar wavelet $h_l(x)$, $x \in [0, 1)$ is defined as [16]:

$$h_l(x) = \begin{cases} 1, & a(l) \le x < b(l); \\ -1, & b(l) \le x < c(l); \\ 0, & \text{otherwise}, \end{cases} \tag{2.1.1}$$

where $a(l) = \frac{k}{m},\ b(l) = \frac{k+0.5}{m},\ c(l) = \frac{k+1}{m},\ l = 2^j + k + 1,\ j = 0, 1, 2, \cdots, J$ is dilation parameter, $m = 2^j$ and $k = 0, 1, 2, \cdots, 2^j - 1$ is translation parameter. When $k = 0,\ j = 0$ we have $l = 2$, which is the minimal value of l and the maximal value of l is $2M$ where $M = 2^J$, J is maximal level of resolution. In particular $h_1(x) := \chi_{[0,1)}(x)$, where $\chi_{[0,1)}(x)$ is characteristic function on interval $[0, 1)$, is the Haar scaling function. For the uniform Haar wavelet, the wavelet-collocation method is applied. The collocation points for the uniform Haar wavelets are usually taken as $x_j = \frac{j+0.5}{2M}$, where $j = 1, 2, ..., 2M$.

2.1.1 Fractional Integral of the Uniform Haar Wavelets

The Riemann-Liouville fractional integral of the Haar scaling function and the uniform Haar wavelets are given as

$$p_{\alpha,1}(x) = I^{\alpha}_{a(1)} h_1(x) = \frac{1}{\Gamma(\alpha)} \int_{a(1)}^{x} (x - s)^{\alpha-1} ds,\ \alpha > 0, \tag{2.1.2}$$

$$p_{\alpha,l}(x) = I^{\alpha}_{a} h_l(x) = \frac{1}{\Gamma(\alpha)} \begin{cases} \int_{a(l)}^{x} (x - s)^{\alpha-1} ds, & a(l) \le x < b(l); \\ \int_{a(l)}^{b(l)} (x - s)^{\alpha-1} ds - \int_{b(l)}^{x} (x - s)^{\alpha-1} ds, & b(l) \le x < c(l); \\ \int_{a(l)}^{b(l)} (x - s)^{\alpha-1} ds - \int_{b(l)}^{c(l)} (x - s)^{\alpha-1} ds, & x \ge c(l). \end{cases} \tag{2.1.3}$$

Equation (2.1.2) and (2.1.3) imply

$$p_{\alpha,1}(x) = \frac{(x-a(1))^{\alpha}}{\Gamma(\alpha+1)}, \tag{2.1.4}$$

and

$$p_{\alpha,l}(x) = \frac{1}{\Gamma(\alpha+1)} \begin{cases} (x - a(l))^{\alpha}, & a(l) \le x < b(l); \\ (x - a(l))^{\alpha} - 2(x - b(l))^{\alpha}, & b(l) \le x < c(l); \\ (x - a(l))^{\alpha} - 2(x - b(l))^{\alpha} + (x - c(l))^{\alpha}, & x \ge c(l). \end{cases} \tag{2.1.5}$$

The uniform grids are useful for the treatment of differential equations whose solution have smooth behavior.

2.2 The Non-uniform Haar Wavelets

There are some problems for which the uniform Haar wavelet method may be unsuitable, for example differential equations under the local excitation, boundary layer problems and asymptotic behavior of solutions, etc. In such cases it is reasonable to increase the number of the collocation points in subregions of rapid change and make use of the non-uniform Haar wavelet method [71]. That is, if solution have abrupt behavior in a given domain then we use non-uniform grids for better approximations.

The variable step-size is small when abrupt behavior of solution occurs and is large otherwise. The main idea of a non-uniform Haar wavelet method was proposed by F. Dubeau et al. [27] and later U. Lepik [72] used the modified form of the non-uniform Haar wavelet for the solution of integral and differential equations. Different non-uniform structures, according to boundary layers, for the numerical solution of singularly perturbed two-point boundary value problems were considered by Fazal-i-Haq et al. [55].

The lth non-uniform Haar wavelet $h_l(x)$, $x \in [a, b]$ is defined as

$$h_l(x) = \begin{cases} 1, & \xi_1(l) \le x < \xi_2(l); \\ -\gamma_l, & \xi_2(l) \le x < \xi_3(l); \\ 0, & \text{otherwise}, \end{cases} \tag{2.2.1}$$

where $l = 2^j + k + 1$; $j = 0, 1, 2, \cdots, J$ is dilation parameter and $k = 0, 1, 2, \cdots, 2^j - 1$ is translation parameter, J is maximal level of resolution and the maximal value of l is $2M$, $M = 2^J$. In particular $h_1(x) := \chi_{[a,b]}(x)$ is the Haar scaling function. The interval $[a, b]$ is partitioned into $2M$ subintervals having grid points $x(j),\ j = 0, 1, 2, \cdots, 2M$. The collocation points for the Haar wavelets are taken as $x_c(i) = \frac{i+0.5}{2M}$, where $i = 1, 2, ..., 2M$. Furthermore, $\xi_j(l)'s$, $j = 1, 2, 3$, are defined as

$$\xi_1(l) = x(2k\eta), \quad \xi_2(l) = x((2k+1)\eta),$$
$$\xi_3(l) = x((2k+2)\eta), \quad \eta = M/m,\ m = 2^j \quad and \quad \gamma_l = \frac{\xi_2(l) - \xi_1(l)}{\xi_3(l) - \xi_2(l)}.$$

2.2.1 Fractional Integral of the Non-uniform Haar Wavelets

In the following, we introduce the Riemann-Liouville fractional integral of the non-uniform Haar scaling and wavelets function by similar procedure as for the uniform Haar wavelets, i.e.,

$$p_{\alpha,1}(x) = I_a^\alpha h_1(x) = \tfrac{(x-a)^\alpha}{\Gamma(\alpha+1)}, \tag{2.2.2}$$

and

$$p_{\alpha,l}(x) = I_a^\alpha h_l(x) = \frac{1}{\Gamma(\alpha+1)} \begin{cases} (x - \xi_1(l))^\alpha, & \xi_1(l) \le x < \xi_2(l); \\ (x - \xi_1(l))^\alpha - (1+\gamma_l)(x - \xi_2(l))^\alpha, & \xi_2(l) \le x < \xi_3(l); \\ (x - \xi_1(l))^\alpha - (1+\gamma_l)(x - \xi_2(l))^\alpha + (x - \xi_3(l))^\alpha, & x \ge \xi_3(l). \end{cases} \tag{2.2.3}$$

The non-uniform Haar wavelets provide approximation to the solution of differential equations on non-uniform grids.

2.3 Function Approximations and Haar Matrices

Any function $y \in L_2[0,1]$ can be represented in term of the non-uniform Haar series as

$$y(x) = \sum_{l=1}^{\infty} b_l h_l(x), \tag{2.3.1}$$

where b_l are the Haar wavelet coefficients given by $b_l = \int_0^1 y(x)h_l(x)dx$.
The function $y(x)$ can be approximated by the truncated Haar wavelet series as

$$y(x) \approx y_M(x) = \sum_{l=1}^{2M} b_l h_l(x),\ l = 2^j + k + 1,\ j = 0, 1, 2, ..., J,\ k = 0, 1, 2, ..., 2^j - 1. \tag{2.3.2}$$

The wavelets coefficients b_l are determined in such away that the integral square error E

$$E = \int_0^1 \left[y(x) - \sum_{l=1}^{2M} b_l h_l(x)\right]^2 dx \tag{2.3.3}$$

is minimized.
In order to find the numerical approximations of a function, we put the Haar wavelets into a discrete form. For this purpose, we utilized the collocation method.

The collocation points for the Haar wavelets are taken as $x_c(i) = \frac{i+0.5}{2M}$, where $i = 1, 2, ..., 2M$. In discrete form, equation (2.3.3) is written as

$$E_M = \triangle x \sum_{i=1}^{2M} \left[y(x_c(i)) - \sum_{l=1}^{2M} b_l h_l(x_c(i))\right]^2.$$

2.3.1 Haar Matrix

Chen and Hsiao [16] established an operational matrix for integration via Haar wavelets, and a procedure for applying the matrix to analyse lumped and distributed- parameters dynamic systems is formulated. The highest derivatives appearing in the differential equations are first expanded into Haar series. The lower order derivatives and the solution functions can then be obtained quite easily by using Haar operational matrix of integration.

The discrete form of (2.3.2) is

$$y_M(x_c(i)) = \sum_{l=1}^{2M} b_l h_l(x_c(i)),\ i = 1, 2, \cdots, 2M. \tag{2.3.4}$$

We can represent (2.3.4) in vector form as

$$\mathbf{y} = \mathbf{bH}, \tag{2.3.5}$$

where $\mathbf{b} = [b_1\ b_2\ \cdots\ b_{2M}]$ and $\mathbf{y} = [y_M(x_c(1))\ y_M(x_c(2))\ \cdots\ y_M(x_c(2M))]$ are $2M$ dimensional row vectors and

$$\mathbf{H}_{2M\times 2M} = \begin{bmatrix} h_1(x_c(1)) & h_1(x_c(2)) & \cdots & h_1(x_c(2M)) \\ h_2(x_c(1)) & h_2(x_c(2)) & \cdots & h_2(x_c(2M)) \\ \vdots & \vdots & \ddots & \vdots \\ h_{2M}(x_c(1)) & h_{2M}(x_c(2)) & \cdots & h_{2M}(x_c(2M)) \end{bmatrix}.$$

In particular, for $J = 2$, we get $2M = 8$ and the Haar matrix is given as

$$\mathbf{H}_{8\times 8} = \begin{bmatrix} 1 & 1 & 1 & 1 & 1 & 1 & 1 & 1 \\ 1 & 1 & 1 & 1 & -1 & -1 & -1 & -1 \\ 1 & 1 & -1 & -1 & 0 & 0 & 0 & 0 \\ 0 & 0 & 0 & 0 & 1 & 1 & -1 & -1 \\ 1 & -1 & 0 & 0 & 0 & 0 & 0 & 0 \\ 0 & 0 & 1 & -1 & 0 & 0 & 0 & 0 \\ 0 & 0 & 0 & 0 & 1 & -1 & 0 & 0 \\ 0 & 0 & 0 & 0 & 0 & 0 & 1 & -1 \end{bmatrix}.$$

The Haar coefficients b_l can be determined by matrix inversion

$$\mathbf{b} = \mathbf{y}\mathbf{H}^{-1}, \tag{2.3.6}$$

where $\mathbf{H}^{-1}$ is the inverse of $\mathbf{H}$. Equation (2.3.6) gives the Haar coefficients b_l which are used in (2.3.2) to get the solution $y(x)$.

2.3.2 Haar Wavelet Operational Matrix of Fractional Integration

Haar matrix $\mathbf{H}$ is obtained by using the collocation points in (2.2.1), $H(l,i) = h_l(x_c(i))$. Similarly, we can obtain the fractional order integration matrix $\mathbf{P}$ of Haar function by substituting the collocation points in equations (2.2.2) and (2.2.3), $\mathbf{P}(l,i) = p_{\alpha,l}(x_c(i))$, as

$$\mathbf{P}_{2M\times 2M} = \begin{bmatrix} p_{\alpha,1}(x_c(1)) & p_{\alpha,1}(x_c(2)) & \cdots & p_{\alpha,1}(x_c(2M)) \\ p_{\alpha,2}(x_c(1)) & p_{\alpha,2}(x_c(2)) & \cdots & p_{\alpha,2}(x_c(2M)) \\ \vdots & \vdots & \ddots & \vdots \\ p_{\alpha,2M}(x_c(1)) & p_{\alpha,2M}(x_c(2)) & \cdots & p_{\alpha,2M}(x_c(2M)) \end{bmatrix}.$$

In particular, we fix $J = 2,\ \alpha = 0.75$, we get $2M = 8$ and the Haar wavelet operational matrix of fractional integration is

$$\mathbf{P}_{8\times 8} = \begin{bmatrix} 0.1360 & 0.3100 & 0.4548 & 0.5853 & 0.7067 & 0.8215 & 0.9312 & 1.0367 \\ 0.1360 & 0.3100 & 0.4548 & 0.5853 & 0.4347 & 0.2014 & 0.0216 & -0.1340 \\ 0.1360 & 0.3100 & 0.1828 & -0.0347 & -0.0668 & -0.0391 & -0.0275 & -0.0210 \\ 0 & 0 & 0 & 0 & 0.1360 & 0.3100 & 0.1828 & -0.0347 \\ 0.1360 & 0.0380 & -0.0293 & -0.0142 & -0.0091 & -0.0066 & -0.0051 & -0.0042 \\ 0 & 0 & 0.1360 & 0.0380 & -0.0293 & -0.0142 & -0.0091 & -0.0066 \\ 0 & 0 & 0 & 0 & 0.1360 & 0.0380 & -0.0293 & -0.0142 \\ 0 & 0 & 0 & 0 & 0 & 0 & 0.1360 & 0.0380 \end{bmatrix}.$$

2.3.3 Haar Wavelet Operational Matrix of Fractional Integration for Boundary Value Problems

We drive another operational matrix of fractional integration to solve the fractional boundary value problems. Let $\eta > 0$ and $g : [0, \eta] \to \mathbb{R}$ be a continuous function and assume that Haar functions have $[0, \eta]$ as compact support, then

$$\begin{aligned} g(x)I_0^\alpha h_1(\eta) &= g(x)\int_0^\eta (\eta - s)^{\alpha-1} ds, \\ v^{\alpha,\eta,1} &= g(x)C_{\alpha,1}, \end{aligned} \tag{2.3.7}$$

and

$$\begin{aligned} g(x)I_0^\alpha h_l(\eta) &= g(x)\Big[\int_{a(l)}^{b(l)} (\eta - s)^{\alpha-1} ds - \int_{b(l)}^{c(l)} (\eta - s)^{\alpha-1} ds\Big], \\ v^{\alpha,\eta,l} &= g(x)C_{\alpha,l}, \end{aligned} \tag{2.3.8}$$

where $v^{\alpha,\eta,1} = g(x)I_0^\alpha h_1(\eta)$, $v^{\alpha,\eta,l} = g(x)I_0^\alpha h_l(\eta)$, $C_{\alpha,1} = \frac{\eta^\alpha}{\Gamma(\alpha+1)}$ and $C_{\alpha,l} = \frac{1}{\Gamma(\alpha+1)}\big[(\eta - a(l))^\alpha - 2(\eta - b(l))^\alpha + (\eta - c(l))^\alpha\big]$. Also $l = 2^j + k + 1$, $j = 0, 1, 2, \cdots, J$ and $k = 0, 1, 2, \cdots, 2^j - 1$. Let $x_c(i) = \eta\frac{i-0.5}{2M}$, $i = 1, 2, \cdots, 2M$ and define a matrix $\mathbf{V}$ by using the collocation points, x_c, in (2.3.7) and (2.3.8), we get

$$\mathbf{V}^{\alpha,\eta}_{\mathbf{2M}\times\mathbf{2M}} = \begin{bmatrix} g(x_c(1))I_0^\alpha h_1(\eta) & g(x_c(2))I_0^\alpha h_1(\eta) & \cdots & g(x_c(2M))I_0^\alpha h_1(\eta) \\ g(x_c(1))I_0^\alpha h_2(\eta) & g(x_c(2))I_0^\alpha h_2(\eta) & \cdots & g(x_c(2M))I_0^\alpha h_2(\eta) \\ \vdots & \vdots & \ddots & \vdots \\ g(x_c(1))I_0^\alpha h_{2M}(\eta) & g(x_c(2))I_0^\alpha h_{2M}(\eta) & \cdots & g(x_c(2M))I_0^\alpha h_{2M}(\eta) \end{bmatrix}.$$

In particular, for $\eta = 1$, $g(x) = x^2$, $\alpha = 1.25, J = 2$, we get

$$\mathbf{V}_{\mathbf{8\times 8}}^{\mathbf{1.25,1}} = \begin{bmatrix} 0.0034 & 0.0310 & 0.0862 & 0.1689 & 0.2793 & 0.4172 & 0.5827 & 0.7757 \\ 0.0005 & 0.0049 & 0.0137 & 0.0269 & 0.0444 & 0.0664 & 0.0927 & 0.1234 \\ 0.0001 & 0.0008 & 0.0021 & 0.0041 & 0.0069 & 0.0102 & 0.0143 & 0.0190 \\ 0.0002 & 0.0021 & 0.0058 & 0.0113 & 0.0187 & 0.0279 & 0.0390 & 0.0519 \\ 0.0000 & 0.0002 & 0.0005 & 0.0009 & 0.0015 & 0.0023 & 0.0032 & 0.0042 \\ 0.0000 & 0.0002 & 0.0006 & 0.0012 & 0.0019 & 0.0029 & 0.0041 & 0.0054 \\ 0.0000 & 0.0003 & 0.0009 & 0.0017 & 0.0029 & 0.0043 & 0.0060 & 0.0080 \\ 0.0001 & 0.0009 & 0.0024 & 0.0048 & 0.0079 & 0.0117 & 0.0164 & 0.0218 \end{bmatrix}.$$

The Haar matrices **H, P** and **V** are constructed to solve the fractional order initial and boundary value problems.

2.4 Convergence of Haar Wavelet Method

Let $y(x)$ be a differentiable function and assume that $y(x)$ have bounded first derivative on $(0,1)$, i.e., there exist $K > 0$; for all $x \in (0,1)$

$$|y'(x)| \leq K.$$

Haar wavelet approximation for the function $y(x)$ is mentioned in (2.3.2). Babolian and Shahsavaran [4] gave L_2-error norm for Haar wavelet approximation, which is

$$\|y(x) - y_M(x)\|^2 \leq \frac{K^2}{3}.\frac{1}{(2M)^2},$$

or

$$\|y(x) - y_M(x)\| \leq O(\frac{1}{M}), \tag{2.4.1}$$

where $M = 2^J$ and J is the maximal level of resolution. From (2.4.1), we observe that error is inversely proportional to the level of resolution. Thus the convergence of Haar wavelet approximation is ensured at higher level of resolution i.e., when M is increased.

2.5 Nonuniform Haar Wavelet Method

This section is based on our paper [114], where we have generated different structures of nonuniform collocation points and applied the non-uniform Haar wavelet methods to different classes of fractional order ordinary differential equations which has abrupt behavior of solution. The uniform and nonuniform Haar wavelet methods are compared. We consider fractional initial as well as boundary value problems with constant and variable coefficients.

2.5.1 Initial Value Problems

Example 1: Consider the α^{th} order linear fractional ordinary differential equation with variable coefficients whose solution also depends on the order of differential equation,

$$ {}^{c}D^{\alpha}y(x) + a(x)y = f(x),\ 0 \le x \le 10,\ 1 < \alpha < 2, \tag{2.5.1} $$

with $y(0) = 1,\ y'(0) = \alpha$ and $f(x) = x^{-\alpha}E_{1,1-\alpha}(\alpha x) + a(x)E_{1,1}(\alpha x)$, where E is Mittag-Leffler function. Furthermore, we choose $a(x) = x$.

The exact solution of initial value problem (2.5.1) is $y(x) = e^{\alpha x}$. The solution procedure is as under: We approximate the higher order derivative term by Haar wavelet series as

$$ {}^{c}D^{\alpha}y(x) \approx \sum_{l=1}^{2M} b_l h_l(x). \tag{2.5.2} $$

Lower order derivatives are obtained by integrating (2.5.2)

$$ y(x) \approx \sum_{l=1}^{2M} b_l p_{\alpha,l}(x) + \alpha x + 1. \tag{2.5.3} $$

Substitute (2.5.2) and (2.5.3) in (2.5.1), we get

$$ \sum_{l=1}^{2M} b_l [h_l(x) + x p_{\alpha,l}(x)] \approx f(x) - \alpha x^2 - x. \tag{2.5.4} $$

Let us divide the interval $[0, 10]$ into two subintervals $[0, 8]$ and $[8, 10]$, let $A = 0, B = 8, C = 10$, step-size for each subintervals are

$\Delta x_1 = \frac{(B-A)}{M}$,

$\Delta x_2 = \frac{(C-B)}{M}$.

Here $\Delta x_2 \ll \Delta x_1$.

The coordinates of the grid points are

For j=1,2,...,$M + 1$

x(j)=A+(i-1)Δx_1,

For j=1,2,..,M

x(j+$M + 1$)=B+(i)Δx_2,

And collocation points are

For j=1,2,...,2M

$x_c(j) = \frac{x(j)+x(j+1)}{2}$.

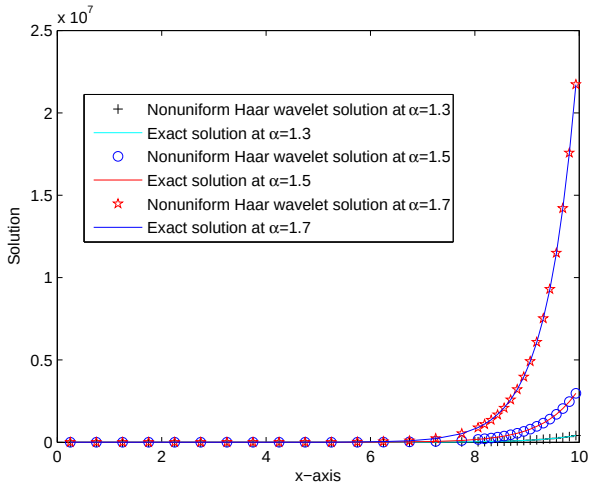

Figure 2.1: Comparison of exact solution with non-uniform Haar wavelet solution for $\alpha = 1.3,\ \alpha = 1.5$ and $\alpha = 1.7$.

	L_∞-error for Non-uniform Haar wavelet solution			L_∞-error for Uniform Haar wavelet solution		
α	$J = 6$	$J = 7$	$J = 8$	$J = 6$	$J = 7$	$J = 8$
1.1	8.6077	1.9960	8.737e-1	2.0229e+2	1.0409e+2	5.2925e+1
1.3	3.4434e+1	8.1861	1.9291	1.5297e+3	7.8965e+2	4.0155e+2
1.5	1.8100e+2	4.4065e+1	1.0791e+1	1.3109e+4	6.7965e+3	3.4602e+3

Table 2.1: L_∞-error for Example 1.

Numerical solution for different order, α, of fractional differential equation at different levels of resolution, J, is considered for both uniform and non-uniform grids. The solution have abrupt behavior so non-uniform Haar wavelets provide better results as compared to uniform Haar wavelet as shown in Table 2.1. The non-uniform Haar wavelet solution and exact solution at different value of α are shown in Figure 2.1.

Example 2: Consider the linear fractional ordinary differential equation with constant coefficients

$$ {}^cD^\alpha y(x) + y'(x) + y(x) = f(x),\ 0 \le x \le 1,\ 1 < \alpha < 2, \tag{2.5.5}$$

with $y(0) = 0,\ y'(0) = 0$, where $f(x) = -\frac{2\Gamma(51)x^{50-\alpha}}{\Gamma(51-\alpha)} + \frac{2\Gamma(101)x^{100-\alpha}}{\Gamma(101-\alpha)} - \frac{\Gamma(\frac{21}{10})x^{\frac{11}{10}-\alpha}}{\Gamma(\frac{21}{10}-\alpha)} - 100x^{49} + 200x^{99} - \frac{11x^{\frac{1}{10}}}{50} - 2x^{50} + 2x^{100} - \frac{x^{\frac{11}{10}}}{5}$.

Exact solution of (2.5.5) is $y(x) = -2x^{50} + 2x^{100} - \frac{x^{\frac{11}{10}}}{5}$, and approximation of higher order term by

the Haar wavelets is

$$ {}^{c}D^{\alpha}y(x) \approx \sum_{l=1}^{2M} b_l h_l(x). \tag{2.5.6} $$

Other derivative terms are obtained by integrating (2.5.6)

$$ \begin{aligned} y(x) &\approx \sum_{l=1}^{2M} b_l p_{\alpha,l}(x), \\ y^{'}(x) &\approx \sum_{l=1}^{2M} b_l p_{\alpha-1,l}(x). \end{aligned} \tag{2.5.7} $$

Substituting (2.5.6) and (2.5.7) in (2.5.5), we get

$$ \sum_{l=1}^{2M} b_l[h_l(x) + p_{\alpha,l}(x) + p_{\alpha-1,l}(x)] \approx f(x). \tag{2.5.8} $$

The exact solution $y(x) = -2x^{50} + 2x^{100} - \frac{x^{\frac{11}{10}}}{5}$ has minimum value Y_{min} at $x = 0.9863$. We observe that the solution initially decreases slowly as x approaches to 0.88, decreases rapidly when x vary from 0.88 to 0.9863 and then it increases rapidly. Therefore we divide the interval $[0, 1]$ into three subintervals $[0, 0.88]$, $[0.88, 0.9863]$ and $[0.9863, 1]$, let $A = 0, B = 0.88, C = 0.9863, D = 1$, and step-size for each subintervals are

$\Delta x_1 = \frac{2(B-A)}{M}$,
$\Delta x_2 = \frac{(C-B)}{M}$,
$\Delta x_3 = \frac{2(D-C)}{M}$.
Here $\Delta x_1 > \Delta x_2 > \Delta x_3$.
The coordinates of the grid points are
For j=1,2,...,$\frac{M}{2} + 1$
x(j)=A+(i-1)Δx_1,
For j=1,2,..,M
x(j+$\frac{M}{2} + 1$)=B+(i)Δx_2,
For j=1,2,...,$\frac{M}{2}$
x(j+1+$\frac{3M}{2}$)=C+(i)Δx_3,
And collocation points are
For j=1,2,...,2M
$x_c(j) = \frac{x(j)+x(j+1)}{2}$.

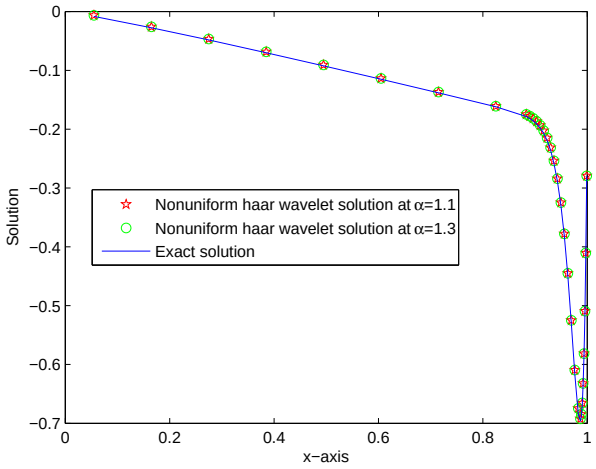

Figure 2.2: Non-uniform Haar wavelet solution at $\alpha = 1.1,\ \alpha = 1.3$ and exact solution.

Table 2.2: Comparison of numerical results by non-uniform Haar wavelets and uniform Haar wavelets with exact solution, at different level of resolution J and for different values of α.

		L_∞- error for Non-uniform Haar wavelet solution			
α	$J=4$	$J=5$	$J=6$	$J=7$	$J=8$
1.1	8.3734e-3	2.8987e-3	8.1917e-4	2.1882e-4	7.6632e-5
1.3	1.0135e-2	3.7616e-3	1.2634e-3	4.5917e-4	2.0132e-4
1.5	1.5592e-2	7.2314e-3	3.4244e-3	1.8563e-3	1.1179e-3
1.7	3.0194e-2	1.8103e-2	1.1610e-2	8.1744e-3	6.0322e-3
		L_∞-error for Uniform Haar wavelet solution			
α	$J=4$	$J=5$	$J=6$	$J=7$	$J=8$
1.1	1.0245e+0	2.6536e-1	6.0917e-2	1.2686e-2	2.1391e-3
1.3	1.1184e+0	2.5716e-1	5.5018e-2	1.1632e-2	2.4754e-3
1.5	1.3520e+0	2.9487e-1	6.8696e-2	1.8905e-2	6.4434e-3
1.7	1.8857e+0	4.2629e-1	1.1869e-1	4.2828e-2	1.9471e-2

Table 2.2 shows that the non-uniform Haar wavelet is good for approximating solution having abrupt behaviour on its domain of definition and provides relatively accurate results as compared to uniform Haar wavelet. Non-uniform grids are generated, in such a away, to reduce the absolute error as much as possible. Since solution of problem in Example 2 attains its minimum value at $x = 0.9863$ and suddenly increases when $x > 0.9863$, that is the reason for using non-uniform grids as shown in

Figure 2.2.

Locally fractionally disturbed vibrations

Example 3: Consider the linear fractional ordinary differential equation with constant coefficients [72],

$$ {}^{c}D^{\alpha}y(x) + \pi^2 y(x) = f(x),\ 0 \le x \le 0.5,\ 1 < \alpha < 2, \tag{2.5.9} $$

with $y(0) = 1,\ y'(0) = 0$, where

$$ f(x) = \begin{cases} 400\sin(40\pi x), & 0.2 \le x \le 0.25; \\ 0, & \text{elsewhere.} \end{cases} $$

Consider the Haar wavelet approximation of higher order derivative in (2.5.9)

$$ {}^{c}D^{\alpha}y(x) \approx \sum_{l=1}^{2M} b_l h_l(x). \tag{2.5.10} $$

Lower order derivatives are obtained by integrating (2.5.10)

$$ y(x) \approx \sum_{l=1}^{2M} b_l p_{\alpha,l}(x) + 1. \tag{2.5.11} $$

Substituting (2.5.10) and (2.5.11) in (2.5.9), we obtain

$$ \sum_{l=1}^{2M} b_l [h_l(x) + \pi^2 p_{\alpha,l}(x)] \approx f(x) - \pi^2. \tag{2.5.12} $$

Here we use same non-uniform grids for fractional order ordinary differential equation as in [72] for non-fractional order ordinary differential equation, interval $[0, 0.5]$ is divided into three subintervals $[0.0.2]$, $[0.2, 0.25]$ and $[0.25, 0.5]$, step-size for each subintervals are

$\Delta x_1 = \frac{0.4}{M}$,

$\Delta x_2 = \frac{0.05}{M}$,

$\Delta x_3 = \frac{0.5}{M}$.

The coordinates of the grid points are

For l=1,2,..,$\frac{M}{2} + 1$

$x(l) = l\Delta x_1$,

For l=1,2,..,M

$x(l + \frac{M}{2} + 1) = 0.2 + l\Delta x_2$,

For l=1,2,..,$\frac{M}{2}$

$x(l + \frac{3M}{2} + 1) = 0.25 + l\Delta x_3$,

And collocation points are

For l=1,2,...,$2M$

$x_c(l) = \frac{x(l)+x(l+1)}{2}$.

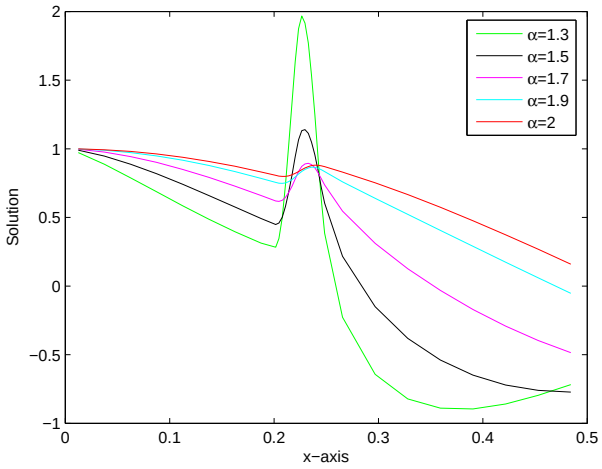

Figure 2.3: Nonuniform Haar wavelet solution at $\alpha = 1.3,\ \alpha = 1.5,\ \alpha = 1.7,\ \alpha = 1.9$ and $\alpha = 2$.

In [72], equation (2.5.9) is solved for $\alpha = 2$, we showed that the solution of equation (2.5.9) converged to the solution at $\alpha = 2$ when α approaches to 2 as shown in Figure 2.3.

Example 4: Consider the α^{th} order fractional ordinary differential equation with variable coefficients,

$$ {}^{c}D^{\alpha}y(x) + e^{x}y = f(x),\ 0 \le x \le 1,\ 0 < \alpha < 1, \tag{2.5.13} $$

with $y(0) = 0$ and $f(x) = \frac{5\Gamma(11)x^{10-\alpha}}{\Gamma(11-\alpha)} - \frac{4\Gamma(6)x^{5-\alpha}}{\Gamma(6-\alpha)} + e^{x}(5x^{10} - 4x^{5})$.
The exact solution of initial value problem (2.5.13) is $y(x) = 5x^{10} - 4x^{5}$.
We approximate the higher order derivative term by Haar wavelet series as

$$ {}^{c}D^{\alpha}y(x) \approx \sum_{l=1}^{2M} b_l h_l(x). \tag{2.5.14} $$

Lower order derivatives are obtained by integrating (2.5.14)

$$ y(x) \approx \sum_{l=1}^{2M} b_l p_{\alpha,l}(x). \tag{2.5.15} $$

Substitute (2.5.14) and (2.5.15) in (2.5.13), we get the following form:

$$ \sum_{l=1}^{2M} b_l[h_l(x) + e^{x}p_{\alpha,l}(x)] \approx f(x). \tag{2.5.16} $$

Since the behavior of the solution changes near $x = 0.8$, therefore, we divide the interval $[0, 1]$ into two subintervals $[0, 0.8]$ and $[0.8, 1]$. Let $A = 0, B = 0.8, C = 1$, and step-size for each subintervals are
$\Delta x_1 = \frac{(B-A)}{M}$,
$\Delta x_2 = \frac{(C-B)}{M}$.

Here $\Delta x_2 \ll \Delta x_1$.

The coordinates of the grid points are

For j=1,2,...,$M+1$

x(j)=A+(i-1)Δx_1,

For j=1,2,..,M

x(j+$M+1$)=B+(i)Δx_2,

And collocation points are

For j=1,2,...,2M

$x_c(j) = \frac{x(j)+x(j+1)}{2}$.

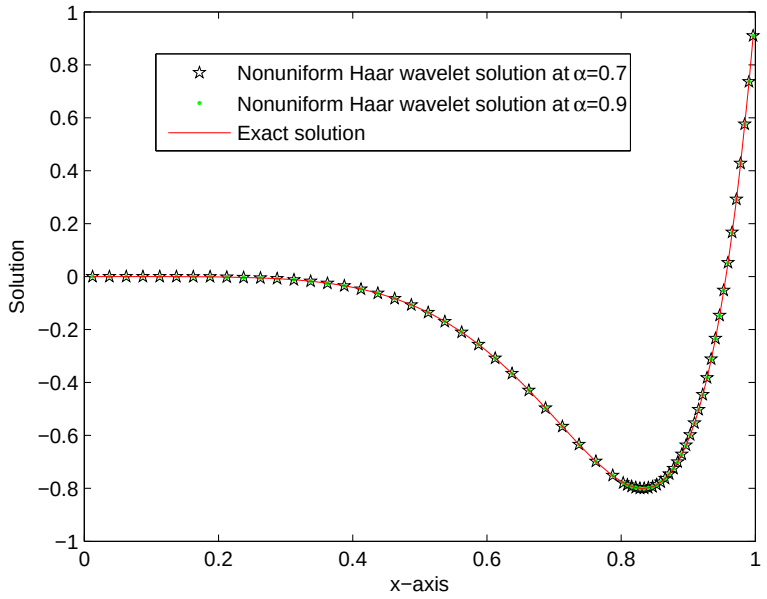

Figure 2.4: Comparison of exact solution with non-uniform Haar wavelet solution at $\alpha = 0.7$, and $\alpha = 0.9$.

	L_∞-error for Non-uniform Haar wavelet solution			L_∞-error for Uniform Haar wavelet solution		
α	$J=5$	$J=6$	$J=7$	$J=5$	$J=6$	$J=7$
0.5	2.4323e-03	8.4575e-04	2.9406e-04	9.4314e-03	3.3157e-03	1.1523e-03
0.7	1.6592e-03	5.1638e-04	1.5997e-04	8.2594e-03	2.5151e-03	7.5543e-04
0.9	1.5639e-03	4.5507e-04	1.2499e-04	6.5167e-03	1.7602e-03	4.6737e-04

Table 2.3: L_∞-error for different α and J.

Table 2.3 shows that the non-uniform Haar wavelets provide better results as compared to uniform Haar wavelets because the solution of the problem have abrupt behavior.

2.5.2 Boundary Value Problems

Example 5: Consider the second order linear fractional ordinary differential equation with variable coefficients,

$$y''(x) + a(x)^c D^\alpha y(x) + b(x)y(x) = f(x),\ 0 \le x \le 1,\ 1 < \alpha < 2, \tag{2.5.17}$$

with $y(0) = 0,\ y(1) = 0$, where $f(x) = 2 - 4830x^{68} + \frac{\Gamma(3)x^{2-\alpha}}{\Gamma(3-\alpha)} - \frac{\Gamma(71)x^{70-\alpha}}{\Gamma(71-\alpha)} + x^2 - x^{70}$.
The exact solution of boundary value problem (2.5.17) is $y(x) = x^2 - x^{70}$.
Consider the Haar wavelet approximation for $y''(x)$ as

$$y''(x) \approx \sum_{l=1}^{2M} b_l h_l(x). \tag{2.5.18}$$

Lower order derivatives are approximated by integrating (2.5.18)

$$\begin{aligned} y(x) &\approx \sum_{l=1}^{2M} b_l (p_{2,l}(x) - xC_{2,l}), \\ {}^cD^\alpha y(x) &\approx \sum_{l=1}^{2M} b_l p_{2-\alpha,l}(x), \end{aligned} \tag{2.5.19}$$

where $C_{\alpha,l}$ is given in (2.3.8). Substitute (2.5.18) and (2.5.19) in (2.5.17), take $a(x) = e^x$ and $b(x) = \sin(x)$, we get the following form:

$$\sum_{l=1}^{2M} b_l [h_l(x) + e^x p_{2-\alpha,l}(x) + \sin(x) p_{2,l}(x) - x\sin(x) C_{2,l}] \approx f(x). \tag{2.5.20}$$

Exact solution $y(x) = x^2 - x^{70}$ has maximum value Y_{max} at $x = (\frac{1}{35})^{(\frac{1}{68})}$. Therefore divide the interval $[0, 1]$ into three subintervals $[0, 0.9]$, $[0.9, (\frac{1}{35})^{(\frac{1}{68})}]$, $[(\frac{1}{35})^{(\frac{1}{68})}, 1]$, let $A = 0, B = 0.9, C = (\frac{1}{35})^{(\frac{1}{68})}, D = 1$ and step-size for each subintervals are
$\Delta x_1 = \frac{4(B-A)}{3M}$,
$\Delta x_2 = \frac{4(C-B)}{M}$,
$\Delta x_3 = \frac{(D-C)}{M}$.
Here $\Delta x_3 \ll \Delta x_1,\ \Delta x_2$.
The coordinates of the grid points are
For j=1:$\frac{3M}{4} + 1$
x(j)=A+(i-1)Δx_1,
For j=1:$\frac{M}{4}$
x(j+$\frac{3M}{4} + 1$)=B+(i)Δx_2,

For j=1:M

x(j+1+M)=C+(i)Δx_3,

And collocation points are

For j=1,2,...,2M

$x_c(j) = \frac{x(j)+x(j+1)}{2}$.

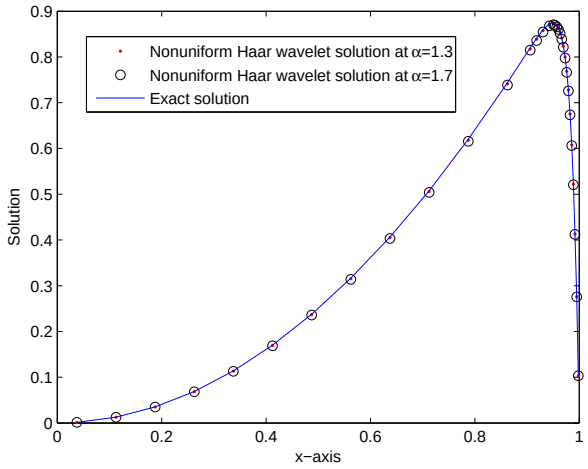

Figure 2.5: Non-uniform Haar wavelet solution at $\alpha = 1.3,\ \alpha = 1.7$ and exact solution.

Table 2.4: Comparison of numerical results by non-uniform Haar wavelets and uniform Haar wavelets with exact solution, at different level of resolution J and order α.

		L_∞-error for Non-uniform Haar wavelet solution			
α	$J=4$	$J=5$	$J=6$	$J=7$	$J=8$
1.1	2.2827e-3	9.0688e-4	2.7620e-4	7.3601e-5	1.8858e-5
1.3	2.6304e-3	1.0321e-3	3.2093e-4	9.0173e-5	2.4710e-5
1.5	3.6424e-3	1.4603e-3	4.9544e-4	1.5983e-4	5.1733e-5
1.7	5.3347e-3	2.3109e-3	8.9327e-4	3.4001e-4	1.3157e-4
1.9	5.2355e-3	2.4560e-3	1.0336e-3	4.3941e-4	1.9339e-4
		L_∞-error for Uniform Haar wavelet solution			
α	$J=4$	$J=5$	$J=6$	$J=7$	$J=8$
1.1	7.2378e-1	2.3554e-1	8.9974e-2	3.8429e-2	1.7646e-2
1.3	7.0842e-1	2.1793e-1	8.2622e-2	3.4997e-2	1.5973e-2
1.5	6.9719e-1	2.0808e-1	7.8037e-2	3.2571e-2	1.4674e-2
1.7	7.1624e-1	2.1195e-1	7.9057e-2	3.2570e-2	1.4442e-2
1.9	8.2296e-1	2.3659e-1	8.9121e-2	3.7229e-2	1.6675e-2

Figure 2.5 shows that solution of boundary value problem (2.5.17) attains its maximum value at $x = (\frac{1}{35})^{(\frac{1}{68})}$ and suddenly decreases when $x > (\frac{1}{35})^{(\frac{1}{68})}$, that is the reason for using non-uniform grids. Table 2.4 shows that uniform grids are not suitable here because we need more points when $x > (\frac{1}{35})^{(\frac{1}{68})}$ and the non-uniform Haar wavelet solution is suitable.

Example 6: Consider the singularly perturbed problem [55] of fractional order:

$$-\epsilon\ {}^cD^\alpha y(x) + (1 + x(1-x))y(x) = f(x),\ 0 \le x \le 1,\ 1 < \alpha < 2, \tag{2.5.21}$$

with $y(0) = 0,\ y(1) = 0$, where $f(x) = 1+x(1-x)+(2\sqrt{\epsilon}-x^2(1-x))e^{\frac{-(1-x)}{\sqrt{\epsilon}}}+(2\sqrt{\epsilon}-x(1-x)^2)e^{\frac{-x}{\sqrt{\epsilon}}}$ and ϵ is a small positive parameter, $0 < \epsilon << 1$.

The exact solution of boundary value problem (2.5.21) is $y(x) = 1+x(1-x)e^{\frac{-x}{\sqrt{\epsilon}}}-xe^{\frac{-(1-x)}{\sqrt{\epsilon}}}$. Consider the Haar wavelet approximation of higher order derivative term in (2.5.21) as

$${}^cD^\alpha y(x) \approx \sum_{l=1}^{2M} b_l h_l(x). \tag{2.5.22}$$

Lower order derivatives are obtained by integrating (2.5.22),

$$y(x) \approx \sum_{l=1}^{2M} b_l(p_{\alpha,l}(x) - xC_{\alpha,l}), \tag{2.5.23}$$

where $C_{\alpha,l}$ is given in (2.3.8). Put (2.5.22) and (2.5.23) in (2.5.21),

$$\sum_{l=1}^{2M} b_l[-\epsilon h_l(x) + (1 + x(1-x))(p_{\alpha,l}(x)) - xC_{\alpha,l}] \approx f(x). \tag{2.5.24}$$

Keeping in view the nature of exact solution given in [55], we need more grid points at end of the interval $(0, 1)$. We generate the collocation points that fulfil the requirement of the solution.
Here, we consider $q = 1.3$, $p = 0.75$, the coordinates of the grid points are
For j=1:1,2,...,$M + 1$
$x(j) = \frac{(q^j-1)}{2(q^{M+1}-1)}$,
For j=1:1,2,...,M
$x(j + M + 1) = x(M + 1) + \frac{(p^j-1)}{2(p^M-1)}$,
And collocation points are
For j=1:1,2,...,$2M$
$x_c(j) = \frac{x(j)+x(j+1)}{2}$.

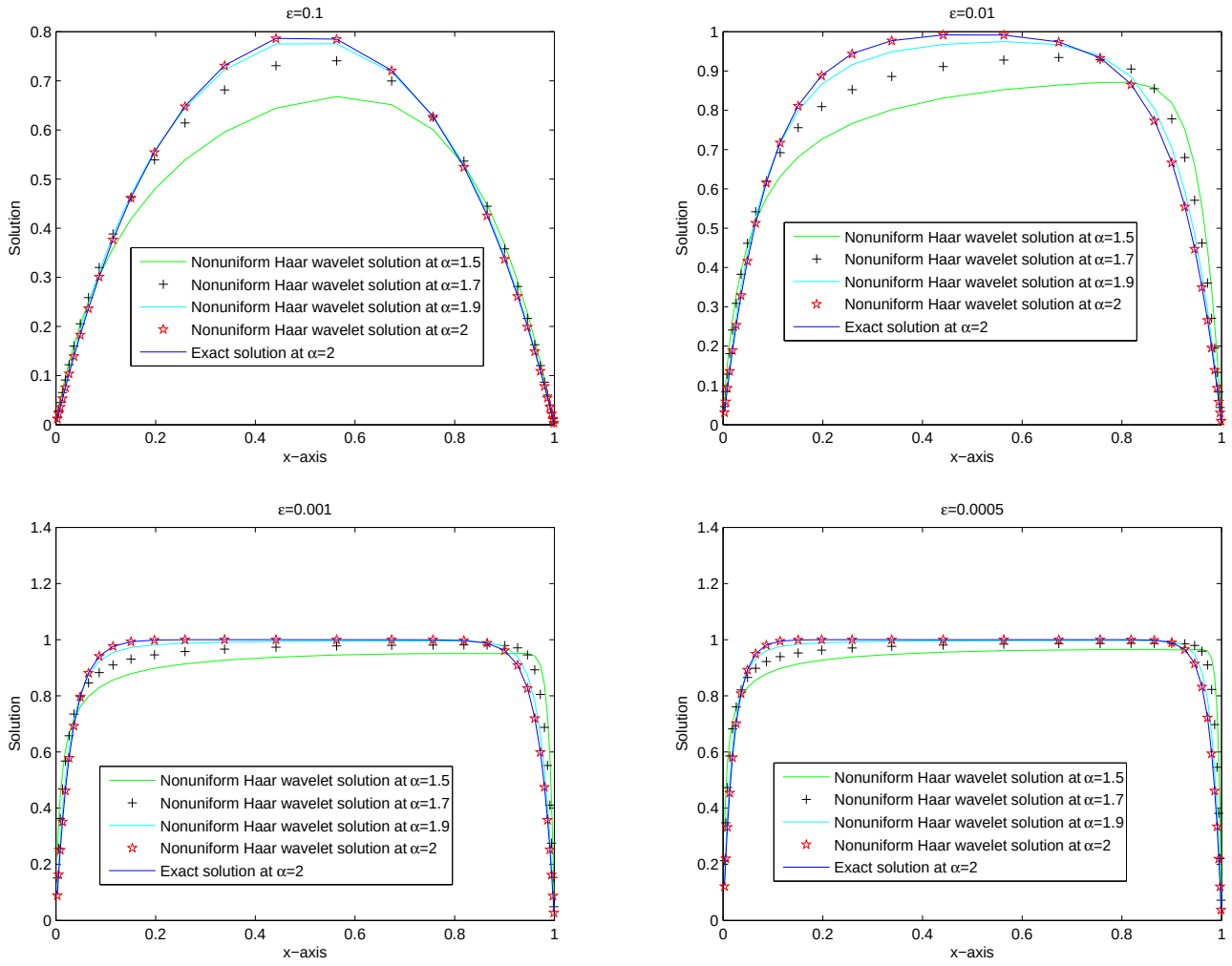

Figure 2.6: Non-uniform Haar wavelet solution at $\alpha = 1.5$, $\alpha = 1.7$, $\alpha = 1.9$, $\alpha = 2$ and exact solution at $\alpha = 2$.

Figure 2.6 showed that the problem converged to the exact solution [55] at different value of ϵ, when α approaches to 2.

2.5.3 Conclusion

The error for the non-uniform Haar wavelet is less than the error for the uniform Haar wavelet. In Examples (3) and (6), we showed that the solution of fractional order ordinary differential equations by the non-uniform Haar wavelet converged to the non-fractional order ordinary differential equation. In Examples (1),(2), (4) and (5), we generated the non-uniform grids according to the behavior of the solution and compared the results with exact and the uniform Haar wavelet solutions. The purpose of including the Example (4) is to show that the method works for any order α. The present method

provided the more accurate results even if the level of resolution is low. Also, the non-uniform Haar wavelet solutions are in good agreement with exact solutions.

Chapter 3

Haar Wavelet-Quasilinearization Technique for Fractional Nonlinear Differential Equations

This chapter is based on our paper [115]. We introduce a numerical method for the solution of fractional nonlinear ordinary differential equation, which is the combinations of two numerical techniques, Haar wavelet and quasilinearization technique. Quasilinearization technique is used to linearize the nonlinear fractional ordinary differential equation and then the Haar wavelet method is applied to linearized fractional ordinary differential equations. In each iteration of quasilinearization technique, solution is updated by the Haar wavelet method. The main aim of the present chapter is to present a numerical method for the solution of nonlinear fractional initial and boundary value problems over a uniform as well as non uniform grids.

3.1 Quasilinearization Technique

The quasilinearization approach [7,74,82] is a generalized Newton-Raphson technique for functional equations. It converges quadratically to the exact solution, if there is convergence at all, and it has monotone convergence. Let us consider the nonlinear second order differential equation [74]

$$y''(x) = f(y(x), x),\ a \leq x \leq b, \tag{3.1.1}$$

with the boundary conditions

$$y(a) = \alpha, \quad y(b) = \beta.$$

Choose an initial approximation of the function $y(x)$, let say $y_0(x)$, it may be $y_0(x) = \alpha$, for $a \leq x \leq b$. The function f can now be expanded around y_0 by the use of the Taylor series

$$f(y(x), x) = f(y_0(x), x) + (y(x) - y_0(x)) f_{y_0}(y_0(x), x), \tag{3.1.2}$$

where we have ignored the second and higher order terms. Using (3.1.2) in (3.1.1), we get

$$y''(x) = f(y_0(x), x) + (y(x) - y_0(x))f_{y_0}(y_0(x), x). \tag{3.1.3}$$

We solve equation (3.1.3) for $y(x)$, call it $y_1(x)$. Now by expanding (3.1.1) about $y_1(x)$,

$$y''(x) = f(y_1(x), x) + (y(x) - y_1(x))f_{y_1}(y_1(x), x), \tag{3.1.4}$$

we obtain a third approximation for $y(x)$, call it $y_2(x)$. Assume that the problem converges and continue the procedure until the desired accuracy is obtained. Consequently, recurrence relation is of the form

$$y''_{r+1}(x) = f(y_r(x), x) + (y_{r+1}(x) - y_r(x))f_{y_r}(y_r(x), x), \tag{3.1.5}$$

where $y_r(x)$ is known and can be used for obtaining $y_{r+1}(x)$. Equation (3.1.5) is always a linear differential equation with boundary conditions

$$y_{r+1}(a) = \alpha, \quad y_{r+1}(b) = \beta.$$

Next we consider a general class of nonlinear second order differential equation of the form [74]

$$y''(x) = f(y'(x), y(x), x), \tag{3.1.6}$$

with the boundary conditions

$$y(a) = \alpha, \quad y(b) = \beta.$$

Here the first derivative $y'(x)$ can be considered as another function and equation (3.1.6) implies

$$\begin{aligned} y''_{r+1}(x) &= f(y'_r(x), y_r(x), x) + (y_{r+1}(x) - y_r(x))f_{y_r}(y'_r(x), y_r(x), x) \\ &+ (y'_{r+1}(x) - y'_r(x))f_{y'_r}(y'_r(x), y_r(x), x), \end{aligned} \tag{3.1.7}$$

with boundary conditions

$$y_{r+1}(a) = \alpha, \quad y_{r+1}(b) = \beta.$$

Similarly, for the higher order nonlinear differential equations, following the same procedure one can obtain the recurrence relation [82],

$$\begin{aligned} L^n y_{r+1}(x) &= f(y_r(x), y'_r(x), ..., y_r^{n-1}(x), x) \\ &+ \sum_{j=0}^{n-1} (y^j_{r+1}(x) - y^j_r(x))f_{y^j}(y_r(x), y'_r(x), ..., y_r^{n-1}(x), x), \end{aligned} \tag{3.1.8}$$

where n is order of the differential equation. Equation (3.1.8) is always a linear differential equation and can be solved recursively, where $y_r(x)$ is known and one can use it to get $y_{r+1}(x)$.

3.1.1 Convergence of Quasilinearization Technique

Consider the nonlinear second order differential equation

$$y''(x) = f(y), \quad y(0) = y(b) = 0. \tag{3.1.9}$$

Application of quasilinearization technique to (3.1.9) yields

$$y''_{r+1}(x) = f(y_r) + (y_{r+1} - y_r)f'(y_r), \quad y_{r+1}(0) = y_{r+1}(b) = 0. \tag{3.1.10}$$

Let $y_0(x)$ be some initial approximation. Each function $y_{r+1}(x)$ is a solution of a linear equation (3.1.10), where y_r is always known and is obtained from the previous iteration. Subtract the r^{th} equation from the $(r+1)^{st}$ equation (3.1.10), we get

$$(y_{r+1} - y_r)'' = f(y_r) - f(y_{r-1}) + (y_{r+1} - y_r)f'(y_r) - (y_r - y_{r-1})f'(y_{r-1}). \tag{3.1.11}$$

By considering (3.1.11) as a differential equation for $(y_{r+1} - y_r)$ and converting into corresponding integral equation

$$(y_{r+1} - y_r) = \int_0^b K(x,y)\{f(y_r) - f(y_{r-1}) + (y_{r+1} - y_r)f'(y_r) - (y_r - y_{r-1})f'(y_{r-1})\}dy. \tag{3.1.12}$$

Where $K(x,y)$ is the Green's function defined by

$$K(x,y) = \begin{cases} x(y-b)/b, & 0 \le x < y \le b, \\ (x-b)y/b, & b \ge x > y \ge 0. \end{cases}$$

Observe that $\max_{x,y} |K(x,y)| = \frac{b}{4}$, where the maximization is over the region $0 \le x, y \le b$. The Taylor series expansion for f with centre at y_{r-1} is

$$f(y_r) = f(y_{r-1}) + (y_r - y_{r-1})f'(y_{r-1}) + \frac{(y_r - y_{r-1})^2}{2}f''(u), \quad y_{r-1} < u < y_r.$$

Letting $\max_y(|f(y)|, |f'(y)|) = s < \infty$ and $k = \max_u |f''(u)|$.
Equation (3.1.12) implies [7]:

$$|y_{r+1} - y_r| \le \int_0^b |K(x,y)| \left\{ |y_{r+1} - y_r||f'(y_r)| + \frac{(y_r - y_{r-1})^2}{2}|f''(u)| \right\} dy,$$

or

$$\max_x |y_{r+1} - y_r| \le \frac{b}{4} \int_0^b \left\{ \max_x |y_{r+1} - y_r| s + \frac{(y_r - y_{r-1})^2}{2} k \right\} dy,$$

$$\max_x |y_{r+1} - y_r| \le \frac{b^2 s}{4} \max_x |y_{r+1} - y_r| + \frac{b^2 k}{8} (\max_x(|y_r - y_{r-1}|)^2,$$

$$\max_x |y_{r+1} - y_r| \le \frac{b^2 \frac{k}{8}}{1 - \frac{b^2 s}{4}} (\max_x(|y_r - y_{r-1}|)^2.$$

This shows that there is quadratic convergence, if there is convergence at all.

3.2 Haar Wavelets Quasilinearization Method

In the Haar wavelet quasilinearization technique, the nonlinear differential equation is solved recursively by a series of linear differential equations. We describe the procedure for both initial and boundary value problem.

3.2.1 Initial Value Problems

Consider the following nonlinear initial value problem

$$\begin{aligned} &{}_cD^{\alpha}y = f(x, y, {}_cD^{\beta}y, y'),\ 0 \le x \le \eta,\ 1 < \alpha < 2,\ 0 < \beta < 1, \\ &y(0) = A,\ y'(0) = B, \end{aligned} \tag{3.2.1}$$

where A and B are constants. Apply the quasilinearization technique to equation (3.2.1), we get

$$\begin{aligned} &{}_cD^{\alpha}y_{r+1} - f_{y'_r}(x, y_r, {}_cD^{\beta}y_r, y'_r)y'_{r+1} - f_{y_r^{\beta}}(x, y_r, {}_cD^{\beta}y_r, y'_r)y^{\beta}_{r+1} - f_{y_r}(x, y_r, {}_cD^{\beta}y_r, \\ &y'_r)y_{r+1} = f(x, y_r, {}_cD^{\beta}y_r, y'_r)) - y_r f_{y_r}(x, y_r, {}_cD^{\beta}y_r, y'_r) - y^{\beta}_r f_{y_r^{\beta}}(x, y_r, {}_cD^{\beta}y_r, y'_r) \\ &-y'_r f_{y'_r}(x, y_r, {}_cD^{\beta}y_r, y'_r),\ y_{r+1}(0) = A,\ y'_{r+1}(0) = B,\ r \ge 0. \end{aligned} \tag{3.2.2}$$

where $\frac{\partial f}{\partial y_r} = f_{y_r}(x, y_r, {}_cD^{\beta}y_r, y'_r)$, $\frac{\partial f}{\partial y'_r} = f_{y'_r}(x, y_r, {}_cD^{\beta}y_r, y'_r)$ and $\frac{\partial f}{\partial y_r^{\beta}} = f_{y_r^{\beta}}(x, y_r, {}_cD^{\beta}y_r, y'_r)$. Implement the Haar wavelet method to the series of differential equation (3.2.2). Approximate the higher order derivative term in Haar wavelet series as

$${}_cD^{\alpha}y_{r+1} = \sum_{l=1}^{2M} b_l^{r+1} h_l(x). \tag{3.2.3}$$

Integrate the equation (3.2.3) and use the initial conditions, to obtain

$$y_{r+1} = \sum_{l=1}^{2M} b_l^{r+1} p_{\alpha,l}(x) + Bx + A. \tag{3.2.4}$$

Differentiation of equation (3.2.4) implies

$$\begin{aligned} y'_{r+1} &= \sum_{l=1}^{2M} b_l^{r+1} p_{\alpha-1,l}(x) + B, \\ {}_cD^{\beta}y_{r+1} &= \sum_{l=1}^{2M} b_l^{r+1} p_{\alpha-\beta,l}(x) + B\tfrac{x^{1-\beta}}{\Gamma(2-\beta)}. \end{aligned} \tag{3.2.5}$$

Where $p_{\alpha,l}(x)$, $p_{\alpha-1,l}(x)$ and $p_{\alpha-\beta,l}(x)$ are given in equations (2.1.4) and (2.1.5). Let $g_r(x, y_r, {}_cD^{\beta}y_r, y'_r) = f(x, y_r, {}_cD^{\beta}y_r, y'_r) - y_r f_{y_r}(x, y_r, {}_cD^{\beta}y_r, y'_r) - y^{\beta}_r f_{y_r^{\beta}}(x, y_r, {}_cD^{\beta}y_r, y'_r) - y'_r f_{y'_r}(x, y_r, {}_cD^{\beta}y_r, y'_r)$ and use equations (3.2.3), (3.2.4) and (3.2.5) in equation (3.2.2) to obtain

$$\begin{aligned} &\sum_{l=1}^{2M} b_l^{r+1}\big[h_l(x) - f_{y'_r}(x, y_r, {}_cD^{\beta}y_r, y'_r)p_{\alpha-1,l}(x) - f_{y_r^{\beta}}(x, y_r, {}_cD^{\beta}y_r, y'_r)p_{\alpha-\beta,l}(x) \\ &-f_{y_r}(x, y_r, {}_cD^{\beta}y_r, y'_r)p_{\alpha,l}(x)\big] = g_r(x, y_r, {}_cD^{\beta}y_r, y'_r) + Bf_{y'_r}(x, y_r, {}_cD^{\beta}y_r, y'_r) \\ &+Bf_{y_r^{\beta}}(x, y_r, {}_cD^{\beta}y_r, y'_r)\tfrac{x^{1-\beta}}{\Gamma(2-\beta)} + (Bx + A)f_{y_r}(x, y_r, {}_cD^{\beta}y_r, y'_r). \end{aligned} \tag{3.2.6}$$

Let $G_r(x, y_r, {}_c D^\beta y_r, y_r') = g_r(x, y_r, {}_c D^\beta y_r, y_r') + B f_{y_r'}(x, y_r, {}_c D^\beta y_r, y_r') + B f_{y_r^\beta}(x, y_r, {}_c D^\beta y_r, y_r') \frac{x^{1-\beta}}{\Gamma(2-\beta)} + (Bx + A) f_{y_r}(x, y_r, {}_c D^\beta y_r, y_r')$. According to the Haar wavelet collocation method, the residual is set to zero at the collocation points, $x_c(j) = \eta \frac{j+0.5}{2M}$, $j = 1, 2, \cdots, 2M$.

$$\begin{aligned}
&\sum_{l=1}^{2M} b_l^{r+1} \big[h_l(x_c(j)) - f_{y_r'}(x_c(j), y_r(x_c(j)), {}_c D^\beta y_r(x_c(j)), y_r'(x_c(j))) p_{\alpha-1,l}(x_c(j)) \\
&- f_{y_r^\beta}(x_c(j), y_r(x_c(j)), {}_c D^\beta y_r(x_c(j)), y_r'(x_c(j))) p_{\alpha-\beta,l}(x_c(j)) - f_{y_r}(x_c(j), y_r(x_c(j)), \\
&{}_c D^\beta y_r(x_c(j)), y_r'(x_c(j))) p_{\alpha,l}(x_c(j)) \big] = G_r(x_c(j), y_r(x_c(j)), {}_c D^\beta y_r(x_c(j)), y_r'(x_c(j))).
\end{aligned} \tag{3.2.7}$$

In vector form, we have

$$(\mathbf{H} - \mathbf{F_r'} \mathbf{P}_{\alpha-1} - \mathbf{F_r^\beta} \mathbf{P}_{\alpha-\beta} - \mathbf{F_r} \mathbf{P}_\alpha)(\mathbf{b}^{r+1})^T = \mathbf{K}^r, \tag{3.2.8}$$

where $\mathbf{b}^{r+1} = [b_1^{r+1}\ b_2^{r+1} \cdots b_{2M}^{r+1}]$ is an unknown vector, $\mathbf{K}^r = [G_r\big|_{x_c(1)}\ G_r\big|_{x_c(2)} \cdots G_r\big|_{x_c(2M)}]$ is known vector, $\mathbf{H}$, $\mathbf{P}_{\alpha-1}$, $\mathbf{P}_{\alpha-\beta}$ and $\mathbf{P}_\alpha$ are $2M \times 2M$ matrices and are derived in section 2.3. Where $\mathbf{F_r}$, $\mathbf{F_r'}$ and $\mathbf{F_r^\beta}$ are the diagonal matrices and are given by

$$\mathbf{F_r} = \begin{bmatrix} f_{y_r}\big|_{x_c(1)} & 0 & \cdots & 0 \\ 0 & f_{y_r}\big|_{x_c(2)} & \cdots & 0 \\ \vdots & \vdots & \ddots & \vdots \\ 0 & 0 & \cdots & f_{y_r}\big|_{x_c(2M)} \end{bmatrix}, \ \mathbf{F_r'} = \begin{bmatrix} f_{y_r'}\big|_{x_c(1)} & 0 & \cdots & 0 \\ 0 & f_{y_r'}\big|_{x_c(2)} & \cdots & 0 \\ \vdots & \vdots & \ddots & \vdots \\ 0 & 0 & \cdots & f_{y_r'}\big|_{x_c(2M)} \end{bmatrix}$$

and $\mathbf{F_r^\beta} = \begin{bmatrix} f_{y_r^\beta}\big|_{x_c(1)} & 0 & \cdots & 0 \\ 0 & f_{y_r^\beta}\big|_{x_c(2)} & \cdots & 0 \\ \vdots & \vdots & \ddots & \vdots \\ 0 & 0 & \cdots & f_{y_r^\beta}\big|_{x_c(2M)} \end{bmatrix}$.

The notation $f_{y_r}\big|_{x_c(1)}$ is used to represent evaluation of f_{y_r} at $x = x_c(1)$. Haar coefficients, $\mathbf{b}^{r+1} = [b_1^{r+1}\ b_2^{r+1} \cdots b_{2M}^{r+1}]$ can be obtained from equation (3.2.8) for each $r \geq 0$ and use these in equations (3.2.3), (3.2.4) and (3.2.5) to get the approximate values of ${}_c D^\alpha y_{r+1}$, y_{r+1}, $y_{r+1}'$and ${}_c D^\beta y_{r+1}$ at the collocation points, $x_c(j)$, $j = 1, 2, \cdots, 2M$. In particular, for $r = 0$ we get a linear differential equation in $y_1(x)$, from equation (3.2.2), and use equation (3.2.8) to obtain $\mathbf{b}^1 = [b_1^1\ b_2^1, \cdots, b_{2M}^1]$ which are used in (3.2.3), (3.2.4) and (3.2.5) to get the approximate values of ${}_c D^\alpha y_1$, y_1, $y_1'$and ${}_c D^\beta y_1$ at the collocation points. Similarly, for $r = 1$ we obtain $y_2(x)$ and so on. In this way, we obtain a sequence of approximations $y_1(x)$, $y_2(x), \cdots$. We may get more accurate approximation while increasing r.

3.2.2 Boundary Value Problems

Consider the fractional nonlinear boundary value problem

$$\begin{aligned} &{}_cD^{\alpha}y = f(x, y, {}_{c}D^{\beta}y, y'),\ 0 \le x \le \eta,\ 1 < \alpha < 2,\ 0 < \beta < 1, \\ &y(0) = \gamma_1,\ y(\eta) = \gamma_2. \end{aligned} \tag{3.2.9}$$

Implement the quasilinearization technique to equation (3.2.9), we get

$$\begin{aligned} &{}_cD^{\alpha}y_{r+1} - f_{y'_r}(x, y_r, {}_{c}D^{\beta}y_r, y'_r))y'_{r+1} - f_{y_r^{\beta}}(x, y_r, {}_{c}D^{\beta}y_r, y'_r))y^{\beta}_{r+1} - f_{y_r}(x, y_r, {}_{c}D^{\beta}y_r, y'_r)) \\ &y_{r+1} = f(x, y_r, {}_{c}D^{\beta}y_r, y'_r)) - y_r f_{y_r}(x, y_r, {}_{c}D^{\beta}y_r, y'_r)) - y^{\beta}_r f_{y_r^{\beta}}(x, y_r, {}_{c}D^{\beta}y_r, y'_r)) \\ &-y'_r f_{y'_r}(x, y_r, {}_{c}D^{\beta}y_r, y'_r)),\ y_{r+1}(0) = \gamma_1,\ y_{r+1}(\eta) = \gamma_2,\ r \ge 0. \end{aligned} \tag{3.2.10}$$

Now apply the Haar wavelet method to the series of differential equation (3.2.10)

$${}_cD^{\alpha}y_{r+1} = \sum_{l=1}^{2M} b_l^{r+1} h_l(x). \tag{3.2.11}$$

Integrate the equation (3.2.11) and use the boundary conditions to obtain

$$y_{r+1} = \sum_{l=1}^{2M} b_l^{r+1} p_{\alpha,l}(x) + \tfrac{x}{\eta}(\gamma_2 - \gamma_1 - \sum_{l=1}^{2M} b_l^{r+1} C_{\alpha,l}) + \gamma_1. \tag{3.2.12}$$

First and β order derivative of y_{r+1} can be obtained from equation (3.2.12) as

$$\begin{aligned} y'_{r+1} &= \sum_{l=1}^{2M} b_l^{r+1} p_{\alpha-1,l}(x) + \tfrac{1}{\eta}(\gamma_2 - \gamma_1 - \sum_{l=1}^{2M} b_l^{r+1} C_{\alpha,l}), \\ {}_cD^{\beta}y_{r+1} &= \sum_{l=1}^{2M} b_l^{r+1} p_{\alpha-\beta,l}(x) + \tfrac{x^{1-\beta}}{\eta\Gamma(2-\beta)}(\gamma_2 - \gamma_1 - \sum_{l=1}^{2M} b_l^{r+1} C_{\alpha,l}). \end{aligned} \tag{3.2.13}$$

Use equations (3.2.11), (3.2.12) and (3.2.13) in equation (3.2.10) to obtain

$$\begin{aligned} &\sum_{l=1}^{2M} b_l^{r+1}\big[h_l(x) - f_{y'_r}(x, y_r, {}_{c}D^{\beta}y_r, y'_r)p_{\alpha-1,l}(x) - f_{y_r^{\beta}}(x, y_r, {}_{c}D^{\beta}y_r, y'_r)p_{\alpha-\beta,l}(x) - \\ &f_{y_r}(x, y_r, {}_{c}D^{\beta}y_r, y'_r)p_{\alpha,l}(x) + g_r(x, y_r, {}_{c}D^{\beta}y_r, y'_r)C_{\alpha,l}\big] = Q_r(x, y_r, {}_{c}D^{\beta}y_r, y'_r), \end{aligned} \tag{3.2.14}$$

where $Q_r(x, y_r, {}_{c}D^{\beta}y_r, y'_r) = f(x, y_r, {}_{c}D^{\beta}y_r, y'_r) - y_r f_{y_r}(x, y_r, {}_{c}D^{\beta}y_r, y'_r) - y^{\beta}_r f_{y_r^{\beta}}(x, y_r, {}_{c}D^{\beta}y_r, y'_r) - y'_r f_{y'_r}(x, y_r, {}_{c}D^{\beta}y_r, y'_r) + (\frac{f_{y'_r}}{\eta}(x, y_r, {}_{c}D^{\beta}y_r, y'_r) + f_{y_r^{\beta}}(x, y_r, {}_{c}D^{\beta}y_r, y'_r)\frac{x^{1-\beta}}{\eta\Gamma(2-\beta)} + f_{y_r}(x, y_r, {}_{c}D^{\beta}y_r, y'_r)\frac{x}{\eta})(\gamma_2 - \gamma_1) + f_{y_r}(x, y_r, {}_{c}D^{\beta}y_r, y'_r)\gamma_1,$

$g_r(x, y_r, {}_{c}D^{\beta}y_r, y'_r) = \frac{f_{y'_r}}{\eta}(x, y_r, {}_{c}D^{\beta}y_r, y'_r) + f_{y_r^{\beta}}(x, y_r, {}_{c}D^{\beta}y_r, y'_r)\frac{x^{1-\beta}}{\eta\Gamma(2-\beta)} + f_{y_r}(x, y_r, {}_{c}D^{\beta}y_r, y'_r)\frac{x}{\eta}.$

Set the residual equal to zero at the collocation points, $x_c(j) = \eta\frac{j+0.5}{2M}$, $j = 1, 2, \cdots, 2M$.

$$\begin{aligned} &\sum_{l=1}^{2M} b_l^{r+1}\big[h_l(x_c(j)) - f_{y'_r}(x_c(j), y_r(x_c(j)), {}_{c}D^{\beta}y_r(x_c(j)), y'_r(x_c(j))))p_{\alpha-1,l}(x_c(j)) - \\ &f_{y_r^{\beta}}(x_c(j), y_r(x_c(j)), {}_{c}D^{\beta}y_r(x_c(j)), y'_r(x_c(j))))p_{\alpha-\beta,l}(x_c(j)) \\ &-f_{y_r}(x_c(j), y_r(x_c(j)), {}_{c}D^{\beta}y_r(x_c(j)), y'_r(x_c(j))))p_{\alpha,l}(x_c(j)) \\ &+g_r(x_c(j), y_r(x_c(j)), {}_{c}D^{\beta}y_r(x_c(j)), y'_r(x_c(j))))C_{\alpha,l}\big] \\ &= Q_r(x_c(j), y_r(x_c(j)), {}_{c}D^{\beta}y_r(x_c(j)), y'_r(x_c(j)))). \end{aligned} \tag{3.2.15}$$

In vector form, we have

$$(\mathbf{H} - \mathbf{F}'_{\mathbf{r}}\mathbf{P}_{\alpha-1} - \mathbf{F}^{\beta}_{\mathbf{r}}\mathbf{P}_{\alpha-\beta} - \mathbf{F}_{\mathbf{r}}\mathbf{P}_{\alpha} + \mathbf{V}^{\alpha,\eta})(\mathbf{b}^{r+1})^T = \mathbf{D}^r, \tag{3.2.16}$$

where $\mathbf{b}^{r+1} = [b_1^{r+1}\ b_2^{r+1}, \cdots, b_{2M}^{r+1}]$ is an unknown vector, $\mathbf{D}^r = [Q_r|_{x_c(1)}, Q_r|_{x_c(2)} \cdots Q_r|_{x_c(2M)}]$ is known vector and $\mathbf{H},\ \mathbf{P}_{\alpha-1},\ \mathbf{P}_{\alpha-\beta},\ \mathbf{P}_{\alpha}$ and $\mathbf{V}^{\alpha,\eta}$ are $2M \times 2M$ matrices and are given in section 2.3. For each $r \geq 0$, we obtain approximate values of $y(x),\ y'(x),\ {}_cD^{\beta}y(x)$ and ${}_cD^{\alpha}y(x)$ at the collocation points. We get more accurate results while increasing r.

3.2.3 Convergence Analysis of Haar Wavelet Quasilinearization Method

Let $y_{r+1}(x)$ be a differentiable function and have bounded first derivative on interval $(0, 1)$, that is, there exist $K > 0$, for all $x \in (0, 1)$, we have

$$|y'_{r+1}(x)| \leq K.$$

Suppose $y^M_{r+1}(x)$ be the Haar wavelet approximation for the function $y(x)$ at the $(r+1)th$ iteration

$$y^M_{r+1}(x) = \sum_{l=1}^{2M} b_l^{r+1} h_l(x), \tag{3.2.17}$$

where $M = 2^J,\ J = 0, 1, 2, \cdots$, then L^2 error norm for the Haar wavelet approximation of $y(x)$ at the $(r+1)th$ iteration is given as

$$\begin{aligned} \|y_{r+1}(x) - y^M_{r+1}(x)\|^2 &= \int_0^1 (y_{r+1}(x) - y^M_{r+1}(x))^2 dx, \\ &= \sum_{l=2M+1}^{\infty} \sum_{l'=2M+1}^{\infty} b_l^{r+1} b_{l'}^{r+1} \int_0^1 h_l(x) h_{l'}(x) dx, \\ &= \sum_{l=2M+1}^{\infty} (b_l^{r+1})^2, \end{aligned} \tag{3.2.18}$$

where

$$b_l^{r+1} = \langle y_{r+1}(x), h_l(x) \rangle = \int_0^1 y_{r+1}(x) h_l(x) dx. \tag{3.2.19}$$

Since Haar wavelet can be represented as $h_l(x) = 2^{\frac{j}{2}} H(2^j x - k)$, where $2^{\frac{j}{2}}$ is the normalizing factor, $k = 0, 1, 2, \cdots, 2^j - 1,\ j = 0, 1, 2, \cdots, J$, and

$$H(2^j x - k) = \begin{cases} 1, & \frac{k}{m} \leq x < \frac{k+0.5}{m}; \\ -1, & \frac{k+0.5}{m} \leq x < \frac{k+1}{m}; \\ 0, & \text{otherwise}, \end{cases} \tag{3.2.20}$$

where $m = 2^j$, equation (3.2.19) implies

$$b_l^{r+1} = 2^{\frac{j}{2}} \left\{ \int_{\frac{k}{m}}^{\frac{k+0.5}{m}} y_{r+1}(x) dx - \int_{\frac{k+0.5}{m}}^{\frac{k+1}{m}} y_{r+1}(x) dx \right\}. \tag{3.2.21}$$

By using the mean value theorem, we get

$$\exists\ x_1,\ x_2\ : \frac{k}{m} \leq x_1 < \frac{k+0.5}{m},\ \frac{k+0.5}{m} \leq x_2 < \frac{k+1}{m},$$

$$\begin{aligned} b_l^{r+1} &= 2^{\frac{j}{2}}\left\{\left(\tfrac{k+0.5}{m} - \tfrac{k}{m}\right)y_{r+1}(x_1) - \left(\tfrac{k+1}{m} - \tfrac{k+0.5}{m}\right)y_{r+1}(x_2)\right\}, \\ &= 2^{\frac{-j}{2}-1}\big(y_{r+1}(x_1) - y_{r+1}(x_2)\big), \end{aligned}$$

or

$$(b_l^{r+1})^2 = 2^{-j-2}\big(y_{r+1}(x_1) - y_{r+1}(x_2)\big)^2.$$

Again using mean value theorem to obtain

$$\begin{aligned} (b_l^{r+1})^2 &= 2^{-j-2}\big(x_2 - x_1\big)^2(y'_{r+1}(x_0))^2,\ x_1 < x_0 < x_2, \\ &\leq 2^{-j-2}2^{-2j}K^2, \\ &= 2^{-3j-2}K^2. \end{aligned}$$

Equation (3.2.18) implies

$$\begin{aligned} \|y_{r+1}(x) - y_{r+1}^M(x)\|^2 &= \sum_{l=2^{J+1}+1}^{\infty}(b_l^{r+1})^2, \\ &= \sum_{j=J+1}^{\infty}\left(\sum_{l=2^j+1}^{2^{j+1}}(b_l^{r+1})^2\right), \\ &\leq \sum_{j=J+1}^{\infty}\left(\sum_{l=2^j+1}^{2^{j+1}}2^{-3j-2}K^2\right), \\ &= K^2\sum_{j=J+1}^{\infty}2^{-2(j+1)}, \\ &= K^2\tfrac{2^{-2(J+1)}}{3}, \\ &= \tfrac{K^2}{3}\tfrac{1}{(2M)^2}. \end{aligned}$$

This implies that

$$\|y_{r+1}(x) - y_{r+1}^M(x)\|^2 \leq \tfrac{K^2}{3}\tfrac{1}{(2M)^2} = O(\tfrac{1}{M}). \tag{3.2.22}$$

Since $M = 2^J$, J is the maximal level of resolution. According to (3.2.22), we conclude that error at the $(r+1)th$ iteration is inversely proportional to the maximal level of resolution.
This implies that $y_{r+1}^M(x)$ converges to $y_{r+1}(x)$ as $J \to \infty$. Since $y_{r+1}(x)$ is the $(r+1)th$ iteration of the quasilinearization technique and according to the convergence analysis of quasilinearization technique as given in subsection 3.1.1, we have

$$\max_x |y_{r+1}(x) - y_r(x)| \leq \tfrac{b^2\frac{k}{8}}{1-\frac{b^2 s}{4}}(\max_x |y_r(x) - y_{r-1}(x)|)^2, \tag{3.2.23}$$

where b, k and s are positive finite constants. Equation (3.2.23) implies that $y_{r+1} \to y(x)$ as $r \to \infty$, if there is convergence at all. Thus we conclude that Haar wavelet approximation, $y_{r+1}^M(x)$, converges to $y(x)$ as J and r approaches to infinity.

3.3 Nonlinear Fractional Differential Equations

In this section, we implement the Haar wavelet quasilinearization method to fractional nonlinear initial and boundary value problems. The obtained results are compared with the exact solution and solution obtained by other numerical methods.

3.3.1 Initial Value Problems

Example 1: Consider the α^{th} order fractional Riccati equation

$$ {}^{c}D^{\alpha}y(x) = -y^2(x) + 1,\ x > 0,\ 0 < \alpha \leq 1, \tag{3.3.1} $$

subject to the initial condition $y(0) = 0$.
The exact solution, when $\alpha = 1$, is given by [94]

$$ y(x) = \tfrac{e^{2x}-1}{e^{2x}+1}. $$

Applying the quasilinearized technique to equation (3.3.1), we get

$$ {}^{c}D^{\alpha}y_{r+1}(x) + 2y_r(x)y_{r+1}(x) = y_r^2(x) + 1,\ x > 0,\ 0 < \alpha \leq 1, \tag{3.3.2} $$

with the initial condition $y_{r+1}(0) = 0$.
Now we apply the Haar wavelet method to equation (3.3.2), we approximate the higher order derivative term by the Haar wavelet series as

$$ {}^{c}D^{\alpha}y_{r+1}(x) = \sum_{l=1}^{2M} b_l h_l(x). \tag{3.3.3} $$

Lower order derivatives are obtained by integrating equation (3.3.3) and use the initial condition

$$ y_{r+1}(x) = \sum_{l=1}^{2M} b_l p_{\alpha,l}(x). \tag{3.3.4} $$

Substitute equations (3.3.3) and (3.3.4) in (3.3.2), we get

$$ \sum_{l=1}^{2M} b_l[h_l(x) + 2y_r(x)p_{\alpha,l}(x)] = y_r^2(x) + 1, \tag{3.3.5} $$

with the initial approximation $y_0(x) = 0$.

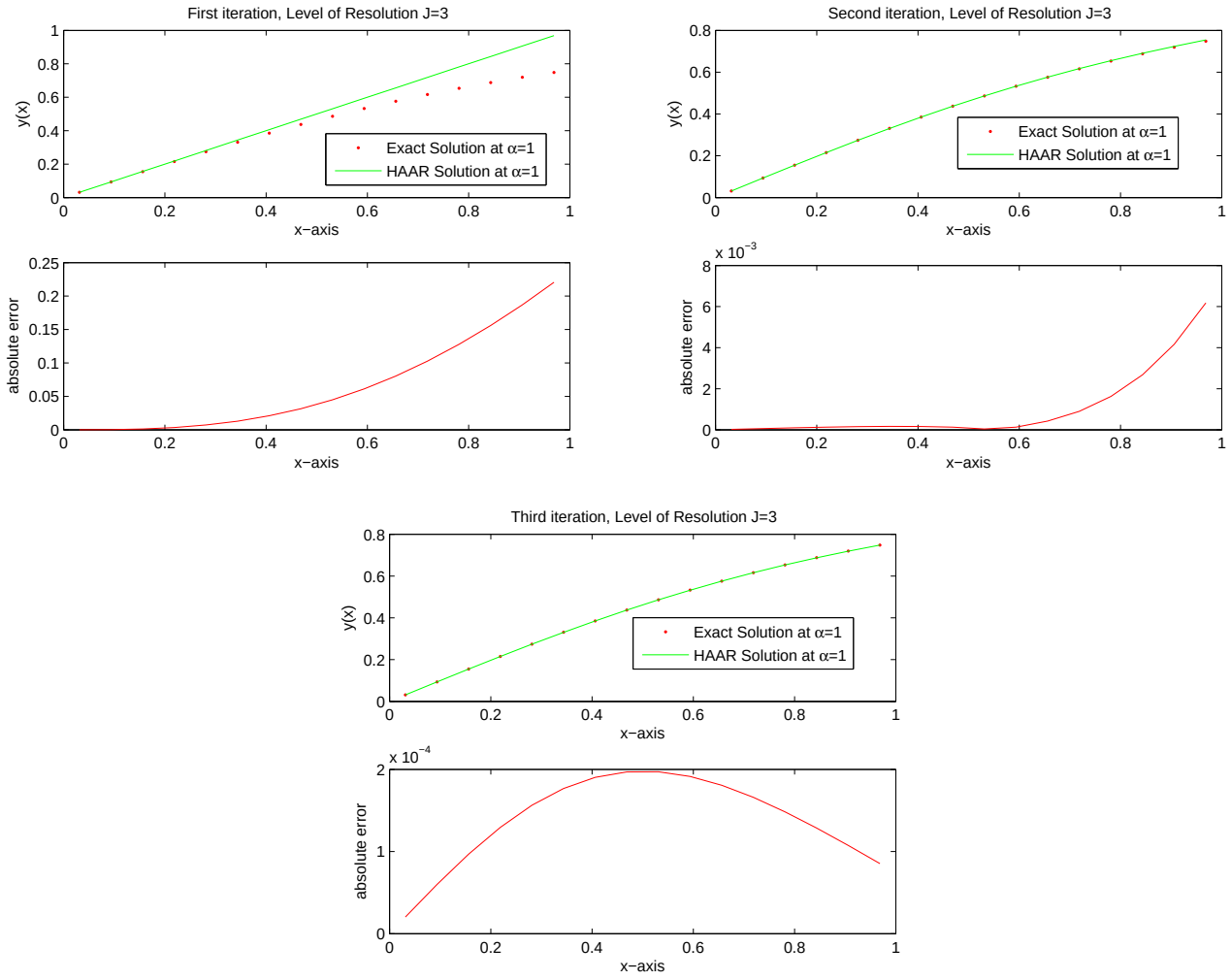

Figure 3.1: Comparison of exact solution and solutions by the Haar wavelet-quasilinearization technique at $J = 3$ for different iterations and $\alpha = 1$.

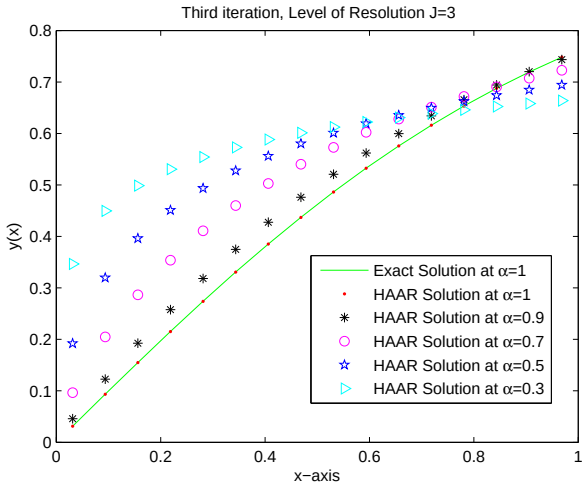

Figure 3.2: Exact solution at $\alpha = 1$ and the Haar wavelet-quasilinearization solution at $\alpha = 1$, $\alpha = 0.9$, $\alpha = 0.7$, $\alpha = 0.5$ and $\alpha = 0.3$.

			$\alpha = 1$			
$r = 4$	$J = 6$	$J = 7$	$J = 8$	$J = 9$		
x	y_{Haar}	y_{Haar}	y_{Haar}	y_{HAAR}	y_{HPM} [94]	y_{Exact}
0.0	0.0	0.0	0.0	0.0	0.0	0.0
0.1	0.099667	0.099668	0.099668	0.099668	0.099668	0.099668
0.2	0.197373	0.197375	0.197375	0.197375	0.197375	0.197375
0.3	0.291310	0.291312	0.291312	0.291313	0.291312	0.291313
0.4	0.379946	0.379948	0.379949	0.379949	0.379944	0.379949
0.5	0.462114	0.462116	0.462117	0.462117	0.462078	0.462117
0.6	0.537047	0.537049	0.537049	0.537050	0.536857	0.537050
0.7	0.604365	0.604367	0.604368	0.604368	0.603631	0.604368
0.8	0.664035	0.664036	0.664037	0.664037	0.661706	0.664037
0.9	0.716296	0.716297	0.716298	0.716298	0.709919	0.716298
1.0	0.761593	0.761594	0.761594	0.761594	0.746032	0.761594

Table 3.1: Comparison of solutions by the Haar wavelet-quasilinearization technique at 4^{th} iteration and different level of resolutions and modified homotopy perturbation method [94].

We fix the order of the differential equation (3.3.1), $\alpha = 1$, and level of resolution, $J = 3$. The graph in Fig. 3.1 shows the exact solution and approximate solution by Haar wavelet method at three iterations. The absolute error reduces with increasing iterations.

Results of third iteration by quasilinearization approach at fixed level of resolution, are shown in Fig. 3.2 with the exact solution at $\alpha = 1$ and the Haar wavelet solution at different values of α. Fig. 3.2 shows that the numerical solutions converge to the exact solution when α approaches to 1.
For $\alpha = 1$ and at different levels of resolution, the numerical results, by the Haar wavelet method, at fourth iteration are shown in Table 3.1. The Haar solutions are in good agreement with exact solution and Haar solution is also compared with the results obtained by modified homotopy perturbation method [94].

Example 2: Consider the fractional Riccati equation

$$^{c}D^{\alpha}y(x) = 2y(x) - y^2(x) + 1,\ x > 0,\ 0 < \alpha \leq 1, \tag{3.3.6}$$

subject to the initial condition $y(0) = 0$.
The exact solution, when $\alpha = 1$, is [94]

$$y(x) = 1 + \sqrt{2}\tanh(\sqrt{2}x + \tfrac{1}{2}\log(\tfrac{\sqrt{2}-1}{2} + 1)).$$

Applying the quasilinearized technique to equation (3.3.6), we get

$$^{c}D^{\alpha}y_{r+1}(x) - (2 - 2y_r(x))y_{r+1}(x) = y_r^2(x) + 1,\ x > 0,\ 0 < \alpha \leq 1, \tag{3.3.7}$$

with the initial condition $y_{r+1}(0) = 0$.
Now apply the Haar wavelet method to equation (3.3.7).We approximate the higher order derivative term by the Haar wavelet series as

$$^{c}D^{\alpha}y_{r+1}(x) = \sum_{l=1}^{2M} b_l h_l(x). \tag{3.3.8}$$

Now to get the Haar wavelet series for lower order derivative terms we integrate equation (3.3.8) and use the initial condition, to get

$$y_{r+1}(x) = \sum_{l=1}^{2M} b_l p_{\alpha,l}(x). \tag{3.3.9}$$

Substitute equations (3.3.8) and (3.3.9) in (3.3.7), we get

$$\sum_{l=1}^{2M} b_l[h_l(x) - (2 - 2y_r(x))p_{\alpha,l}(x)] = y_r^2(x) + 1, \tag{3.3.10}$$

with the initial approximation $y_0(x) = 0$.

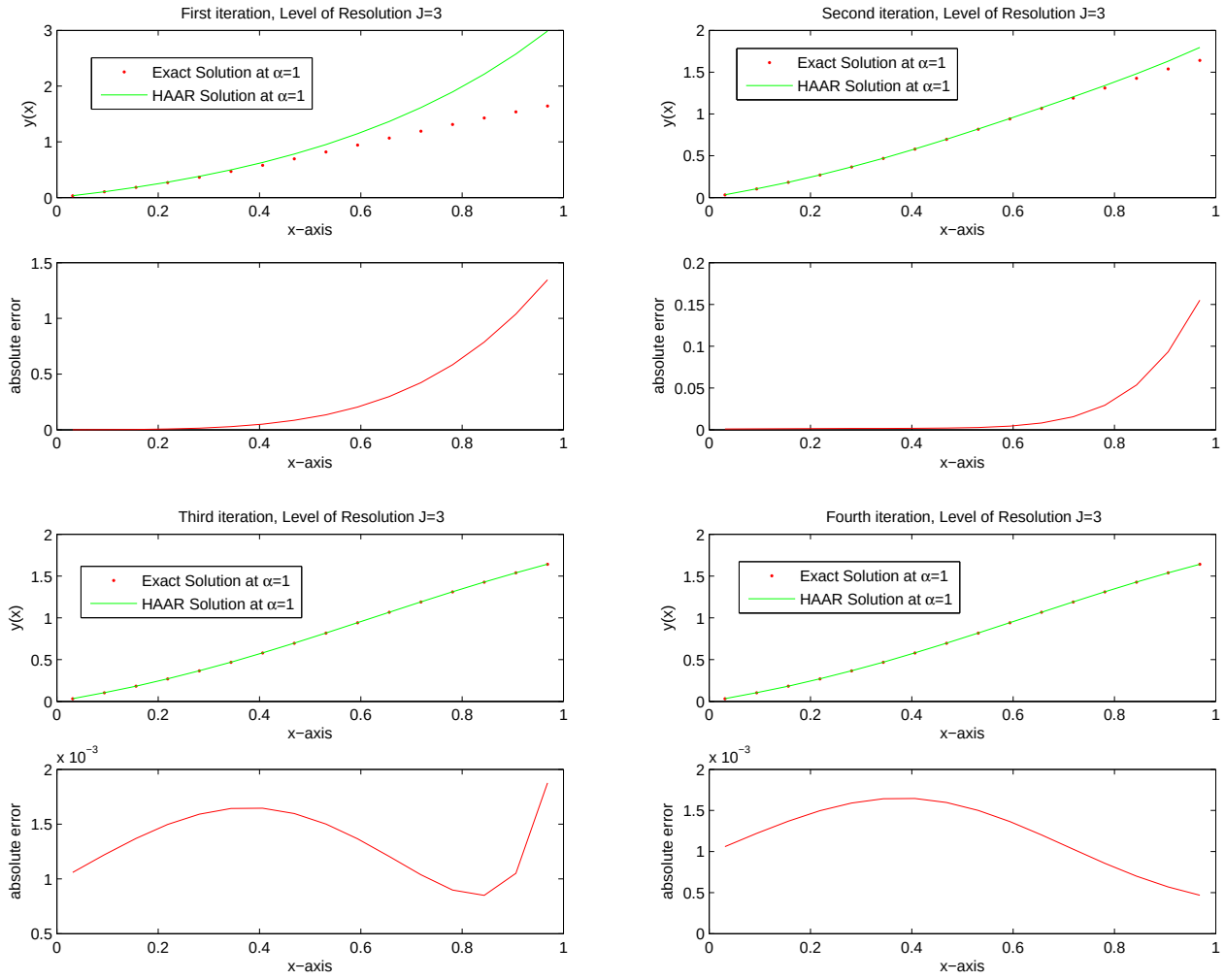

Figure 3.3: Comparison of exact solution and solution by Haar wavelet-quasilinearization technique at $J = 3$, for different iterations, and $\alpha = 1$.

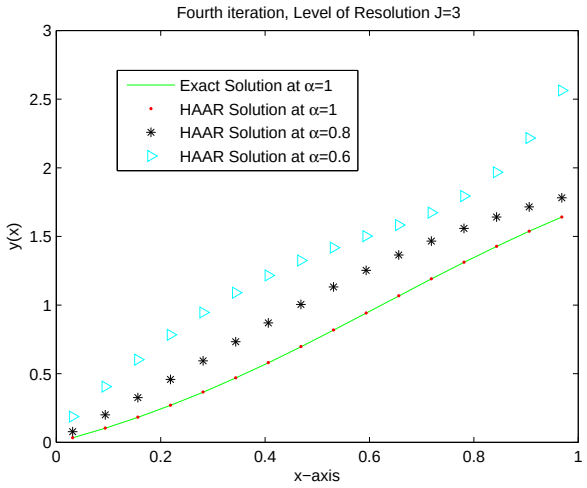

Figure 3.4: Exact solution at $\alpha = 1$ and the Haar wavelet-quasilinearization solution at $\alpha = 1,\ \alpha = 0.8,$ and $\alpha = 0.6$.

$\alpha = 1$						
$r = 4$	$J = 6$	$J = 7$	$J = 8$	$J = 9$		
x	y_{Haar}	y_{Haar}	y_{Haar}	y_{HAAR}	y_{HPM} [94]	y_{Exact}
0.0	0.0	0.0	0.0	0.0	0.0	0.0
0.1	0.110314	0.110300	0.110296	0.110295	0.110294	0.110295
0.2	0.242000	0.241983	0.241978	0.241977	0.241965	0.241977
0.3	0.395130	0.395111	0.395106	0.395105	0.395106	0.395105
0.4	0.567838	0.567819	0.567814	0.567813	0.568115	0.567812
0.5	0.756039	0.756020	0.756016	0.756015	0.757564	0.756014
0.6	0.953587	0.953571	0.953568	0.953567	0.958259	0.953566
0.7	1.152966	1.152953	1.152950	1.152949	1.163459	1.152949
0.8	1.346376	1.346367	1.346364	1.346364	1.365240	1.346364
0.9	1.526920	1.526914	1.526912	1.526911	1.554960	1.526911
1.0	1.689505	1.689500	1.689499	1.689499	1.723810	1.689498

Table 3.2: Haar wavelet with quasilinearization technique at 4^{th} iteration and different level of resolutions and comparison with modified homotopy perturbation method [94].

We fix the level of resolution, $J = 3$, and order of differential equation (3.3.6), $\alpha = 1$. The exact solution and the Haar solution at different iterations along with the absolute error are shown in Fig. 3.3. We observe that error reduces with increase in iterations.

Exact solution at $\alpha = 1$ and the Haar solution at different values of α, are displayed in Fig. 3.4. It is observed that solutions of fractional Riccati equation (3.3.6) converge to the solution of first order Riccati equation, when α approaches to 1.

Table 3.2 shows the Haar solution at fourth iteration and at $\alpha = 1$ with different level of resolutions. The Haar solution approaches to exact solution while increasing J. The Haar solution is also compared with the modified homotopy perturbation method [94].

Example 3: Consider the following α^{th} order fractional Van der Pol oscillator problem

$$ {}^cD^{\alpha}y(x) + \frac{dy(x)}{dx} + y(x) + y^2(x)\frac{dy(x)}{dx} = 2\cos(x) - \cos^3(x),\ 1 < \alpha \leq 2, \tag{3.3.11} $$

subject to the initial conditions: $y(0) = 0$, $y'(0) = 1$.

The exact solution, when $\alpha = 2$, is [8] $y(x) = \sin(x)$.

Quasilinearization technique to equation (3.3.11) implies

$$ \begin{aligned} {}^cD^{\alpha}y_{r+1}(x) + (1 + 2y_r(x)y_r'(x))y_{r+1}(x) + (1 + y_r^2(x))y_{r+1}'(x) \\ = 2y_r^2(x)y_r'(x) + 2\cos(x) - \cos^3(x), \end{aligned} \tag{3.3.12} $$

with the initial conditions $y_{r+1}(0) = 0$, $y_{r+1}'(0) = 1$.

Consider the Haar wavelet approximation of higher order derivative term in equation (3.3.12)

$$ {}^cD^{\alpha}y_{r+1}(x) = \sum_{l=1}^{2M} b_l h_l(x). \tag{3.3.13} $$

Lower order derivatives are obtained by integrating equation (3.3.13) and use the initial conditions, we get

$$ y_{r+1}(x) = \sum_{l=1}^{2M} b_l p_{\alpha,l}(x) + x, \tag{3.3.14} $$

$$ y_{r+1}'(x) = \sum_{l=1}^{2M} b_l p_{\alpha-1,l}(x) + 1. \tag{3.3.15} $$

Substitute equations (3.3.13), (3.3.14) and (3.3.15) in (3.3.12), we obtain

$$ \begin{aligned} \sum_{l=1}^{2M} b_l[h_l(x) + (1 + 2y_r(x)y_r'(x))p_{\alpha,l}(x) + (1 + y_r^2(x))p_{\alpha-1,l}(x)] = 2y_r^2(x)y_r'(x) \\ -(1 + 2y_r(x)y_r'(x))x - 1 - y_r^2(x) + 2\cos(x) - \cos^3(x), \end{aligned} \tag{3.3.16} $$

with the initial approximations $y_0(x) = 0$, $y_0'(x) = 1$.

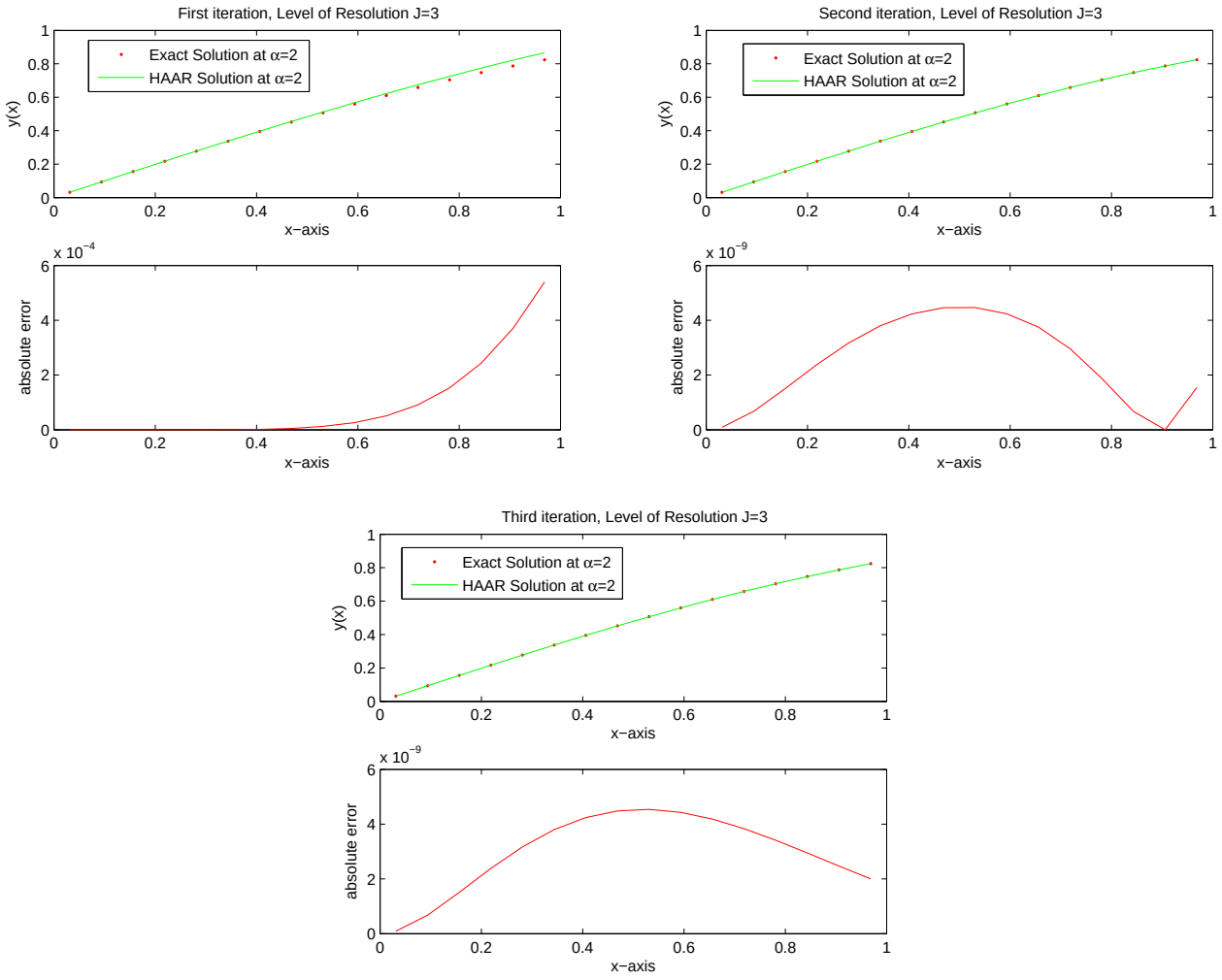

Figure 3.5: Comparison of exact solution and solutions by the Haar wavelet-quasilinearization technique at $J = 3,$ for different iterations, and $\alpha = 2.$

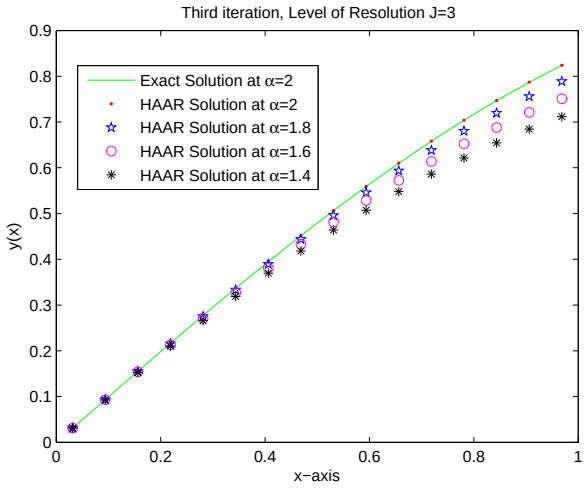

Figure 3.6: Exact solution at $\alpha = 2$ and the Haar wavelet-quasilinearization solution at $\alpha = 2$, $\alpha = 1.8$, $\alpha = 1.6$and $\alpha = 1.4$.

				$\alpha = 2$		
$r = 3$	$J = 8$	$J = 9$	$J = 10$			
x	y_{Haar}	y_{Haar}	y_{Haar}	y_{VIM} [9]	y_{HPM} [9]	y_{Exact}
0.0	0.0000000000	0.0000000000	0.0000000000	0.0000000000	0.0000000000	0.0000000000
0.1	0.0998333872	0.0998334093	0.0998334148	0.0998333893	0.0998334161	0.0998334166
0.2	0.1986692768	0.1986693173	0.1986693274	0.1986676148	0.1986692604	0.1986693308
0.3	0.2955201331	0.2955201883	0.2955202021	0.2955011070	0.2955190492	0.2955202067
0.4	0.3894182543	0.3894183203	0.3894183368	0.3893138342	0.3894101010	0.3894183423
0.5	0.4794254413	0.4794255143	0.4794255325	0.4790386507	0.4793884172	0.4794255386
0.6	0.5646423719	0.5646424480	0.5646424671	0.563525292	0.5645175388	0.5646424734
0.7	0.6442175863	0.6442176620	0.6442176809	0.6415028932	0.6438744431	0.6442176872
0.8	0.7173559950	0.7173560669	0.7173560849	0.7115469778	0.7165444751	0.7173560909
0.9	0.7833268225	0.7833268880	0.7833269044	0.7720563532	0.7816179472	0.7833269096
1.0	0.8414709106	0.8414709675	0.8414709817	0.8212443348	0.8381911175	0.8414709848

Table 3.3: Solution by the Haar wavelet-quasilinearization technique at 3^{rd} iteration and different level of resolutions compared with homotopy perturbation method [9], variational iteration method [9] and exact solution.

The Haar solution at three iterations by fixing order of differential equation (3.3.11), $\alpha = 2$, and level of resolution, $J = 3$, are shown in Fig. 3.5. Absolute error is computed for each iteration.

We fix the solutions at third iteration and level of resolution, $J = 3$ are shown in Fig. 3.6. Exact solution at $\alpha = 2$ is plotted and Fig. 3.6 shows that the Haar solution converges to the exact solution, when α approaches to 2. From the numerical results in Table 3.3, it is clear that the approximate solution by Haar wavelet method are close to exact solutions, when $\alpha = 2$, and the Haar solution is compared with variational iteration method [9] and homotopy perturbation method [9].

Example 4: Consider the α^{th} order nonlinear oscillator ordinary differential equation

$$ {}^cD^{\alpha}y(x) - y(x) + y^2(x) + y'^2(x) - 1 = 0,\ 1 < \alpha \leq 2, \tag{3.3.17} $$

subject to the initial conditions: $y(0) = 2$, $y'(0) = 0$.

The exact solution, when $\alpha = 2$, is [46] $y(x) = 1 + \cos(x)$.

Quasilinearization technique to equation (3.3.17) implies

$$ {}^cD^{\alpha}y_{r+1}(x) + 2y'_r(x)y'_{r+1}(x) - (1 - 2y_r(x))y_{r+1}(x) = y_r^2(x) + y_r'^2(x) + 1,\ 0 < \alpha \leq 2, \tag{3.3.18} $$

with the initial conditions $y_{r+1}(0) = 2$, $y'_{r+1}(0) = 0$.

Apply the Haar wavelet method to equation (3.3.18)

$$ {}^cD^{\alpha}y_{r+1}(x) = \sum_{l=1}^{2M} b_l h_l(x). \tag{3.3.19} $$

Lower order derivatives are obtained by integrating equation (3.3.19) and use the initial conditions

$$ y_{r+1}(x) = \sum_{l=1}^{2M} b_l p_{\alpha,l}(x) + 2, \tag{3.3.20} $$

$$ y'_{r+1}(x) = \sum_{l=1}^{2M} b_l p_{\alpha-1,l}(x). \tag{3.3.21} $$

Substitute equations (3.3.19), (3.3.20) and (3.3.21) in (3.3.18), we get

$$ \sum_{l=1}^{2M} b_l[h_l(x) + 2y'_r(x)p_{\alpha-1,l}(x) - (1 - 2y_r(x))p_{\alpha,l}(x)] = y_r^2(x) + y_r'^2(x) + 2(1 - 2y_r(x)) + 1, \tag{3.3.22} $$

with the initial approximations $y_0(x) = 2$, $y'_0(x) = 0$.

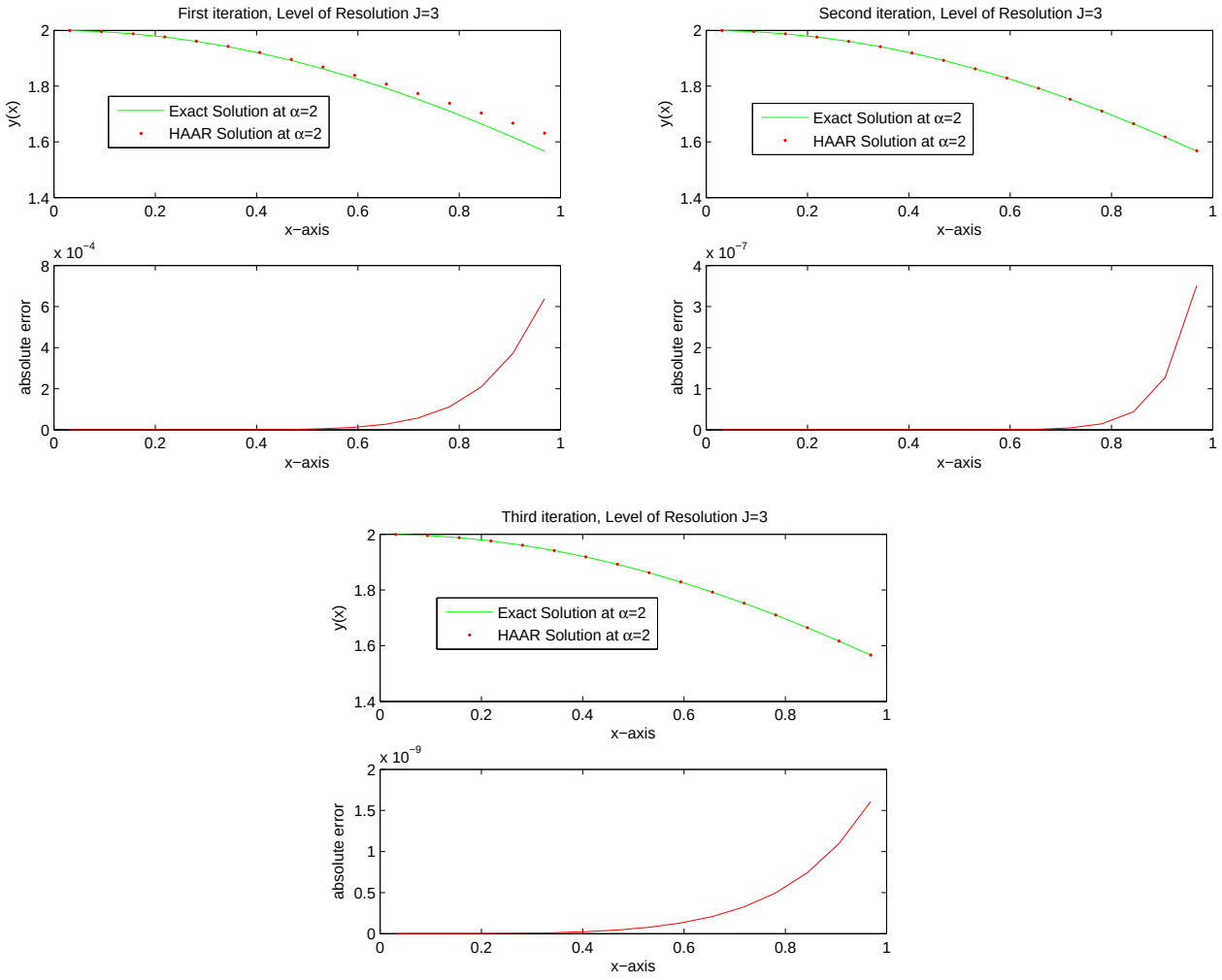

Figure 3.7: Comparison of exact solution and solutions by Haar wavelet-quasilinearization technique at $J = 3$, for different iterations, and $\alpha = 2$.

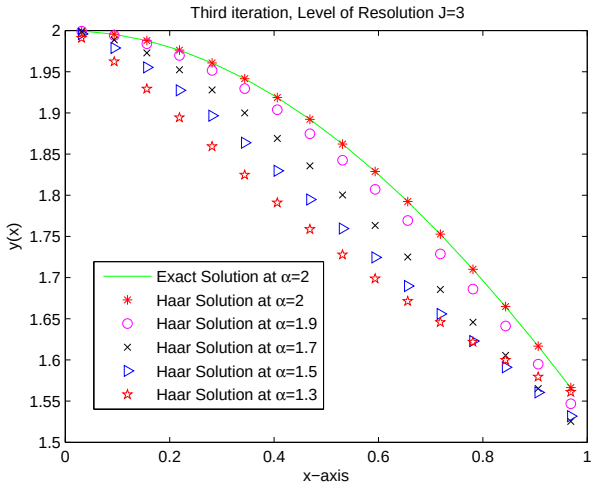

Figure 3.8: Exact solution at $\alpha = 2$ and the Haar wavelet-quasilinearization solution at $\alpha = 2$, $\alpha = 1.9$, $\alpha = 1.7$, $\alpha = 1.5$and $\alpha = 1.3$.

				$\alpha = 2$		
$r = 3$	$J = 8$	$J = 9$	$J = 10$			
x	y_{Haar}	y_{Haar}	y_{Haar}	y_{VIM} [9]	y_{HPM} [9]	y_{Exact}
0.0	2.000000000	2.000000000	2.000000000	2.000000000	2.000000000	2.000000000
0.1	1.995004166	1.995004165	1.995004165	1.994995832	1.995012500	1.995004165
0.2	1.980066581	1.980066579	1.980066578	1.979933244	1.980200000	1.980066578
0.3	1.955336496	1.955336491	1.955336490	1.954661486	1.956012500	1.955336489
0.4	1.921061007	1.921060997	1.921060995	1.918927628	1.923200000	1.921060994
0.5	1.877582583	1.877582567	1.877582563	1.872374035	1.882812500	1.877582562
0.6	1.825335647	1.825335623	1.825335617	1.814534782	1.836200000	1.825335615
0.7	1.764842233	1.764842199	1.764842190	1.744830994	1.785012500	1.764842187
0.8	1.696706772	1.696706725	1.696706713	1.662565054	1.731200000	1.696706709
0.9	1.621610051	1.621609989	1.621609973	1.566913614	1.677012500	1.621609968
1.0	1.540302414	1.540302333	1.540302313	1.456919365	1.625000000	1.540302306

Table 3.4: Haar wavelet-quasilinearization technique at 3^{rd} iteration and for different level of resolutions compared with homotopy perturbation method [9], variational iteration method [9] and exact solution.

The exact and the Haar solutions, at different iterations are shown in Fig. 3.7. Here we fix order of differential equation (3.3.17), $\alpha = 2$, and level of resolution, $J = 3$. Absolute error is given at

each iteration. The results in Fig. 3.8 indicate that the Haar solution converge to the exact solution when α approaches to 2.

Numerical solution of present method at different level of resolution is shown in Table 3.4 and the results are in high agreement with the exact solution. Haar solutions are also compared with solutions obtained by variational iteration method and homotopy perturbation method [9].

3.3.2 Boundary Value Problems

Example 5: Consider the fractional order nonlinear Troesch's boundary value problem

$$ {}^{c}D^{\alpha}y(x) - \lambda \sinh(\lambda y(x)) = 0,\ 0 \le x \le 1,\ 1 < \alpha \le 2, \tag{3.3.23} $$

subject to the boundary conditions: $y(0) = 0,\ \ y(1) = 1$. The exact solution, when $\alpha = 2$, is given in [101].

The quasilinearized form of equation (3.3.23) is

$$ {}^{c}D^{\alpha}y_{r+1}(x) - \lambda^2 \cosh(\lambda y_r(x)) y_{r+1}(x) = \lambda \sinh(\lambda y_r(x)) - \lambda^2 y_r(x) \cosh(\lambda y_r(x)), \tag{3.3.24} $$

with the boundary conditions: $y_{r+1}(0) = 0$, $y_{r+1}(1) = 1$.

Apply the Haar wavelet method to equation (3.3.24), Haar wavelet approximation of higher order derivative is

$$ {}^{c}D^{\alpha}y_{r+1}(x) = \sum_{l=1}^{2M} b_l h_l(x). \tag{3.3.25} $$

Lower order derivatives are obtained by integrating equation (3.3.25) and use the boundary conditions, we get

$$ y_{r+1}(x) = \sum_{l=1}^{2M} b_l (p_{\alpha,l}(x) - x C_{\alpha,l}) + x, \tag{3.3.26} $$

where $C_{\alpha,l}$ is given in equation (2.3.7) and (2.3.8). Substitute equations (3.3.25) and (3.3.26) in (3.3.24), we get

$$ \begin{aligned} &\sum_{l=1}^{2M} b_l [h_l(x) - \lambda^2 \cosh(\lambda y_r(x)) p_{\alpha,l}(x) + x\lambda^2 \cosh(\lambda y_r(x)) C_{\alpha,l}] \\ &= x\lambda^2 \cosh(\lambda y_r(x)) + \lambda \sinh(\lambda y_r(x)) - \lambda^2 y_r(x) \cosh(\lambda y_r(x)), \end{aligned} \tag{3.3.27} $$

with the initial approximations $y_0(x) = 0$.

				$\alpha = 2$		
$r = 6$	$J = 8$	$J = 9$	$J = 10$			
x	y_{Haar}	y_{Haar}	y_{Haar}	y_{HPM} [40]	y_{DM} [28]	y_{Exact}
0.1	0.0959443490	0.0959443492	0.0959443493	0.0959395656	0.0959383534	0.0959443493
0.2	0.1921287470	0.1921287475	0.1921287476	0.1921193244	0.1921180592	0.1921287477
0.3	0.2887944000	0.2887944007	0.2887944008	0.2887806940	0.2887803297	0.2887944009
0.4	0.3861848453	0.3861848461	0.3861848463	0.3861675428	0.3861687095	0.3861848464
0.5	0.4845471635	0.4845471644	0.4845471647	0.4845274183	0.4845302901	0.4845471647
0.6	0.5841332472	0.5841332481	0.5841332484	0.5841127822	0.5841169798	0.5841332484
0.7	0.6852011471	0.6852011480	0.6852011482	0.6851822495	0.6851868451	0.6852011483
0.8	0.7880165217	0.7880165224	0.7880165226	0.7880018367	0.7880055691	0.7880165227
0.9	0.8928542155	0.8928542160	0.8928542161	0.8928462193	0.8928480234	0.8928542161

Table 3.5: Results of Troeschs problem for $\lambda = 0.5$.
The Haar wavelet-quasilinearization technique at 6^{th} iteration and different level of resolutions compared with homotopy perturbation method [40], decomposition method [28] and exact solution

				$\alpha = 2$		
$r = 6$	$J = 8$	$J = 9$	$J = 10$			
x	y_{Haar}	y_{Haar}	y_{Haar}	y_{HPM} [40]	y_{DM} [28]	y_{Exact}
0.1	0.0846612520	0.0846612554	0.0846612563	0.0843817004	0.084248760	0.0846612565
0.2	0.1701713492	0.1701713559	0.1701713576	0.1696207644	0.169430700	0.1701713582
0.3	0.2573938951	0.2573939048	0.2573939073	0.2565929224	0.256414500	0.2573939080
0.4	0.3472228388	0.3472228510	0.3472228541	0.3462107378	0.346085720	0.3472228551
0.5	0.4405998164	0.4405998305	0.4405998340	0.4394422743	0.439401985	0.4405998351
0.6	0.5385343780	0.5385343931	0.5385343968	0.5373300622	0.537365700	0.5385343980
0.7	0.6421285897	0.6421286043	0.6421286080	0.6410104651	0.641083800	0.6421286091
0.8	0.7526080774	0.7526080899	0.7526080930	0.7517335467	0.751788000	0.7526080939
0.9	0.8713625092	0.8713625172	0.8713625191	0.8708835371	0.870908700	0.8713625196

Table 3.6: Results of Troeschs problem for $\lambda = 1$.
The Haar wavelet-quasilinearization technique at 6^{th} iteration and for different level of resolutions compared with homotopy perturbation method [40], decomposition method [28] and exact solution

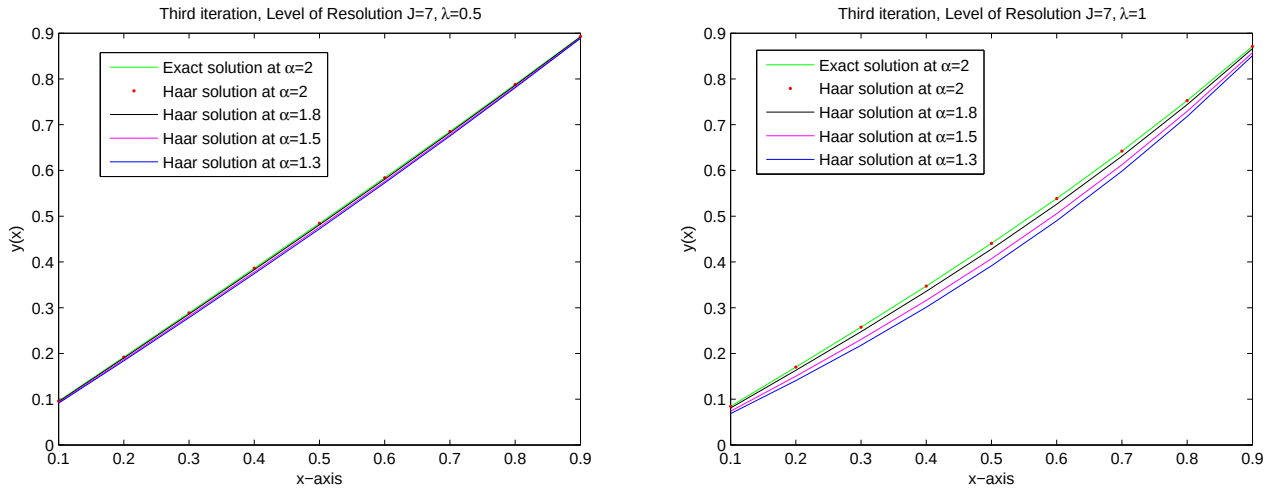

Figure 3.9: Exact solution at $\alpha = 2$ and the Haar wavelet-quasilinearization solution at $\alpha = 2$, $\alpha = 1.8$, $\alpha = 1.5$, and $\alpha = 1.3$.

Numerical solution by the Haar wavelet method is shown in Table 3.5 and Table 3.6 at different levels of resolutions. The results in Table 3.5 and Table 3.6 are obtained for $\lambda = 0.5$ and $\lambda = 1.0$ respectively. Solution by present method are in good agreement with exact solution and also better than the solution obtained by homotopy perturbation method [40] and decomposition method [28]. Numerical results at third iteration, with fixed resolution level $J = 7$ and $\lambda = 0.5$, $\lambda = 1.0$; for different values of α are plotted in Fig. 3.9. We use the MATLAB command of one-dimensional data interpolation using spline to get the values at $x = 0.1, x = 0.2, ..., x = 0.9$ and plot the exact and the Haar solution at these points. It is also shown that the Haar solution converges to the exact solution when α approaches to 2.

Comparison of Uniform and Nonuniform Haar Wavelet Quasilinearization Technique

Example 6: Consider the α^{th} order fractional nonlinear boundary value problem,

$$ {}^{c}D^{\alpha}y(x) + a(x)y'^{2}(x) + b(x)y(x)y'(x) = f(x),\ 1 < \alpha \leq 2, \tag{3.3.28} $$

subject to the boundary conditions $y(0) = 0,\ y(1) = 0$.
The exact solution is given by

$$ y(x) = x^{\alpha} - x^{70-\alpha}, $$

where

$$ f(x) = \Gamma(\alpha+1) - \tfrac{71-\alpha}{71-2\alpha}x^{70-2\alpha} + a(x)(\alpha x^{\alpha-1} - (70-\alpha)x^{69-\alpha})^2 \\ +b(x)(\alpha x^{\alpha-1} - (70-\alpha)x^{69-\alpha})(x^{\alpha} - x^{70-\alpha}). $$

Applying the quasilinearized technique to equation (3.3.28), we get

$$\begin{aligned} {}^cD^{\alpha}y_{r+1}(x) + b(x)y'_r(x)y_{r+1}(x) + (2a(x)y'_r(x) + b(x)y_r(x))y'_{r+1}(x) = f(x) \\ +a(x)y'^2_r(x) + b(x)y_r(x)y'_r(x), \end{aligned} \tag{3.3.29}$$

with the boundary conditions $y_{r+1}(0) = 0,\ \ y_{r+1}(1) = 0$.
Now apply the Haar wavelet method to equation (3.3.29), we approximate the higher order derivative term by the Haar wavelet series as

$${}^cD^{\alpha}y_{r+1}(x) = \sum_{l=1}^{2M} b_l h_l(x). \tag{3.3.30}$$

Lower order derivatives are obtained by integrating equation (3.3.30) and use the initial condition

$$y_{r+1}(x) = \sum_{l=1}^{2M} b_l(p_{\alpha,l}(x) - xC_{\alpha,l}), \tag{3.3.31}$$

$$y'_{r+1}(x) = \sum_{l=1}^{2M} b_l(p_{\alpha-1,l}(x) - C_{\alpha,l}), \tag{3.3.32}$$

where $C_{\alpha,l}$ is given in (2.3.7) and (2.3.8). Substitute equations (3.3.30), (3.3.31) and (3.3.32) in (3.3.29), we get

$$\begin{aligned} \sum_{l=1}^{2M} b_l[h_l(x) + b(x)y'_r(x)p_{\alpha,l}(x) - b(x)y'_r(x)C_{\alpha,l} + (2a(x)y'_r(x) + b(x)y_r(x))p_{\alpha-1,l}(x) \\ -(2a(x)y'_r(x) + b(x)y_r(x))C_{\alpha,l}] = f(x) + a(x)y'^2_r(x) + b(x)y_r(x)y'_r(x), \end{aligned} \tag{3.3.33}$$

with the initial approximation $y_0(x) = 0,\ \ y'_0(x) = 0$. Here we consider $a(x) = e^x$ and $b(x) = x$.
As the non-uniform Haar wavelets are useful for the treatment of abrupt solution of differential equations. The solution of Problem (3.3.28) have abrupt behavior near point $x = 0.95$, so we use the non-uniform grid structure for better approximations.
Let us divide the interval $[0, 1]$ into two subintervals $[0, 0.94]$ and $[0.94, 1]$, let $A = 0, B = 0.94, C = 1$, step-size for each subintervals are
$\Delta x_1 = \frac{(B-A)}{\frac{3M}{2}}$,
$\Delta x_2 = \frac{(C-B)}{\frac{M}{2}}$.
Here $\Delta x_2 \ll \Delta x_1$.
The coordinates of the grid points are
For j=1,2,...,$\frac{3M}{2} + 1$
x(j)=A+(i-1)Δx_1,
For j=1,2,..,$\frac{M}{2}$
x(j+$\frac{3M}{2} + 1$)=B+(i)Δx_2.
And collocation points are
For j=1,2,...,2M

$x_c(j) = \frac{x(j)+x(j+1)}{2}$.

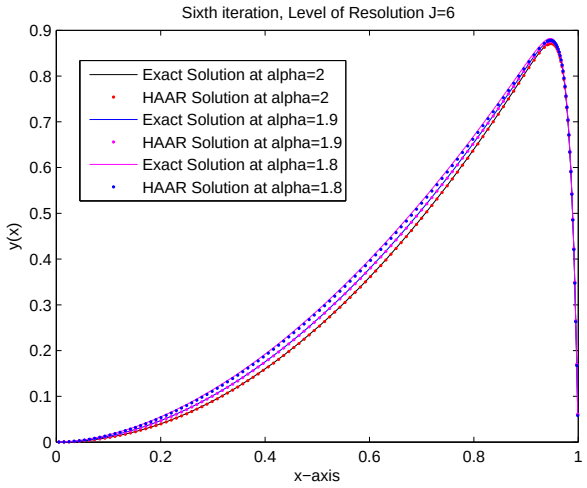

Figure 3.10: Exact solution and the Haar wavelet-quasilinearization solution at $\alpha = 2$, $\alpha = 1.9$, and $\alpha = 1.8$.

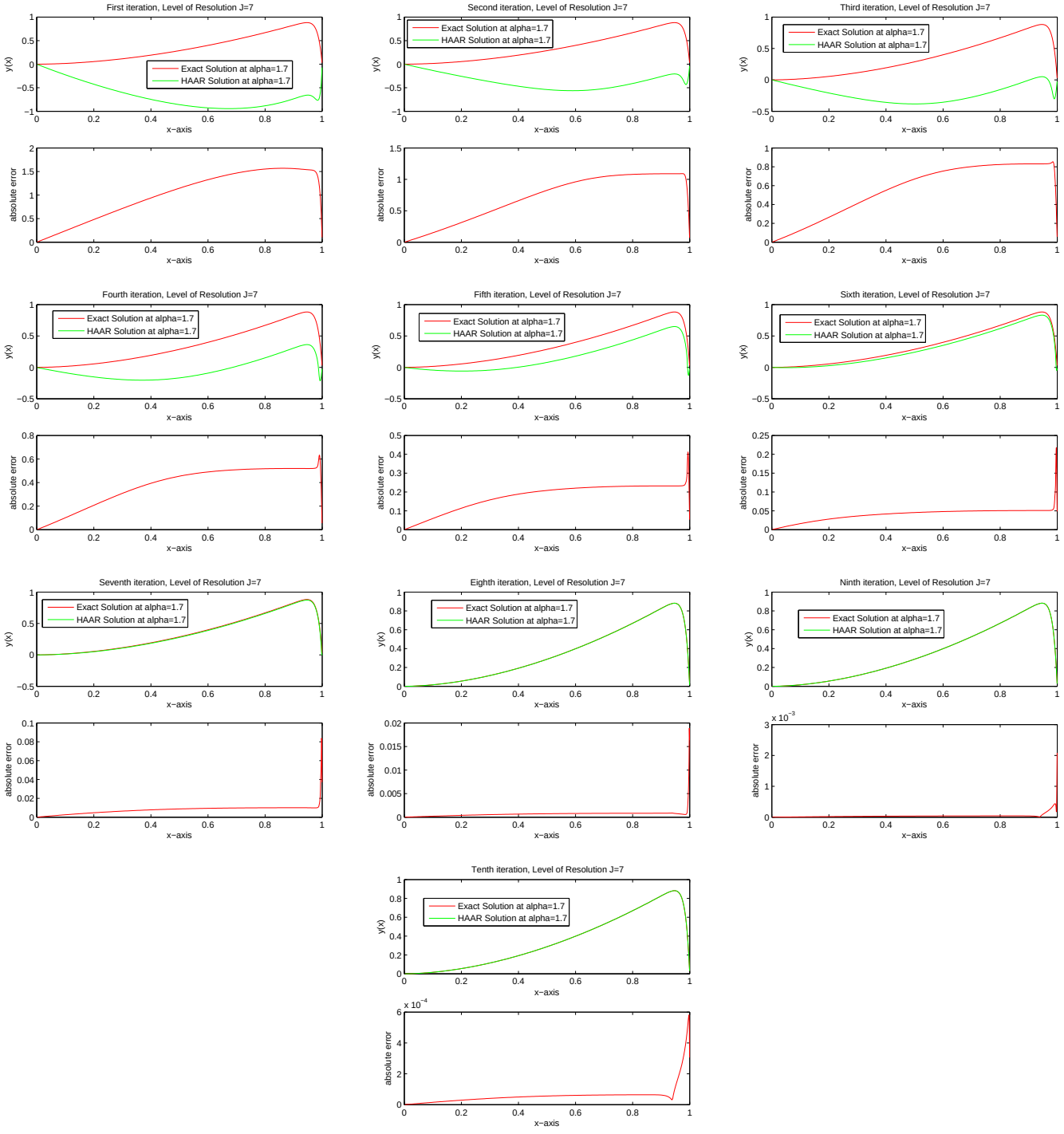

Figure 3.11: Comparison of exact solution and solution by the Haar wavelet-quasilinearization technique at $J = 7$, for different iterations, and $\alpha = 1.7$.

		Non-uniform Haar wavelet solution		Uniform Haar wavelet solution	
α	$r = 10$	$J = 8$	$J = 9$	$J = 8$	$J = 9$
1.8		5.4361e-004	2.5395e-004	8.2879e-002	2.2821e-002
1.9		2.7391e-004	1.1097e-004	6.4336e-002	2.2824e-002
2.0		8.0791e-005	2.0363e-005	1.0221e-002	2.3951e-003

Table 3.7: L_∞-error

Numerical solution for different order α of fractional differential equation (3.3.28) at different level of resolution J is considered for both uniform and non-uniform grids. The solution have abrupt behavior so non-uniform Haar wavelets provide better results as compared to uniform Haar wavelet as shown in Table 3.7. The results in Table 3.7 are at 10^{th} iteration. The non-uniform Haar wavelet solution and exact solution at 10^{th} iteration, fixed level of resolution $J = 7$ and for different value of α are plotted in Fig. 3.10. The advantage of quasilinearization technique for nonlinear differential equations are shown in Fig. 3.11. Here we fix level of resolution and order of equation (3.3.28) $\alpha = 1.7$.

3.3.3 Conclusion

It is shown that Haar wavelet method with quasilinearization technique gives good results when applied to different fractional order nonlinear initial and boundary value problems. The results obtained from Haar wavelet quasilinearization technique are better from the results obtained by other methods and are in good agreement with exact solutions. The solution of the fractional order, nonlinear ordinary differential equation converge to the solution of integer order differential equation as shown in Figures 3.2, 3.4, 3.6, 3.8, 3.9 and 3.10. The graphical analysis shows that approximate solution converge to the exact solution while iterations are increased and absolute error goes down. Different type of non-linearities can easily be handled by the Haar wavelet with quasilinearization method.

Chapter 4

Haar Wavelet-Quasilinearization Technique for Heat Convection–Radiation and Fractional Oscillation Equations

Many physical problems such as heat transfer equations are nonlinear. Due to their nonlinear nature, analytic solutions of these equations are not available in general. Therefore different numerical methods have been applied for providing approximate solutions. Some of these techniques include, generalized approximation method [62], variational iteration methods [47] and homotopy- perturbation method [48].

In the last few decades a considerable attention has been devoted to the study of nonlinear oscillators due to their potential applications in diverse areas of engineering and science [83]. The oscillator equation arises in a number of models describing various phenomena in nonlinear dynamics. Different numerical methods have been introduced for finding the approximate solution of nonlinear oscillator equations such as a differential transform method [80], modified homotopy perturbation method and the max-min approach [45], and homotopy analysis method [63].

This chaper is used to find the approximate solutions of the heat convection radiation and nonlinear fractional oscillator equations by using Haar wavelet method in conjunction with quasilinearization technique.

4.1 Assessment of Haar Wavelet-Quasilinearization Technique in Heat Convection–Radiation Equations

In this section, we will discuss solutions by the Haar wavelet-quasilinearization technique for the two problems, namely, (i) temperature distribution equation in lumped system of combined convection-radiation in a slab made of materials with variable thermal conductivity and (ii) cooling of a lumped system by combined convection and radiation are strongly reliable and also more accurate than the other numerical methods and are in good agreement with exact solution. According to the Haar wavelet-quasilinearization technique, we convert the nonlinear heat transfer equation to linear discretized equation with the help of quasilinearization technique and apply the Haar wavelet method at each iteration of quasilinearization technique to get the solution. The main aim of present work [116] is to show the reliability of the Haar wavelet-quasilinearization technique for heat transfer equations.

4.1.1 Temperature Distribution in Lumped System of Combined Convection-Radiation in a Slab Made of Materials with Variable Thermal Conductivity

Let the lumped system have volume V, surface area A, density ρ, specific heat c, the initial temperature T_i, temperature of the convection environment T_a, heat transfer coefficient h and c_a is specific heat at temperature T_a. Consider the mathematical model describing the temperature distribution in lumped system of combined convection–radiation in a slab made of materials with variable thermal conductivity is given by the following nonlinear boundary value problem:

$$\begin{array}{ll} \frac{d^2y(x)}{dx^2} & -\varepsilon y^4(x) = 0,\ 0 \le x \le 1, \\ \frac{dy(0)}{dx} & = 0,\ y(1) = 1. \end{array} \tag{4.1.1}$$

Where $y = \frac{T-T_a}{T_i-T_a}$ is dimensionless temperature, $x = \frac{t}{\rho V c_a/hA}$ is dimensionless time and $\varepsilon = \beta(T-T_a)$.

Haar Wavelet-Quasilinearization Technique

Applying the quasilinearization technique to (4.1.1), we get

$$\begin{array}{ll} \frac{d^2y_{r+1}(x)}{dx^2} & -4\varepsilon y_r^3(x)y_{r+1}(x) = -3\varepsilon y_r^4(x),\ 0 \le x \le 1, \\ \frac{dy_{r+1}(0)}{dx} & = 0,\ y_{r+1}(1) = 1. \end{array} \tag{4.1.2}$$

Now we implement the Haar wavelet method to equation (4.1.2), we approximate the higher order derivative term by the Haar wavelet series as

$$\frac{d^2y_{r+1}(x)}{dx^2} = \sum_{l=1}^{2M} b_l^{r+1} h_l(x). \tag{4.1.3}$$

Lower order derivatives are obtained by integrating equation (4.1.3) and use the boundary conditions

$$y_{r+1}(x) = \sum_{l=1}^{2M} b_l^{r+1} p_{2,l}(x) - C_{2,l} + 1, \tag{4.1.4}$$

where $C_{\alpha,l}$ is given in (2.3.8). Substitute equations (4.1.3) and (4.1.4) in (4.1.2), to obtain

$$\sum_{l=1}^{2M} b_l^{r+1}[h_l(x) - 4\varepsilon y_r^3(x) p_{2,l}(x) + 4\varepsilon y_r^3(x) C_{2,l}] = -3\varepsilon y_r^4(x) + 4\varepsilon y_r^3(x), \tag{4.1.5}$$

with the initial approximation $y_0(x) = 0$.

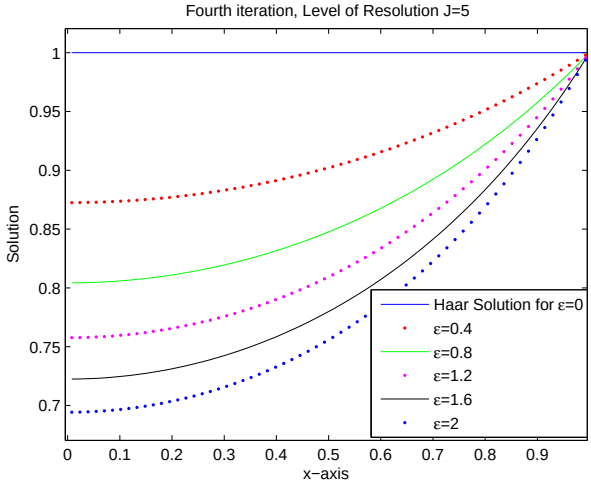

Figure 4.1: Solutions by Haar wavelet-quasilinearization technique for different ε at $J = 5$ and $r = 4$.

4^{th} *iteration*				$J = 8$
x	*Maple*	y_{GA} [62]	y_{HPM} [62]	y_{Haar}
0.0	0.834542	0.963536	0.640000	0.834543
0.2	0.840390	0.964009	0.652096	0.840391
0.4	0.858269	0.965742	0.689536	0.858269
0.6	0.889247	0.969893	0.755776	0.889248
0.8	0.935346	0.979233	0.866576	0.935346

Table 4.1: Numerical results for temperature distribution equation for $\varepsilon = 0.6$: Haar wavelet-quasilinearization technique at 4^{th} iteration and level of resolutions $J = 8$.

4^{th} *iteration*				$J = 8$
x	*Maple*	y_{GA} [62]	y_{HPM} [62]	y_{Haar}
0.0	0.694318	0.968771	-0.666667	0.694362
0.2	0.703698	0.968804	-0.625600	0.703739
0.4	0.732894	0.969008	-0.489600	0.732927
0.6	0.785488	0.970024	-0.220267	0.785510
0.8	0.869161	0.975059	-0.246400	0.869176

Table 4.2: Numerical results for temperature distribution equation for $\varepsilon = 2.0$: Haar wavelet-quasilinearization technique at 4^{th} iteration and level of resolutions $J = 8$.

Figure 4.1 shows the temperature y_{Haar} by Haar wavelet quasilinearization technique for different ε at $J = 5$ and at 4^{th} iteration. According to Figure 4.1 and Table 4.1 and 4.2, temperature increases with decreasing ε, also temperature vary with time x. Table 4.1 and 4.2 shows that obtained solution are in good agreement with numerical solution provided by Maple and are better than generalized approximation method y_{GA} [62] and homotopy perturbation method y_{HPM} [62].

4.1.2 Cooling of a Lumped System by Combined Convection and Radiation

Consider the system have volume V, surface area A, density ρ, specific heat c, emissivity E, the initial temperature T_i, temperature of the convection environment T_a, heat transfer coefficient h and c_a is specific heat at temperature T_a. In this case system loses heat through radiation and the effective sink temperature is T_s. The mathematical model describing the cooling of a lumped system by combined convection and radiation is given by the following nonlinear initial value problem:

$$\begin{aligned} \rho V c\frac{dT(t)}{dt} + hA(T - T_a) + E\sigma A(T^4 - T_s^4) = 0, \\ T(t = 0) = T_i. \end{aligned} \tag{4.1.6}$$

For the solution of (4.1.6), we do the certain changes in parameters:
$y = \frac{T}{T_i}$, $y_a = \frac{T_a}{T_i}$, $y_s = \frac{T_s}{T_i}$, $x = \frac{t}{\rho V c_a/hA}$, $\varepsilon = \frac{E\sigma T_i^3}{h}$.
Equation (4.1.6) implies after changing the parameters:

$$\begin{aligned} \frac{dy(x)}{dx} + (y - y_a) + \varepsilon(y^4 - y_s^4) = 0, \\ y(x = 0) = 1. \end{aligned} \tag{4.1.7}$$

For the sake of simplicity we assume that $y_a = y_s = 0$, equation (4.1.7) becomes

$$\begin{aligned} \frac{dy(x)}{dx} + y + \varepsilon y^4 = 0, \\ y(x = 0) = 1. \end{aligned} \tag{4.1.8}$$

Haar Wavelet-Quasilinearization Technique

Implementation of the quasilinearization technique to (4.1.8) gives

$$\begin{aligned} \frac{dy_{r+1}(x)}{dx} + (1 + 4\varepsilon y_r^3)y_{r+1} = 3\epsilon y_r^4, \\ y_{r+1}(x = 0) = 1. \end{aligned} \tag{4.1.9}$$

According to the Haar wavelet method to equation (4.1.9), approximate the higher order derivative term by the Haar wavelet series as

$$\frac{dy_{r+1}(x)}{dx} = \sum_{l=1}^{2M} b_l^{r+1} h_l(x). \tag{4.1.10}$$

Solution can be obtained by integrating equation (4.1.10) and use the initial condition to yield

$$y_{r+1}(x) = \sum_{l=1}^{2M} b_l^{r+1} p_{1,l}(x) + 1. \tag{4.1.11}$$

Substitute equations (4.1.10) and (4.1.11) in (4.1.9),

$$\sum_{l=1}^{2M} b_l^{r+1}[h_l(x) + (1 + 4\varepsilon y_r^3(x))p_{1,l}(x)] = 3\varepsilon y_r^4(x) - (1 + 4\varepsilon y_r^3(x)), \tag{4.1.12}$$

with the initial approximation $y_0(x) = 1$.

To get the solution on large interval, say $[0, 5]$, we divide the interval $[0, 5]$ into three subintervals $[0, 1.25]$, $[1.25, 3.75]$ and $[3.75, 5]$, let $A = 0,\ B = 1.25,\ C = 3.75,\ D = 5$, step-size for each subintervals are

$\Delta x_1 = \frac{(B-A)}{\frac{M}{2}}$,

$\Delta x_2 = \frac{(C-B)}{M}$,

$\Delta x_3 = \frac{(D-C)}{\frac{M}{2}}$,

The coordinates of the grid points are

For j=1,2,...,$\frac{M}{2} + 1$

x(j)=A+(i-1)Δx_1,

For j=1,2,..,M

x(j+$\frac{M}{2} + 1$)=B+(i)Δx_2,

For j=1,2,..,$\frac{M}{2}$

x(j+$\frac{3M}{2} + 1$)=C+(i)Δx_3.

And collocation points are

For j=1,2,...,2M

$x_c(j) = \frac{x(j)+x(j+1)}{2}$.

4^{th} *iteration*				$J = 8$
ε	*Exact*	y_{VIM} [47]	y_{HPM} [47]	y_{Haar}
0.0	0.606531	0.606531	0.606531	0.606531
0.1	0.591591	0.591617	0.591638	0.591592
0.2	0.578023	0.578207	0.578371	0.578023
0.3	0.565620	0.566185	0.566732	0.565620
0.4	0.554217	0.555440	0.556720	0.554217
0.5	0.543681	0.545868	0.548335	0.543681
0.6	0.533903	0.537369	0.541576	0.533904
0.7	0.524793	0.529850	0.536445	0.524793
0.8	0.516275	0.523226	0.532940	0.516275
0.9	0.508284	0.517412	0.531062	0.508284
1.0	0.500765	0.512333	0.530812	0.500765

Table 4.3: Numerical results for cooling equation for different ε and $x = 0.5$: Haar wavelet-quasilinearization technique at 4^{th} iteration and level of resolutions $J = 8$.

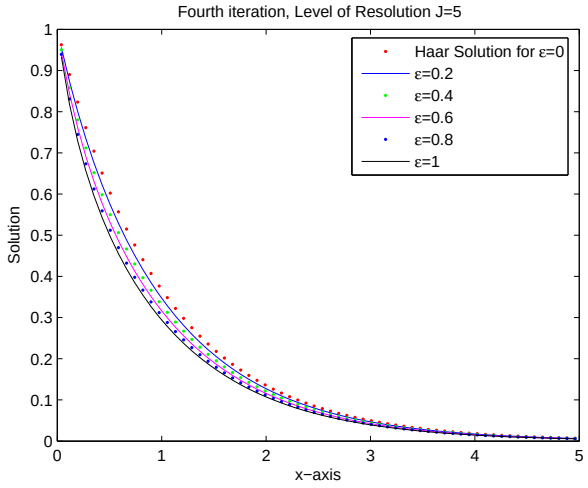

Figure 4.2: Solutions by Haar wavelet-quasilinearization technique for different ε at $J = 5$ and $r = 4$.

Temperature y_{Haar} at higher interval, $[0, 5]$, by Haar wavelet quasilinearization technique at $J = 5$ and iteration $r = 4$, of the cooling equation for different values of ε is shown in Figure 4.2. It shows that temperature decreases with increasing ε, also shows that temperature reduces to zero when time x is increasing. According to Table 4.3, we conclude that our results are in good agreement with exact solution and more accurate than variational iteration method y_{VIM} [47] and

homotopy perturbation method y_{HPM} [47].

We can get more accurate results while increasing level of resolution J or iteration r or both, according to convergence analysis given in section (3.2.3).

4.1.3 Conclusion

The main purpose of the present chapter is to show the applicability of Haar wavelet quasilinearization technique for the solution of heat convection radiation equations, because when some numerical method applied for the solution of heat convection radiation equations they becomes unstable when we increase the value of parameter epsilon, which appears in heat convection radiation equations, as shown in Table 4.1, 4.2 and 4.3. This is the main advantage for implementing the Haar wavelet quasilinearization technique on heat convection radiation equations, because it gives stable and accurate results.

4.2 Haar Wavelet Operational Matrix Method for Fractional Oscillation Equations

The fractional order forced duffing-Van der Pol oscillator is given by the following second order differential equation [83].

$$y''(t) - \mu(1 - y^2(t))y'(t) + ay(t) + by^3(t) = g(f, \omega, t),$$

where $g(f, \omega, t) = f\cos(\omega t)$ represents the periodic driving function of time with period $T = 2\pi/\omega$, where ω is the angular frequency of the driving force, f is the forcing strength, $\mu > 0$ is the damping parameter of the system. Duffing–Van der Pol oscillator equation can be expressed in three physical situations

(1) Single-well $a > 0, b > 0$,

(2) Double-well $a < 0, b > 0$,

(3) Double-hump $a > 0, b < 0$.

In this section, we present Haar wavelet quasilinearization technique for the solution of force-free duffing-Van der Pol oscillator of fractional order, forced duffing-Van der Pol oscillator of fractional order and higher order fractional duffing equation and compare the results with those obtained by other methods and exact solution.

4.2.1 Forced Duffing-Van Der Pol Oscillator Equation

Consider the α^{th} order fractional forced DVP oscillator equation

$$^cD^{\alpha}y(x) - \mu(1 - y^2(x))y'(x) + ay(x) + by^3(x) = f\cos(\omega x),\ 1 < \alpha \leq 2, \tag{4.2.1}$$

subject to the initial conditions $y(0) = 1,\ y'(0) = 0$.
Apply the quasilinearization technique to (4.2.1), we obtain

$$\begin{aligned} {}^cD^{\alpha}y_{n+1}(x) - \mu(1 - y_n^2(x))y'_{n+1}(x) + (a + 2\mu y_n(x)y'_n(x) + 3by_n^2(x))y_{n+1}(t) \\ = f\cos(\omega x) + 2\mu y_n^2(x)y'_n(x) + 2by_n^3(x), \end{aligned} \tag{4.2.2}$$

with the initial conditions $y_{n+1}(0) = 1,\ y'_{n+1}(0) = 0$.
Now we apply the Haar wavelet method to equation (4.2.2), we approximate the higher order derivative term by the Haar wavelet series as

$${}^cD^{\alpha}y_{n+1}(x) = \sum_{l=1}^{2M} b_l h_l(x). \tag{4.2.3}$$

Lower order derivatives are obtained by integrating equation (4.2.3) and use the initial condition

$$y_{n+1}(x) = \sum_{l=1}^{2M} b_l p_{\alpha,l}(x) + 1, \quad y'_{n+1}(x) = \sum_{l=1}^{2M} b_l p_{\alpha-1,l}(x). \tag{4.2.4}$$

Substitute equations (4.2.3) and (4.2.4) in (4.2.2) to get

$$\begin{aligned} &\sum_{l=1}^{2M} b_l[h_l(x) - \mu(1 - y_n^2(x))p_{\alpha-1,l}(x) + (a + 2\mu y_n(x)y'_n(x) + 3by_n^2(x))p_{\alpha,l}(x)] \\ &\quad = f\cos(\omega x) + 2\mu y_n^2(x)y'_n(x) + 2by_n^3(x) - (a + 2\mu y_n(x)y'_n(x) + 3by_n^2(x)). \end{aligned} \tag{4.2.5}$$

with the initial approximations $y_0(x) = 1,\ y'_0(x) = 0$.
(1) (Single–well $a > 0,\ b > 0.$) $a = 0.5,\ b = 0.5,\ \mu = 0.1,\ f = 0.5,\ \omega = 0.79$.
(2) (Double–well $a < 0,\ b > 0.$) $a = -0.5,\ b = 0.5,\ \mu = 0.1,\ f = 0.5,\ \omega = 0.79$.
(3) (Double–hump $a > 0,\ b < 0.$) $a = 0.5,\ b = -0.5,\ \mu = 0.1,\ f = 0.5,\ \omega = 0.79$.

$\alpha = 2$					
5^{th} *iteration*			$J = 9$		
x	y_{RK}	y_{HPM} [117]	y_{VIM} [117]	y_{Haar}	Absolute Error
0.2	0.9900451	0.99004	0.99004	0.9900451	3.1e-8
0.4	0.9607026	0.96075	0.9607	0.9607024	1.5e-7
0.6	0.9134154	0.91383	0.91341	0.9134150	3.5e-7
0.8	0.8502496	0.85216	0.85025	0.8502491	5.8e-7
1.0	0.773523	0.77973	0.77353	0.773522	8.0e-7

Table 4.4: Single-well situation: Comparison of solutions by the Haar wavelet-quasilinearization technique y_{Haar} at 5^{th} iteration and level of resolutions $J = 9$ with numerical methods [117] and numerical solution based on the fourth-order Runge-Kutta.

$\alpha = 2$					
5^{th} *iteration*			$J = 9$		
x	y_{RK}	y_{VIM} [117]	y_{HPM} [117]	y_{Haar}	Absolute Error
0.2	1.009945	1.00994	1.00994	1.009945	9.8e-9
0.4	1.039114	1.03911	1.03918	1.039114	6.7e-8
0.6	1.085448	1.08544	1.08621	1.085448	1.9e-7
0.8	1.145384	1.14539	1.14937	1.145384	3.9e-7
1.0	1.213777	1.21382	1.22785	1.213778	6.4e-7

Table 4.5: Double-well situation: Comparison of solutions by the Haar wavelet-quasilinearization technique y_{Haar} at 5^{th} iteration and level of resolutions $J = 9$ with numerical methods [117] and numerical solution based on the fourth-order Runge-Kutta.

$\alpha = 2$					
5^{th} *iteration*			$J = 9$		
x	y_{RK}	y_{VIM} [117]	y_{HPM} [117]	y_{Haar}	Absolute Error
0.1	1.00250	1.0025	1.0025	1.00250	2.5e-9
0.2	1.01001	1.01001	1.01001	1.01001	4.3e-11
0.5	1.06301	1.063	1.06296	1.06301	4.3e-8
0.75	1.14347	1.14346	1.14209	1.14347	9.8e-8
1.0	1.26039	1.26035	1.25055	1.26039	3.9e-7

Table 4.6: Double-hump situation: Comparison of solutions by the Haar wavelet-quasilinearization technique y_{Haar} at 5^{th} iteration and level of resolutions $J = 9$ with numerical methods [117] and numerical solution based on the fourth-order Runge-Kutta.

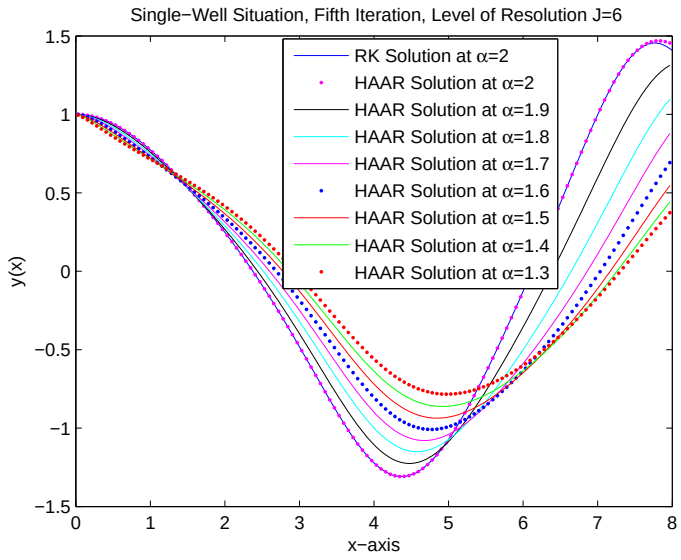

Figure 4.3: Solution by RK method (RK Solution) at $\alpha = 2$ and solution by Haar wavelet-quasilinearization technique (HAAR Solution) at $J = 6$ and different values of α for $a = 0.5,\ b = 0.5, \mu = 0.1,\ f = 0.5,\ \omega = 0.79$.

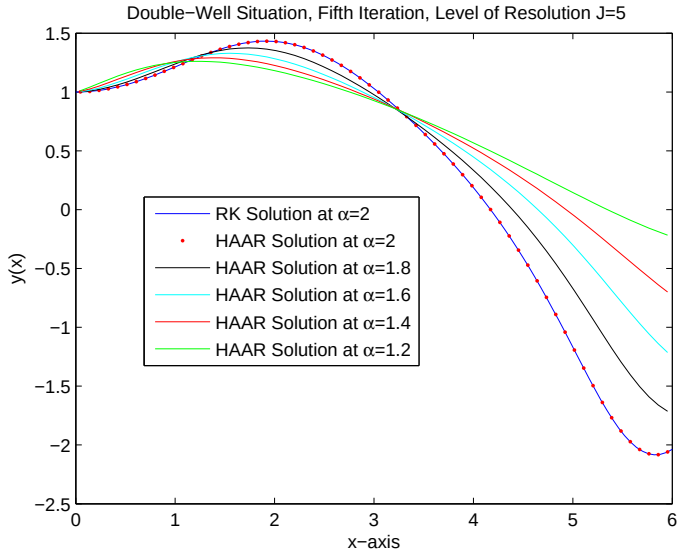

Figure 4.4: Solution by RK method (RK Solution) at $\alpha = 2$ and solution by Haar wavelet-quasilinearization technique (HAAR Solution) at $J = 5$ and different values of α for $a = -0.5,\ b = 0.5, \mu = 0.1,\ f = 0.5,\ \omega = 0.79$.

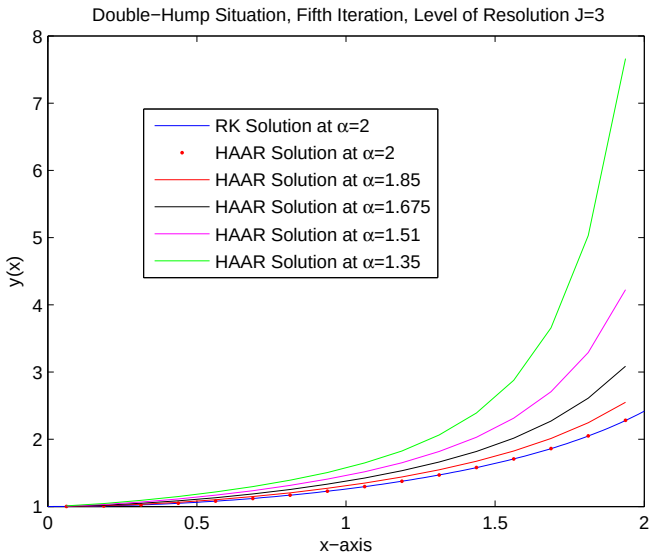

Figure 4.5: Solution by RK method (RK Solution) at $\alpha = 2$ and solution by Haar wavelet-quasilinearization technique (HAAR Solution) at $J = 3$ and different values of α for $a = 0.5,\ b = -0.5, \mu = 0.1,\ f = 0.5,\ \omega = 0.79$

The results obtained using the Haar wavelet quasilinearization technique at fifth iteration for the three situations, single-well, double-well and double-hump are given in Table 4.4, 4.5 and 4.6 respectively. Here we fix the order of equation, $\alpha = 2$, and level of resolution $J = 9$. We compared the obtained solution with variational iteration method [117], homotopy perturbation method [117] and numerical solution based on the fourth–order Runge-Kutta (RK) method. Also the absolute error relative to RK method is shown in Tables 4.4, 4.5 and 4.6. It shows that obtained results are more accurate as compared to variational iteration method and homotopy perturbation method.

Figure 4.3, 4.4 and 4.5 showed the solution of equation (4.2.1) for single-well, double-well and double-hump situation respectively. We plot the solutions at different order α of equation (4.2.1). Here we fixed the solution at fifth iteration and level of resolution $J = 5$ or $J = 6$. Also solution by fourth order Runge-Kutta method (RK Solution) at $\alpha = 2$ is also plotted along with the solution obtained by the Haar wavelet quasilinearization technique (HAAR Solution) and Figures 4.3, 4.4 and 4.5 shows that Haar solution converges to the RK solution when α approaches to 2.

4.2.2 Force-Free Duffing-Van Der Pol Oscillator Equation

Consider the α^{th} order fractional force-free DVP oscillator equation

$$ {}^{c}D^{\alpha}y(x) - \mu(1 - y^2(x))y'(x) + ay(x) + by^3(x) = 0,\ 1 < \alpha \leq 2, \tag{4.2.6}$$

subject to the initial conditions $y(0) = 1,\ y'(0) = 0$.

Haar wavelet–quasilinearization technique on (4.2.6) gives

$$\begin{aligned}\sum_{l=1}^{2M} b_l[h_l(x) - \mu(1 - y_n^2(x))p_{\alpha-1,l}(x) + (a + 2\mu y_n(x)y_n'(x) + 3by_n^2(x))p_{\alpha,l}(x)] \\ = 2\mu y_n^2(x)y_n'(x) + 2by_n^3(x) - (a + 2\mu y_n(x)y_n'(x) + 3by_n^2(x)),\end{aligned} \tag{4.2.7}$$

with the initial approximations $y_0(x) = 1,\ y_0'(x) = 0$.

$\alpha = 2$				
5^{th} *iteration*			$J = 9$	
x	y_{RK}	y_{ADM} [17]	y_{Haar}	Absolute Error
0.0	2.00000	1.99750	2.00000	2.1e-12
0.1	1.98971	1.98724	1.98971	1.7e-7
0.2	1.95936	1.95697	1.95936	3.5e-7
0.3	1.90980	1.90758	1.90980	5.4e-7
0.4	1.84202	1.84008	1.84202	7.3e-7
0.5	1.75702	1.75552	1.75702	9.2e-7
0.6	1.65586	1.65493	1.65586	1.1e-6
0.7	1.53958	1.53937	1.53958	1.3e-6
0.8	1.40923	1.53937	1.40923	1.4e-6
0.9	1.26586	1.26726	1.26586	1.6e-6
1.0	1.11054	1.11267	1.11054	1.7e-6
1.1	0.94435	0.94704	0.94435	1.9e-6
1.2	0.76846	0.77147	0.76846	2.0e-6
1.3	0.58411	0.58715	0.58410	2.1e-6
1.4	0.39267	0.39545	0.39267	2.3e-6
1.5	0.19567	0.19795	0.19566	2.4e-6

Table 4.7: Force-Free Duffing-Van der Pol Oscillator Equation: Comparison of solutions by the Haar wavelet-quasilinearization technique y_{Haar} at 5^{th} iteration and level of resolutions $J = 9$ with Adomian decomposition method y_{ADM} [17] and numerical solution based on the fourth-order Runge-Kutta.

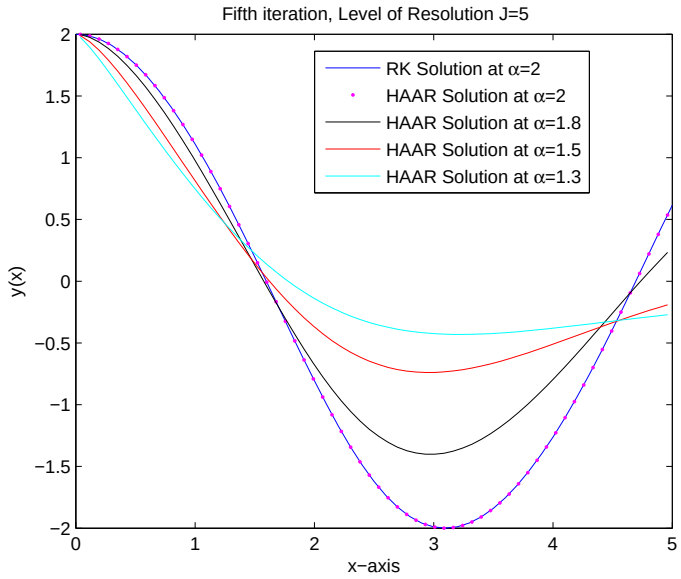

Figure 4.6: Solution by RK method (RK Solution) at $\alpha = 2$ and solution by Haar wavelet-quasilinearization technique (HAAR Solution) at $J = 5$ and different values of α for $a = 1,\ \mu = 0.1,\ b = 0.01,\ f = 0$.

Results of fifth iteration by the Haar wavelet quasilinearization technique at fixed level of resolution $J = 9$ and at $\alpha = 2$ are shown in Table 4.7. Here we consider $\mu = 0.1,\ a = 1,\ b = 0.01$ and compare the obtained solution with Adomian decomposition method [17]. Equation (4.2.6) is also solved by fourth order Runge-Kutta method to show the applicability of the Haar wavelet quasilinearization technique. Table 4.7 shows that solution by the Haar wavelet quasilinearization technique gives more accurate results as compared to Adomian decomposition method.

Results of fifth iteration by the Haar wavelet quasilinearization technique at fixed level of resolution $J = 5$ and at different values of α, are shown in Figure 4.6, along with the RK solution at $\alpha = 2$. Figure 4.6 showed that obtained solution converge to the RK solution when α approaches to 2.

4.2.3 Higher Order Oscillation Equation

Consider the α^{th} order fractional Duffing equation

$$ {}^{c}D^{\alpha}y(x) + 5y''(x) + 4y(x) - \tfrac{1}{6}y^3(x) = 0,\ 3 < \alpha \leq 4, \tag{4.2.8} $$

subject to the initial condition
$y(0) = 0,\ y'(0) = 1.91103,\ y''(0) = 0,\ y'''(0) = -1.15874.$

The exact solution, when $\alpha = 4$, is given by

$$y(x) = 2.1906\sin(0.9x) - 0.02247sin(2.7x) + 0.000045sin(4.5x).$$

Quasilinearization technique to (4.2.8) gives

$${}^cD^{\alpha}y_{n+1}(x) + 5y''_{n+1}(x) + (4 - \tfrac{1}{2}y_n^2(x))y_{n+1}(x) = -\tfrac{1}{3}y_n^3(x),\ 3 < \alpha \leq 4, \tag{4.2.9}$$

with the initial conditions
$y_{n+1}(0) = 0,\ y'_{n+1}(0) = 1.91103,\ y''_{n+1}(0) = 0,\ y'''_{n+1}(0) = -1.15874$. Implement the Haar wavelet method to equation (4.2.9) as

$${}^cD^{\alpha}y_{n+1}(x) = \sum_{l=1}^{2M} b_l h_l(x). \tag{4.2.10}$$

Lower order derivatives are obtained by integrating equation (4.2.10) and use the initial condition

$$\begin{aligned}
y_{n+1}(x) &= \sum_{l=1}^{2M} b_l p_{\alpha,l}(x) - \tfrac{1.15874}{6}x^3 + 1.91103x, \\
y'_{n+1}(x) &= \sum_{l=1}^{2M} b_l p_{\alpha-1,l}(x) - \tfrac{1.15874}{2}x^2 + 1.91103, \\
y''_{n+1}(x) &= \sum_{l=1}^{2M} b_l p_{\alpha-2,l}(x) - 1.15874x, \\
y'''_{n+1}(x) &= \sum_{l=1}^{2M} b_l p_{\alpha-3,l}(x) - 1.15874.
\end{aligned} \tag{4.2.11}$$

Substitute equations (4.2.10) and (4.2.11) in (4.2.9), we get

$$\begin{aligned}
\sum_{l=1}^{2M} b_l[h_l(x) + 5p_{\alpha-2,l}(x) + (4 - \tfrac{1}{2}y_n^2(x))p_{\alpha,l}(x)] = -\tfrac{1}{3}y_n^3(x) + 5(1.15874)x \\
-(4 - \tfrac{1}{2}y_n^2(x))(1.91103x - \tfrac{1.15874}{6}x^3),
\end{aligned} \tag{4.2.12}$$

with the initial approximations
$y_0(x) = 0,\ y'_0(x) = 1.91103,\ y''_0(x) = 0,\ y'''_0(x) = -1.15874.$

$\alpha = 4$					
6^{th} *iteration*				$J = 10$	
x	y_{Exact} [75]	y_{GDQR} [75]	E_{GDQR} [75]	y_{Haar}	E_{Haar}
0.0	0	0	0	0	0
0.7	1.2692	1.2693	-0.002	1.2692	0.0025
1.4	2.0990	2.0993	-0.010	2.0990	0.0037
2.1	2.0929	2.0933	-0.019	2.0928	0.0048
2.8	1.2541	1.2545	-0.027	1.2541	0.0059
3.5	-0.0179	-0.0177	0.813	-0.0179	-0.1679
4.2	-1.2843	-1.2842	0.003	-1.2843	-0.0010
4.9	1.0880	-2.1051	-0.004	1.0879	0.0063
5.6	-2.0866	-2.0868	-0.014	-2.0865	-0.0046
6.3	-1.2390	-1.2395	-0.039	-1.2389	-0.0083
7.0	0.0357	0.0352	1.276	0.0358	0.2095
7.7	1.2992	1.2990	0.013	1.2992	0.0010
8.4	2.1109	2.1111	-0.009	2.1108	0.0031
9.1	2.0801	2.0805	-0.021	2.0800	0.0056
9.8	1.2237	1.2243	-0.044	1.2236	0.0099
10.5	-0.0536	-0.0529	1.146	-0.0537	-0.1965
11.2	-1.3141	-1.3136	0.037	-1.3141	-0.0042
11.9	-2.1166	-2.1166	-0.002	-2.1166	-0.0022
12.6	-2.0734	-2.0741	-0.030	-2.0733	-0.0068
13.3	-1.2084	-1.2093	-0.071	-1.2082	-0.0136
14.0	0.0714	0.0706	1.057	0.0715	0.1888

Table 4.8: Higher order oscillation equation: Comparison of solutions by the Haar wavelet-quasilinearization technique at 6^{th} iteration and level of resolutions $J = 10$ with generalized differential quadrature rule (GDQR) method [75]and exact solution.

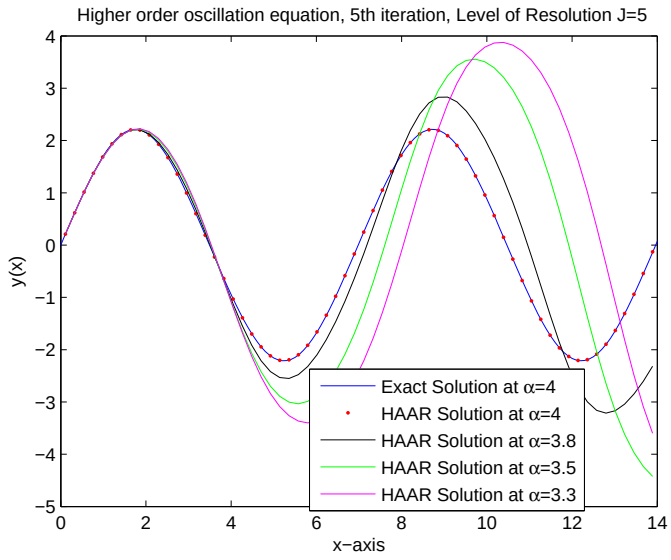

Figure 4.7: Higher order oscillation equation: Exact solution at $\alpha = 4$ and solution by Haar wavelet-quasilinearization technique at $J = 5$ and different values of α.

Solution by the Haar wavelet quasilinearization technique at 6^{th}, fixed level of resolution $J = 10$ and order of equation (4.2.8) $\alpha = 4$ is shown in Table 4.8. It shows that obtained solution is more accurate as compared to generalized differential quadrature rule (GDQR) [75]. E_{GDQE} and E_{Haar} represent the percentage error of generalized differential quadrature rule and the Haar wavelet quasilinearization technique respectively.
We fix the solutions at fifth iteration, level of resolution $J = 5$ and plot the solution at different values of α are shown in Figure 4.7 along with the exact solution at $\alpha = 4$ and Figure 4.7 shows that solution by the Haar wavelet quasilinearization technique converge to the exact solution, when α approaches to 4.

4.2.4 Conclusion

It is shown that Haar wavelet method with quasilinearization technique gives good results when applied to fractional order nonlinear oscillation equations. The results obtained from Haar wavelet quasilinearization technique are better from the results obtained by other methods and are in good agreement with exact solutions or solution by fourth order Runge-Kutta method, as shown in Tables and Figures. The solution of the fractional order, nonlinear oscillation equation converge to the solution of integer order nonlinear oscillation differential equation as shown in Figures 4.3, 4.4, 4.5, 4.6 and 4.7.

Chapter 5

Haar Wavelet Operational Matrix Method for Fractional Nonlinear Partial Differential Equations

The wavelet algorithms for solving partial differential equations are based on the Galerkin techniques or on the collocation method. Haar wavelet algorithm is based on the collocation method. Numerical solution of linear fractional partial differential equations by Haar wavelet method has been given in [131]. Convergence analysis of Haar wavelet method is also discussed. Lepik [73] organized a method by using two dimensional Haar wavelets for solving partial differential equations, he considered the diffusion and Poisson equations as test problems. An efficient numerical method for the solution of nonlinear partial differential equations based on the Haar wavelets approach is introduced by Celik [22,23], and tested in the case of generalized Burgers−Huxley equation and magnetohydrodynamic flow equations. Hariharan et al. [53,54] developed a solution for Fisher′s equation, Nowell−whitehead equation, Cahn−Allen equation, FitzHugh−Nagumo equation, Burger′s equation and the Burgers−Fisher equation by Haar wavelet method.

In this chapter, we developed a method by combining the Haar wavelet method and quasilinearization technique for numerical solutions of nonlinear fractional partial differential equations. We discretize the nonlinear fractional partial differential equation by quasilinearization technique and then convert the obtained discretized equation into a Sylvester equation by the Haar wavelet technique to get the solution. The convergence analysis of the method is also investigated. The obtained numerical results are compared with the exact solution and the numerical solution obtained by other methods. Several problems are solved to show the applicability of the Haar wavelet method with quasilinearization technique.

5.1 Quasilinearization for Partial Differential Equation

The quasilinearization approach [7] is a generalized Newton-Raphson technique for functional equations. It converges quadratically to the exact solution, if there is convergence at all, and it has monotone convergence.

Quasilinearization for the nonlinear partial differential equations is as follows. Consider a class of nonlinear fractional partial differential equations

$$\frac{\partial^\alpha u}{\partial t^\alpha} = u_{xx} + h(u, u_x),\ 0 < x < 1,\ t \geq 0, 0 < \alpha < 1, \tag{5.1.1}$$

with the initial condition

$$u(x, 0) = g(x),$$

and boundary conditions

$$u(0, t) = u(1, t) = 0,$$

where h is the nonlinear function of u and u_x. Quasilinearization approach for equation (5.1.1) implies

$$\begin{aligned} \tfrac{\partial^\alpha u_{r+1}}{\partial t^\alpha} = (u_{r+1})_{xx} + h(u_r, (u_r)_x) + (u_{r+1} - u_r)h_u(u_r, (u_r)_x) \\ +((u_{r+1})_x - (u_r)_x)h_{u_x}(u_r, (u_r)_x),\ r \geq 0, \end{aligned} \tag{5.1.2}$$

with the initial and boundary conditions

$$u_{r+1}(x, 0) = g(x),\ 0 < x < 1,$$

$$u_{r+1}(0, t) = u_{r+1}(1, t) = 0,\ t \geq 0.$$

Starting with an initial approximation $u_0(x, t)$, we have a linear equation for each $u_{r+1},\ r \geq 0$.

5.2 Implementation of Method

In this section, we describes the procedure of implementing the method for fractional nonlinear partial differential equation. The first step is to convert the fractional nonlinear partial differential equation into discrete fractional partial differential equation by quasilinearization technique, as described in section 5.1. The next step is to solve the obtained discretized fractional partial differential equation by the Haar wavelet operational matrix method. Consider the following fractional nonlinear partial differential equation

$$\begin{aligned} \tfrac{\partial^\alpha u}{\partial t^\alpha} - a(x)\tfrac{\partial^\beta u}{\partial x^\beta} + b(x)u\tfrac{\partial^\gamma u}{\partial x^\gamma} + d(x)u^p = f(t, x), \\ 0 < \alpha \leq 2,\ 1 < \beta \leq 2,\ 0 < \gamma \leq 1,\ p \geq 1, \end{aligned} \tag{5.2.1}$$

with the initial and boundary conditions,

$$u(x, 0) = g_1(x),\quad \frac{\partial u}{\partial t}|_{t=0} = g_2(x),\ 0 < x < 1,$$

$$u(0,t) = Y_1(t), \quad u(1,t) = Y_2(t),\ t \geq 0.$$

Apply the quasilinearization technique to equation (5.2.1), we get

$$\begin{aligned} \frac{\partial^\alpha u_{r+1}}{\partial t^\alpha} - a(x)\frac{\partial^\beta u_{r+1}}{\partial x^\beta} + b(x,u_r)\frac{\partial^\gamma u_{r+1}}{\partial x^\gamma} + d(x,u_r,\frac{\partial^\gamma u_r}{\partial x^\gamma})u_{r+1} = f(t,x,u_r,\frac{\partial^\gamma u_r}{\partial x^\gamma}), \\ 0 < \alpha \leq 2,\ 1 < \beta \leq 2,\ 0 < \gamma \leq 1,\ r \geq 0, \end{aligned} \tag{5.2.2}$$

with the initial and boundary conditions,

$$u_{r+1}(x,0) = g_1(x), \quad \frac{\partial u_{r+1}}{\partial t}|_{t=0} = g_2(x),\ 0 < x < 1,$$

$$u_{r+1}(0,t) = Y_1(t), \quad u_{r+1}(1,t) = Y_2(t),\ t \geq 0,$$

where $b(x,u_r) = b(x)u_r$, $d(x,u_r,\frac{\partial^\gamma u_r}{\partial x^\gamma}) = b(x)\frac{\partial^\gamma u_r}{\partial x^\gamma} + d(x)pu_r^{p-1}$ and
$f(t,x,u_r,\frac{\partial^\gamma u_r}{\partial x^\gamma}) = f(t,x) - b(x)u_r\frac{\partial^\gamma u_r}{\partial x^\gamma} - d(x)u_r^p + u_r\Big(b(x)\frac{\partial^\gamma u_r}{\partial x^\gamma} + d(x)pu_r^{p-1}\Big) + b(x)u_r\frac{\partial^\gamma u_r}{\partial x^\gamma}$.
Apply the Haar wavelet method to equation (5.2.2), we approximate the higher order term by the Haar wavelet series as

$$\frac{\partial^\beta u_{r+1}}{\partial x^\beta} = \sum_{l=1}^{2M}\sum_{i=1}^{2M} c_{l,i}^{r+1}h_l(x)h_i(t) = H^T(x)C^{r+1}H(t). \tag{5.2.3}$$

Apply the fractional integral operator I_x^β on equation (5.2.3)

$$u_{r+1}(x,t) = \sum_{l=1}^{2M}\sum_{i=1}^{2M} c_{l,i}^{r+1}I_x^\beta h_l(x)h_i(t) + p(t)x + q(t), \tag{5.2.4}$$

where $p(t)$ and $q(t)$ are functions of t. Use the boundary conditions and equations (2.1.2) and (2.1.3), we get

$$q(t) = Y_1(t),$$

$$p(t) = -\sum_{l=1}^{2M}\sum_{i=1}^{2M} c_{l,i}^{r+1}(\frac{1}{\Gamma(\beta)}\int_0^1 (1-s)^{\beta-1}h_l(s)ds)h_i(t) + Y_2(t) - Y_1(t),$$

or

$$p(t) = -\sum_{l=1}^{2M}\sum_{i=1}^{2M} c_{l,i}^{r+1}(I_1^\beta h_l(x))h_i(t) + Y_2(t) - Y_1(t).$$

Equation (5.2.4) can be written as

$$u_{r+1}(x,t) = \sum_{l=1}^{2M}\sum_{i=1}^{2M} c_{l,i}^{r+1}p_{\beta,l}(x)h_i(t) - x(\sum_{l=1}^{2M}\sum_{i=1}^{2M} c_{l,i}^{r+1}(I_1^\beta h_l(x))h_i(t)) + x(Y_2(t)-Y_1(t)) + Y_1(t). \tag{5.2.5}$$

Take the Caputo fractional derivative $\frac{\partial^\gamma}{\partial x^\gamma}$, of order γ, to equation (5.2.5)

$$\begin{aligned} \frac{\partial^\gamma u_{r+1}}{\partial x^\gamma} = \sum_{l=1}^{2M}\sum_{i=1}^{2M} c_{l,i}^{r+1}p_{\beta-\gamma,l}(x)h_i(t) - \frac{x^{1-\gamma}}{\Gamma(2-\gamma)}(\sum_{l=1}^{2M}\sum_{i=1}^{2M} c_{l,i}^{r+1}(I_1^\beta h_l(x))h_i(t)) + \\ \frac{x^{1-\gamma}}{\Gamma(2-\gamma)}(Y_2(t) - Y_1(t)). \end{aligned} \tag{5.2.6}$$

We introduce some notations which will be used in this section for simplification,

$$\begin{aligned} S(x,t) &= \frac{-b(x,u_r)x^{1-\gamma}}{\Gamma(2-\gamma)}(Y_2(t)-Y_1(t)) - xd(x,u_r,\frac{\partial^\gamma u_r}{\partial x^\gamma})(Y_2(t)-Y_1(t)) - d(x,u_r,\frac{\partial^\gamma u_r}{\partial x^\gamma})Y_1(t) \\ &\quad + f(t,x,u_r,\frac{\partial^\gamma u_r}{\partial x^\gamma}) \\ &= \sum_{l=1}^{2M}\sum_{i=1}^{2M} m_{l,i}h_l(x)h_i(t), \end{aligned}$$

where $m_{l,i} =< h_l(x), < S(x,t), h_i(t) >>$. Use equations (5.2.3), (5.2.5) and (5.2.6) in equation (5.2.2), to obtain

$$\begin{aligned} \frac{\partial^\alpha u_{r+1}}{\partial t^\alpha} =& a(x)\sum_{l=1}^{2M}\sum_{i=1}^{2M} c_{l,i}^{r+1}h_l(x)h_i(t) - b(x,u_r)\sum_{l=1}^{2M}\sum_{i=1}^{2M} c_{l,i}^{r+1}p_{\beta-\gamma,l}(x)h_i(t) \\ &+ \frac{b(x,u_r)x^{1-\gamma}}{\Gamma(2-\gamma)}(\sum_{l=1}^{2M}\sum_{i=1}^{2M} c_{l,i}^{r+1}C_{\beta,l}h_i(t)) - d(x,u_r,\frac{\partial^\gamma u_r}{\partial x^\gamma})\sum_{l=1}^{2M}\sum_{i=1}^{2M} c_{l,i}^{r+1}p_{\beta,l}(x)h_i(t) \\ &+ xd(x,u_r,\frac{\partial^\gamma u_r}{\partial x^\gamma})(\sum_{l=1}^{2M}\sum_{i=1}^{2M} c_{l,i}^{r+1}C_{\beta,l}h_i(t)) + \sum_{l=1}^{2M}\sum_{i=1}^{2M} m_{l,i}h_l(x)h_i(t). \end{aligned} \tag{5.2.7}$$

where $C_{\beta,l} = I_1^\beta h_l(x)$ and is given in section 2.3. Apply fractional integral operator I_t^α to (5.2.7) and use the initial conditions to obtain,

$$\begin{aligned} u_{r+1}(x,t) =& a(x)\sum_{l=1}^{2M}\sum_{i=1}^{2M} c_{l,i}^{r+1}h_l(x)p_{\alpha,i}(t) - b(x,u_r)\sum_{l=1}^{2M}\sum_{i=1}^{2M} c_{l,i}^{r+1}p_{\beta-\gamma,l}(x)p_{\alpha,i}(t) + \\ &\frac{b(x,u_r)x^{1-\gamma}}{\Gamma(2-\gamma)}(\sum_{l=1}^{2M}\sum_{i=1}^{2M} c_{l,i}^{r+1}C_{\beta,l}p_{\alpha,i}(t)) - d(x,u_r,\frac{\partial^\gamma u_r}{\partial x^\gamma})\sum_{l=1}^{2M}\sum_{i=1}^{2M} c_{l,i}^{r+1}p_{\beta,l}(x)p_{\alpha,i}(t) \\ &+ xd(x,u_r,\frac{\partial^\gamma u_r}{\partial x^\gamma})(\sum_{l=1}^{2M}\sum_{i=1}^{2M} c_{l,i}^{r+1}C_{\beta,l}p_{\alpha,i}(t)) + \sum_{l=1}^{2M}\sum_{i=1}^{2M} m_{l,i}h_l(x)p_{\alpha,i}(t) + g_2(x)t \\ &+ g_1(x). \end{aligned} \tag{5.2.8}$$

Let $K(x,t) = -g_2(x)t - g_1(x) + x(Y_2(t) - Y_1(t)) + Y_1(t)$. From equation (5.2.5) and (5.2.8),

$$\begin{aligned} &\sum_{l=1}^{2M}\sum_{i=1}^{2M} c_{l,i}^{r+1}p_{\beta,l}(x)h_i(t) - x(\sum_{l=1}^{2M}\sum_{i=1}^{2M} c_{l,i}^{r+1}C_{\beta,l}h_i(t)) + K(x,t) = a(x)\sum_{l=1}^{2M}\sum_{i=1}^{2M} c_{l,i}^{r+1}h_l(x)p_{\alpha,i}(t) \\ &- b(x,u_r)\sum_{l=1}^{2M}\sum_{i=1}^{2M} c_{l,i}^{r+1}p_{\beta-\gamma,l}(x)p_{\alpha,i}(t) + \frac{b(x,u_r)x^{1-\gamma}}{\Gamma(2-\gamma)}(\sum_{l=1}^{2M}\sum_{i=1}^{2M} c_{l,i}^{r+1}C_{\beta,l}p_{\alpha,i}(t)) \\ &- d(x,u_r,\frac{\partial^\gamma u_r}{\partial x^\gamma})\sum_{l=1}^{2M}\sum_{i=1}^{2M} c_{l,i}^{r+1}p_{\beta,l}(x)p_{\alpha,i}(t) + xd(x,u_r,\frac{\partial^\gamma u_r}{\partial x^\gamma})(\sum_{l=1}^{2M}\sum_{i=1}^{2M} c_{l,i}^{r+1}C_{\beta,l}p_{\alpha,i}(t)) \\ &+ \sum_{l=1}^{2M}\sum_{i=1}^{2M} m_{l,i}h_l(x)p_{\alpha,i}(t). \end{aligned} \tag{5.2.9}$$

In discrete form, equation (5.2.9) can be written as

$$\begin{aligned}
&\sum_{l=1}^{2M}\sum_{i=1}^{2M} c_{l,i}^{r+1} p_{\beta,l}(x_c(j))h_i(t_c(n)) - x_c(j)(\sum_{l=1}^{2M}\sum_{i=1}^{2M} c_{l,i}^{r+1} C_{\beta,l} h_i(t_c(n))) + K(x_c(j),t_c(n)) \\
&= a(x_c(j))\sum_{l=1}^{2M}\sum_{i=1}^{2M} c_{l,i}^{r+1} h_l(x_c(j))p_{\alpha,i}(t_c(n)) - b(x_c(j),u_r)\sum_{l=1}^{2M}\sum_{i=1}^{2M} c_{l,i}^{r+1} p_{\beta-\gamma,l}(x_c(j))p_{\alpha,i}(t_c(n)) \\
&+ \frac{b(x_c(j),u_r)x_c(j)^{1-\gamma}}{\Gamma(2-\gamma)}(\sum_{l=1}^{2M}\sum_{i=1}^{2M} c_{l,i}^{r+1} C_{\beta,l} p_{\alpha,i}(t_c(n))) - d(x_c(j),u_r,\frac{\partial^\gamma u_r}{\partial x^\gamma}) \\
&\sum_{l=1}^{2M}\sum_{i=1}^{2M} c_{l,i}^{r+1} p_{\beta,l}(x_c(j))p_{\alpha,i}(t_c(n)) + x_c(j)d(x_c(j),u_r,\frac{\partial^\gamma u_r}{\partial x^\gamma})(\sum_{l=1}^{2M}\sum_{i=1}^{2M} c_{l,i}^{r+1} C_{\beta,l} p_{\alpha,i}(t_c(n))) \\
&+ \sum_{l=1}^{2M}\sum_{i=1}^{2M} m_{l,i} h_l(x_c(j))p_{\alpha,i}(t_c(n)),
\end{aligned} \tag{5.2.10}$$

where $x_c(j) = \frac{2j-1}{4M},\ t_c(n) = \frac{2j-1}{4M},\ j,n = 1,2,...,2M$, are collocation points.
In matrix form, equation (5.2.10) can be written as

$$\begin{aligned}
&P^\beta C^{r+1}H - \mathbf{V}^{\beta,1,f(x)}C^{r+1}H - (AH^TC^{r+1}\mathbf{P}_t^\alpha - B\mathbf{P}_x^{\beta-\gamma}C^{r+1}\mathbf{P}_t^\alpha + \mathbf{V}^{\beta,1,g(x)}C^{r+1}\mathbf{P}_t^\alpha \\
&- D\mathbf{P}_x^\beta C^{r+1}\mathbf{P}_t^\alpha + D\mathbf{V}^{\beta,1,f(x)}C^{r+1}\mathbf{P}_t^\alpha) - H^TM'\mathbf{P}_t^\alpha + \mathbf{K} = 0,
\end{aligned} \tag{5.2.11}$$

where H is the $2M \times 2M$ Haar matrix, $\mathbf{V}^{\beta,1,f(x)} = f(x)I_1^\beta H^T$ and $\mathbf{V}^{\beta,1,g(x)} = u_r g(x) I_1^\beta H^T$ are the $2M \times 2M$ fractional integration matrices for boundary value problem and $\mathbf{P}_x^\beta = I_x^\beta H^T$, $\mathbf{P}_t^\alpha = I_t^\alpha H$, and $\mathbf{P}_x^{\beta-\gamma} = I_x^{\beta-\gamma}H^T$ are the $2M\times 2M$ matrices of fractional integration of the Haar functions. These matrices are derived in section 2.3. Also $\mathbf{K} = K(x_c(j),t_c(j)),\ j = 1,2,\cdots,2M$ is the $2M \times 2M$ matrix determined at the collocation points, M' is $2M \times 2M$ coefficient matrix determined by the inner products $m_{l,i} =< h_l(x), < S(x,t), h_i(t) >>$, and $f(x) = x$, $g(x) = \frac{b(x)x^{1-\gamma}}{\Gamma(2-\gamma)}$.
Let $Q := (AH^T - B\mathbf{P}_x^{\beta-\gamma} + \mathbf{V}^{\beta,1,g(x)} - D\mathbf{P}_x^\beta + D\mathbf{V}^{\beta,1,f(x)})^{-1}$ is the $2M \times 2M$ matrix, where A, B and D are the diagonal matrices and are given by

$$A = \begin{bmatrix} a(x_1) & 0 & \cdots & 0 \\ 0 & a(x_2) & \cdots & 0 \\ \vdots & \vdots & \ddots & \vdots \\ 0 & 0 & \cdots & a(x_{2M}) \end{bmatrix},\ B = \begin{bmatrix} b(x_1) & 0 & \cdots & 0 \\ 0 & b(x_2) & \cdots & 0 \\ \vdots & \vdots & \ddots & \vdots \\ 0 & 0 & \cdots & b(x_{2M}) \end{bmatrix}$$

$$\text{and } D = \begin{bmatrix} d(x_1) & 0 & \cdots & 0 \\ 0 & d(x_2) & \cdots & 0 \\ \vdots & \vdots & \ddots & \vdots \\ 0 & 0 & \cdots & d(x_{2M}) \end{bmatrix}$$

Equation (5.2.11) can be written as

$$Q(\mathbf{P}_x^{\beta} - \mathbf{V}^{\beta,1,f(x)})C^{r+1} - C^{r+1}\mathbf{P}_t^{\alpha}H^{-1} + Q(\mathbf{K} - H^T M'\mathbf{P}_t^{\alpha})H^{-1} = 0, \tag{5.2.12}$$

which is the Sylvester equation. Solve equation (5.2.12) for C^{r+1}, which is $2M \times 2M$ coefficient matrix, and substituting C^{r+1} in equation (5.2.5) or (5.2.8), we get solution $u_{r+1}(x,t)$ at the collocation points.

In particular, given an initial approximation $u_0(x,t)$, we get a linear fractional partial differential equation in $u_1(x,t)$ by substituting $r = 0$ in equation (5.2.2), which is solved by above procedure to get $u_1(x,t)$ at the collocation points. Similarly for $r = 1$, we obtain $u_2(x,t)$ and so on.

5.3 Convergence of Method

Let us assume that $u_{r+1}(x,t)$ be a continuously differentiable function on $[0,1)\times[0,1)$, and $|\frac{\partial u_{r+1}(x,t)}{\partial x}| \leq K$, for all $(x,t) \in [0,1) \times [0,1)$, $K > 0$.

Suppose $u_{r+1}^M(x,t)$ be the Haar wavelet approximation for the function $u(x,t)$ at the $(r+1)th$ iteration, that is,

$$u_{r+1}(x,t) \approx u_{r+1}^M(x,t) = \sum_{l=1}^{2M}\sum_{p=1}^{2M} c_{lp}^{r+1} h_l(x) h_p(t). \tag{5.3.1}$$

L^2 error norm for the Haar wavelet approximation of $u(x,t)$ at the $(r+1)th$ iteration is given as

$$\begin{aligned}
&\|u_{r+1}(x,t) - u_{r+1}^M(x,t)\|^2 = \int_0^1\int_0^1 (u_{r+1}(x,t) - u_{r+1}^M(x,t))^2 dxdt,\\
&= \sum_{l=2M+1}^{\infty}\sum_{p=2M+1}^{\infty}\sum_{l'=2M+1}^{\infty}\sum_{p'=2M+1}^{\infty} c_{lp}^{r+1} c_{l'p'}^{r+1}\Big(\int_0^1 h_l(x)h_{l'}(x)dx\Big)\Big(\int_0^1 h_p(t)h_{p'}(t)dt\Big).
\end{aligned}$$

By using orthogonality of Haar wavelet, we get

$$\|u_{r+1}(x,t) - u_{r+1}^M(x,t)\|^2 = \sum_{l=2M+1}^{\infty}\sum_{p=2M+1}^{\infty}\big(c_{lp}^{r+1}\big)^2, \tag{5.3.2}$$

where $c_{lp}^{r+1} = \langle h_l(x), \langle u_{r+1}(x,t), h_p(t)\rangle\rangle$. Consider the inner product of $u_{r+1}(x,t)$ and $h_p(t)$, we get

$$\begin{aligned}
\langle u_{r+1}(x,t), h_p(t)\rangle &= \int_0^1 u_{r+1}(x,t)h_p(t)dt,\\
&= 2^{\frac{j}{2}}\left\{\int_{\frac{k}{m}}^{\frac{k+0.5}{m}} u_{r+1}(x,t)dt - \int_{\frac{k+0.5}{m}}^{\frac{k+1}{m}} u_{r+1}(x,t)dt\right\},
\end{aligned} \tag{5.3.3}$$

where $2^{\frac{j}{2}}$ is the normalizing factor of the Haar wavelet. By using the mean value theorem

$$\exists\ t_1,\ t_2\ : \frac{k}{m} \leq t_1 < \frac{k+0.5}{m},\ \frac{k+0.5}{m} \leq t_2 < \frac{k+1}{m}$$

such that

$$\begin{aligned}
\langle u_{r+1}(x,t), h_p(t)\rangle &= 2^{\frac{j}{2}}\big\{(\tfrac{k+0.5}{m} - \tfrac{k}{m})u_{r+1}(x,t_1) - (\tfrac{k+1}{m} - \tfrac{k+0.5}{m})u_{r+1}(x,t_2)\big\},\\
&= 2^{-\frac{j}{2}-1}\big(u_{r+1}(x,t_1) - u_{r+1}(x,t_2)\big).
\end{aligned} \tag{5.3.4}$$

Taking the inner product of $h_l(x)$ with the obtained function (5.3.4), we have

$$\begin{aligned}
c_{lp}^{r+1} &= \langle h_l(x), \langle u_{r+1}(x,t), h_p(t)\rangle\rangle, \\
&= 2^{-\frac{j}{2}-1}\int_0^1 h_l(x)\big(u_{r+1}(x,t_1) - u_{r+1}(x,t_2)\big)dx, \\
&= 2^{-\frac{j}{2}-1}\bigg(\int_0^1 h_l(x)u_{r+1}(x,t_1)dx - \int_0^1 h_l(x)u_{r+1}(x,t_2)dx\bigg), \\
&= 2^{-\frac{j}{2}-1}\bigg\{2^{\frac{j}{2}}\bigg[\int_{\frac{k}{m}}^{\frac{k+0.5}{m}} u_{r+1}(x,t_1)dx - \int_{\frac{k+0.5}{m}}^{\frac{k+1}{m}} u_{r+1}(x,t_1)dx \\
&\quad - \int_{\frac{k}{m}}^{\frac{k+0.5}{m}} u_{r+1}(x,t_2)dx + \int_{\frac{k+0.5}{m}}^{\frac{k+1}{m}} u_{r+1}(x,t_2)dx\bigg]\bigg\},
\end{aligned}$$

Using the mean value theorem to obtain

$$\exists\ x_1,\ x_2,\ x_3,\ x_4,\ \text{such that } \frac{k}{m} \le x_1,\ x_2 < \frac{k+0.5}{m},\ \frac{k+0.5}{m} \le x_3,\ x_4 < \frac{k+1}{m}$$

$$\begin{aligned}
c_{lp}^{r+1} &= \tfrac{1}{2}\bigg[(\tfrac{k+0.5}{m} - \tfrac{k}{m})u_{r+1}(x_1,t_1) - (\tfrac{k+1}{m} - \tfrac{k+0.5}{m})u_{r+1}(x_3,t_1) - (\tfrac{k+0.5}{m} - \tfrac{k}{m})u_{r+1}(x_2,t_2) \\
&\quad +(\tfrac{k+1}{m} - \tfrac{k+0.5}{m})u_{r+1}(x_4,t_2)\bigg], \\
&= \tfrac{1}{2^{j+2}}\bigg[(u_{r+1}(x_1,t_1) - u_{r+1}(x_3,t_1)) - (u_{r+1}(x_2,t_2) - u_{r+1}(x_4,t_2))\bigg],
\end{aligned}$$

or

$$(c_{lp}^{r+1})^2 = \tfrac{1}{2^{2j+4}}\bigg[(u_{r+1}(x_1,t_1) - u_{r+1}(x_3,t_1)) - (u_{r+1}(x_2,t_2) - u_{r+1}(x_4,t_2))\bigg]^2. \tag{5.3.5}$$

Again using mean value theorem

$$\exists\ \eta_1, \eta_2\ :\ x_1 \le \eta_1 < x_3,\ x_2 \le \eta_2 < x_4$$

such that

$$\begin{aligned}
(c_{lp}^{r+1})^2 &= \tfrac{1}{2^{2j+4}}\bigg[(x_3 - x_1)\tfrac{\partial u(\eta_1,t_1)}{\partial x} - (x_4 - x_2)\tfrac{\partial u(\eta_2,t_2)}{\partial x}\bigg]^2, \\
&\le \tfrac{1}{2^{2j+4}}\bigg[(x_3 - x_1)^2\bigg(\tfrac{\partial u(\eta_1,t_1)}{\partial x}\bigg)^2 + (x_4 - x_2)^2\bigg(\tfrac{\partial u(\eta_2,t_2)}{\partial x}\bigg)^2 \\
&\quad +2(x_3 - x_1)(x_4 - x_2)\big|\tfrac{\partial u(\eta_1,t_1)}{\partial x}\big|\big|\tfrac{\partial u(\eta_2,t_2)}{\partial x}\big|\bigg], \\
&\le \tfrac{1}{2^{2j+4}}\big(2^{-2j}K^2 + 2^{-2j}K^2 + 2\times 2^{-2j}K^2\big), \\
&= \tfrac{K^2}{2^{4j+2}}.
\end{aligned} \tag{5.3.6}$$

Using $(c_{lp}^{r+1})^2$ in equation (5.3.2), we get

$$
\begin{aligned}
\|u_{r+1}(x,t) - u^M_{r+1}(x,t)\|^2 &= \sum_{l=2M+1}^{\infty}\sum_{p=2M+1}^{\infty}\left(c^{r+1}_{lp}\right)^2, \\
&= \sum_{j=J+1}^{\infty}\left(\sum_{l=2^j+1}^{2^{j+1}}\sum_{p=2^j+1}^{2^{j+1}}\left(c^{r+1}_{lp}\right)^2\right), \\
&\leq \sum_{j=J+1}^{\infty}\left(\sum_{l=2^j+1}^{2^{j+1}}\sum_{p=2^j+1}^{2^{j+1}}\frac{K^2}{2^{4j+2}}\right), \\
&= K^2\sum_{j=J+1}^{\infty}\frac{2^{2j}}{2^{2(2j+1)}}, \\
&= K^2\sum_{j=J+1}^{\infty}\frac{1}{2^{2j+2}}, \\
&= K^2\frac{2^{-2(J+1)}}{3}.
\end{aligned}
$$

This implies that

$$
\|u_{r+1}(x,t) - u^M_{r+1}(x,t)\|^2 \leq \frac{K^2}{3}\frac{1}{(2M)^2}, \tag{5.3.7}
$$

where $M = 2^J$ and equation (5.3.7) implies that error between the exact and approximate solution at the $(r+1)th$ iteration is inversely proportional to the maximal level of resolution, J. This implies that $u^M_{r+1}(x,t)$ converges to $u_{r+1}(x,t)$ as $J \to \infty$. Since $u_{r+1}(x,t)$ is obtained at $(r+1)th$ iteration of quasilinearization technique, according to convergence analysis of quasilinearization technique [7] which states that $u_{r+1}(x,t)$ converges to $u(x,t)$ as r approaches to infinity, if there is convergence at all. This suggest that solution by Haar wavelet quasilinearization technique, $u^M_{r+1}(x,t)$, converges to $u(x,t)$ as J and r approaches to infinity.

5.4 Solution of Nonlinear Fractional Partial Differential Equation

In this section, we implement the Haar wavelet quasilinearization method on some nonlinear fractional initial boundary value problems and compare the results with exact solution and results obtained by the other methods.

5.4.1 Fractional Generalized Burger–Fisher Equation

Consider the fractional time derivative generalized Burger–Fisher equation,

$$
\frac{\partial^\alpha u}{\partial t^\alpha} - \frac{\partial^2 u}{\partial x^2} + au^\gamma\frac{\partial u}{\partial x} + bu(u^\gamma - 1) = 0, 0 \leq x \leq 1,\ t \geq 0,\ 0 < \alpha \leq 1, \tag{5.4.1}
$$

subject to the initial and boundary conditions

$$
u(x,0) = (\frac{1}{2} - \frac{1}{2}\tanh(\frac{a\gamma}{2(1+\gamma)}x))^{\frac{1}{\gamma}} = L(x),
$$

$$
u(0,t) = (\frac{1}{2} - \frac{1}{2}\tanh(\frac{a\gamma}{2(1+\gamma)}[-(\frac{a^2 + b(1+\gamma^2)}{a(1+\gamma)})t]))^{\frac{1}{\gamma}} = E(t),
$$

$$u(1,t) = (\frac{1}{2} - \frac{1}{2}\tanh(\frac{a\gamma}{2(1+\gamma)}[1 - (\frac{a^2 + b(1+\gamma^2)}{a(1+\gamma)})t]))^{\frac{1}{\gamma}} = F(t),$$

The exact solution, when $\alpha = 1$, is [18]:

$$u(x,t) = (\frac{1}{2} - \frac{1}{2}\tanh(\frac{a\gamma}{2(1+\gamma)}[x - (\frac{a^2 + b(1+\gamma^2)}{a(1+\gamma)})t]))^{\frac{1}{\gamma}}. \tag{5.4.2}$$

Applying the quasilinearized technique to equation (5.4.1), we get

$$\frac{\partial^\alpha u_{r+1}}{\partial t^\alpha} - \frac{\partial^2 u_{r+1}}{\partial x^2} - u_{r+1}(b+Y) + V(u_{r+1})_x = Z,\ 0 \le x \le 1,\ t \ge 0,\ r \ge 0 \tag{5.4.3}$$

with the initial and boundary conditions

$$u_{r+1}(x,0) = L(x),$$

$$u_{r+1}(0,t) = E(t),\ u_{r+1}(1,t) = F(t),$$

where $Y = -a\gamma(u_r)^{\gamma-1}(u_r)_x - b(\gamma+1)(u_r)^\gamma,\ Z = -b(u_r)^{\gamma+1} - Yu_r,\ V = a(u_r)^\gamma$.
Now we apply the Haar wavelet method to discretized equation (5.4.3), as described in section 5.2, we get the solution at the collocation points.

3^{rd} *iteration*		$J = 5$				
x	t	u_{Haar}	u_{Exact}	E_{Haar}	E_{RDTM} [64]	E_{VIM} [64]
0.01	0.02	0.49999875125	0.49999875125	5.55112e-017	0.49994e-05	2.50311e-03
	0.04	0.49999875250	0.49999875250	1.11022e-016	0.49994e-05	2.50811e-03
	0.06	0.49999875375	0.49999875375	1.11022e-016	1.49994e-05	2.51312e-03
	0.08	0.49999875500	0.49999875500	1.11022e-016	1.99994e-05	2.51812e-03
0.04	0.02	0.49999500125	0.49999500125	5.55112e-017	0.49975e-05	9.99620e-03
	0.04	0.49999500250	0.49999500250	1.11022e-016	0.99975e-05	1.00012e-02
	0.06	0.49999500375	0.49999500375	5.55112e-017	1.49975e-05	1.00062e-02
	0.08	0.49999500500	0.49999500500	1.11022e-016	1.99975e-05	1.00112e-02
0.08	0.02	0.49999000125	0.49999000125	1.66533e-016	0.49950e-05	1.99794e-02
	0.04	0.49999000250	0.49999000250	1.11022e-016	0.99950e-05	1.99844e-02
	0.06	0.49999000375	0.49999000375	1.11022e-016	1.49950e-05	1.99894e-02
	0.08	0.49999000500	0.49999000500	5.55112e-017	1.99950e-05	1.99944e-02

Table 5.1: Comparison of solution by the Haar wavelet–quasilinearization technique u_{Haar}, at 3^{rd} iteration with fix level of resolution, $J = 5$ and $\alpha = 1$, with exact solution u_{Exact}, solution by reduced differential transform method and variational iteration method, by fixing $a = 0.001, b = 0.001, \gamma = 1$.

3^{rd} *iteration*		$J = 5$			
t	x	u_{Haar}	u_{Exact}	E_{Haar}	E_{RDTM} [64]
0.01	0.02	0.707104	0.707104	3.98681e-013	4.7133e-06
	0.04	0.707102	0.707102	1.11466e-013	9.4271e-06
	0.06	0.707100	0.707100	5.05040e-013	1 .4142e-05
	0.08	0.707097	0.707097	5.23914e-013	1 .8855e-05
0.04	0.02	0.707104	0.707104	3.80584e-013	4.7117e-06
	0.04	0.707102	0.707102	7.54951e-014	9.4260e-06
	0.06	0.707100	0.707100	4.51750e-013	1 .4140e-05
	0.08	0.707097	0.707097	4.54081e-013	1 .8854e-05
0.08	0.02	0.707104	0.707104	3.68705e-013	4.7104e-06
	0.04	0.707102	0.707102	5.19584e-014	9.4241e-06
	0.06	0.707100	0.707100	4.16667e-013	1 .4138e-05
	0.08	0.707097	0.707097	4.07896e-013	1.8852e-05

Table 5.2: Comparison of solution by the Haar wavelet–quasilinearization technique u_{Haar}, at 3^{rd} iteration, level of resolution $J = 5$ and $\alpha = 1$, with exact solution u_{Exact} and solution by reduced differential transform method, by fixing $a = 0.001, b = 0.001, \gamma = 2$.

3^{rd} *iteration*			$J = 2$		$J = 2$		$J = 2$
		E_{HPM} [102]	E_{Haar}	E_{HPM} [102]	E_{Haar}	E_{HPM} [102]	E_{Haar}
x	t	$a = b = 0.01$	$a = b = 0.01$	$a = b = 0.1$	a=b=0.1	$a = b = 0.5$	a=b=0.5
0.1	0.2	6.28000e-11	2.69179e-12	4.32620e-8	3.78398e-9	6.17680e-6	9.57046e-7
	0.4	5.08000e-11	1.02440e-11	1.08832e-7	1.38803e-8	1.60295e-5	3.50199e-6
	0.6	1.63800e-10	1.64766e-11	1.74575e-7	2.23361e-8	2.58023e-5	5.69371e-6
	0.8	3.02500e-10	9.08112e-12	2.40128e-7	1.48742e-8	3.54471e-5	4.76851e-6
0.4	0.2	3.50000e-10	2.94909e-12	3.85160e-7	6.66689e-9	7.87747e-5	3.83906e-6
	0.4	6.02000e-10	1.06882e-11	6.65330e-7	1.87074e-8	7.89518e-5	7.95768e-6
	0.6	1.65600e-9	1.69744e-11	1.71580e-6	2.76171e-8	2.36284e-4	1.02360e-5
	0.8	2.71000e-9	9.43595e-12	2.76581e-6	1.8565e-8	3.92443e-4	7.75145e-6
0.8	0.2	6.69900e-9	2.94531e-12	7.28031e-6	7.3431e-9	1.24466e-3	6.72227e-6
	0.4	2.69600e-9	1.06647e-11	3.08014e-6	1.9471e-8	6.22452e-4	1.19714e-5
	0.6	1.31100e-9	1.69509e-11	1.12091e-6	2.8278e-8	2.80910e-6	1.39281e-5
	0.8	5.32000e-9	9.42751e-12	5.32152e-6	1.8976e-8	6.28040e-4	9.92739e-6

Table 5.3: Comparison of solution by the Haar wavelet–quasilinearization technique, at 3^{rd} iteration, level of resolution $J = 2$ and $\alpha = 1$, with exact solution and solution by homotopy perturbation method at $\gamma = 1$ and different values of $a,\ b$.

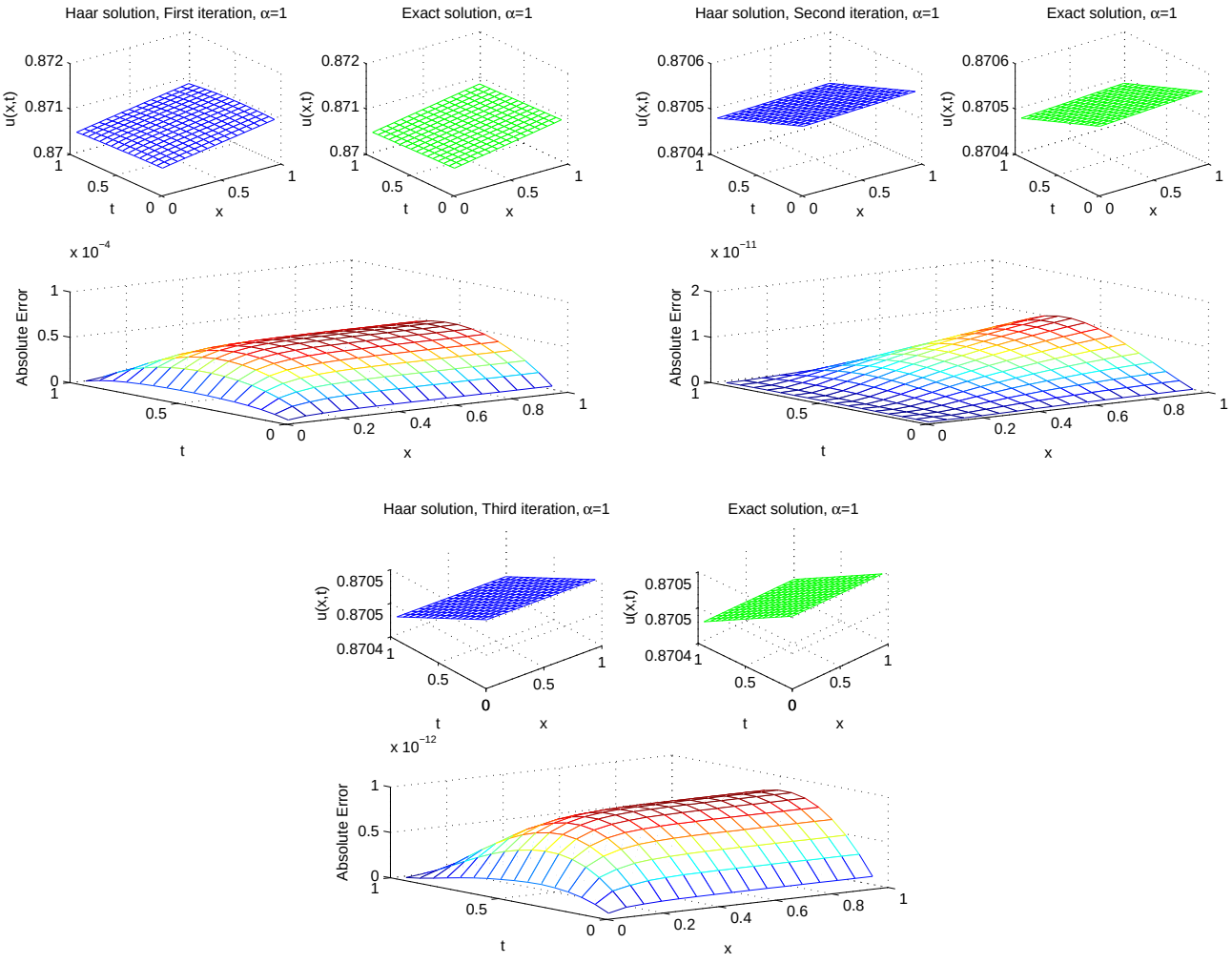

Figure 5.1: Comparison of exact solution and solution by Haar wavelet method of the generalized Burger–Fisher equation ($a = 0.001, b = 0.001, \gamma = 5$) at $\alpha = 1$, level of resolution $J = 3$ and at different iterations.

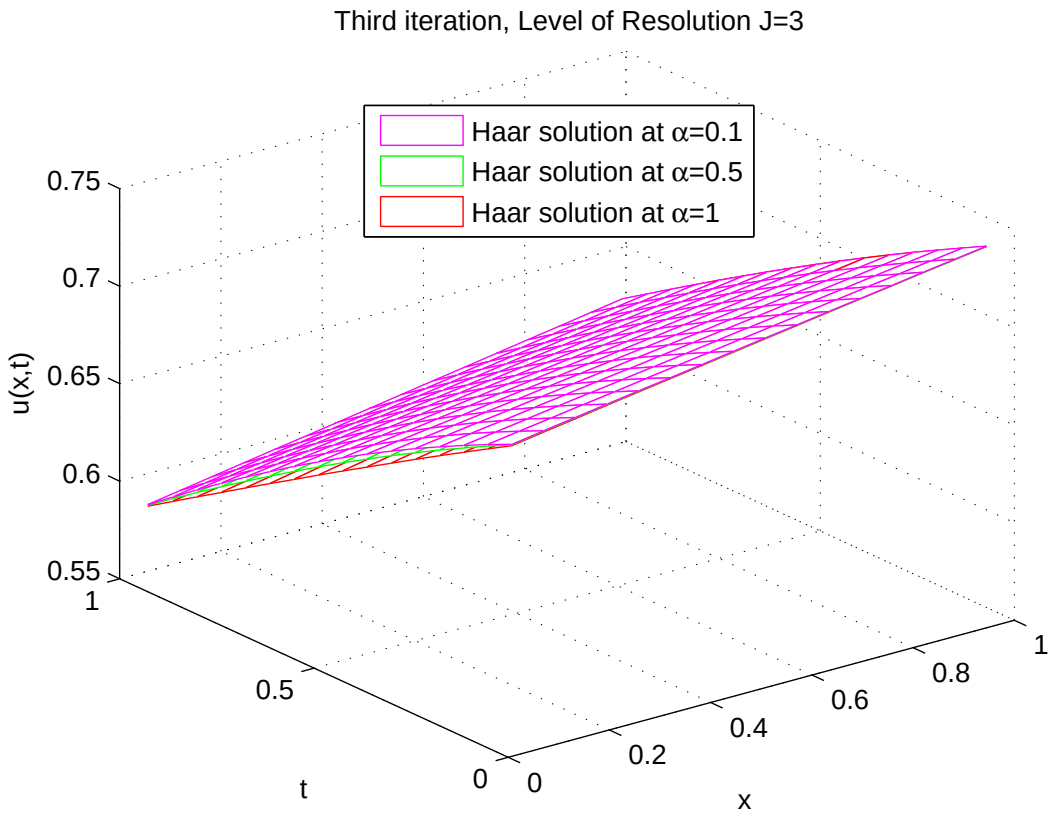

Figure 5.2: Solution by Haar wavelet quasilinearization method of generalized Burger–Fisher equation ($a = 1, b = 1, \gamma = 2$) at different values of α, $J = 3$ and at 3^{rd} iteration.

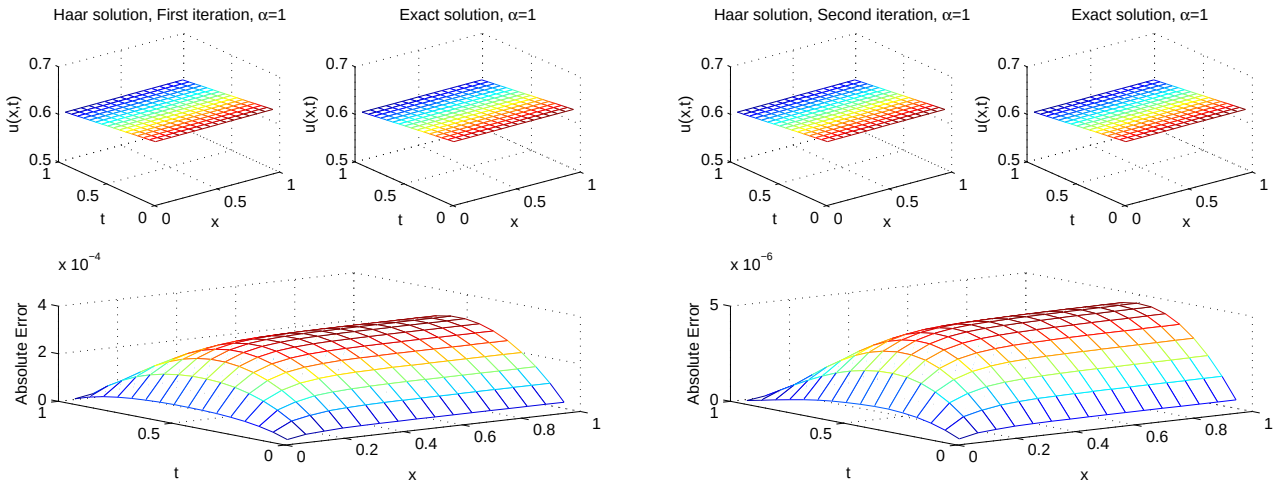

Figure 5.3: Comparison of solutions of generalized Burger equation ($a = 0.2, b = 0, \gamma = 1.5$) by Haar wavelet quasilinearization method with exact solution , at different iteration and $J = 3$.

2^{nd} *iteration*		$J = 2$			$J = 2$		
		u_{Haar}	u_{Exact}	E_{abs}	u_{Haar}	u_{Exact}	E_{abs}
x	t	$a = 0.1$	$a = 0.1$	$a = 0.1$	$a = 0.5$	$a = 0.5$	$a = 0.5$
0.1	0.2	0.4975625	0.4975625	3.7839802e-9	0.4890653	0.4890643	9.5704495e-7
	0.4	0.4950627	0.4950627	1.3880260e-8	0.4765832	0.4765797	3.5019863e-6
	0.6	0.4925630	0.4925630	2.2336092e-8	0.4641300	0.4641243	5.6937119e-6
	0.8	0.4900638	0.4900638	1.4874234e-8	0.4517183	0.4517135	4.7685117e-6
0.4	0.2	0.4977500	0.4977500	6.6668935e-9	0.4937544	0.4937506	3.8390547e-6
	0.4	0.4952502	0.4952501	1.8707414e-8	0.4812670	0.4812590	7.9576764e-6
	0.6	0.4927505	0.4927505	2.7617091e-8	0.4688011	0.4687909	1.0236046e-5
	0.8	0.4902513	0.4902512	1.8564943e-8	0.4563693	0.4563616	7.7514463e-6
0.8	0.2	0.4980000	0.4980000	7.3430706e-9	0.5000072	0.5000005	6.7222677e-6
	0.4	0.4955001	0.4955001	1.9470687e-8	0.4875151	0.4875031	1.1971347e-5
	0.6	0.4930005	0.4930005	2.8277874e-8	0.4750352	0.4750213	1.3928113e-5
	0.8	0.4905012	0.4905011	1.8976366e-8	0.4625806	0.4625707	9.9273816e-6

Table 5.4: Comparison of exact solution of Burger equation ($b = 0,\ \gamma = 1$) at $\alpha = 1$ and solution by Haar wavelet quasilinearization method at second iteration, $J = 2$, for different values of a.

Case 1: Solution of the generalized Burger-Fisher equation at different values of a, b and γ.

We fix the order of the differential equation (5.4.1), $\alpha = 1$, level of resolution, $J = 5$ and take the values $a = 0.001,\ b = 0.001,\ \gamma = 1$. We obtain the results at third iteration and compare with the exact solution, reduced differential transform method [64] and variational iteration method [64] as shown in Table 5.1. Here u_{Haar} represent the solution by Haar wavelet quasilinearization method, u_{Exact} represent the exact solution. E_{Haar}, E_{RDTM} and E_{VIM} represents the absolute error by Haar wavelet quasilinearization method, reduced differential transform method [64] and variational iteration method [64] respectively.

We also solve the generalized Burger–Fisher equation (5.4.1) by taking $a = 0.001$, $b = 0.001$ and $\gamma = 2$, and compare the solution by Haar wavelet quasilinearization method with solution obtained by reduced differential transform method [64] and exact solution as shown in Table 5.2.

We get the solution of the generalized Burger–Fisher equation for $\alpha = 1,\ J = 2, \gamma = 1$ and at different values of a, b as shown in Table 5.3. We compare the solution by Haar wavelet quasilinearization method with homotopy perturbation method [102]. Here E_{Haar}, E_{HPM} denotes the absolute error by Haar wavelet quasilinearization method and homotopy perturbation method [102] respectively.

Table 5.1-5.3 shows that our results are more accurate as compare to reduced differential transform method [64], variational iteration method [64] and homotopy perturbation method [102].

Exact solution at $\alpha = 1$ and the solutions by Haar wavelet quasilinearization method at $\alpha = 1$, $J = 3$ and at different iterations are plotted in Figure 5.1, which shows that absolute error reduces with increasing iterations of Haar wavelet quasilinearization method. Figure 5.1 is used to display the solution of generalized Burger–Fisher equation when $a = 0.001,\ b = 0.001$ and $\gamma = 5$.

Exact solution at $\alpha = 1$ and the solution by Haar wavelet quasilinearization technique at different values of α, are displayed in Figure 5.2. It is observed that solutions of fractional generalized Burger–Fisher equation (5.4.1) converge to the classical generalized Burger-Fisher equation when α approaches to 1.

Case 2: When $b = 0$, equation (5.4.1) is reduced to the generalized Burger equation. Solution by Haar wavelet quasilinearization method of the generalized Burger equation, when $a = 0.2$ and $\gamma = 1.5$, along with exact solution at $\alpha = 1$, is shown in Figure 5.3. It shows that absolute error reduces while increasing iterations.

Case 3: When $b = 0$ and $\gamma = 1$, Equation (5.4.1) is reduced to the Burger equation. Solution by Haar wavelet quasilinearization technique of the Burger equation along with exact solution at $\alpha = 1$ for different values of a are shown in Table 5.4. Here we observe that solution by Haar wavelet quasilinearization method with $J = 2$ and at second iteration are in good agreement with exact solution. Absolute errors E_{abs} are also shown for the sake of accuracy.

5.4.2 Fractional Klein–Gordon Equations

Problem 1 Consider the fractional Klein–Gordon equation,

$$\frac{\partial^\alpha u}{\partial t^\alpha} - \frac{\partial^\beta u}{\partial x^\beta} + u^2 = x^2t^2,\ 1 < \alpha \leq 2,\ 1 < \beta \leq 2. \tag{5.4.4}$$

subject to the initial and boundary conditions

$$u(x,0) = 0,\ u_t(x,0) = x,$$

$$u(0,t) = 0,\ u(1,t) = t.$$

The exact solution, when $\alpha = 2,\ \beta = 2$, is

$$u(x,t) = xt.$$

The quasilinearized form of equation (5.4.4) is

$$\frac{\partial^\alpha u_{r+1}}{\partial t^\alpha} - \frac{\partial^\beta u_{r+1}}{\partial x^\beta} + 2u_r u_{r+1} = x^2t^2 + (u_r)^2,\ 1 < \alpha \leq 2,\ 1 < \beta \leq 2,\ r \geq 0, \tag{5.4.5}$$

subject to the initial and boundary conditions

$$u_{r+1}(x,0) = 0,\ (u_{r+1})_t(x,0) = x,$$

$$u_{r+1}(0,t) = 0,\ u_{r+1}(1,t) = t.$$

Haar wavelet method to discretized equation (5.4.5) gives the following results for all $r \geq 0$.

3^{rd} *iteration*		$J = 3$		
t	x	u_{Haar}	u_{Exact}	E_{abs}
0.1	0.2	0.02	0.02	0
	0.4	0.04	0.04	0
	0.6	0.06	0.06	6.9389e-18
	0.8	0.08	0.08	0
0.5	0.2	0.10	0.10	0
	0.4	0.20	0.20	0
	0.6	0.30	0.30	5.5511e-17
	0.8	0.40	0.40	1.3323e-15
0.9	0.2	0.18	0.18	2.7756e-17
	0.4	0.36	0.36	5.5511e-17
	0.6	0.54	0.54	0
	0.8	0.72	0.72	1.5543e-15

Table 5.5: Comparison of solution by the Haar wavelet–quasilinearization technique, at 3^{rd} iteration, level of resolution $J = 3$ and at $\alpha = 2$, $\beta = 2$, with exact solution.

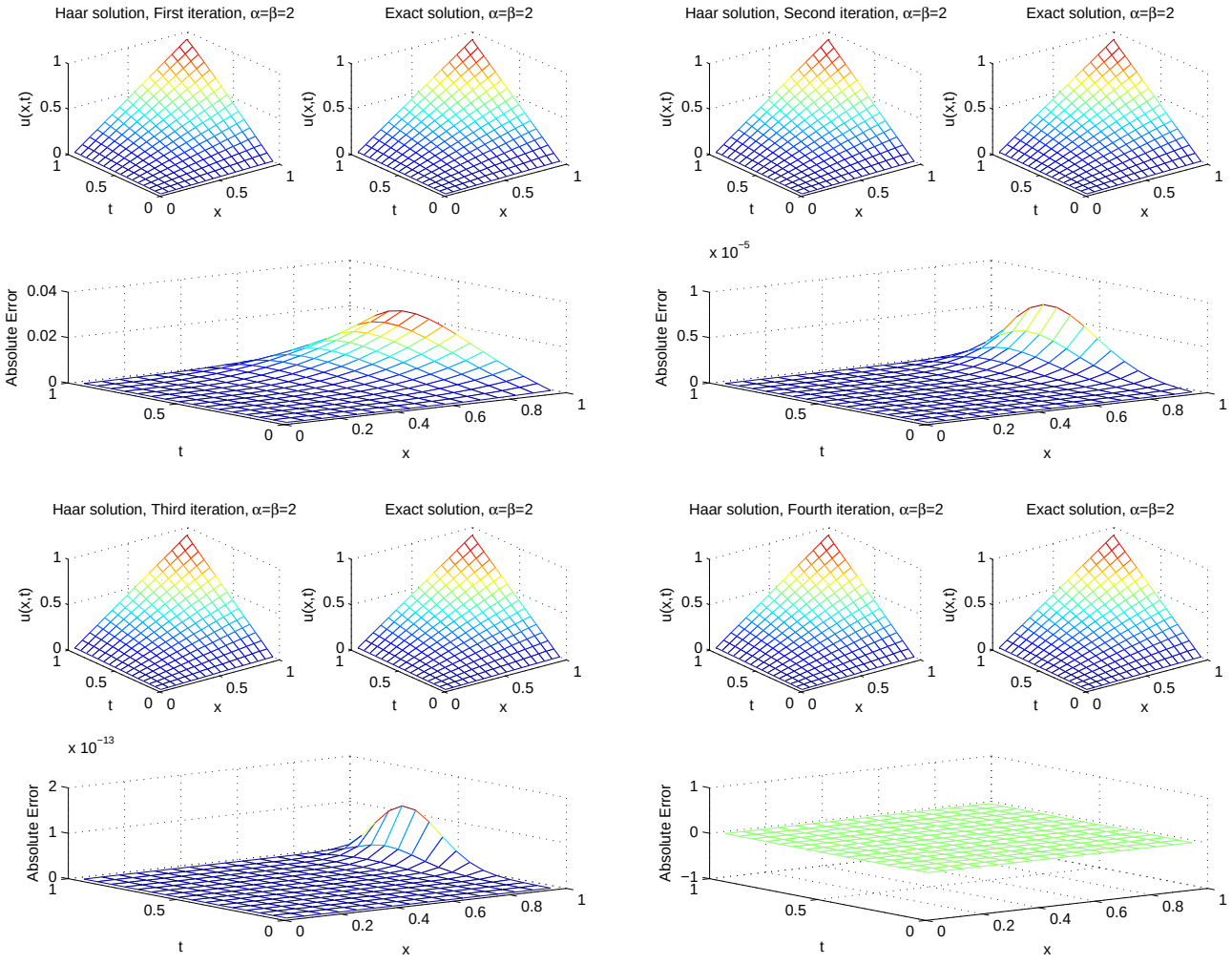

Figure 5.4: Comparison of exact solution and solution by Haar wavelet quasilinearization method for $\alpha = 2,\ \beta = 2$, at different iterations with $J = 3$.

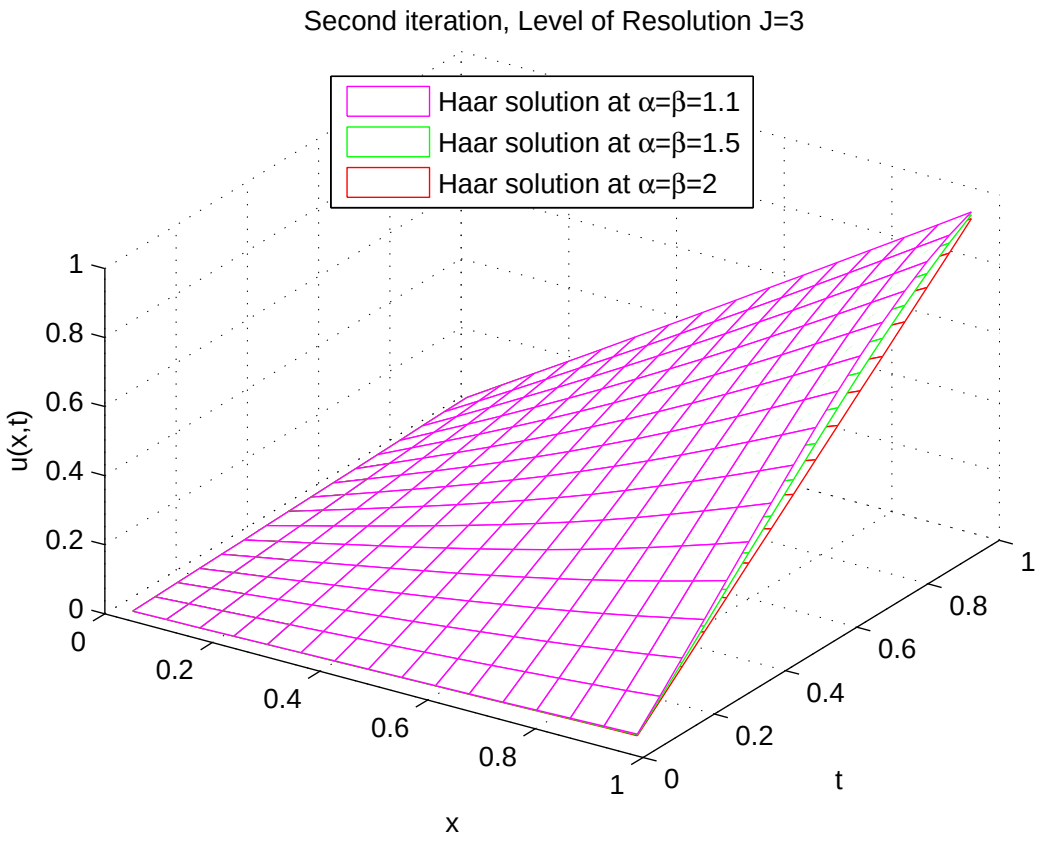

Figure 5.5: Solution by Haar wavelet quasilinearization method, at 2^{nd} iteration with $J = 3$, of Klein Gordon equation at different values of $\alpha,\ \beta$.

We fix $\alpha = 2,\ \beta = 2$ in equation (5.4.4) and apply the Haar wavelet quasilinearization technique with $J = 3$. The results in Table 5.5 is at third iteration. E_{abs} represent the absolute error which shows that solutions by Haar wavelet quasilinearization method are in good agreement with exact solution.

Figure 5.4 shows that solutions by Haar wavelet quasilinearization method of the Klein Gordon equation (5.4.4) are more accurate and absolute error reduces while increasing iterations.
Numerical solution by Haar wavelet quasilinearization method at second iteration, with fixed resolution level $J = 3$ and for different values of α, β are plotted in Figure 5.5. It is observed that solutions by Haar wavelet quasilinearization method of fractional Klein Gordon equation (5.4.4) converge to the solution of classical Klein Gordon equation, when $\alpha,\ \beta$ approaches to 2.
Problem 2 Consider the following fractional time derivative Klein–Gordon equation,

$$\frac{\partial^\alpha u}{\partial t^\alpha} - \frac{\partial^2 u}{\partial x^2} + u^2 = -x\cos(t) + x^2\cos^2(t),\ 1 < \alpha \leq 2, \tag{5.4.6}$$

subject to the initial and boundary conditions

$$u(x,0) = x,\ u_t(x,0) = 0,$$

$$u(0,t) = 0,\ u(1,t) = \cos(t).$$

The exact solution, when $\alpha = 2$, is given by [19]

$$u(x,t) = x\cos(t).$$

Applying the quasilinearization technique to equation (5.4.6), we get the discretize equation

$$\frac{\partial^\alpha u_{r+1}}{\partial t^\alpha} - \frac{\partial^2 u_{r+1}}{\partial x^2} + 2u_r u_{r+1} = -x\cos(t) + x^2\cos^2(t) + (u_r)^2, \tag{5.4.7}$$

subject to the initial and boundary conditions

$$u_{r+1}(x,0) = x,\ (u_{r+1})_t(x,0) = 0,$$

$$u_{r+1}(0,t) = 0,\ u_{r+1}(1,t) = \cos(t).$$

Implement the Haar wavelet method on equation (5.4.7) to get the solution for each $r \geq 0$.

		$\alpha = 1.2$	$\alpha = 2$		
3^{rd} *iteration*		$J = 4$	$J = 7$	$J = 9$	
x	t	u_{Haar}	u_{Haar}	u_{Haar}	u_{Exact}
0.1	0.3	0.08366615	0.09553350	0.09553364	0.09553365
	0.7	0.07232962	0.07648411	0.07648421	0.07648422
	0.9	0.06287309	0.06216098	0.06216000	0.06216000
0.5	0.4	0.42018902	0.46053021	0.46053048	0.46053050
	0.6	0.38907907	0.41266758	0.41266779	0.41266781
	0.8	0.34364615	0.34835287	0.34835332	0.34835335
0.7	0.1	0.66860531	0.69650244	0.69650289	0.69650292
	0.5	0.58480770	0.61430666	0.61430772	0.61430779
	0.9	0.44007916	0.43512674	0.43512696	0.43512698
0.9	0.3	0.84074106	0.85980148	0.85980275	0.85980284
	0.6	0.73431695	0.74280157	0.74280202	0.74280205
	0.9	0.55768597	0.55944861	0.55944895	0.55944897

Table 5.6: Comparison of solution by Haar wavelet quasilinearization method, at 3^{rd} iteration for different values of α and different level of resolution J, with exact solution at $\alpha = 2$.

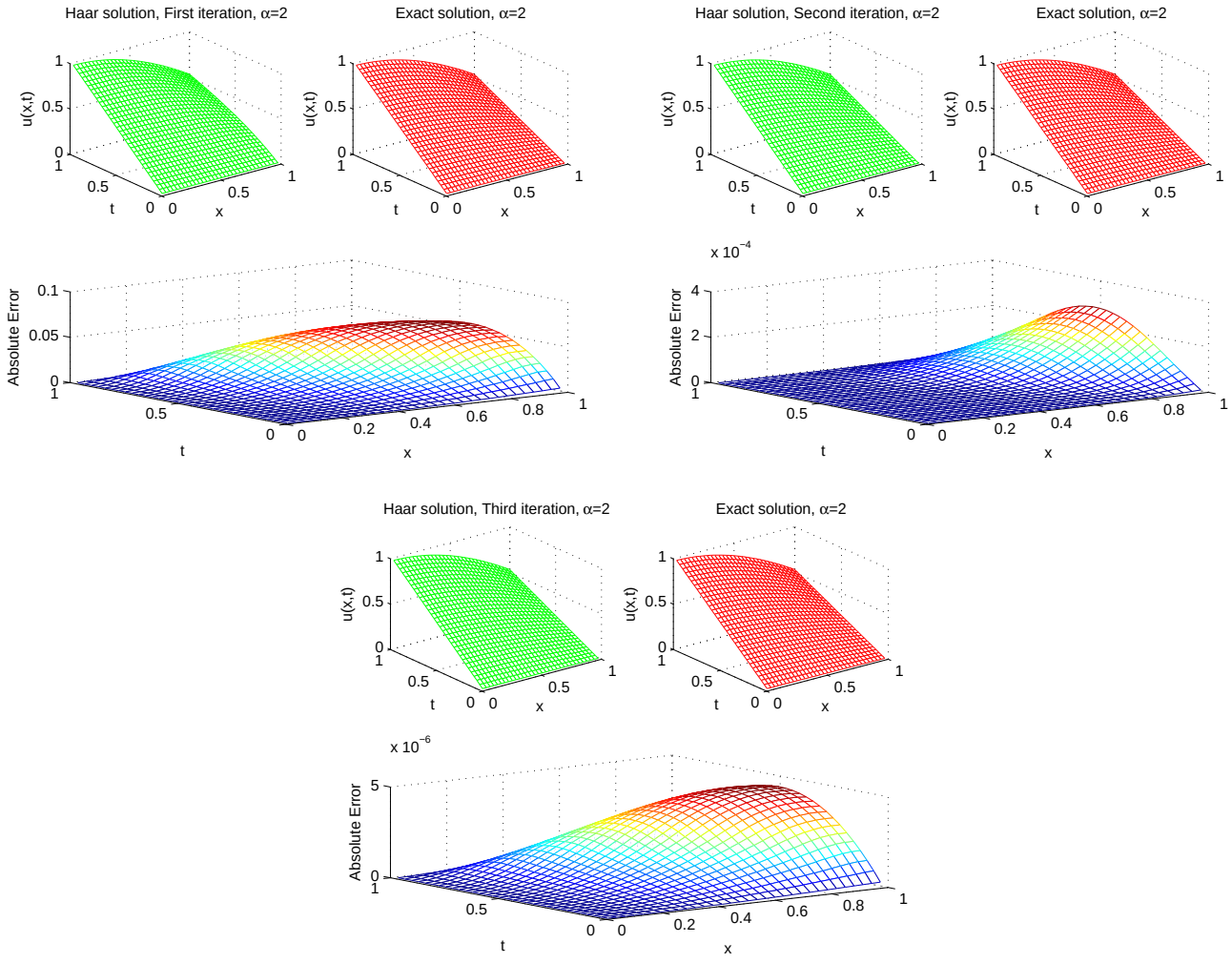

Figure 5.6: Comparison of exact and solution by Haar wavelet quasilinearization method at $\alpha = 2$, $J = 4$ and at different iterations.

Table 5.6 mention the exact solution at $\alpha = 2$ and solution by Haar wavelet quasilinearization technique at different $\alpha's$ and $J's$. The results in Table 5.6 are at third iteration. The data displayed in Table 5.6 shows that solution by the Haar wavelet quasilinearization technique converges to the exact solution at $\alpha = 2$ while increasing level of resolution J, because it shows that we get more accurate results at $J = 9$ as compare to $J = 7$. Table 5.6 shows that solution by Haar wavelet quasilinearization method converge to the exact solution when α approaches to 2.
Comparison of exact solution and solution by the Haar wavelet quasilinearization technique is shown in Figure 5.6. It also shows that we get more accurate results at higher iterations.

5.4.3 Fractional Burgers Equation

Consider the following fractional Burgers equation,

$$\frac{\partial^\alpha u}{\partial t^\alpha} + u\frac{\partial u}{\partial x} = \frac{\partial^\beta u}{\partial x^\beta}, 0 < \alpha \leq 1,\ 1 < \beta \leq 2, \tag{5.4.8}$$

with the following conditions

$$u(x,0) = 2x,$$
$$u(0,t) = 0, u(1,t) = \frac{2}{1+2t},$$

whose exact solution, when $\alpha = 1$, $\beta = 2$, is given [10]

$$u(x,t) = \frac{2x}{1+2t}. \tag{5.4.9}$$

Applying the quasilinearization technique to equation (5.4.8) to obtain the discretized equation

$$\frac{\partial^\alpha u_{r+1}}{\partial t^\alpha} + u_r\frac{\partial u_{r+1}}{\partial x} - \frac{\partial^\beta u_{r+1}}{\partial x^\beta} + u_{r+1}\frac{\partial u_r}{\partial x} = u_r\frac{\partial u_r}{\partial x}, 0 < \alpha \leq 1,\ 1 < \beta \leq 2,\ r \geq 0, \tag{5.4.10}$$

with the following conditions

$$u_{r+1}(x,0) = 2x,$$
$$u_{r+1}(0,t) = 0, u_{r+1}(1,t) = \frac{2}{1+2t}.$$

Apply the Haar wavelet method to discretize equation (5.4.10).

		$\alpha = 0.5, \beta = 2$	$\alpha = 0.7, \beta = 2$	$\alpha = 1, \beta = 2$		
5^{th} *iteration*		$J = 8$	$J = 8$	$J = 7$	$J = 8$	
x	t	u_{Haar}	u_{Haar}	u_{Haar}	u_{Haar}	u_{Exact}
0.1	0.3	0.1200807	0.1220607	0.1250004	0.1250000	0.1250000
	0.7	0.0896191	0.0881609	0.0833335	0.0833334	0.0833333
	0.9	0.0796789	0.0772933	0.0714286	0.0714286	0.0714286
0.5	0.4	0.5543077	0.5576233	0.5555558	0.5555561	0.5555556
	0.6	0.4732065	0.4698999	0.4545457	0.4545459	0.4545455
	0.8	0.4134079	0.4057360	0.3846160	0.3846156	0.3846154
0.7	0.1	1.0861842	1.1088053	1.1666732	1.1666698	1.1666667
	0.5	0.7107272	0.7103718	0.7000023	0.7000007	0.7000000
	0.9	0.5310973	0.5219788	0.5000003	0.5000002	0.5000000
0.9	0.3	1.1171191	1.1212042	1.1250051	1.1250005	1.1250000
	0.6	0.8276398	0.8259672	0.8181826	0.8181824	0.8181818
	0.9	0.6582548	0.6536948	0.6428576	0.6428574	0.6428571

Table 5.7: Comparison of exact solution at $\alpha = 1,\ \beta = 2$ and solution by Haar wavelet quasilinearization technique at different values of α and $\beta = 2$ with different resolution levels J.

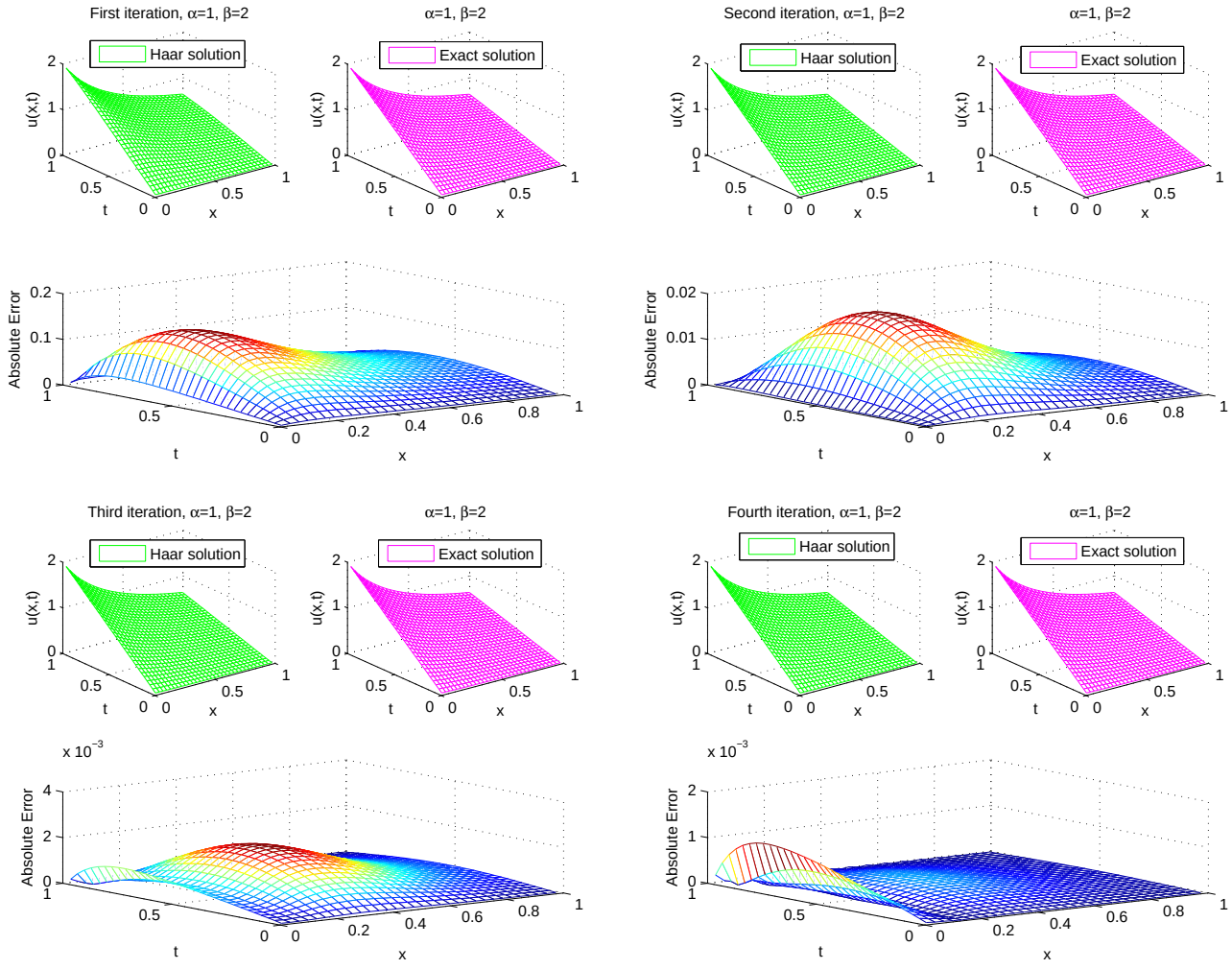

Figure 5.7: Comparison of exact and solution by Haar wavelet quasilinearization method at different iterations with $J = 4$, $\alpha = 1$ and $\beta = 2$.

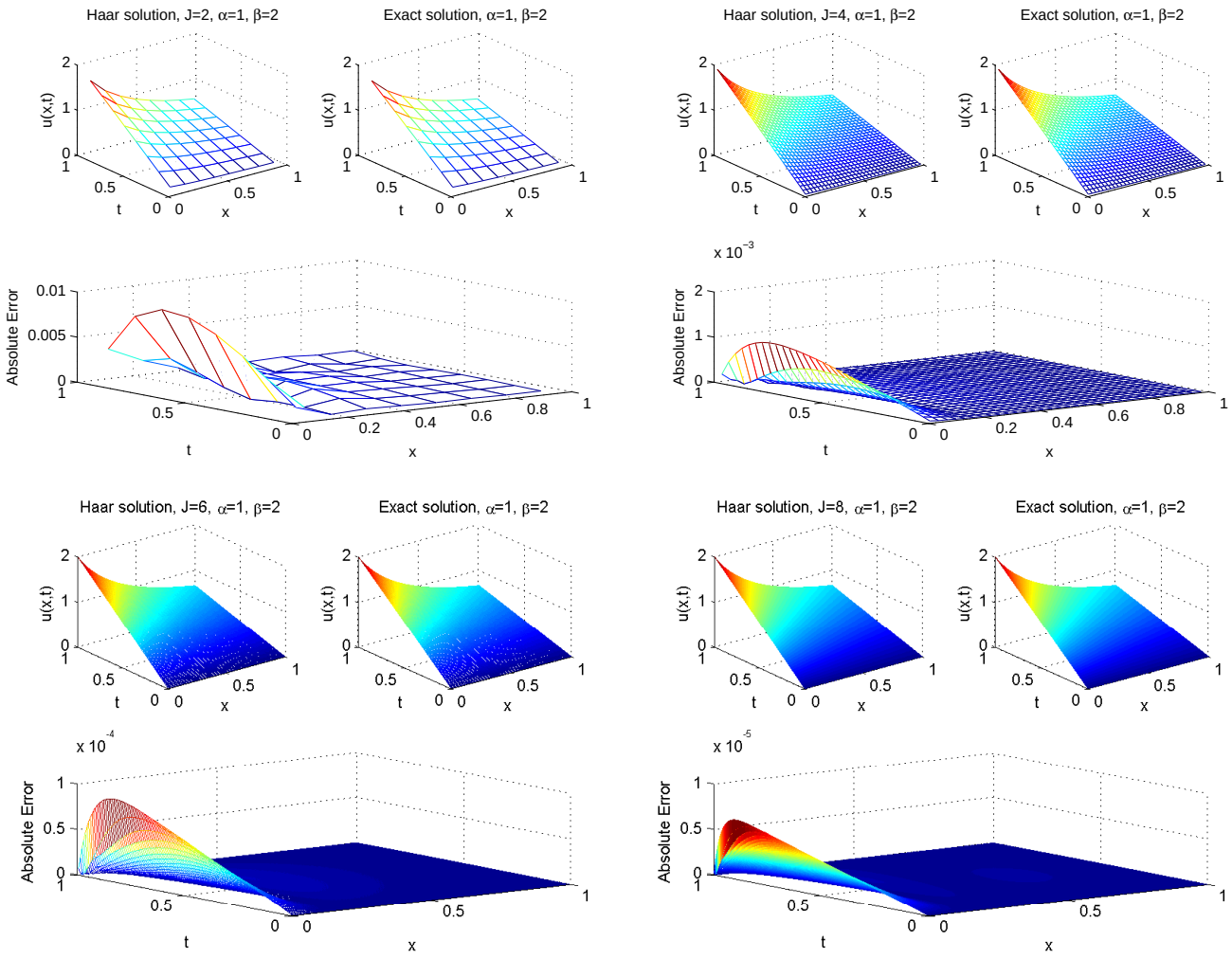

Figure 5.8: Comparison of exact solution and solution by Haar wavelet quasilinearization method at 4^{th} iteration and with different resolution levels J.

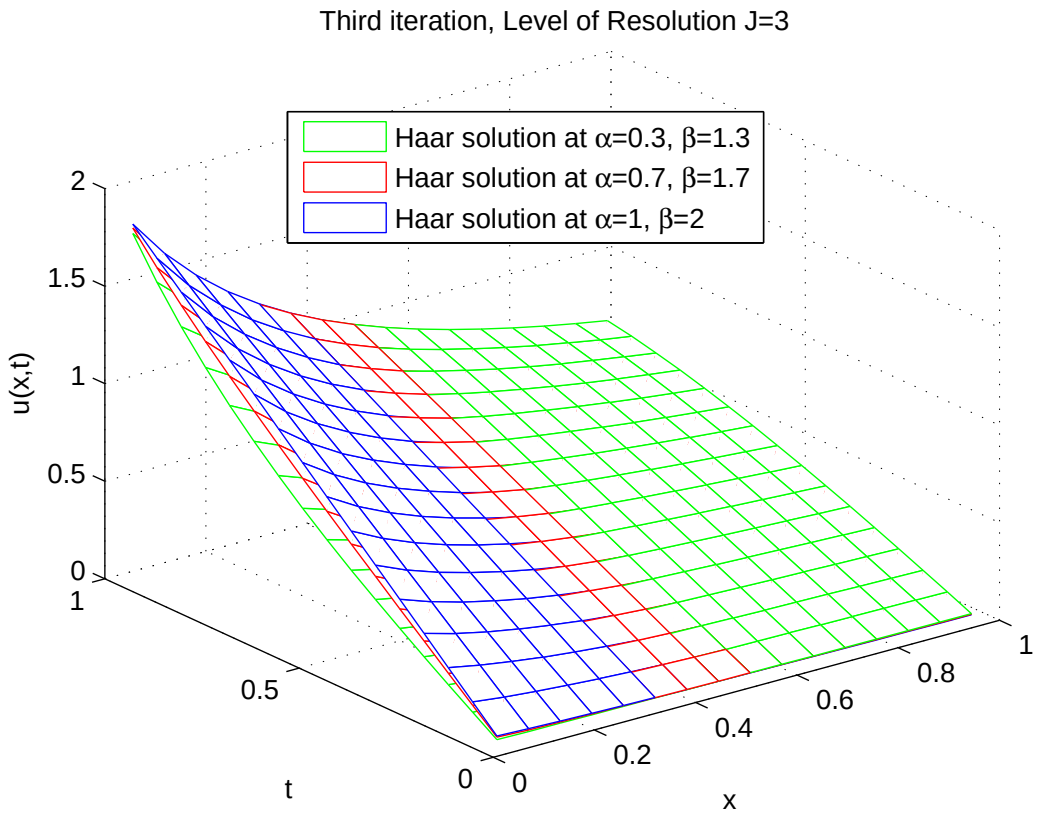

Figure 5.9: Exact solution at $\alpha = 1,\ \beta = 2$ and solution by Haar wavelet quasilinearization method at different α and β with $J = 3$ and at 3^{rd} iteration.

Numerical solution by the Haar wavelet quasilinearization technique is shown in Table 5.7, It shows that solution by Haar wavelet quasilinearization method converges to the exact solution at $\alpha = 1,\ \beta = 2$, when $\beta = 2$ and α approaches to 1. Also it is observed that solution by Haar wavelet quasilinearization method get closer to the exact solution while J is increased.

Result in Figure 5.7 indicate that solution by Haar wavelet quasilinearization method becomes more accurate with increasing iterations. Solution by Haar wavelet quasilinearization method at 4^{th} iteration, $\alpha = 1,\ \beta = 2$ and at different level of resolutions J, are plotted in Figure 5.8. We notice that solution by Haar wavelet quasilinearization method converge to the exact solution while increasing J, i.e., absolute error goes down with increasing J.

Figure 5.9 shows that solution by Haar wavelet quasilinearization method converge to the exact solution when α and β approaches to 1 and 2 respectively.

5.4.4 Conclusion

It is observed that Haar wavelet method with quasilinearization technique gives comparatively good results when applied to different fractional nonlinear initial boundary value problems. The results obtained from Haar wavelet quasilinearization technique are better from the results obtained by other methods [64, 102] and are in good agreement with exact solutions. The numerical solution of the fractional nonlinear partial differential equation converge to the solution of the integer partial differential equation as shown in Table 5.7 and Figures 5.2, 5.5, 5.9. Approximate solution converge to the exact solution while iterations are increased and absolute error goes down. Also solution by Haar wavelet quasilinearization technique becomes more accurate with increasing level of resolution J. Different type of non-linearities can easily be handled by the Haar wavelet with quasilinearization method.

Chapter 6

Haar Wavelet-Picard Technique for Fractional Order Nonlinear Initial and Boundary Value Problems

In this chapter, a technique called Haar wavelet-Picard technique is developed to get the numerical solutions of nonlinear differential equations of fractional order. The Haar wavelet-Picard technique is the combination of Haar wavelet and Picard technique. Picard iteration is used to linearize the nonlinear fractional order differential equations and then Haar wavelet method is applied to linearized fractional ordinary differential equations. In each iteration of Picard iteration, solution is updated by the Haar wavelet method. The results are compared with the exact solution.

6.1 Haar Wavelet Picard Technique

The procedure for implementation of Haar wavelet Picard technique is same as Haar wavelets quasi-linearization method as described in section 3.2.

6.1.1 Convergence Analysis

First we analyze the convergence of both the schemes then we describe the role of their convergence according to the Haar wavelet Picard technique.

Convergence of Picard Technique

Consider the nonlinear second order differential equation

$$y''(x) = f(y), \quad y(0) = y(b) = 0. \tag{6.1.1}$$

Application of Picard technique to (6.1.1) yields

$$y''_{r+1}(x) = f(y_r), \quad y_{r+1}(0) = y_{r+1}(b) = 0. \tag{6.1.2}$$

Let $y_0(x)$ be some initial approximation. Each function $y_{r+1}(x)$ is a solution of a linear equation (6.1.2), where y_r is always considered known and is obtained from the previous iteration.

According to Picard technique [7]:

$$| \, y_{r+1} - y_r \, | \leq k \, | \, y_r - y_{r-1} \, |, \quad \text{where} \quad k < 1. \tag{6.1.3}$$

This shows that there is linear convergence, if there is convergence at all.

Convergence of Haar Wavelet Method

We have already described the convergence of Haar wavelet method in section 2.4 of chapter 2, which shows that the error is inversely proportional to the level of resolution.

Haar wavelet Picard technique first discretizes the nonlinear initial and boundary value problem, then Haar wavelet method is applied on the obtained discretized equation to get the approximate solutions $y_0(x), \ y_1(x), \cdots$, at each iteration of Picard technique. According to the convergence analysis of both Haar and Picard technique, approximate solution by Haar wavelet-Picard technique converges to the exact solution while increasing both level of resolution J and picard iteration r.

6.2 Applications

In this section, we solve nonlinear differential equations of fractional order by the Haar wavelets - Picard technique and compare the results with the exact solution.

Example 1: Consider the αth order fractional nonlinear Bratu type equation

$${}^cD^{\alpha}y(x) - 2e^{y(x)} = 0, \ 1 < \alpha \leq 2, \tag{6.2.1}$$

subject to the initial condition $y(0) = 0, \ y'(0) = 0$.

The exact solution, when $\alpha = 2$, is given by [65]

$$y(x) = -2\ln(\cos x).$$

Applying the Picard iteration to equation (6.2.1), we get

$${}^cD^{\alpha}y_{r+1}(x) = 2e^{y_r(x)}, \ 1 < \alpha \leq 2, \tag{6.2.2}$$

with the initial condition $y_{r+1}(0) = 0, \ y'_{r+1}(0) = 0$.

Now we apply the Haar wavelet method to equation (6.2.2), we approximate the higher order derivative term by the Haar wavelet series as

$$ {}^{c}D^{\alpha} y_{r+1}(x) = \sum_{l=1}^{2M} b_l h_l(x). \tag{6.2.3} $$

Lower order derivatives are obtained by integrating equation (6.2.3) and use the initial conditions

$$ y_{r+1}(x) = \sum_{l=1}^{2M} b_l p_{\alpha,l}(x), \quad y'_{r+1}(x) = \sum_{l=1}^{2M} b_l p_{\alpha-1,l}(x). \tag{6.2.4} $$

Substitute equations (6.2.3) and (6.2.4) in (6.2.2), we get

$$ \sum_{l=1}^{2M} b_l h_l(x) = 2e^{y_r(x)}, \tag{6.2.5} $$

with the initial approximation $y_0(x) = 0$.

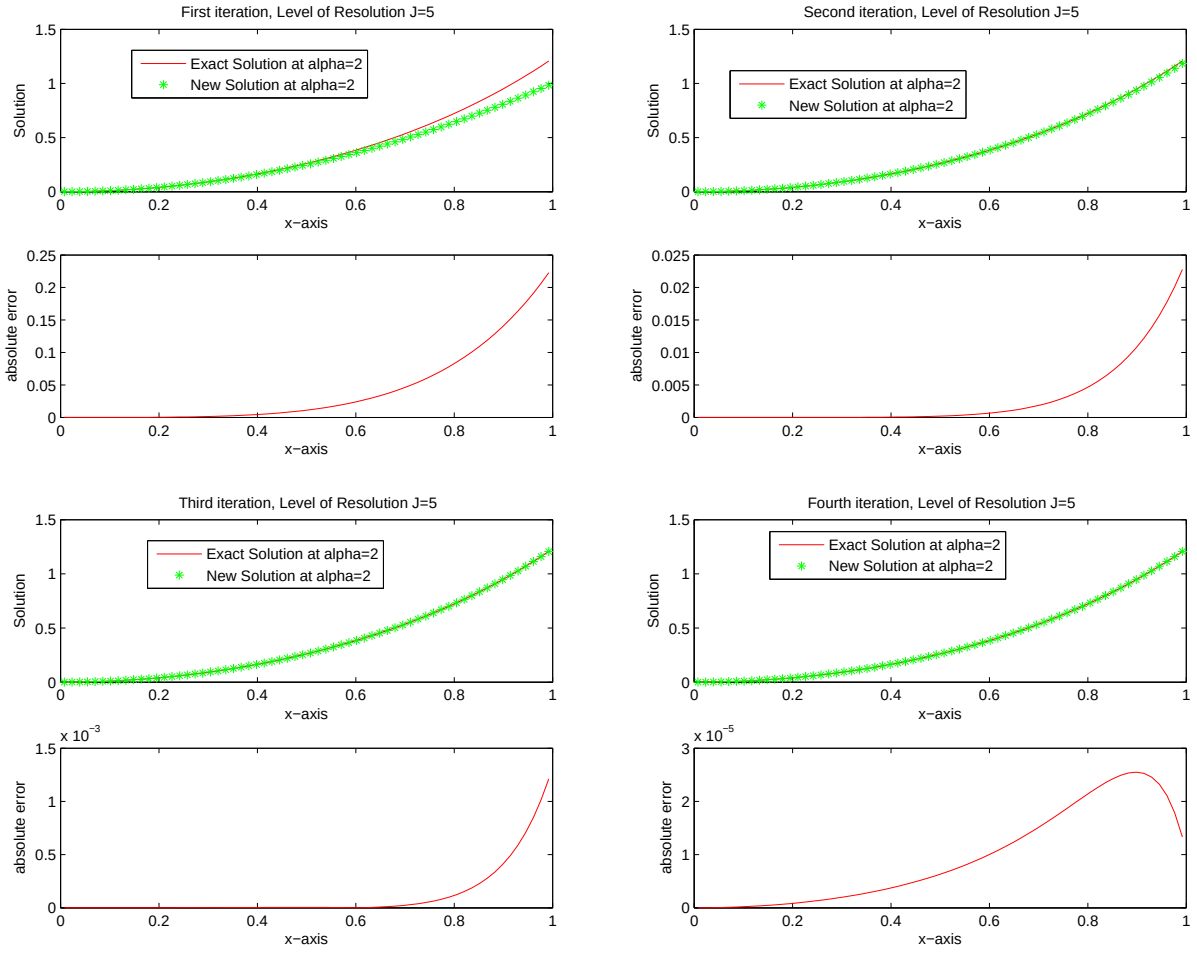

Figure 6.1: Comparison of exact solution and solutions by Haar wavelet-Picard technique, for different iterations at $J = 5$ and $\alpha = 2$.

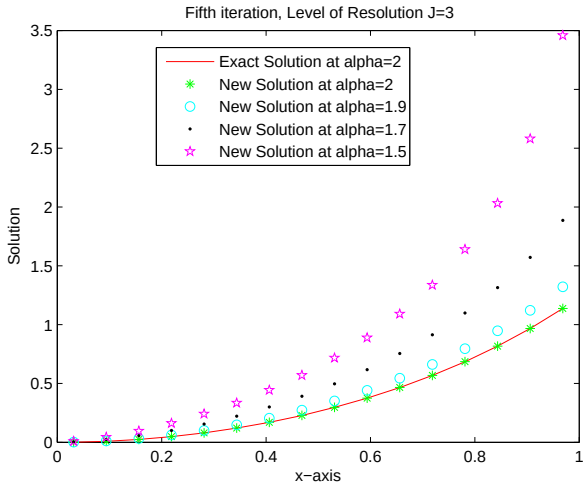

Figure 6.2: Exact solution at $\alpha = 2$ and the Haar wavelet-Picard solution at $\alpha = 2,\ \alpha = 1.9, \alpha = 1.7$ and $\alpha = 1.5$.

We fix the order of the differential equation (6.2.1), $\alpha = 2$, and level of resolution, $J = 5$. The graph in Figure 6.1 shows the exact solution and approximate solution at four iterations. The absolute error reduces with increasing iterations.

Results at fifth iteration of Haar wavelet-Picard technique at fixed level of resolution $J = 3$ and at different values of α are shown in Figure 6.2, with the exact solution at $\alpha = 2$. Figure 6.2 showed that the numerical solutions converge to the exact solution when α approaches to 2.

Example 2: Consider the fractional nonlinear Duffing equation

$$ {}^{c}D^{\alpha}y(x) + y'(x) + y(x) + y(x)^3 = \cos^3(x) - \sin(x),\ 1 < \alpha \leq 2, \tag{6.2.6} $$

subject to the initial conditions $y(0) = 1,\ y'(0) = 0$.

The exact solution, when $\alpha = 2$, is

$$ y(x) = \cos(x). $$

Applying the Picard iteration to equation (6.2.6)

$$ {}^{c}D^{\alpha}y_{r+1}(x) + y'_{r+1}(x) + y_{r+1}(x) = \cos^3(x) - \sin(x) - y_r(x)^3,\ 1 < \alpha \leq 2, \tag{6.2.7} $$

with the initial conditions $y_{r+1}(0) = 1,\ y'_{r+1}(0) = 0$.

Apply the Haar wavelet method to equation (6.2.7). We approximate the higher order derivative term by the Haar wavelet series as

$$ {}^{c}D^{\alpha}y_{r+1}(x) = \sum_{l=1}^{2M} b_l h_l(x). \tag{6.2.8} $$

Now to get the Haar wavelet series for lower order derivative terms we integrate equation (6.2.8) and use the initial condition, to get

$$y_{r+1}(x) = \sum_{l=1}^{2M} b_l p_{\alpha,l}(x) + 1, \quad y'_{r+1}(x) = \sum_{l=1}^{2M} b_l p_{\alpha-1,l}(x). \tag{6.2.9}$$

Substitute equations (6.2.8) and (6.2.9) in (6.2.7)

$$\sum_{l=1}^{2M} b_l [h_l(x) + p_{\alpha-1,l}(x) + p_{\alpha,l}(x)] = \cos^3(x) - \sin(x) - y_r(x)^3 - 1, \tag{6.2.10}$$

with the initial approximations $y_0(x) = 1,\ y'_0(x) = 0$.

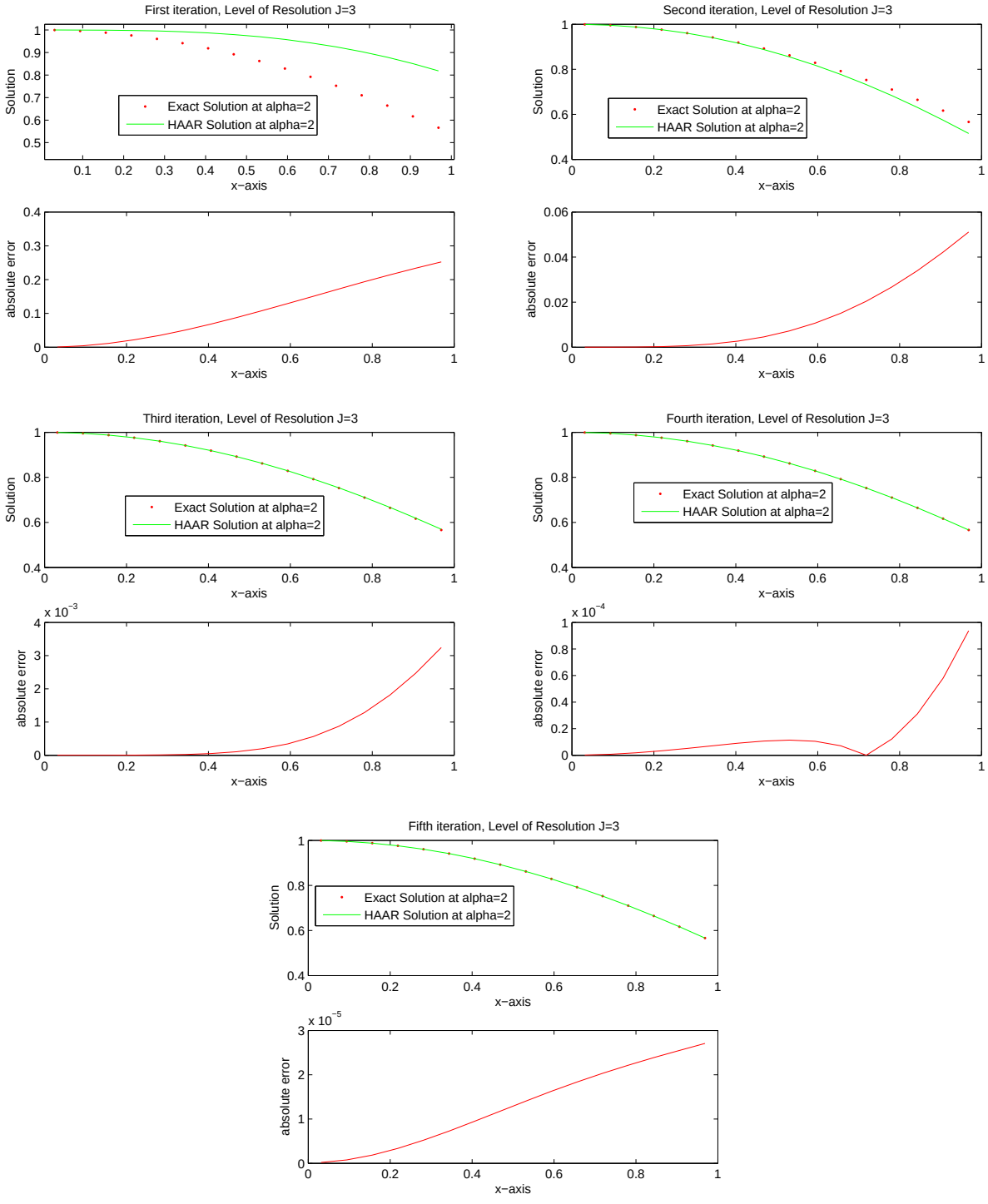

Figure 6.3: Comparison of exact solution and solutions by Haar wavelet-Picard technique for different iterations at $J = 3$ and $\alpha = 2$.

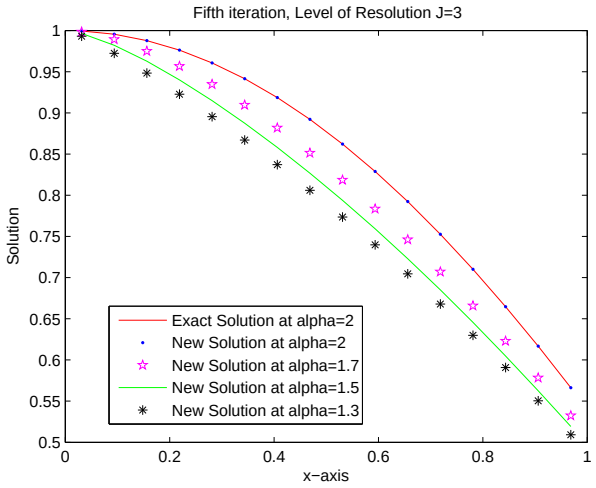

Figure 6.4: Exact solution at $\alpha = 2$ and the Haar wavelet-Picard solution at $\alpha = 2,\ \alpha = 1.8, \alpha = 1.5$ and $\alpha = 1.3$.

We fix the level of resolution, $J = 3$, and order of differential equation (6.2.6), $\alpha = 2$. The exact solution and the numerical solution by Haar wavelet-Picard technique at different iterations along with the absolute error are shown in Figure 6.3.

Exact solution at $\alpha = 2$ and the Haar solution at different values of α, are displayed in Figure 6.4. It is observed that solutions of fractional nonlinear Duffing equation (6.2.6) converge to the solution of second order nonlinear Duffing equation, when α approaches to 2.

Example 3: Consider the α^{th} order nonlinear Lane–Emden type equation [65]:

$$ {}^{c}D^{\alpha}y(x) + \frac{2}{x}y'(x) + 8e^{y(x)} + 4e^{\frac{y(x)}{2}} = 0,\ 1 < \alpha \leq 2, \tag{6.2.11} $$

subject to the initial conditions: $y(0) = 0,\ y'(0) = 0$.

The exact solution, when $\alpha = 2$, is

$$ y(x) = -2\ln(1 + x^2). $$

Picard iteration to equation (6.2.11) implies

$$ {}^{c}D^{\alpha}y_{r+1}(x) + \frac{2}{x}y'_{r+1}(x) = -8e^{y_r(x)} - 4e^{\frac{y_r(x)}{2}},\ 1 < \alpha \leq 2, \tag{6.2.12} $$

with the initial conditions $y_{r+1}(0) = 0,\ y'_{r+1}(0) = 0$.

Apply the Haar wavelet method to equation (6.2.12)

$$ {}^{c}D^{\alpha}y_{r+1}(x) = \sum_{l=1}^{2M} b_l h_l(x). \tag{6.2.13} $$

Lower order derivatives are obtained by integrating equation (6.2.13) and use the initial conditions

$$y_{r+1}(x) = \sum_{l=1}^{2M} b_l p_{\alpha,l}(x), \tag{6.2.14}$$

$$y'_{r+1}(x) = \sum_{l=1}^{2M} b_l p_{\alpha-1,l}(x). \tag{6.2.15}$$

Substitute equations (6.2.13), (6.2.14) and (6.2.15) in (6.2.12), we get

$$\sum_{l=1}^{2M} b_l [h_l(x) + \tfrac{2}{t} p_{\alpha-1,l}(x)] = -8e^{y_r(x)} - 4e^{\frac{y_r(x)}{2}}, \tag{6.2.16}$$

with the initial approximations $y_0(x) = 0$, $y'_0(x) = 0$.

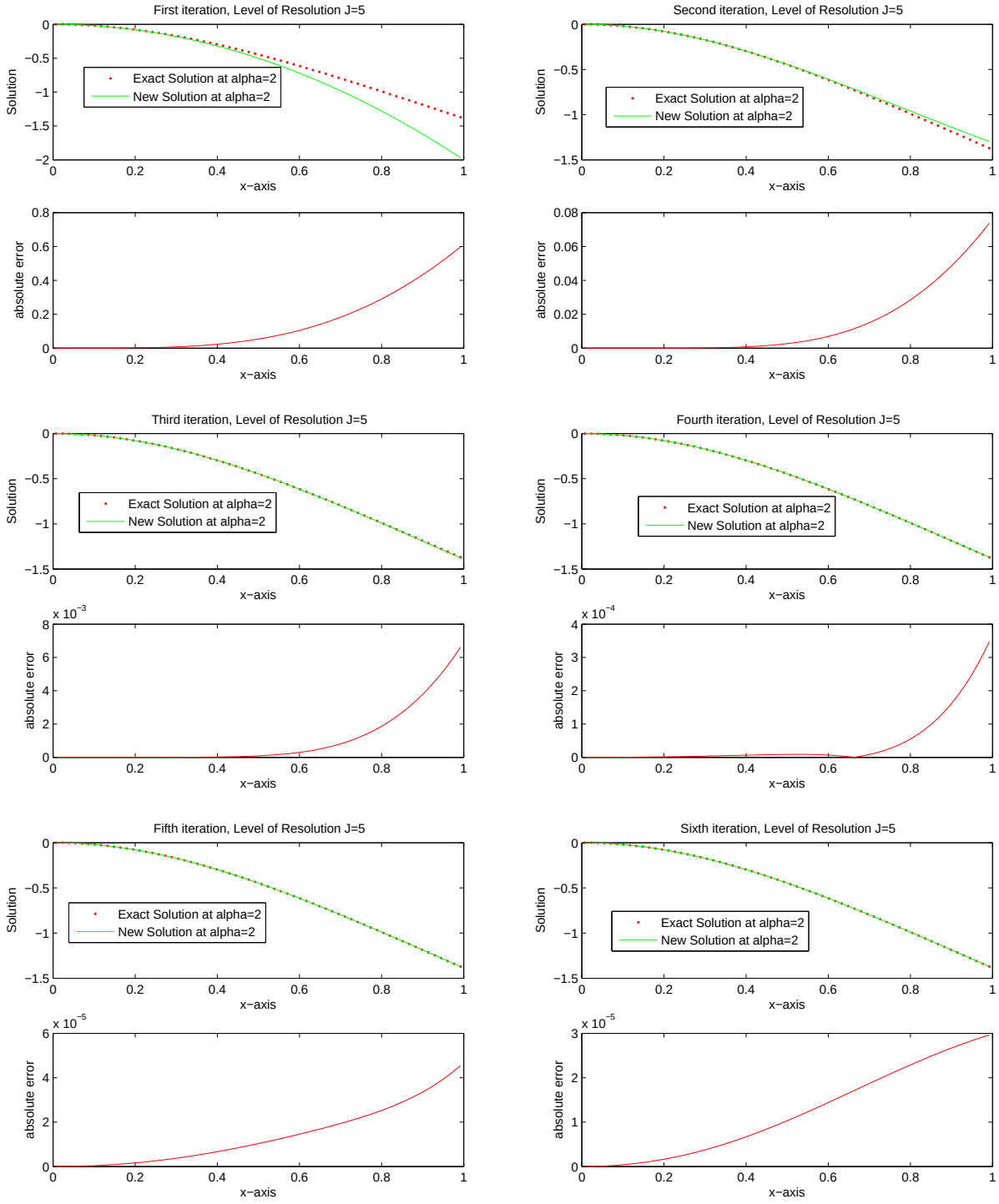

Figure 6.5: Comparison of exact solution and solutions by Haar wavelet-Picard technique at $J = 5$, for different iterations and $\alpha = 2$.

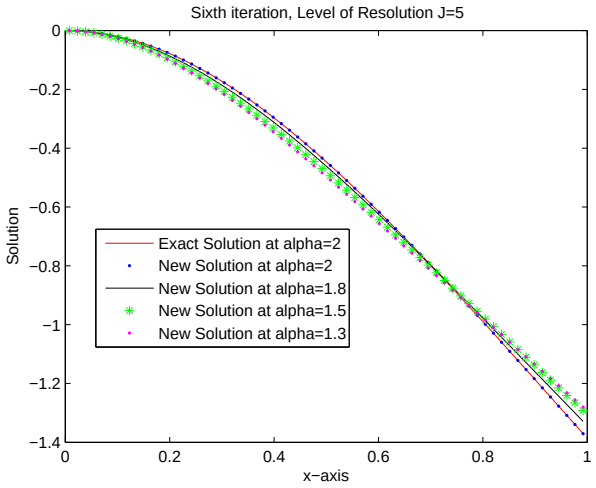

Figure 6.6: Exact solution at $\alpha = 2$ and the Haar wavelet-Picard solution at $\alpha = 2,\ \alpha = 1.8, \alpha = 1.5$ and $\alpha = 1.3$.

Here we fix the order of the differential equation (6.2.11), $\alpha = 2$, and level of resolution, $J = 5$. The graph in Figure 6.5 shows the exact solution and approximate solution by proposed method at six iterations.

Results of sixth iteration by Haar wavelet-Picard technique at $J = 5$ and different values of α, are shown in Figure 6.6 along with the exact solution at $\alpha = 2$. Figure 6.6 showed that the numerical solutions converge to the exact solution when α approaches to 2.

Example 4: Consider the α^{th} order fractional nonlinear boundary value problem,

$$ {}^{c}D^{\alpha}y(x) + a(x)y'^{2}(x) + b(x)y(x)y'(x) = f(x),\ 1 < \alpha \leq 2, \tag{6.2.17} $$

subject to the boundary conditions $y(0) = 0,\ \ y(1) = 0$.

The exact solution is given by

$$ y(x) = x^3 - x^2, $$

where $f(x) = \frac{\Gamma(4)}{\Gamma(4-\alpha)}x^{3-\alpha} - \frac{\Gamma(3)}{\Gamma(3-\alpha)}x^{2-\alpha} + a(x)(3x^2 - 2x)^2 + b(x)(3x^2 - 2x)(x^3 - x^2)$.

Applying the Picard technique to equation (6.2.17), we get

$$ {}^{c}D^{\alpha}y_{r+1}(x) = f(x) - a(x)y_r'^{2}(x) - b(x)y_r(x)y_r'(x),\ 1 < \alpha \leq 2, \tag{6.2.18} $$

with the boundary conditions $y_{r+1}(0) = 0,\ \ y_{r+1}(1) = 0$.

Now apply the Haar wavelet method to equation (6.2.18), we approximate the higher order derivative term by the Haar wavelet series as

$$ {}^{c}D^{\alpha}y_{r+1}(x) = \sum_{l=1}^{2M} b_l h_l(x). \tag{6.2.19} $$

Lower order derivatives are obtained by integrating equation (6.2.19) and use the initial condition

$$y_{r+1}(x) = \sum_{l=1}^{2M} b_l(p_{\alpha,l}(x) - xC_{\alpha,l}), \tag{6.2.20}$$

$$y'_{r+1}(x) = \sum_{l=1}^{2M} b_l(p_{\alpha-1,l}(x) - C_{\alpha,l}), \tag{6.2.21}$$

where $C_{\alpha,l} = \int_0^1 p_{\alpha,l}(x)dx$. Substitute equations (6.2.19), (6.2.20) and (6.2.21) in (6.2.18), we get

$$\sum_{l=1}^{2M} b_l h_l(x) = f(x) - a(x)y'^2_r(x) - b(x)y_r(x)y'_r(x),\ 1 < \alpha \leq 2. \tag{6.2.22}$$

with the initial approximation $y_0(x) = 0,\ \ y'_0(x) = 0$. Here we consider $a(x) = e^x$ and $b(x) = x$.

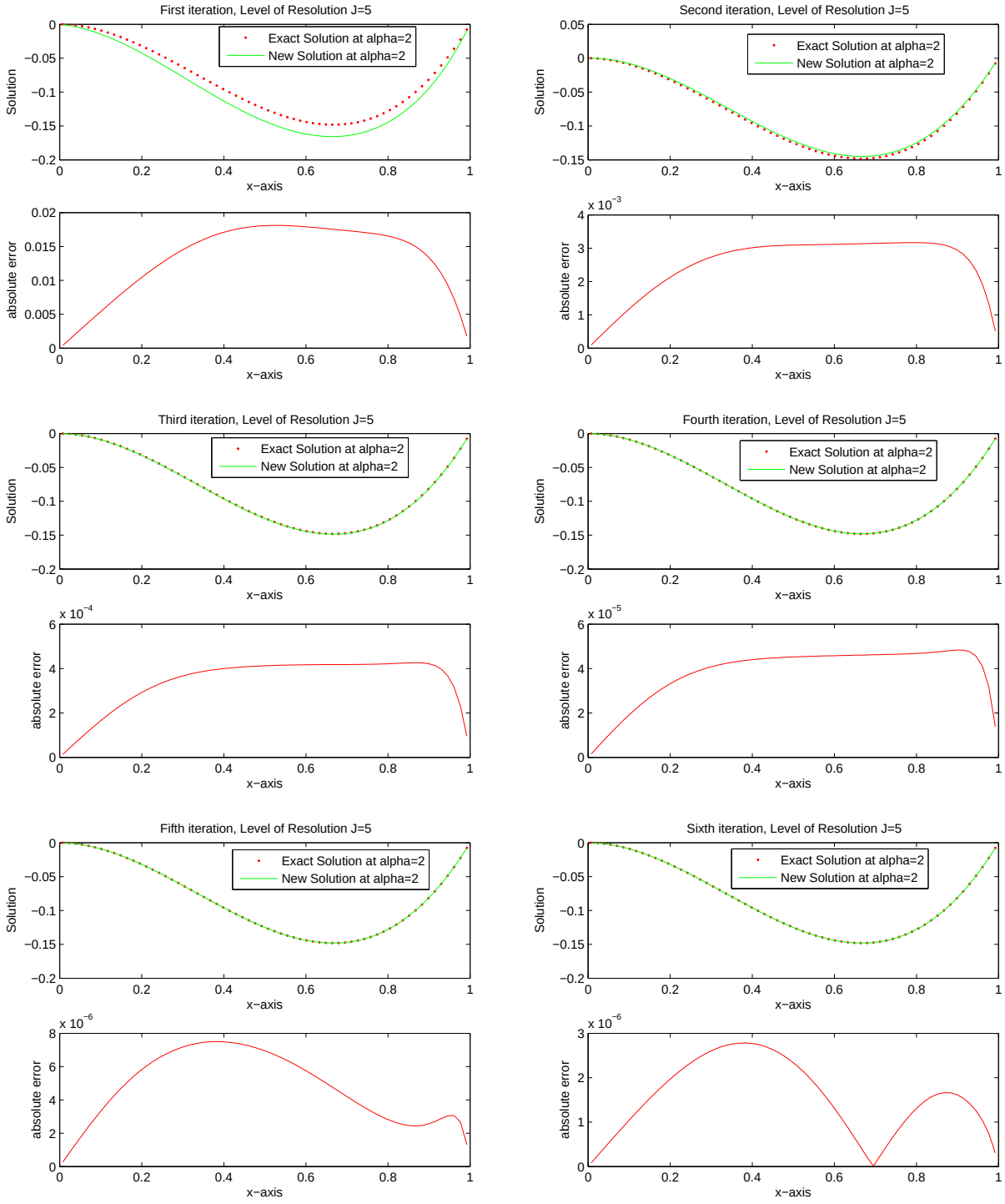

Figure 6.7: Comparison of exact solution and solutions by Haar wavelet-Picard technique at $J = 5$, for different iterations and $\alpha = 2$.

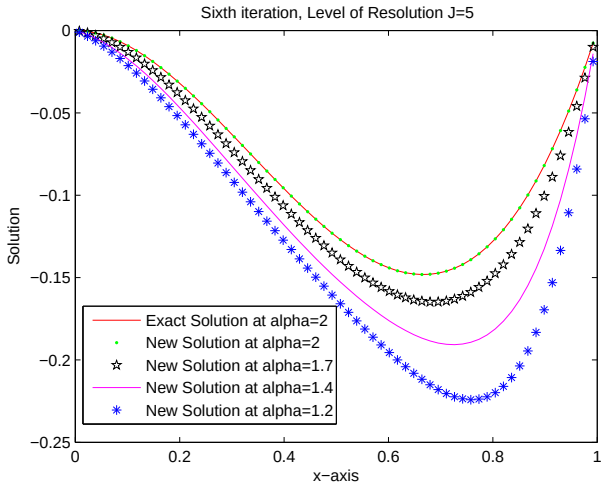

Figure 6.8: Exact solution at $\alpha = 2$ and the Haar wavelet-Picard solution at $\alpha = 2$, $\alpha = 1.7, \alpha = 1.4$ and $\alpha = 1.2$.

We fix the order of the differential equation (6.2.17), $\alpha = 2$, and level of resolution, $J = 5$. The graph in Figure 6.7 shows the exact solution and approximate solution by present method at six iterations.

Results at sixth iteration of present method at fixed level of resolution, $J = 5$, and at different values of α are shown in Figure 6.8 along with the exact solution at $\alpha = 2$. Figure 6.8 showed that the numerical solutions converge to the exact solution when α approaches to 2.

6.2.1 Conclusion

It is shown that Haar wavelet–Picard technique gives excellent results when applied to different fractional order nonlinear initial and boundary value problems. The solution of the fractional order, nonlinear ordinary differential equation converge to the solution of integer order differential equation as shown in Figures 6.2, 6.4, 6.6, and 6.8. Other Figures show that approximate solution converge to the exact solution while iterations are increased and absolute error goes down. Different type of non-linearities can easily be handled by the Haar wavelet–Picard technique.

Chapter 7

Wavelet Galerkin Quasilinearization Method for Nonlinear Boundary Value Problems

The wavelet-Galerkin method does not use a wavelet at all. It actually uses the wavelet's scaling function. Wavelet Galerkin method have been applied for solving linear boundary value problems [3, 92, 93, 99, 113]. The objective of the present work is to develop a method by utilizing the wavelet-Galerkin and quasilinearization technique for the approximation of solutions of nonlinear boundary value problems. The beginning of this chapter is to describe the Daubechies wavelet, and then construct the connection coefficients for the solution of differential equations.

7.1 Daubechies Wavelets

Daubechies [29, 30] constructed a family of compactly supported orthonormal wavelets. A wavelet system consists of a scaling function $\phi(x)$ and a wavelet function $\psi(x)$. There are two important relations in wavelet theory, which we called two-scale relation

$$\phi(x) = \sum_{l=0}^{N-1} p_l \phi_l(2x), \tag{7.1.1}$$

and the equation

$$\psi(x) = \sum_{l=2-N}^{1} (-1)^l p_{1-l} \phi_l(2x), \tag{7.1.2}$$

where $\phi_l(.) := \phi(. - l)$. The coefficients p_l are called the wavelet filter coefficients. Relations (7.1.1) and (7.1.2) are also called refinement relations and N (an even integer) is the number of wavelet filter coefficients in the refinement relations. The supports of the scaling function $\phi(x)$ and wavelet function $\psi(x)$ are $[0, N-1]$ and $[1 - \frac{N}{2}, \frac{N}{2}]$ respectively. Daubechies constructed wavelet

filter coefficients p_l to satisfy the certain conditions and corresponding to these, scaling and wavelet functions have certain properties [20]

$$\sum_{l=0}^{N-1} p_l = 2 \quad \Rightarrow \quad \int_{-\infty}^{\infty} \phi(x)dx = 1, \tag{7.1.3}$$

$$\sum_{l=0}^{N-1} p_l p_{l-2m} = 2\delta_{0,m} \quad \Rightarrow \quad \int_{-\infty}^{\infty} \phi(x)\phi(x-m)dx = \delta_{0,m}, \tag{7.1.4}$$

$$\sum_{l=2-N}^{1} (-1)^l p_{1-l} p_{l-2m} = 0 \quad \Rightarrow \quad \int_{-\infty}^{\infty} \phi(x)\psi(x-m)dx = 0, \quad \text{for any integer } m, \tag{7.1.5}$$

$$\sum_{l=0}^{N-1} (-1)^l l^m p_l = 0 \quad \Rightarrow \quad \int_{-\infty}^{\infty} x^m \psi(x)dx = 0, \quad m = 0, 1, ..., \tfrac{N}{2} - 1, \tag{7.1.6}$$

where δ is the delta function. Relation (7.1.3) shows that scaling function have unit area and relations (7.1.4) and (7.1.5) indicate the orthonormality of ϕ and orthogonality of ϕ and ψ respectively. Relation (7.1.6) shows that m^{th} moment of ψ is zero, i.e., it has m vanishing moments, which implies that we can express the elements of the set $\{1, x, ..., x^{\frac{N}{2}} - 1\}$ as a linear combination of $\phi(x-k)$, integer translate of $\phi(x)$.

Let V_j and W_j be the subspaces of $L^2(\mathbb{R})$, the space of square-integrable functions on the real line, which are generated as the L^2-closure of the linear spans of $\phi_{j,k}(x) = 2^{j/2}\phi(2^j x - k)$ and $\psi_{j,k}(x) = 2^{j/2}\psi(2^j x - k)$, $k \in \mathbb{Z}$ respectively. According to the orthogonality of ϕ and ψ, relation (7.1.5), we have

$$V_{j+1} = V_j \bigoplus W_j. \tag{7.1.7}$$

Relation (7.1.7) implies

$$V_0 \subset V_1 \subset V_2 \subset \cdots \subset V_j \subset V_{j+1} \tag{7.1.8}$$

and we have

$$\begin{aligned} V_{j+1} &= V_j \bigoplus W_j, \\ &= V_{j-1} \bigoplus W_{j-1} \bigoplus W_j, \\ &\vdots \\ &= V_0 \bigoplus W_0 \bigoplus W_1 \bigoplus W_2 \cdots \bigoplus W_j, \end{aligned} \tag{7.1.9}$$

where $\bigoplus$ denotes the orthogonal direct sum, $W_j \perp W_p$ for $j \neq p$ and $W_j \subset V_p$ for $j < p$. Daubechies

wavelets have the following orthogonality properties [20]:

$$\begin{aligned}
\int_{-\infty}^{\infty} \phi_{j,k}(x)\phi_{j,l}(x)dx &= \delta_{k,l}, \\
\int_{-\infty}^{\infty} \psi_{j,k}(x)\psi_{l,m}(x)dx &= \delta_{j,l}\delta_{k,m}, \\
\int_{-\infty}^{\infty} \phi_{j,k}(x)\psi_{j,m}(x)dx &= 0.
\end{aligned}$$

Daubechies wavelet have no explicit expressions for the scaling function $\phi(x)$ and the wavelet function $\psi(x)$ at arbitrary x. The function values of $\phi(x)$ and $\psi(x)$ at the dyadic points $\frac{k}{2^j}$, for integers j and k, can be recursively computed from the two scale relations (7.1.1) and (7.1.2) respectively.

Multi-resolution analysis

The multi-resolution analysis is based on property (7.1.7). It is a decomposition of the Hilbert space $L_2(\mathbb{R})$ on a series of closed subspaces $\{V_j\}_{j\in\mathbb{Z}}$ such that

- $\cdots \subset V_{-2} \subset V_{-1} \subset V_0 \subset V_1 \subset V_2 \subset \cdots V_j \subset V_{j+1} \subset \cdots$
- $\overline{\bigcup_{j\in\mathbb{Z}} V_j} = L^2(\mathbb{R})$
- $\bigcap_{j\in\mathbf{Z}} V_j = \{0\}$
- $f(x) \in V_j \;\Leftrightarrow\; f(2x) \in V_{j+1} \;\forall\; f \in L^2(\mathbb{R}),\; j \in \mathbf{Z}$
- $f(x) \in V_0 \;\Leftrightarrow\; f(x-k) \in V_0 \;\forall\; f \in L^2(\mathbb{R}),\; k \in \mathbf{Z}$
- $\exists \phi \in V_0$ such that $\{\phi(x-k)\}_{k\in\mathbf{Z}}$ forms a Riesz basis for V_0.

Multi-resolution analysis is designed to get good time resolution and poor frequency resolution at high frequencies and good frequency resolution and poor time resolution at low frequencies. The idea of multi-resolution is used in representing functions from the space $L_2(\mathbb{R})$. The wavelet expansion of a function $f(x) \in L_2(\mathbb{R})$ is of the form

$$f(x) = \sum_{k\in\mathbf{Z}} c_{0k}\phi_{0k}(x) + \sum_{j=0}^{\infty}\sum_{k\in\mathbf{Z}} c_{jk}\psi_{jk}(x).$$

This implies that

$$f(x) \in \{V_0 \bigoplus W_0 \bigoplus W_1 \bigoplus W_2 \cdots \bigoplus W_\infty\} = L_2(\mathbb{R}).$$

It is an exact representation of $f(x)$. We can approximate the function $f(x)$ at fixed level of resolution j as

$$\widetilde{f}(x) = \sum_{k\in\mathbf{Z}} c_{jk}\phi_{jk}(x). \tag{7.1.10}$$

For this expansion, we have the following convergence property,

$$\|f - \widetilde{f}\| \leq C2^{-jr}\|f^{(r)}\|, \tag{7.1.11}$$

where

$$c_{jk} = \int \widetilde{f}(x)\phi_{jk}(x)dx,$$

and C, r are constants. Inequality (7.1.11) implies that $\widetilde{f}(x)$ approaches to $f(x)$ as $j \to \infty$.

7.1.1 Construction of Wavelet Filter Coefficients

There are certain restrictions on filter coefficients that is unit area under scaling function (7.1.3), orthonormality of translates of scaling functions (7.1.4), orthonormality of scaling and wavelet functions (7.1.5) and vanishing moments of wavelet functions (7.1.6). We constructed the wavelet filter coefficient for the Daubechies wavelets, which we used for the solution of linear and nonlinear boundary value problems. The simplest Daubechies wavelet is the Haar wavelet, which has explicit expression for calculating the scaling function $\phi(x)$. It is denoted by $D2$, which means Daubechies wavelet having two filter coefficients. It is also denoted by $db1$, which means the Daubechies wavelet having one vanishing moment.
Equation (7.1.3) implies by taking $N = 2$

$$\sum_{l=0}^{N-1} p_l = 2 \quad \Rightarrow \quad p_0 + p_1 = 2. \tag{7.1.12}$$

Since $db1$ has one vanishing moment, therefore from equation (7.1.6), we have

$$\sum_{l=0}^{N-1} (-1)^l p_l = 0 \quad \Rightarrow \quad p_0 - p_1 = 0. \tag{7.1.13}$$

Solving equation (7.1.12) and (7.1.13), we get $p_0 = 1, \quad p_1 = 1.$

Similarly, $db2$ ($D4$) have four wavelet coefficients, i.e., $N = 4$, and two vanishing moments. Using equations (7.1.3), (7.1.4) and (7.1.6), to get

$$\begin{aligned}
\text{Unit area under } \phi \quad &\Rightarrow \quad p_0 + p_1 + p_2 + p_3 = 2. \\
\text{Zeroth moment of } \psi \quad &\Rightarrow \quad p_0 - p_1 + p_2 - p_3 = 0. \\
\text{First moment of } \psi \quad &\Rightarrow \quad 0p_0 - 1p_1 + 2p_2 - 3p_3 = 0.
\end{aligned}$$

$$\text{Orthonormality of } \phi \Rightarrow \begin{cases} p_0p_2 + p_1p_3 = 0, \ m \neq 0, \\ p_0^2 + p_1^2 + p_2^2 + p_3^2 = 2, \ m = 0. \end{cases}$$

Solving system (7.1.1), we get filter coefficients

$p_0 = \frac{1+\sqrt{3}}{4}$, $p_1 = \frac{3+\sqrt{3}}{4}$, $p_2 = \frac{3-\sqrt{3}}{4}$, $p_3 = \frac{1-\sqrt{3}}{4}$.

Similarly, DN has N-coefficients and $\frac{N}{2}$-vanishing moments. We get the other Daubechies filter coefficients by similar procedure. Some are calculated and are shown in Table 7.1.

	$N=2$	$N=4$	$N=6$	$N=8$	$N=10$	$N=12$
p_0	1	0.6830	0.4705	0.3258	0.2264	0.1577
p_1	1	1.1830	1.1411	1.0109	0.8539	0.6995
p_2		0.3170	0.6504	0.8922	1.0243	1.0623
p_3		-0.1830	-0.1909	-0.0396	0.1958	0.4458
p_4			-0.1208	-0.2645	-0.3427	-0.3200
p_5			0.0498	0.0436	-0.0456	-0.1835
p_6				0.0465	0.1097	0.1379
p_7				-0.0150	-0.0088	0.0389
p_8					-0.0178	-0.0447
p_9					0.0047	0.0008
p_{10}						0.0068
p_{11}						-0.0015

Table 7.1: Filter coefficients for the family of Daubechies wavelets DN.

It can be seen that the equation $\sum_{l=0}^{N-1} p_l = 2$ is satisfied.

7.2 Two-term Connection Coefficients

The Daubechies wavelet functions ϕ cannot be represented in closed form for $N > 2$ so analytic calculation of its integrals is not an option, and numerical quadrature is often inaccurate due to highly oscillatory nature of the wavelet basis functions. Latto et al. [76] provide an alternative method for computing the wavelet connection coefficients on unbounded intervals. The two term connection coefficients are defined as

$$\Omega_k^{d_1,d_2} = \int_{-\infty}^{\infty} \phi^{d_1}(x)\phi^{d_2}(x-k)dx. \tag{7.2.1}$$

There is no loss of generality in fixing the shift on the first term at zero because

$$\begin{aligned} \Omega_{k,l}^{d_1,d_2} &= \int_{-\infty}^{\infty} \phi_k^{d_1}(x)\phi_l^{d_2}(x)dx, \\ &= \int_{-\infty}^{\infty} \phi^{d_1}(x)\phi_{l-k}^{d_2}(x)dx, \\ &= \Omega_{l-k}^{d_1,d_2}. \end{aligned}$$

Taking d times derivative of the Daubechies scaling function (7.1.1), by assuming that it is d times differentiable, to obtain

$$\phi^d(x) = 2^d \sum_{l=0}^{N-1} p_l \phi_l^d(2x), \quad \text{where} \quad \phi^d(x) := \tfrac{d^d\phi}{dx^d}. \tag{7.2.2}$$

Use equation (7.2.2) in (7.2.1) and changing variables, we get

$$\begin{aligned}
\Omega_k^{d_1,d_2} &= \tfrac{1}{2}\int_{-\infty}^{\infty}(2^{d_1}\sum_{m=0}^{N-1}p_m\phi_m^{d_1}(2x))(2^{d_2}\sum_{l=0}^{N-1}p_l\phi_{l+2k}^{d_2}(2x))d(2x),\\
&= 2^{d_1+d_2-1}\sum_{m=0}^{N-1}\sum_{l=0}^{N-1}p_mp_l\int_{-\infty}^{\infty}\phi_m^{d_1}(2x)\phi_{l+2k}^{d_2}(2x)d(2x),\\
&= 2^{d_1+d_2-1}\sum_{m,l}p_mp_l\int_{-\infty}^{\infty}\phi_m^{d_1}(x)\phi_{l+2k}^{d_2}(x)dx,\\
&= 2^{d_1+d_2-1}\sum_{m,l}p_mp_l\int_{-\infty}^{\infty}\phi^{d_1}(x)\phi_{l+2k-m}^{d_2}(x)dx.
\end{aligned}$$

Changing indices, to obtain

$$\Omega_k^{d_1,d_2} = 2^{d_1+d_2-1}\sum_{m,l}p_mp_{l-2k+m}\int_{-\infty}^{\infty}\phi^{d_1}(x)\phi^{d_2}(x-l)dx. \tag{7.2.3}$$

Let $\bigwedge^{d_1,d_2}$ be a column vector with $2N-3$ components which are connection coefficients, $\bigwedge^{d_1,d_2} = [\Omega_k^{d_1,d_2}]_{k=2-N:N-2}$. Equation (7.2.3) gives a system of linear equations with $\bigwedge^{d_1,d_2}$ as unknown vector, we can write equation (7.2.3) in vector form as

$$\tfrac{1}{2^{d_1+d_2-1}}\bigwedge^{d_1,d_2} = T\bigwedge^{d_1,d_2}. \tag{7.2.4}$$

We derive an expression of calculating the connection coefficients according to the V_j spaces. Define the connection coefficients as

$$\Omega_k^{d_1,d_2} = 2^j\int_{-\infty}^{\infty}\phi^{d_1}(2^jx)\phi^{d_2}(2^jx-k)dx. \tag{7.2.5}$$

Letting $d_1 = 0,\ d_2 = d$, we make the substitution, $y = 2^jx$, use in [31], through out our work. This substitution provides a way of calculating the connection coefficients for V_j spaces. Here j is an integer and 2^j is scaling factor. Its corresponds to either the expansion ($j > 0$) or contraction ($j < 0$) of the scaling or wavelet function.
Connection coefficients takes the form

$$\Omega_k^{0,d} = 2^{dj}\int\phi^{(0)}(y)\phi^d(y-k)dy. \tag{7.2.6}$$

Similarly, we can obtain

$$\tfrac{1}{2^{d-1}}\bigwedge^{0,d} = T\bigwedge^{0,d}, \tag{7.2.7}$$

where T is a square matrix of order $2N-3$, i.e., $T_{k:l} = \sum_{m=0}^{N-1}p_mp_{l-2k+m}$, where indices k and l vary from $2-N$ to $N-2$. It is homogeneous system and thus does not have a unique nonzero solution. In order to make the system inhomogeneous, one equation is added which is derived from the moment equations of the scaling function.

Moment of Daubechies Scaling Function

The moments M_i^j of ϕ_i are defined as

$$M_i^j = \int_{-\infty}^{\infty} x^j \phi_i(x) dx. \tag{7.2.8}$$

Since $\int_{-\infty}^{\infty} \phi(x)dx = 1$, this implies that $M_0^0 = 1$. To derive an explicit formula to compute the moments, let us consider the jth moment of $\phi(x)$ and use the refinement relation (7.1.1) to obtain

$$\begin{aligned} M_0^j &= \int_{-\infty}^{\infty} x^j \phi(x) dx, \\ &= \int_{-\infty}^{\infty} x^j \sum_{i=0}^{N-1} p_i \phi(2x-i) dx, \\ &= 2^{-j-1} \sum_{i=0}^{N-1} p_i \int_{-\infty}^{\infty} (2x)^j \phi(2x-i) d(2x), \\ M_0^j &= 2^{-j-1} \sum_{i=0}^{N-1} p_i M_i^j. \end{aligned} \tag{7.2.9}$$

By making substitution $x - i = u$ in equation (7.2.8) to get

$$\begin{aligned} M_i^j &= \int_{-\infty}^{\infty} (u+i)^j \phi(u) du, \\ &= \sum_{k=0}^{j} \binom{j}{k} i^{j-k} M_0^k. \end{aligned} \tag{7.2.10}$$

Use equation (7.2.10) in equation (7.2.9)

$$\begin{aligned} M_0^j &= 2^{-j-1} \sum_{i=0}^{N-1} p_i \sum_{k=0}^{j} \binom{j}{k} i^{j-k} M_0^k, \\ &= 2^{-j-1} \sum_{i=0}^{N-1} p_i \Big(\sum_{k=0}^{j-1} \binom{j}{k} i^{j-k} M_0^k + M_0^j \Big), \\ &= 2^{-j-1} \sum_{k=0}^{j-1} \binom{j}{k} M_0^k \Big(\sum_{i=0}^{N-1} p_i i^{j-k} \Big) + 2^{-j-1} M_0^j \sum_{i=0}^{N-1} p_i, \end{aligned}$$

Since $\sum_{i=0}^{N-1} p_i = 2$, we get

$$M_0^j = \frac{1}{2^{j+1}} \Big[\sum_{k=0}^{j-1} \binom{j}{k} M_0^k \Big(\sum_{i=0}^{N-1} p_i i^{j-k} \Big) + 2M_0^j \Big],$$

or

$$M_0^j = \frac{1}{2(2^j-1)} \sum_{k=0}^{j-1} \binom{j}{k} M_0^k \sum_{i=0}^{N-1} p_i i^{j-k}. \tag{7.2.11}$$

By substituting the obtained value of M_0^j in equation (7.2.10), we arrive at the explicit formula which were derived by Latto et al. [76] to compute the moments of $\phi_i(x)$

$$M_i^j = \frac{1}{2(2^j-1)} \sum_{k=0}^{j} \binom{j}{k} i^{j-k} \sum_{l=0}^{k-1} \binom{k}{l} M_0^l \Big(\sum_{i=0}^{N-1} p_i i^{k-l} \Big),$$

where p_i are Daubechies wavelet coefficients.

The whole calculations were made to find the moment of scaling function in V_0 space. Now following [103], we extend the procedure for the moment of scaling function in V_j space for $j \geq 0$. By using the relation (7.1.6), we can represent the monomials x^d, $d = 0, 1, ..., \frac{N}{2} - 1$, as the linear combinations of Daubechies scaling function in V_j space as

$$x^d = \sum_i m_i^d \phi_{j,i}(x), \tag{7.2.12}$$

where m_i^d is the d^{th} moment of $\phi_{j,i}(x) := 2^{\frac{j}{2}}\phi(2^j x - i)$ and is given by using the orthonormality of $\phi(x)$ as

$$m_i^d = \int_{-\infty}^{\infty} x^d 2^{j/2} \phi_i(2^j x) dx. \tag{7.2.13}$$

Consider the substitution $y = 2^j x$ in equation (7.2.12)

$$y^d = 2^{jd} 2^{j/2} \sum_i m_i^d \phi_i(y). \tag{7.2.14}$$

Differentiate equation (7.2.14) d times, to get

$$d! = 2^{jd} 2^{j/2} \sum_i m_i^d \phi_i^d(y). \tag{7.2.15}$$

Taking inner product on both sides of equation (7.2.15) with $\phi(y)$,

$$d! = 2^{j/2} \sum_i m_i^d 2^{jd} \int_{-\infty}^{\infty} \phi(y)\phi_i^d(y) dy,$$

or

$$d! 2^{-j/2} = \sum_i m_i^d \Omega_i^{0,d},$$

$$d! 2^{-j/2} = \mathbf{m}^d \bigwedge^{0,d}, \tag{7.2.16}$$

where $\mathbf{m}^d$ is a row vector with $2N - 3$ components, $\mathbf{m}^d = [m_i^d]_{i=2-N:N-2}$, and can be derive from equation (7.2.13) as

$$\begin{aligned} m_i^d &= \int_{-\infty}^{\infty} \frac{y^d}{2^{jd}} 2^{j/2} \phi_i(y) d\tfrac{y}{2^j}, \\ m_i^d &= 2^{-jd-j/2} \int_{-\infty}^{\infty} y^d \phi_i(y) dy, \\ m_i^d &= 2^{-jd-j/2} M_i^d, \end{aligned} \tag{7.2.17}$$

where $M_i^d = \int x^d \phi_i(x) dx$ is the d^{th} moment of ϕ_i. Equation (7.2.17) shows that d^{th} moment of $\phi_{j,i}(x)$ is equal to the $2^{-jd-j/2}$ times d^{th} moment of $\phi(x - i)$.

Finally, from equation (7.2.7) and (7.2.16), we get the system for the calculation of connection coefficients

$$\begin{pmatrix} T - \frac{1}{2^{d-1}} I \\ \mathbf{m}^d \end{pmatrix} \bigwedge^{0,d} = \begin{pmatrix} 0 \\ d! 2^{-j/2} \end{pmatrix}.$$

This is the over-determined system of order $(2N-2) \times (2N-3)$, which is solved to get column vector $\bigwedge^{0,d}$.

Latto et al. [76] have only computed the two term connection coefficients at $j = 0,\ N = 6,\ d_1 = 0$ and $d_2 = 2$. We provide tables of connection coefficients in the appendix for the two cases $d_1 = 0,\ d_2 = 2$ and $d_1 = 0,\ d_2 = 1$ by using different values of j and N. The purpose of finding the connection coefficients is to use them in the wavelet Galerkin method for the solution of boundary value problems. Without these connection coefficients wavelet Galerkin method does not work.

7.3 Implementation of Wavelet-Galerkin Method

Consider the following class of boundary value problem

$$y''(x) + ay'(x) + by(x) = f(x), \quad y(0) = \alpha, y(1) = \beta, \tag{7.3.1}$$

where a, b, α and β are real constants. A trial solution for (7.3.1) is

$$y(x) \cong \sum_l c_l 2^{j/2} \phi(2^j x - l), \tag{7.3.2}$$

where c_l are the unknown coefficients. Use (7.3.2) in (7.3.1) to obtain

$$\begin{aligned} \tfrac{d^2}{dx^2}\Big(\sum_l c_l 2^{j/2}\phi(2^j x - l)\Big) + a\tfrac{d}{dx}\Big(\sum_l c_l 2^{j/2}\phi(2^j x - l)\Big) \\ + b\sum_l c_l 2^{j/2}\phi(2^j x - l) - f(x) \neq 0. \end{aligned} \tag{7.3.3}$$

For simplicity, we use substitution $y = 2^j x,\ C_l = 2^{j/2} c_l$ in equation (7.3.3), we get

$$\sum_l C_l 2^{2j} \tfrac{d^2}{dy^2}\phi(y-l) + a\sum_l C_l 2^j \tfrac{d}{dy}\phi(y-l) + b\sum_l C_l \phi(y-l) - f(\tfrac{y}{2^j}) \neq 0. \tag{7.3.4}$$

Multiplying $\phi_p(y)$, on both sides of (7.3.4) and integrating over the domain, we get

$$\begin{aligned} \sum_l C_l 2^{2j} \int \phi(y-p)\tfrac{d^2}{dy^2}\phi(y-l)dy + a\sum_l C_l 2^j \int \phi(y-p)\tfrac{d}{dy}\phi(y-l)dy \\ + b\sum_l C_l \int \phi(y-p)\phi(y-l)dy = \int \phi(y-p) f(\tfrac{y}{2^j})dy, \end{aligned} \tag{7.3.5}$$

where $f(x) = \sum_{i=0}^{m} b_i x^i$, is a polynomial of degree m in x.
The orthonormality of Daubechies wavelets implies

$$\int \phi(y-p)\phi(y-l)dy = \delta_{p,l}. \tag{7.3.6}$$

Now use equation (7.2.6) and (7.3.6) in (7.3.5), we have

$$\sum_l C_l(\Omega^{0,2}_{l-p} + a\Omega^{0,1}_{l-p} + b\delta_{p,l}) = \sum_{i=0}^{m} b_i \int \frac{y^i}{2^{ji}}\phi(y-p)dy,$$

or

$$\sum_l C_l(\Omega^{0,2}_{l-p} + a\Omega^{0,1}_{l-p} + b\delta_{p,l}) = h_p, \tag{7.3.7}$$

where $h_p = \sum_{i=0}^{m} \frac{b_i}{2^{ji}} M^i_p$. The indexes l and p have to cover the whole domain. If the original domain is discretized with 2^j functions that is $0 \le l, p \le 2^j - 1$ and $N-1$ functions have to be added both at the left and right of the 2^j functions, as mentioned in [31]. Now the fictitious domain is discretized with $2^j + 2(N-1)$ functions that is $-(N-1) \le l, p \le 2^j - 1 + (N-1)$. This implies that equation (7.3.7) will form an $2^j + 2(N-1)$ by $2^j + 2(N-1)$ linear system

$$\mathbf{AC} = \mathbf{H},$$

where $\mathbf{C}$ and $\mathbf{H}$ are column vectors containing all the C_l and h_p respectively and $\mathbf{A}$ is an square matrix of order $2^j + 2(N-1)$.

Treatment of the boundary conditions [31] is as follows:

Conditions $y(0) = \alpha$ and $y(1) = \beta$ imply

$$\sum_l C_l\phi_l(0) = \alpha, \tag{7.3.8}$$

$$\sum_l C_l\phi_l(1) = \beta. \tag{7.3.9}$$

Since inner product of $\phi_l(y)$ and $\phi_p(y)$ gives the equation (7.3.6), therefore equation (7.3.8) and (7.3.9) implies

$$\sum_l C_l\delta_{l,p}(0) = \alpha, \tag{7.3.10}$$

$$\sum_l C_l\delta_{l,p}(1) = \beta. \tag{7.3.11}$$

First and last equations in (7.3.7) are replaced by (7.3.10) and (7.3.11) respectively. In equations (7.3.10) and (7.3.11), the δ function has to be evaluated at 0 and 1 respectively. So, for the left and right boundary we have $l = p = 0$ and $l = p = 2^j - 1$ respectively and they occupy first and last row in the matrix $\mathbf{A}$.

Solution of Linear Boundary Value Problems

Consider the harmonic wave equation [11]

$$\frac{d^2y}{dx^2} + By = 0,\ y(0) = 0,\ y(1) = 1, \tag{7.3.12}$$

where B is a constant. The exact solution of (7.3.12) is

$$y(x) = \frac{\sin(x\sqrt{B})}{\sin(\sqrt{B})}.$$

Apply the wavelet Galerkin method to equation (7.3.12), we get

$$\sum_l C_l(\Omega_{l-p}^{0,2} + B\delta_{p,l}) = 0,$$

and boundary conditions gives

$$\sum_l C_l\delta_{l,p}(0) = 0, \ \sum_l C_l\delta_{l,p}(1) = 1.$$

Consider $B = 891 = (9.5\pi)^2$ in equation (7.3.12), as given in [11].

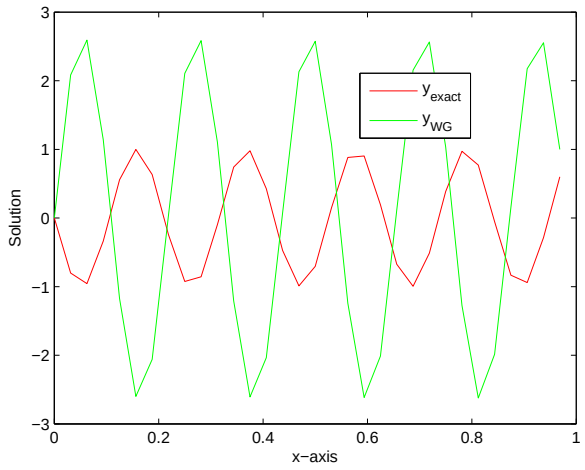

Figure 7.1: Comparison of exact solution and solution by wavelet Galerkin method with $D6$ at $j = 5$.

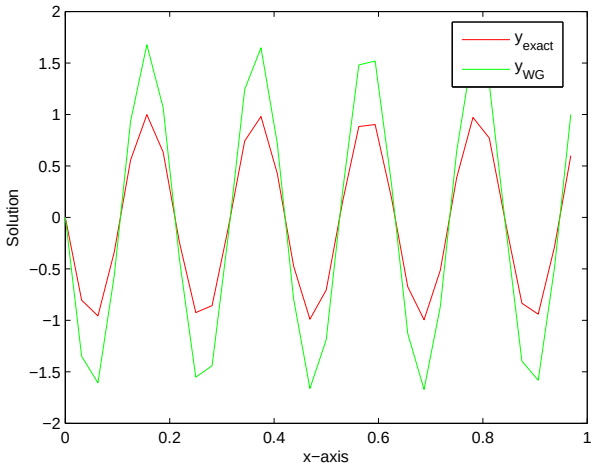

Figure 7.2: Comparison of exact solution and solution by wavelet Galerkin method with $D12$ at $j = 5$.

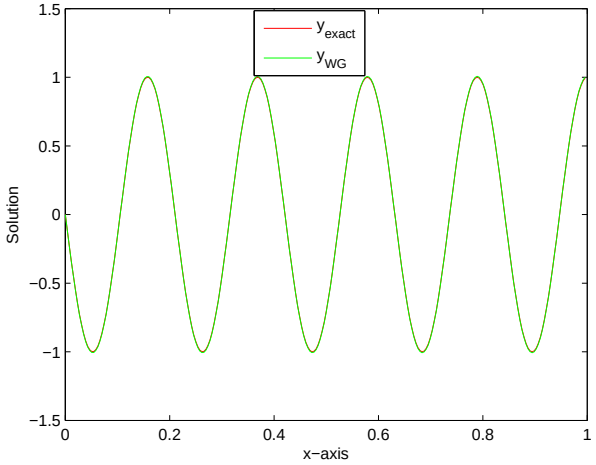

Figure 7.3: Comparison of exact solution and solution by wavelet Galerkin method with $D6$ at $j = 8$.

Figure 7.1 shows the exact solution and solution by wavelet Galerkin method with $D6$ and resolution $j = 5$, that is $2^j = 32$ scaling functions. Figure 7.2 is used to show that wavelet Galerkin method with higher order wavelets $D12$ gives better results as compared to low order wavelets $D6$, as shown in Figure 7.1, with same resolution level $j = 5$. According to the error analysis of Daubechies wavelets as shown in section 7.1, we get more accurate results while increasing level of resolution j as shown in Figure 7.3. The approximate solution by wavelet Galerkin method are in good agreement with exact solution.

7.4 Wavelet Galerkin Quasilinearization Method for Nonlinear Boundary Value Problems

A numerical method is introduced by wavelet-Galerkin and quasilinearization technique for nonlinear boundary value problems. Quasilinearization technique is applied to discretize the nonlinear differential equation and then wavelet-Galerkin method is implemented to discretized differential equations. In each iteration of quasilinearization technique, solution is updated by wavelet- Galerkin method. In order to demonstrate the applicability of method, we consider the various nonlinear boundary value problems.

Example 1: We consider the nonlinear two-point boundary value problem [34]

$$y''(x) + y^2(x) = x^4 + 2, 0 < x < 1, \tag{7.4.1}$$

subject to the boundary conditions $y(0) = 0,\ y(1) = 1$. The exact solution is $y(x) = x^2$. Apply quasilinearization to equation (7.4.1), we get

$$y''_{r+1}(x) + 2y_r(x)y_{r+1}(x) = y_r^2(x) + 2 + x^4, \tag{7.4.2}$$

with the boundary conditions: $y_{r+1}(0) = 0$, $y_{r+1}(1) = 1$.

Apply wavelet–Galerkin method to equation (7.4.2) we have

$$\sum_l C_l(\Omega^{0,2}_{l-p} + 2y_r(x)\delta_{p,l}) = y_r^2(x) + \sum_{i=0}^{4} \frac{b_i}{2^{ji}} M_p^i,$$

and boundary conditions implies

$$\sum_l C_l\delta_{l,p}(0) = 0,\ \sum_l C_l\delta_{l,p}(1) = 1,$$

where $b = [2, 0, 0, 0, 1]$, with the initial approximation $y_0(x) = 0$.

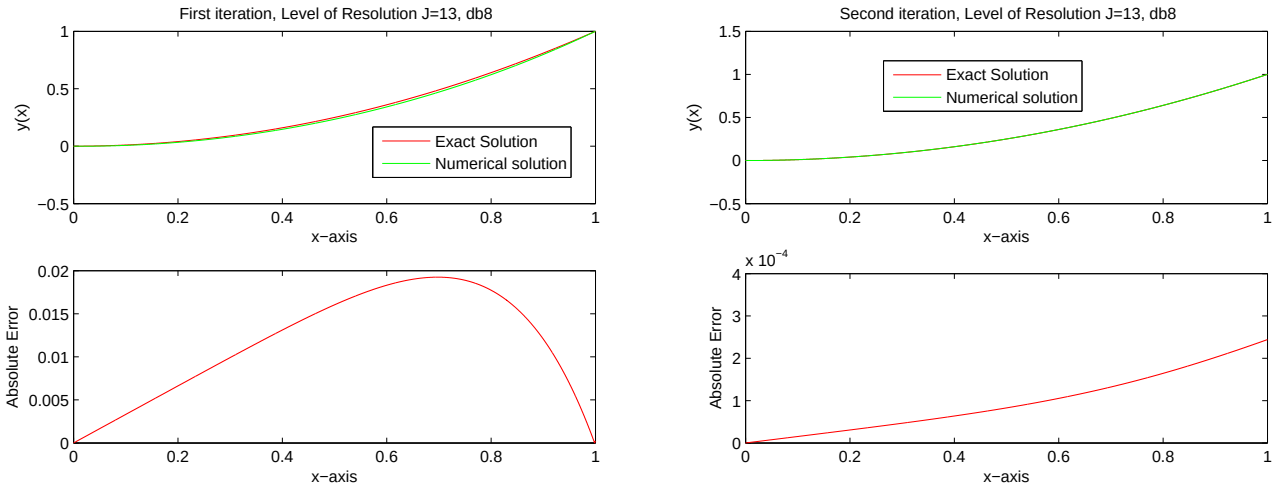

Figure 7.4: Comparison of exact solution and solution by wavelet Galerkin quasilinearization method at $J = 13$, for different iterations, and we used $D16$.

3^{rd} *iteration*	$J = 13$		
x	y_{NEW}	y_{exact}	Absolute Error
0.1	1.0022e-2	1.0e-2	2.2423e-5
0.2	4.0045e-2	4.0e-2	4.4852e-5
0.3	9.0067e-2	9.0e-2	6.7318e-5
0.4	1.6009e-1	1.6e-1	8.9901e-5
0.5	2.5011e-1	2.5e-1	1.1275e-4
0.6	3.6014e-1	3.6e-1	1.3613e-4
0.7	4.9016e-1	4.9e-1	1.6038e-4
0.8	6.4019e-1	6.4e-1	1.8602e-4
0.9	8.1021e-1	8.1e-1	2.1369e-4

Table 7.2: Comparison of exact solution y_{exact} and solution by the wavelet Galerkin quasilinearization method y_{NEW} at 2^{nd} iteration, level of resolution $J = 13$ and $D16$ is used as Galerkin bases.

We solved the equation (7.4.1) by using $D16$ and fixed the level of resolution $J = 13$. Figure 7.4 shows the exact solution and approximate solution at first and second iteration, i.e., $y_0(x)$ is the initial approximation and by using $y_0(x)$ we get $y_1(x)$, that is the solution at first iteration and then $y_1(x)$ is used to get $y_2(x)$, which is the solution of equation (7.4.1) at second iteration. Table 7.2 is used to compares the approximate solution, at second iteration for $J = 13$, with exact solution. We

may get the more accurate results while increasing level of resolution at higher iteration.

Example 2: We consider the nonlinear Bratu's boundary value problem

$$-y''(x) = \lambda e^{y(x)},\ y(0) = 0,\ y(1) = 0. \tag{7.4.3}$$

The quasilinear form of equation (7.4.3) is

$$y''_{r+1}(x) + \lambda e^{y_r(x)} y_{r+1}(x) = -\lambda e^{y_r(x)}(1 - y_r(x)), \tag{7.4.4}$$

with the boundary conditions $y_{r+1}(0) = 0$, $y_{r+1}(1) = 0$.
Wavelet–Galerkin method for equation (7.4.4) implies

$$\sum_l C_l(\Omega^{0,2}_{l-p} + \lambda e^{y_r(x)}\delta_{p,l}) = -\lambda e^{y_r(x)}(1 - y_r(x)),$$

and, from boundary conditions, we have

$$\sum_l C_l \delta_{l,p}(0) = 0,\ \sum_l C_l \delta_{l,p}(1) = 0,$$

with the initial approximation $y_0(x) = 0$.

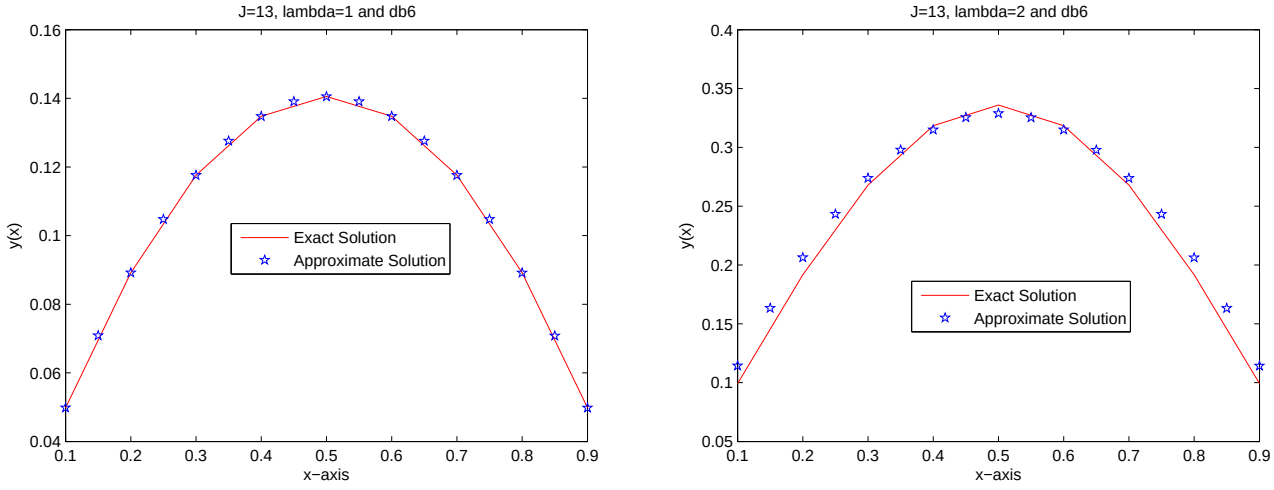

Figure 7.5: Comparison of exact solution and solution by wavelet Galerkin method with quasilinearization technique at level of resolution $J = 13$ and we use $D12$ as Galerkin bases, and at $\lambda = 1$ and $\lambda = 2$ respectively.

		$\lambda = 1$	
2^{nd} *iteration*		$J = 13$	
x	y_{DM} [28]	y_{NEW}	y_{exact}
0.1	0.0471616875	0.0498386633	0.0498467900
0.2	0.0871680000	0.0891737644	0.0891899350
0.3	0.1177614375	0.1175850602	0.1176090956
0.4	0.1369920000	0.1347586231	0.1347902526
0.5	0.1435546875	0.1405003497	0.1405392142
0.6	0.1369920000	0.1347446015	0.1347902526
0.7	0.1177614375	0.1175571769	0.1176090956
0.8	0.0871680000	0.0891323318	0.0891899350
0.9	0.0471616875	0.0497841328	0.0498467900

Table 7.3: Comparison of exact solution y_{exact}, solution by decomposition method y_{DM} and solution by the wavelet Galerkin quasilinearization method y_{NEW} at 2^{nd} iteration and for $D12$.

		$\lambda = 2$	
2^{nd} *iteration*		$J = 13$	
x	y_{DM} [28]	y_{NEW}	y_{exact}
0.1	0.1144107440	0.1143861795	0.0991935000
0.2	0.2064191156	0.2063705472	0.1917440000
0.3	0.2738793116	0.2738079343	0.2679915000
0.4	0.3150893646	0.3149970528	0.3183360000
0.5	0.3289524214	0.3288416969	0.3359375000
0.6	0.3150893646	0.3149632892	0.3183360000
0.7	0.2738793116	0.2737413240	0.2679915000
0.8	0.2064191156	0.2062728271	0.1917440000
0.9	0.1144107440	0.1142597336	0.0991935000

Table 7.4: Comparison of exact solution y_{exact}, solution by decomposition method y_{DM} and solution by the wavelet Galerkin quasilinearization method y_{NEW} at 2^{nd} iteration and for $D12$.

Bratu's boundary value problem is solved by using $D12$ as Galerkin bases and at level of resolution $J = 13$. We compared our results with the results obtained by decomposition method in (7.4.3) and exact solution. For $\lambda = 1$ and $\lambda = 2$, our results are more accurate as compared to decomposition method, as shown in Tables 7.3 and 7.4 respectively. We used the MATLAB command of one-

dimensional data interpolation using spline to get the values at $x = 0.1,\ x = 0.2, ...,\ x = 0.9$ and plot the exact and approximate solutions at these points for $\lambda = 1$ and $\lambda = 2$ as shown in Figure 7.5.

Example 3: Consider the nonlinear Troesch's boundary value problem

$$\begin{aligned} &y''(x) - \lambda \sinh(\lambda y(x)) = 0,\ 0 \le x \le 1, \\ &y(0) = 0,\ y(1) = 1. \end{aligned} \tag{7.4.5}$$

The quasilinearized form of equation (7.4.5) is

$$y''_{r+1}(x) - \lambda^2 \cosh(\lambda y_r(x)) y_{r+1}(x) = \lambda \sinh(\lambda y_r(x)) - \lambda^2 y_r(x) \cosh(\lambda y_r(x)), \tag{7.4.6}$$

where $0 \le x \le 1$, with the boundary conditions $y_{r+1}(0) = 0$, $y_{r+1}(1) = 1$.

Implementation of wavelet–Galerkin method to equation (7.4.6), implies

$$\sum_l C_l(\Omega^{0,2}_{l-p} - \lambda^2 \cosh(\lambda y_r(x))\delta_{p,l}) = \lambda \sinh(\lambda y_r(x)) - \lambda^2 y_r(x) \cosh(\lambda y_r(x)),$$

and boundary conditions leads to

$$\sum_l C_l \delta_{l,p}(0) = 0,\ \sum_l C_l \delta_{l,p}(1) = 1,$$

with the initial approximation $y_0(x) = 0$.

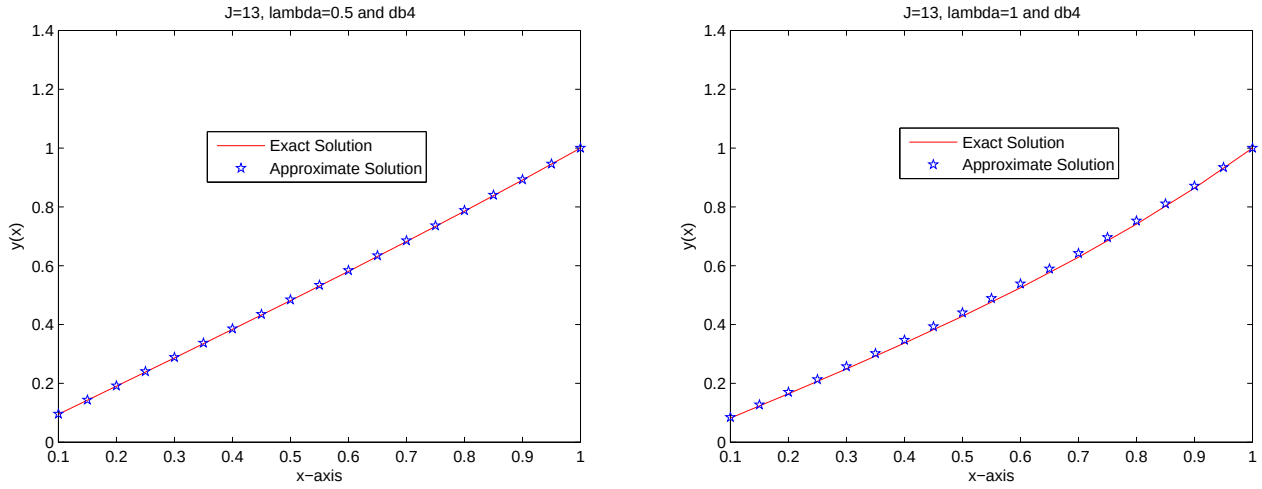

Figure 7.6: Comparison of exact solution and solution by wavelet Galerkin quasilinearization method at level of resolution $J = 13$ and for $D8$, and at $\lambda = 0.5$ and $\lambda = 1$ respectively.

				$\lambda = 0.5$
2^{nd} *iteration*		$J = 11$	$J = 13$	
x	y_{VIM} [84]	y_{NEW}	y_{NEW}	y_{exact}
0.1	0.100042	0.095994	0.095956	0.095177
0.2	0.200334	0.192228	0.192152	0.190634
0.3	0.301128	0.288944	0.288829	0.286653
0.4	0.402677	0.386385	0.386231	0.383523
0.5	0.505241	0.484798	0.484606	0.481537
0.6	0.609082	0.584436	0.584204	0.581002
0.7	0.714470	0.685556	0.685284	0.682235
0.8	0.821682	0.788424	0.788112	0.785572
0.9	0.931008	0.893316	0.892962	0.891367
1.0	1.042740	1.000592	1.000194	1.000000

Table 7.5: Comparison of exact solution y_{exact}, solution by variational iteration method y_{VIM} and solutions by wavelet Galerkin quasilinearization method y_{NEW} at 2^{nd} iteration, at different level of resolutions, while using $D8$ as Galerkin bases.

				$\lambda = 1$
2^{nd} *iteration*		$J = 11$	$J = 13$	
x	y_{VIM} [84]	y_{NEW}	y_{NEW}	y_{exact}
0.1	0.100167	0.084715	0.084674	0.081797
0.2	0.201339	0.170280	0.170197	0.164531
0.3	0.304541	0.257558	0.257433	0.249167
0.4	0.410841	0.347444	0.347275	0.336732
0.5	0.521373	0.440880	0.440666	0.428347
0.6	0.637362	0.538877	0.538616	0.525274
0.7	0.760162	0.642538	0.642226	0.628971
0.8	0.891287	0.753089	0.752722	0.741168
0.9	1.032460	0.871929	0.871495	0.863970
1.0	1.185650	1.000718	1.000226	1.000000

Table 7.6: Comparison of exact solution y_{exact}, solution by variational iteration method y_{VIM} and solutions by wavelet Galerkin quasilinearization method y_{NEW} at 2^{nd} iteration, at different level of resolutions while using $D8$ as Galerkin bases.

Tables 7.5, 7.6 and Figure 7.6 represent the solution of equation (7.4.5) at second iteration. $D8$ is used as Galerkin bases to find the solution of (7.4.5) at different level of resolutions and at $\lambda = 0.5$ and $\lambda = 1$ as shown in Tables 7.5 and 7.6 respectively. Solutions by wavelet Galerkin quasilinearization method are compared with variational iteration method [84] and with exact solution. Our results are in high agreement with exact solution and better than variational iteration method [84].

Example 4: Consider the following nonlinear boundary value problem,

$$y''(x) + y'(x) + y^3(x) + y(x) = f(x), \tag{7.4.7}$$

subject to the boundary conditions $y(0) = 0, \quad y(1) = 0$, where $f(x) = 2 + 2x + x^2 - 20x^3 - 5x^4 - x^5 + x^6 - 3x^9 + 3x^{12} - x^{15}$ and exact solution is given by $y(x) = x^2 - x^5$.
Applying the quasilinearization technique to equation (7.4.7), we get

$$y''_{r+1}(x) + y'_{r+1}(x) + (1 + 3y_r^2(x))y_{r+1}(x) = f(x) + 2y_r^3(x), \tag{7.4.8}$$

with the boundary conditions $y_{r+1}(0) = 0,\ y_{r+1}(1) = 0$.
Now we apply the wavelet–Galerkin method to equation (7.4.8),

$$\sum_l C_l(\Omega^{0,2}_{l-p} + \Omega^{0,1}_{l-p} + (1 + 3y_r^2(x))\delta_{p,l}) = 2y_r^3(x) + \sum_{i=0}^{15} \frac{b_i}{2^{ji}} M_p^i,$$

and boundary conditions implies

$$\sum_l C_l \delta_{l,p}(0) = 0,\ \sum_l C_l \delta_{l,p}(1) = 0,$$

where $b = [2, 2, 1, -20, -5, -1, 1, 0, 0, -3, 0, 0, 3, 0, 0, -1]$, with the initial approximations $y_0(x) = 0$.

2^{nd} *iteration*	$J = 13$		
x	y_{NEW}	y_{exact}	Absolute Error
0.1	0.0100320512	0.0099900000	4.2051152889e-005
0.2	0.0397617227	0.0396800000	8.1722744304e-005
0.3	0.0876864075	0.0875700000	1.1640750572e-004
0.4	0.1499017545	0.1497600000	1.4175454098e-004
0.5	0.2189016605	0.2187500000	1.5166050983e-004
0.6	0.2823782628	0.2822400000	1.3826276219e-004
0.7	0.3220219443	0.3219300000	9.1944320423e-005
0.8	0.3123213602	0.3123199999	1.3602317094e-006
0.9	0.2193634808	0.2195099999	1.4651915492e-004

Table 7.7: Comparison of exact solution y_{exact} and solution by wavelet Galerkin quasilinearization method y_{NEW} at 2^{nd} iteration , level of resolutions $J = 13$ and $D10$ is used as Galerkin bases.

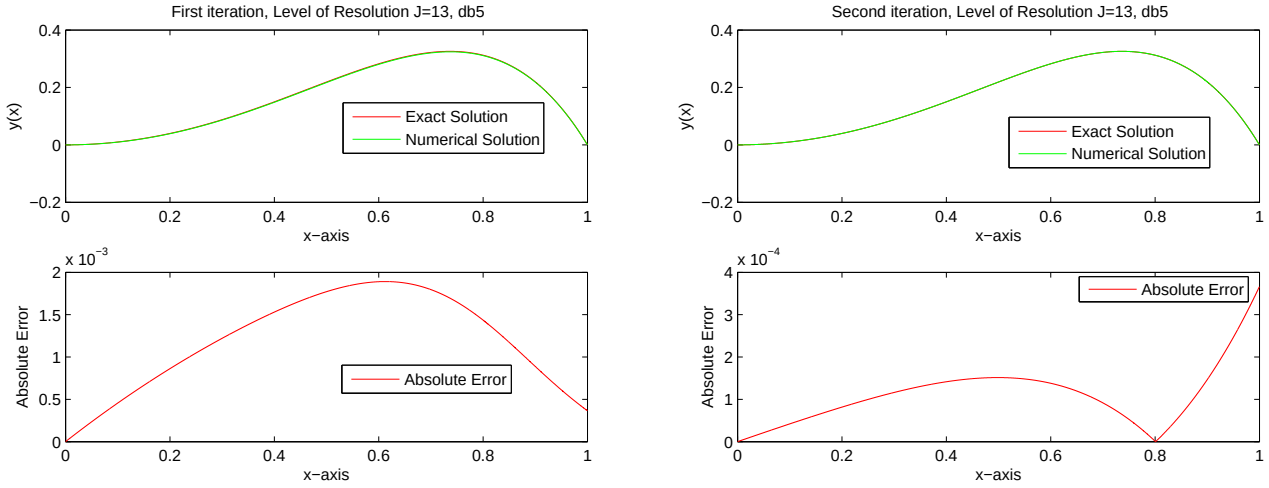

Figure 7.7: Comparison of exact solution and solution by wavelet Galerkin quasilinearization method at $J = 13$, for different iterations, and for $D10$.

Numerical solution by wavelet Galerkin quasilinearization method for (7.4.7) at second iteration and level of resolution $J = 13$, are stable and accurate as shown in Table 7.7. To get the more accurate results increase the iteration or level of resolution or both. Figure 7.7 shows that approximate solution converge to the exact solution while increasing iterations. Here $D10$ is used as Galerkin bases.

7.4.1 Conclusion

We have successfully constructed the wavelet filter coefficients, and two term connection coefficients which are used in wavelet Galerkin quasilinearization method for solving linear and nonlinear boundary value problems. It is shown that the wavelet–Galerkin method with quasilinearization method gives stable and accurate results when applied to different nonlinear boundary value problems. The method provides better and more accurate results as compared to variational iteration method and decomposition method, as shown in Tables 7.3–7.6. Also results are in good agreement with exact solutions. Figures 7.4 and 7.7 shows that approximate solution converge to the exact solution while iterations are increased and absolute error goes down. The main advantage of the method is that the different type of non-linearities can easily be handled.

Chapter 8

Numerical Techniques for Nonlinear Fractional Differential Equations

Fractional differential equation is a generalization of the ordinary and partial differential equation to arbitrary non-integer order. During the last decade, several papers have been devoted to the study of the numerical solution of fractional differential equations. Therefore different numerical methods have been introduced and utilized for providing approximate solutions. Some of these methods include, the Adomian decomposition method [44], the homotopy perturbation method [60] and Haar wavelets method [115, 130].

In this chapter, we introduce two approximate methods for solving nonlinear fractional differential equation. The first method is the combinations of Chebyshev wavelet method with quasilinearization technique and second method is developed by using Legendre wavelet method in conjunction with quasilinearization technique. We discuss these methods in the present chapter.

8.1 Chebyshev Wavelet Quasilinearization Technique for Nonlinear Fractional Differential Equations

Chebyshev wavelets are orthonormal and have compact support. The advantage of Chebyshev wavelets operational matrices approach is that it reduces the differential equation to a system of algebraic equations. The first kind Chebyshev wavelets is utilized in [70], authors constructed operational matrices of integration and solve the linear ordinary differential equations. It also utilized for solving fractional nonlinear integro–differential equations in [57]. According to [127], authors derived operational matrices by using second kind Chebyshev wavelets for solving fractional linear and nonlinear ordinary differential equation, they dealt only with the quadratic nonlinearity. Chebyshev wavelets method is also used for solving linear partial differential equation in [58], authors focused on the solution of the second order linear hyperbolic telegraph equation.

We developed a solution method, Chebyshev wavelet quasilinearization technique, for fractional nonlinear differential equation. The method utilizes the Chebyshev wavelets in conjunction with quasilinearization technique. The operational matrices are derived and utilized to reduce the fractional differential equation to a system of algebraic equations. Convergence analysis for the present method is also investigated. Numerical examples are provided to illustrate the efficiency and accuracy of the technique.

8.1.1 Second Kind Chebyshev Wavelets and Operational Matrices

The second kind Chebyshev polynomials [86], $U_m(x)$, of order m are defined for $m \in \mathbf{Z}^+$, on the interval $[-1, 1]$ and given by the following recurrence formulae

$$U_0(x) = 1, \quad U_1(x) = 2x, \quad U_{m+1}(x) = 2xU_m(x) - U_{m-1}(x), \quad m = 1, 2, 3, \cdots .$$

The second kind Chebyshev polynomials are orthogonal on $[-1, 1]$ with respect to the weight function $\sqrt{1-x^2}$ as

$$\int_{-1}^{1} \sqrt{1-x^2} U_m(x) U_n(x) dx = \frac{\pi}{2} \delta_{mn},$$

where $\frac{\pi}{2}$ is the normalizing factor and δ is the Kronecker delta function.
Scaling and translation of the basic wavelet (mother wavelet) $\psi(x)$ define the basis

$$\psi_{p,q}(x) = \frac{1}{\sqrt{|p|}} \psi\Big(\frac{x-q}{p}\Big), \quad p, q \in \mathbb{R},\ p \neq 0,$$

where p is scaling parameter and q is the translation parameter. By restricting p, q to discrete values as: $p = p_0^{-k}$, $q = nq_0p_0^{-k}$, where $p_0 > 1$, $q_0 > 0$ and $k, n \in \mathbb{N}$, we get the following family of discrete wavelets as

$$\psi_{k,n}(x) = p_0^{\frac{k}{2}} \psi(p_0^k x - nq_0). \tag{8.1.1}$$

The set of wavelets (8.1.1) forms an orthogonal basis of $L^2[0, 1)$. In particular, when $p_0 = 2$ and $q_0 = 1$, then $\psi_{k,n}$ form an orthonormal basis. That is

$$\langle\, \psi_{k,n}(x), \psi_{l,m}(x) \rangle = \delta_{kl}\delta_{nm}.$$

The discrete wavelets transform is defined as

$$\psi_{k,n}(x) = 2^{\frac{k}{2}} \psi(2^k x - n).$$

The second kind Chebyshev wavelets are defined on interval $[0, 1)$ by

$$\psi_{n,m}(x) = \begin{cases} \sqrt{\frac{2}{\pi}} 2^{\frac{k}{2}} U_m(2^k x - \hat{n}), & \frac{\hat{n}-1}{2^k} \leq x < \frac{\hat{n}+1}{2^k}, \\ 0, & elsewhere, \end{cases} \tag{8.1.2}$$

where $k = 1, 2, 3, \cdots$, is the level of resolution, $\hat{n} = 2n - 1$, $n = 1, 2, 3, \cdots, 2^{k-1}$, is the translation parameter, $m = 0, 1, 2, \cdots, M - 1$, $M \in \mathbb{N}$, is the order of the second kind Chebyshev polynomials.

Function Approximations and the Second Kind Chebyshev Wavelets Matrix

We can expand any function $y(x) \in L^2[0,1)$ into truncated second kind Chebyshev wavelets series as

$$y(x) \approx \sum_{n=1}^{2^{k-1}} \sum_{m=0}^{M-1} c_{nm}\psi_{n,m}(x) = \mathbf{C}^T \mathbf{\Psi}(x), \tag{8.1.3}$$

where $\mathbf{C}$ and $\Psi(x)$ are $\hat{m} \times 1$, $(\hat{m} = 2^{k-1}M)$, matrices, given by

$\mathbf{C}$=$[c_{10}, c_{11}, \cdots, c_{1M-1}, c_{20}, c_{21}, \cdots, c_{2M-1}, \cdots, c_{2^{k-1}0}, c_{2^{k-1}1}, \cdots, c_{2^{k-1}M-1}]^T$,

$\mathbf{\Psi}(x) = [\psi_{1,0}(x), \psi_{1,1}(x), \cdots, \psi_{1M-1}(x), \psi_{2,0}(x), \psi_{2,1}(x), \cdots, \psi_{2,M-1}(x)$

$, \cdots, \psi_{2^{k-1},0}(x), \psi_{2^{k-1},1}(x), \cdots, \psi_{2^{k-1},M-1}(x)]^T$.

The collocation points for the second kind Chebyshev wavelets are taken as $x_i = \frac{2i-1}{2^k M}$, $i = 1, 2, ..., 2^{k-1}M$. The second kind Chebyshev wavelets matrix $\mathbf{\Psi}_{\hat{m},\hat{m}}$ is given as

$$\mathbf{\Psi}_{\hat{m}\times\hat{m}} = \left[\mathbf{\Psi}\left(\frac{1}{2^k M}\right), \mathbf{\Psi}\left(\frac{3}{2^k M}\right), ..., \mathbf{\Psi}\left(\frac{2^k M - 1}{2^k M}\right)\right]. \tag{8.1.4}$$

In particular, we fix $k = 2,\ M = 3$, we have $n = 1, 2$; $m = 0, 1, 2$ and $i = 1, 2, ..., 6$, the second kind Chebyshev wavelets matrix is given as

$$\Psi_{6\times 6} = \begin{pmatrix} 1.2732 & 1.2732 & 1.2732 & 0 & 0 & 0 \\ 0 & 0 & 0 & 1.2732 & 1.2732 & 1.2732 \\ -1.6977 & 0 & 1.6977 & 0 & 0 & 0 \\ 0 & 0 & 0 & -1.6977 & 0 & 1.6977 \\ 0.9903 & -1.2732 & 0.9903 & 0 & 0 & 0 \\ 0 & 0 & 0 & 0.9903 & -1.2732 & 0.9903 \end{pmatrix}$$

Any function of two variables $u(x,t) \in L_2\left([0,1] \times [0,1]\right)$ can be approximated as

$$u(x,t) \approx \sum_{n=1}^{2^{k-1}} \sum_{m=0}^{M-1} \sum_{i=1}^{2^{k-1}} \sum_{j=0}^{M-1} c_{nm,ij}\psi_{n,m}(x)\psi_{i,j}(t),$$

or

$$u(x,t) \approx \sum_{l=1}^{\hat{m}} \sum_{p=1}^{\hat{m}} c_{l,p}\psi_l(x)\psi_p(t) = \mathbf{\Psi}^T(x)\mathbf{C}\mathbf{\Psi}(t),$$

where C is $\hat{m} \times \hat{m}$ coefficient matrix and its entries are $c_{l,p} =< \psi_l(x), < u(x,t), \psi_p(t) >> .$

Second Kind Chebyshev Wavelets Operational Matrix of Fractional Order Integration

For simplicity, we write (8.1.3) as

$$y(x) \approx \sum_{i=1}^{\hat{m}} c_i\psi_i(x) = \mathbf{C}^T \mathbf{\Psi}(x), \tag{8.1.5}$$

where $c_i = c_{nm}$, $\psi_i = \psi_{n,m}(x)$. The index i is determined by the equation $i = M(n-1) + m + 1$ and $\hat{m} = 2^{k-1}M$. Also, $\mathbf{C} = [c_1, c_2, \cdots, c_{\hat{m}}]^T$, $\mathbf{\Psi}(x) = [\psi_1(x), \psi_2(x), \cdots, \psi_{\hat{m}}(x)]^T$.
An arbitrary function $y \in L_2[0,1)$, can be expanded into block-pulse functions [68] as

$$y(x) \approx \sum_{i=0}^{\hat{m}-1} a_i b_i(x) = \mathbf{a}^T \mathbf{B}(x),$$

where a_i are the coefficients of the block-pulse functions $b_i(x)$. The second kind Chebyshev wavelets can be expanded into $\hat{m}-$set of block-pulse functions as

$$\mathbf{\Psi}(x) = \mathbf{\Psi}_{\hat{m}\times\hat{m}} \mathbf{B}(x). \tag{8.1.6}$$

The fractional integral of block-pulse function vector can be written as

$$(\mathcal{I}^\alpha \mathbf{B})(x) = \mathbf{F}^\alpha_{\hat{m}\times\hat{m}}\ \mathbf{B}(x), \tag{8.1.7}$$

where $\mathbf{F}^\alpha_{\hat{m}\times\hat{m}}$ is given in [68] with

$$\mathbf{P}^\alpha_{\hat{m}\times\hat{m}} = \mathbf{\Psi}_{\hat{m}\times\hat{m}} \mathbf{F}^\alpha (\mathbf{\Psi}_{\hat{m}\times\hat{m}})^{-1}. \tag{8.1.8}$$

The second kind Chebyshev wavelets operational matrix of integration $\mathbf{P}^\alpha_{\hat{m}\times\hat{m}}$ of fractional order α are utilize for solving differential equations.
In particular, for $k = 2$, $M = 3$, $\alpha = 0.75$, the second kind Chebyshev wavelet operational matrix of fractional order integration $\mathbf{P}^{0.75}_{6\times6}$ is given by

$$\mathbf{P}^{0.75}_{6\times6} = \begin{pmatrix} 0.3718 & 0.5024 & 0.1505 & -0.0405 & -0.0115 & 0.0092 \\ 0 & 0.3718 & 0 & 0.1505 & 0 & -0.0115 \\ -0.1966 & 0.0467 & 0.0721 & -0.0196 & 0.0983 & 0.0074 \\ 0 & -0.1966 & 0 & 0.0721 & 0 & 0.0983 \\ 0.0525 & 0.0991 & -0.0304 & -0.0119 & 0.0427 & 0.0039 \\ 0 & 0.0525 & 0 & -0.0304 & 0 & 0.0427 \end{pmatrix}$$

This phenomena makes calculations fast because the operational matrix $\mathbf{P}^\alpha_{\hat{m}\times\hat{m}}$ contains many zero entries.

Chebyshev Wavelets Operational Matrix of Fractional Integration for Boundary Value Problems

We need another operational matrix of fractional integration while solving fractional boundary value problems. In this subsection, we drive an operational matrix of fractional integration for dealing with the boundary conditions while solving fractional boundary value problem. Let $f(x) \in L_2[0,1)$ be a given function, then

$$f(x)I_1^{\alpha}\psi_{n,m}(x) \;\; = \frac{f(x)}{\Gamma(\alpha)}\int_0^1 (1-s)^{\alpha-1}\psi_{n,m}(s)ds. \tag{8.1.9}$$

Since the second kind Chebyshev wavelets are supported on the intervals $[\frac{2n-2}{2^k}, \frac{2n}{2^k})$, therefore

$$\begin{aligned} f(x)I_1^{\alpha}\psi_{n,m}(x) &= \frac{f(x)2^{\frac{k+1}{2}}}{\sqrt{\pi}\Gamma(\alpha)}\int_{\frac{2n-2}{2^k}}^{\frac{2n}{2^k}} (1-s)^{\alpha-1}U_m(2^k s-2n+1)ds, \\ &= f(x)W_{n,m}^{\alpha}, \end{aligned} \tag{8.1.10}$$

where $W_{n,m}^{\alpha} = \frac{2^{\frac{k+1}{2}}}{\sqrt{\pi}\Gamma(\alpha)}\int_{\frac{2n-2}{2^k}}^{\frac{2n}{2^k}} (1-s)^{\alpha-1}U_m(2^k s-2n+1)ds.$

Expand the equation (8.1.10) at the collocation points, $x_i = \frac{2i-1}{2^k M}$, $i = 1, 2, ..., \hat{m}$, to obtain

$$\mathbf{K}_{\hat{\mathbf{m}}\times\hat{\mathbf{m}}}^{\mathbf{f},\alpha} = \mathbf{W}_{\hat{\mathbf{m}}\times\mathbf{1}}^{\alpha}\mathbf{H}_{\mathbf{1}\times\hat{\mathbf{m}}}, \tag{8.1.11}$$

where $\mathbf{H}_{\mathbf{1}\times\hat{\mathbf{m}}} = [f(x_1), f(x_2), ..., f(x_{\hat{m}})]$,
$\mathbf{W}_{\hat{\mathbf{m}}\times\mathbf{1}}^{\alpha} = [W_{1,0}^{\alpha}, W_{1,1}^{\alpha}, \cdots, W_{1M-1}^{\alpha}, W_{2,0}^{\alpha}, W_{2,1}^{\alpha}, \cdots, W_{2,M-1}^{\alpha}, \cdots, W_{2^{k-1},0}^{\alpha}, W_{2^{k-1},1}^{\alpha}, \cdots, W_{2^{k-1},M-1}^{\alpha}]^T$.
In particular, for $k = 2,\ M = 3,\ \alpha = 0.75,$ and $f(x) = x\cos(x)$, we have

$$\mathbf{K}_{\mathbf{6}\times\mathbf{6}}^{\mathbf{f},\mathbf{0.75}} = \begin{bmatrix} 0.0466 & 0.1360 & 0.2140 & 0.2734 & 0.3082 & 0.3133 \\ 0.0684 & 0.1995 & 0.3139 & 0.4011 & 0.4520 & 0.4595 \\ 0.0027 & 0.0078 & 0.0122 & 0.0156 & 0.0176 & 0.0179 \\ 0.0195 & 0.0570 & 0.0897 & 0.1146 & 0.1292 & 0.1313 \\ 0.0159 & 0.0462 & 0.0727 & 0.0929 & 0.1047 & 0.1065 \\ 0.0346 & 0.1011 & 0.1590 & 0.2031 & 0.2290 & 0.2327 \end{bmatrix}$$

8.1.2 Procedure of Implementation to Fractional Nonlinear Ordinary Differential Equation

In this section, we describe the procedure of implementation of the method to fractional nonlinear ordinary differential equations.

Fractional Nonlinear Duffing Oscillator with Damping Effect

Consider the following order Duffing oscillator equation

$$\begin{aligned} &\frac{d^{\alpha}y}{dt^{\alpha}} + a\frac{dy}{dt} + by + dy^3 = f(t), \quad 1 < \alpha \leq 2,\ t \geq 0, \\ &y(0) = A,\ \frac{dy}{dt}(0) = B, \end{aligned} \tag{8.1.12}$$

where $A,\ B,\ a,\ b,$ and d, are constants.

Quasilinearization technique to equation (8.1.12) implies

$$\begin{aligned} &\frac{d^\alpha y_{r+1}}{dt^\alpha} + a\frac{dy_{r+1}}{dt} + (b + 3dy_r^2)y_{r+1} = f(t) + 2dy_r^3, \quad 1 < \alpha \leq 2,\ t \geq 0, \\ &y_{r+1}(0) = A,\ \frac{dy_{r+1}}{dt}(0) = B, \end{aligned} \tag{8.1.13}$$

where $r = 0, 1, 2, ..., N$, $N \in \mathbb{N}$. At this stage, we approximate the higher order derivative term in equation (8.1.13) by Chebyshev wavelets series as

$$\frac{d^\alpha y_{r+1}}{dt^\alpha} = \mathbf{C^{r+1}}^T \mathbf{\Psi}(t). \tag{8.1.14}$$

The integration of (8.1.14) along with initial conditions yields

$$\begin{aligned} y_{r+1} &= (\mathbf{C^{r+1}})^T I_x^\alpha \mathbf{\Psi}(t) + Bt + A, \\ \frac{dy_{r+1}}{dx} &= (\mathbf{C^{r+1}})^T I_x^{\alpha-1} \mathbf{\Psi}(t) + B. \end{aligned} \tag{8.1.15}$$

Substituting the equations (8.1.14) and (8.1.15) in equation (8.1.13), we get

$$(\mathbf{C^{r+1}})^T [\mathbf{\Psi}(t) + aI_x^{\alpha-1}\mathbf{\Psi}(t) + (b + 3dy_r^2) I_x^\alpha \mathbf{\Psi}(t)] = f(t) + 2dy_r^3 - aB - (b + 3dy_r^2)(Bt + A), \tag{8.1.16}$$

with the initial approximations $y_0(x) = A,\ y_0'(x) = B$.

By considering $a = b = d = 1$, $A = 1$ and $B = 0$, equation (8.1.12) implies

$$\begin{aligned} &\frac{d^\alpha y}{dt^\alpha} + \frac{dy}{dt} + y + y^3 = \cos^3(t) - \sin(t), \quad 1 < \alpha \leq 2,\ t \geq 0, \\ &y(0) = 1,\ \frac{dy}{dt}(0) = 0. \end{aligned} \tag{8.1.17}$$

The exact solution at $\alpha = 2$ is given by $y(t) = \cos(t)$.

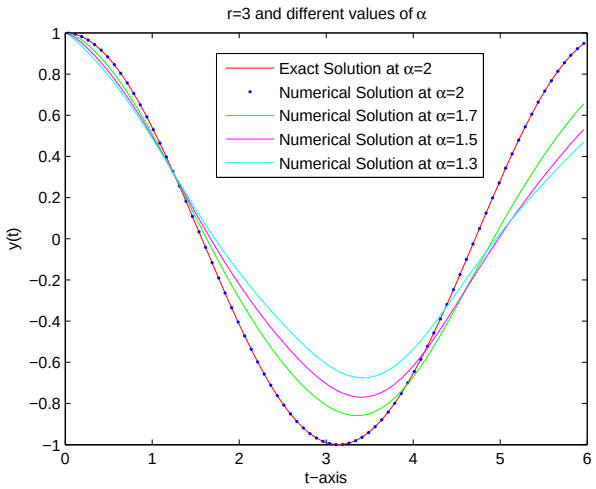

Figure 8.1: Exact solution at $\alpha = 2$ and numerical solutions at $k = 5$, $M = 5$, $r = 3$, and at different values of α.

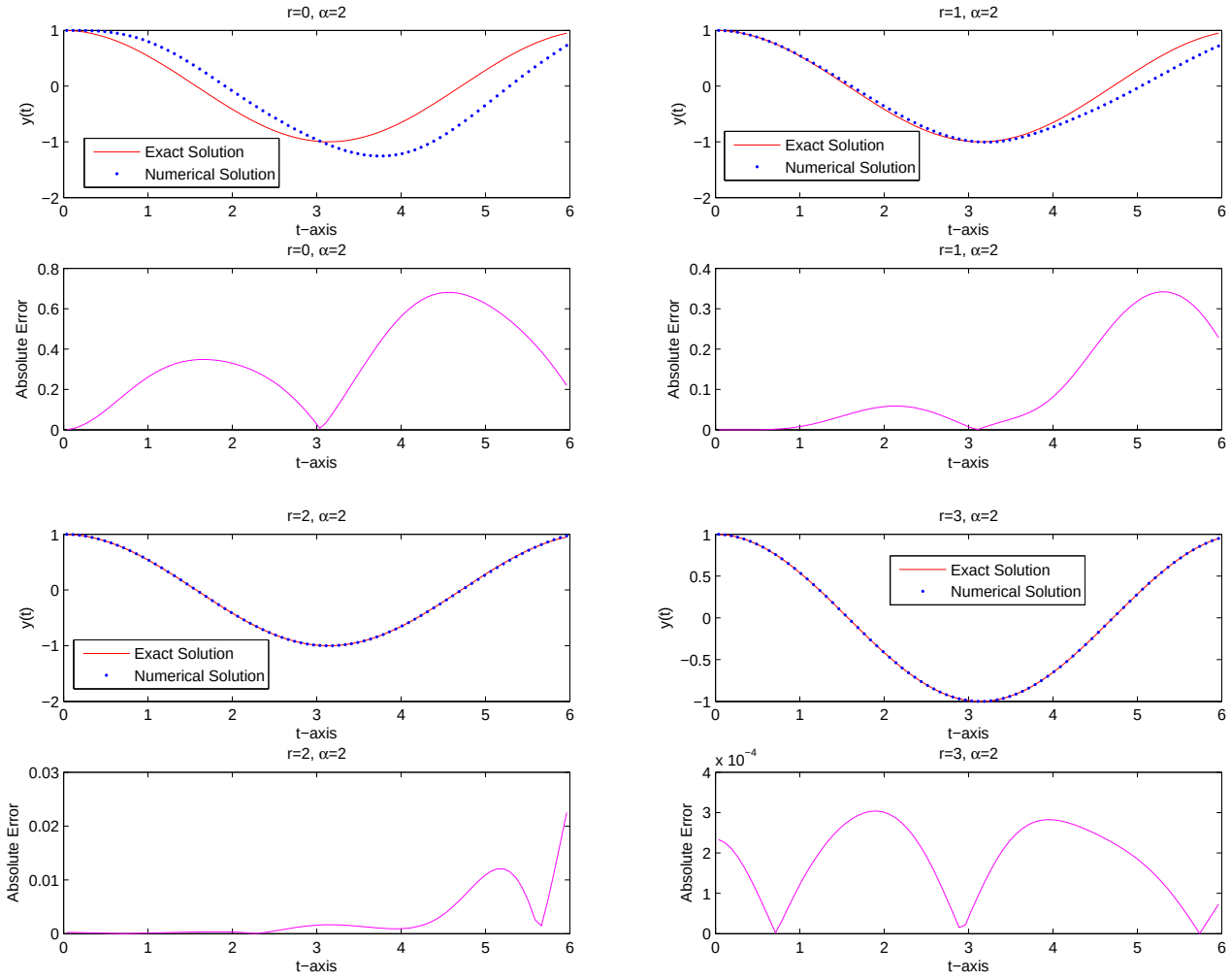

Figure 8.2: Comparison of exact solution and solutions by the Chebyshev wavelet quasilinearization technique at $k = 5,\ M = 5,\ \alpha = 2$ and for different iterations r.

Figure 8.1 indicates that approximate solution converge to the solution of integer order differential equation when α approaches to 2. Figure 8.2 shows that approximate solution approaches to the exact solution while increasing iteration r and absolute error goes down. Here we fix $k = 5,\ M = 5$ and $\alpha = 2$.

Fractional Nonlinear Lane Emden Initial Value Problem

Consider the following initial value problem

$$\begin{aligned} &\frac{d^\alpha y}{dx^\alpha} + \frac{2}{x}\frac{d^\beta y}{dx^\beta} + 4(2e^y + e^{\frac{y}{2}}) = 0, \quad 1 < \alpha \leq 2,\ 0 < \beta \leq 1,\ x \geq 0, \\ &y(0) = 0,\ \frac{dy}{dx}(0) = 0. \end{aligned} \tag{8.1.18}$$

The exact solution at $\alpha = 2,\ \beta = 1$, is given by $y(x) = -2\ln(1+x^2)$.
We first linearized the equation (8.1.18) by applying the Quasilinearization technique, we obtain

$$\begin{aligned} \frac{d^\alpha y_{r+1}}{dx^\alpha} + \frac{2}{x}\frac{d^\beta y_{r+1}}{dx^\beta} + 2(4e^{y_r} + e^{\frac{y_r}{2}})y_{r+1} &= 8e^{y_r}(y_r - 1) + 2e^{\frac{y_r}{2}}(y_r - 2), \\ 1 < \alpha \leq 2,\ 0 < \beta \leq 1,\ x \geq 0, & \\ y_{r+1}(0) = 0,\ \frac{dy_{r+1}}{dx}(0) = 0, & \end{aligned} \tag{8.1.19}$$

where $r = 0, 1, 2, ..., N$, $N \in \mathbb{N}$. Now approximate the solution of the equation (8.1.19) by Chebyshev wavelet method. We approximate the higher order derivative term in equation (8.1.19) by Chebyshev wavelets series as

$$\frac{d^\alpha y_{r+1}}{dx^\alpha} = \mathbf{C^{r+1}}^T \mathbf{\Psi}(x). \tag{8.1.20}$$

Integrate the equation (8.1.20) and use the initial conditions to get the lower order derivatives as

$$\begin{aligned} y_{r+1} &= (\mathbf{C^{r+1}})^T I_x^\alpha \mathbf{\Psi}(x), \\ \frac{d^\beta y_{r+1}}{dx^\beta} &= (\mathbf{C^{r+1}})^T I_x^{\alpha-\beta} \mathbf{\Psi}(x). \end{aligned} \tag{8.1.21}$$

Use equations (8.1.20) and (8.1.21) in equation (8.1.19), we get

$$(\mathbf{C^{r+1}})^T[\mathbf{\Psi}(x) + \frac{2}{x} I_x^{\alpha-\beta}\mathbf{\Psi}(x) + 2(4e^{y_r} + e^{\frac{y_r}{2}})I_x^\alpha \mathbf{\Psi}(x)] = 8e^{y_r}(y_r - 1) + 2e^{\frac{y_r}{2}}(y_r - 2), \tag{8.1.22}$$

with the initial approximations $y_0(x) = 0$.

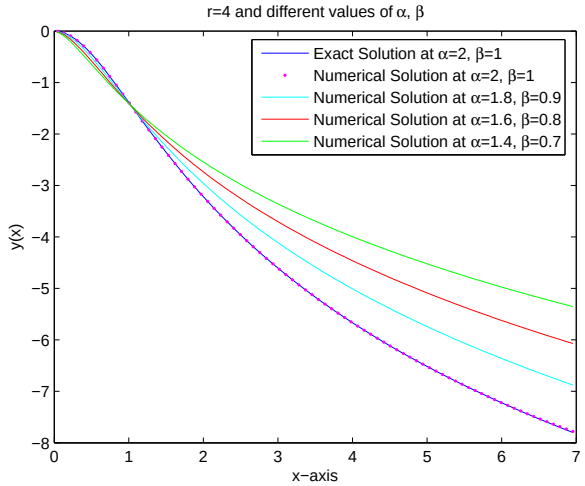

Figure 8.3: Exact solution at $\alpha = 2$ and solution by the Chebyshev wavelet quasilinearization technique at $k = 5,\ M = 5,\ r = 4,$ and at different values of α and β.

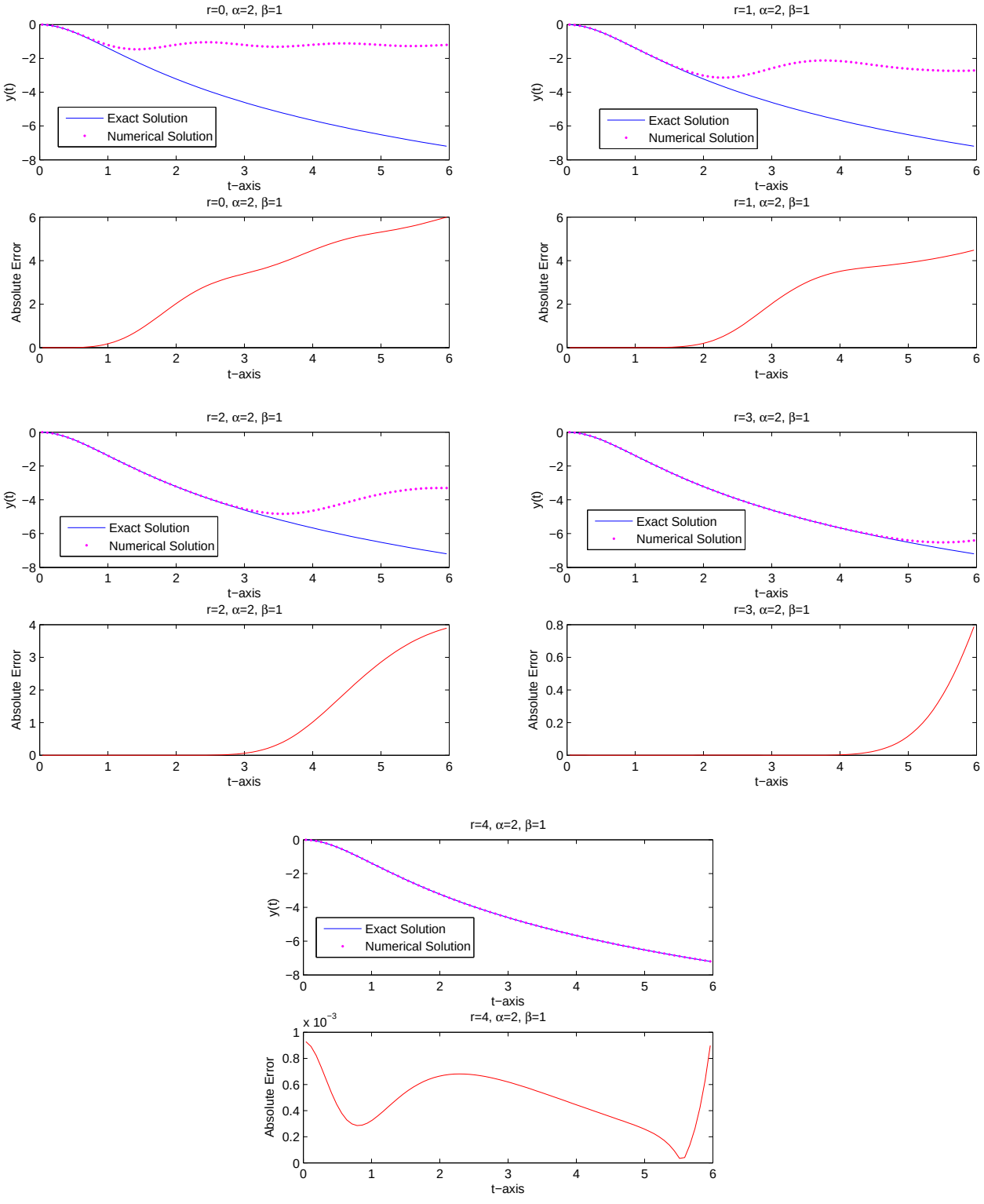

Figure 8.4: Comparison of exact solution and approximate solutions at $k = 5$, $M = 5$, $\alpha = 2$ and for different iterations r.

Table 8.1: Comparison of present solution with exact solution, at different level of resolution k and different order of Chebyshev polynomials M at $r = 4$.

	L_∞-error for proposed solution				
x	$k = 2,\ M = 3$	$k = 4,\ M = 4$	$k = 6,\ M = 5$	$k = 7,\ M = 6$	$k = 8,\ M = 7$
0.1	4.220e-3	1.568e-4	6.277e-6	1.090e-6	2.002e-7
0.3	3.413e-3	1.190e-4	4.762e-6	8.268e-7	1.519e-7
0.5	2.151e-3	7.569e-5	3.027e-6	5.256e-7	9.653e-8
0.7	1.469e-3	5.222e-5	2.087e-6	3.623e-7	6.654e-8
0.9	1.584e-3	5.091e-5	2.034e-6	3.532e-7	6.487e-8

In Table 8.1, we consider $0 \leq x \leq 1,\ \alpha = 2,$ and $\beta = 1$. The results shows that absolute error decreases while increasing k and M. According to the Table 8.1 and Figure 8.4, we get more accurate results while increasing $k,\ M$ and r. Figure 8.3 shows that solution by Chebyshev wavelet quasilinearization technique approaches to the solution of integer order differential equation when α and β approaches to 2 and 1 respectively.

Fractional Nonlinear Lane Emden Boundary Value Problem

Consider the following fractional order boundary value problem

$$\begin{aligned} &\frac{d^\alpha y}{dx^\alpha} + \frac{2}{x}\frac{dy}{dx} - 6y^2 = 6 + \frac{2}{x} - 6(x^2+x)^2, \quad 1 < \alpha \leq 2,\ 0 \leq x \leq 1, \\ &y(0) = 0,\ y(1) = 2. \end{aligned} \tag{8.1.23}$$

The exact solution, when $\alpha = 2$, is given by $y(x) = x^2 + x$.
Apply the Quasilinearization technique to equation (8.1.23)

$$\begin{aligned} &\frac{d^\alpha y_{r+1}}{dx^\alpha} + \frac{2}{x}\frac{dy_{r+1}}{dx} - 12y_r y_{r+1} = 6 + \frac{2}{x} - 6(x^2+x)^2 - 6y_r^2, \quad 1 < \alpha \leq 2,\ 0 \leq x \leq 1, \\ &y_{r+1}(0) = 0,\ y_{r+1}(1) = 2,\ r = 0, 1, 2, ..., N,\ N \in \mathbb{N}. \end{aligned} \tag{8.1.24}$$

We approximate the higher order derivative term in equation (8.1.24) by Chebyshev wavelets series as

$$\frac{d^\alpha y_{r+1}}{dx^\alpha} = \mathbf{C^{r+1}}^T \mathbf{\Psi}(x). \tag{8.1.25}$$

Integrate the equation (8.1.25) and use the boundary conditions, we obtain

$$\begin{aligned} y_{r+1} &= \left(\mathbf{C^{r+1}}\right)^T I_x^\alpha \mathbf{\Psi}(x) + 2x - f_1(x)\mathbf{W}^\alpha_{\hat{\mathbf{m}}\times\mathbf{1}}, \\ \frac{dy_{r+1}}{dx} &= \left(\mathbf{C^{r+1}}\right)^T I_x^{\alpha-1} \mathbf{\Psi}(x) + 2 - f_2(x)\mathbf{W}^\alpha_{\hat{\mathbf{m}}\times\mathbf{1}}, \end{aligned} \tag{8.1.26}$$

where $f_1(x) = x$ and $f_2(x) = 1$. Use equations (8.1.25) and (8.1.26) in equation (8.1.24), we get

$$(\mathbf{C^{r+1}})^T[\mathbf{\Psi}(x) + \frac{2}{x}I_x^{\alpha-1}\mathbf{\Psi}(x) - g_1(x)\mathbf{W}^{\alpha}_{\hat{\mathbf{m}}\times\mathbf{1}} - 12y_r I_x^{\alpha}\mathbf{\Psi}(x) + g_2(x)\mathbf{W}^{\alpha}_{\hat{\mathbf{m}}\times\mathbf{1}}] = 6 + \frac{2}{x} - 6(x^2+x)^2 - 6y_r^2 - \frac{4}{x} + 24xy_r, \tag{8.1.27}$$

with the initial approximations $y_0(x) = 0$. where $r = 0, 1, 2, ..., \mathbb{N}$, $g_1(x) = \frac{2}{x}$ and $g_2(x) = 12xy_r$.

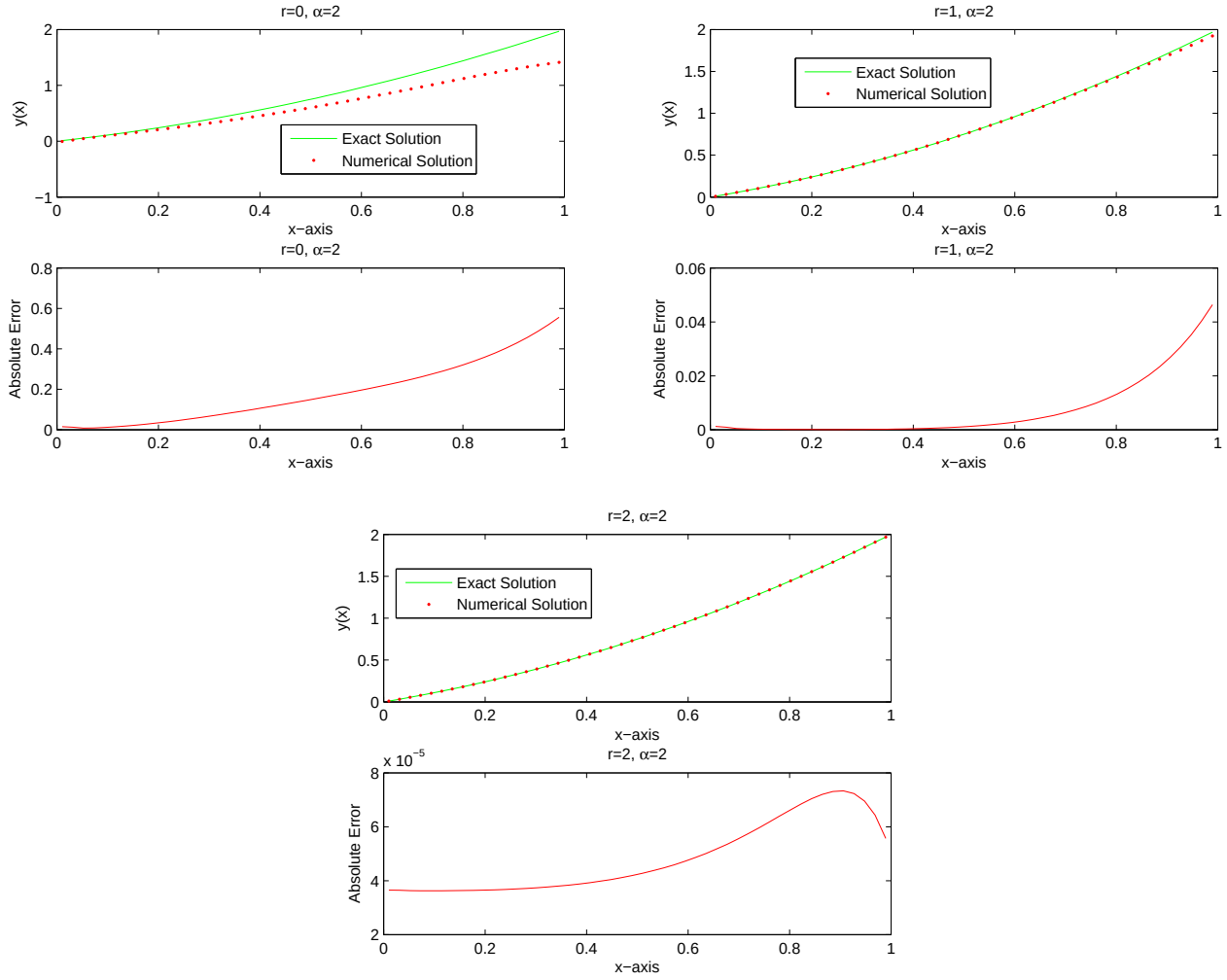

Figure 8.5: Comparison of exact solution and solutions by Chebyshev wavelet quasilinearization technique at $k = 5,\ M = 5,\ \alpha = 2$ and for different iterations r.

Figure 8.5 is used to plot exact solution of integer order differential equation and approximate solutions at different iteration r and $\alpha = 2$, along with the absolute error.

8.1.3 Procedure of Implementation to Fractional Nonlinear Partial Differential Equation

We describe the procedure of implementation of the method to fractional nonlinear partial differential equation.

Fractional Burgers Equations

We describes the procedure of implementing the method for fractional Burgers equation. Consider

$$\frac{\partial^\alpha u}{\partial t^\alpha} + au\frac{\partial u}{\partial x} = \nu\frac{\partial^\beta u}{\partial x^\beta}, \quad 0 < \alpha \leq 1,\ 1 < \beta \leq 2,\ t > 0,\ 0 \leq x \leq b, \tag{8.1.28}$$

with the initial and boundary conditions

$$u(x,0) = f(x),\ u(0,t) = g_1(t), \quad u(b,t) = g_2(t),$$

where $\nu,\ a,\ b > 0$. Apply the Quasilinearization technique to equation (8.1.28), we obtain

$$\begin{gathered}\frac{\partial^\alpha u_{r+1}}{\partial t^\alpha} + au_r\frac{\partial u_{r+1}}{\partial x} - \nu\frac{\partial^\beta u_{r+1}}{\partial x^\beta} + a\frac{\partial u_r}{\partial x}u_{r+1} = au_r\frac{\partial u_r}{\partial x}, \\ 0 < \alpha \leq 1,\ 1 < \beta \leq 2,\ t > 0,\ 0 \leq x \leq b,\end{gathered} \tag{8.1.29}$$

where $r = 0, 1, 2, ..., N$, $N \in \mathbb{N}$, $u_r(x,t)$ is known and can be used for obtaining $u_{r+1}(x,t)$. Equation (8.1.29) is always a linear differential equation with initial and boundary conditions are

$$u_{r+1}(x,0) = f(x),\ u_{r+1}(0,t) = g_1(t), \quad u_{r+1}(b,t) = g_2(t).$$

We implement the Chebyshev wavelets method to equation (8.1.29) as

$$\frac{\partial^\beta u_{r+1}}{\partial x^\beta} = \sum_{l=1}^{\hat{m}}\sum_{i=1}^{\hat{m}} c_{l,i}^{r+1}\psi_l(x)\psi_i(t) = \Psi^T(x)C^{r+1}\Psi(t). \tag{8.1.30}$$

Apply the fractional integral operator I_x^β on equation (8.1.30)

$$u_{r+1}(x,t) = I_x^\beta\Psi^T(x)C^{r+1}\Psi(t) + h_1(t)x + h_2(t). \tag{8.1.31}$$

Differentiate the equation (8.1.31) with respect to x, we get

$$\frac{\partial u_{r+1}}{\partial x} = I_x^{\beta-1}\Psi^T(x)C^{r+1}\Psi(t) + h_1(t). \tag{8.1.32}$$

Use the boundary conditions, to obtain

$$h_2(t) = g_1(t),\ h_1(t) = \frac{1}{b}\bigg(g_2(t) - g_1(t) - (I_{x=b}^\beta\Psi^T(x))C^{r+1}\Psi(t)\bigg).$$

Equations (8.1.31) and (8.1.32) implies

$$u_{r+1}(x,t) = I_x^\beta\Psi^T(x)C^{r+1}\Psi(t) + \frac{x}{b}\bigg(g_2(t) - g_1(t)\bigg) - \frac{x}{b}\bigg(I_{x=b}^\beta\Psi^T(x)\bigg)C^{r+1}\Psi(t) + g_1(t). \tag{8.1.33}$$

$$\frac{\partial u_{r+1}}{\partial x} = I_x^{\beta-1}\Psi^T(x)C^{r+1}\Psi(t) + \frac{1}{b}\Big(g_2(t) - g_1(t)\Big) - \frac{1}{b}\Big(I_{x=b}^{\beta}\Psi^T(x)\Big)C^{r+1}\Psi(t). \tag{8.1.34}$$

Equation (8.1.29) can be written as

$$\frac{\partial^\alpha u_{r+1}}{\partial t^\alpha} = au_r\frac{\partial u_r}{\partial x} - au_r\frac{\partial u_{r+1}}{\partial x} + \nu\frac{\partial^\beta u_{r+1}}{\partial x^\beta} - a\frac{\partial u_r}{\partial x}u_{r+1}. \tag{8.1.35}$$

Use equations (8.1.30), (8.1.33) and (8.1.34) in equation (8.1.35), to obtain

$$\begin{aligned}\frac{\partial^\alpha u_{r+1}}{\partial t^\alpha} =&\Big(- au_r(I_x^{\beta-1}\Psi^T(x)) + \frac{a}{b}u_r(I_{x=b}^{\beta}\Psi^T(x)) + \nu\Psi^T(x) - a\frac{\partial u_r}{\partial x}(I_x^{\beta}\Psi^T(x)) \\ &+ \frac{ax}{b}\frac{\partial u_r}{\partial x}(I_{x=b}^{\beta}\Psi^T(x))\Big)C^{r+1}\Psi(t) + \Psi^T(x)S^{r+1}\Psi(t),\end{aligned} \tag{8.1.36}$$

where

$$S^{r+1} = (\Psi^T(x))^{-1}\Big(au_r\frac{\partial u_r}{\partial x} - \frac{au_r}{b}(g_2(t) - g_1(t)) - \frac{ax}{b}\frac{\partial u_r}{\partial x}(g_2(t) - g_1(t)) - a\frac{\partial u_r}{\partial x}g_1(t)\Big)(\Psi(t))^{-1}.$$

Apply fractional integral operator I_t^α to (8.1.36) and use the initial condition to obtain

$$\begin{aligned}u_{r+1}(x,t) =&\Big(- au_r(I_x^{\beta-1}\Psi^T(x)) + \frac{a}{b}u_r(I_{x=b}^{\beta}\Psi^T(x)) + \nu\Psi^T(x) - a\frac{\partial u_r}{\partial x}(I_x^{\beta}\Psi^T(x)) \\ &+ \frac{ax}{b}\frac{\partial u_r}{\partial x}(I_{x=b}^{\beta}\Psi^T(x))\Big)C^{r+1}(I_t^\alpha\Psi(t)) + \Psi^T(x)S^{r+1}(I_t^\alpha\Psi(t)) + f(x).\end{aligned} \tag{8.1.37}$$

From equation (8.1.33) and (8.1.37)

$$\begin{aligned}&\Big(I_x^{\beta}\Psi^T(x) - \frac{x}{b}(I_{x=b}^{\beta}\Psi^T(x))\Big)C^{r+1}\Psi(t)) + \frac{x}{b}(g_2(t) - g_1(t)) + g_1(t) \\ &= \Big(- au_r(I_x^{\beta-1}\Psi^T(x)) + \frac{a}{b}u_r(I_{x=b}^{\beta}\Psi^T(x)) + \nu\Psi^T(x) - a\frac{\partial u_r}{\partial x}(I_x^{\beta}\Psi^T(x)) \\ &+ \frac{ax}{b}\frac{\partial u_r}{\partial x}(I_{x=b}^{\beta}\Psi^T(x))\Big)C^{r+1}(I_t^\alpha\Psi(t)) + \Psi^T(x)S^{r+1}(I_t^\alpha\Psi(t)) + f(x),\end{aligned} \tag{8.1.38}$$

or

$$G\big(I_x^{\beta}\Psi^T(x) - \frac{x}{b}(I_{x=b}^{\beta}\Psi^T(x))\big)C^{r+1} - C^{r+1}(I_t^\alpha\Psi(t))(\Psi(t))^{-1} + GF(\Psi(t))^{-1} = 0, \tag{8.1.39}$$

where

$$G = \Big(- au_r(I_x^{\beta-1}\Psi^T(x)) + \frac{a}{b}u_r(I_{x=b}^{\beta}\Psi^T(x)) + \nu\Psi^T(x) - a\frac{\partial u_r}{\partial x}(I_x^{\beta}\Psi^T(x)) + \frac{ax}{b}\frac{\partial u_r}{\partial x}(I_{x=b}^{\beta}\Psi^T(x))\Big)^{-1}$$

and

$$F = \Big(\frac{x}{b}(g_2(t) - g_1(t)) + g_1(t) - (\Psi^T(x)S^{r+1}(I_t^\alpha\Psi(t)) + f(x))\Big).$$

Equation (8.1.39) is the Sylvester equation. We solve equation (8.1.39) for C^{r+1} and substituting C^{r+1} in equation (8.1.33) or (8.1.37), to get solution $u(x,t)$ at $(r+1)th$ iteration of quasilinearization technique, at the collocation points.

Example: Consider the following fractional problem

$$\frac{\partial^\alpha u}{\partial t^\alpha} + u\frac{\partial u}{\partial x} = \frac{\partial^\beta u}{\partial x^\beta}, \quad 0 < \alpha \leq 1,\ 1 < \beta \leq 2,\ t > 0,\ 0 \leq x \leq 1, \tag{8.1.40}$$

with the initial and boundary conditions

$$u(x,0) = 2x,\ u(0,t) = 0, \quad u(1,t) = \frac{2}{1+2t}.$$

The exact solution of (8.1.40), when $\alpha = 1$ and $\beta = 2$, is given in [13], $u(x,t) = \frac{2x}{1+2t}$.

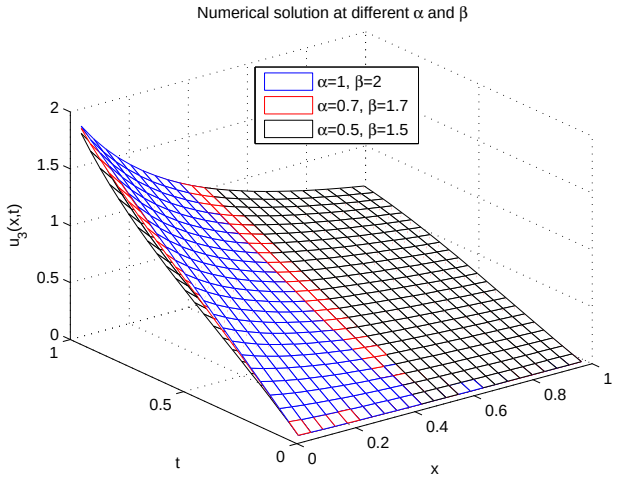

Figure 8.6: Solutions by the method at $k = 4,\ M = 3$ and at different α and β.

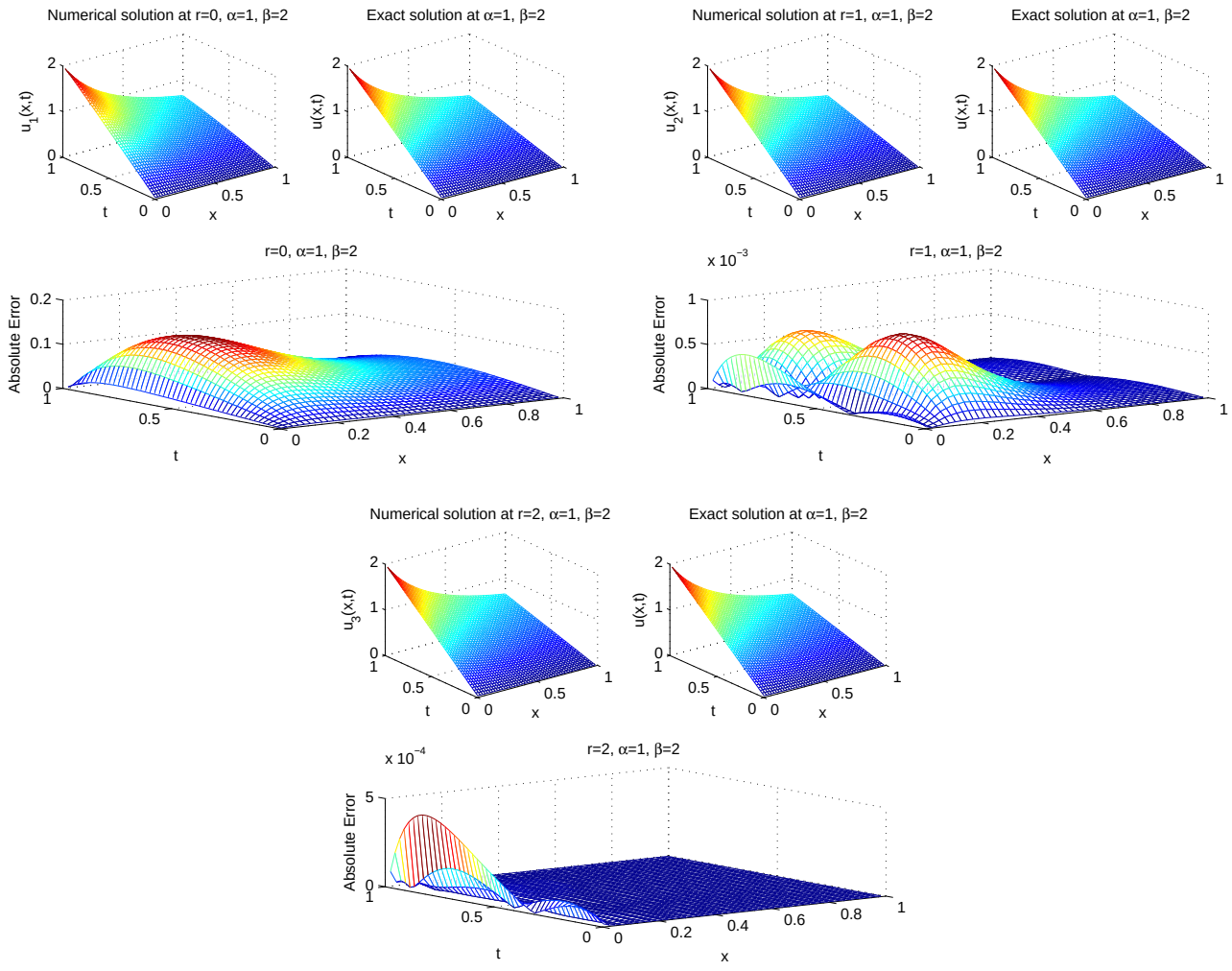

Figure 8.7: Comparison of exact solution at $\alpha = 1,\ \beta = 2$ and solutions by the method at $k = 5,\ M = 3,\ \alpha = 2$ and for different iterations r.

Solution of the fractional order differential equation converge to the solution of the integer order differential equation when α and β approaches to 1 and 2 respectively, as shown in Figure 8.6. Figure 8.7 compares the exact solution and approximate solution for $\alpha = 1$ and $\beta = 2$, at different iteration r and $k = 5,\ M = 3$.

Fractional Klein Gordon Equation

Consider the following fractional Klein Gordon equation,

$$\frac{\partial^\alpha u}{\partial t^\alpha} + a\frac{\partial^\beta u}{\partial x^\beta} + u^b = f(x,t), \quad 1 < \alpha \leq 2,\ 1 < \beta \leq 2,\ t > 0,\ 0 \leq x \leq 1, \tag{8.1.41}$$

with the initial and boundary conditions

$$\begin{aligned} u(x,0) &= g_1(x), \quad u_t(x,0) = g_2(x), \\ u(0,t) &= f_1(t), \quad u(1,t) = f_2(t), \end{aligned} \tag{8.1.42}$$

where a is a constant and $b > 1$. We linearized the nonlinear equation (8.1.41) that is

$$\begin{aligned} \frac{\partial^\alpha u_{r+1}}{\partial t^\alpha} + a\frac{\partial^\beta u_{r+1}}{\partial x^\beta} + b u_r^{b-1} u_{r+1} = f(x,t) + u_r^b(b-1), \\ 1 < \alpha \le 2,\ 1 < \beta \le 2,\ t > 0,\ 0 \le x \le 1, \end{aligned} \tag{8.1.43}$$

subject to the conditions

$$\begin{aligned} u_{r+1}(x,0) &= g_1(x), \quad (u_{r+1})_t(x,0) = g_2(x), \\ u_{r+1}(0,t) &= f_1(t), \quad u_{r+1}(1,t) = f_2(t), \end{aligned} \tag{8.1.44}$$

where $r = 0, 1, 2, ..., N$, $N \in \mathbb{N}$, $u_0(x,t)$ is a initial approximation which is used to get $u_1(x,t)$ and use $u_1(x,t)$ to get $u_2(x,t)$ and so on. In this way, we may get more accurate results while increasing N.

Apply the Chebyshev wavelets method to equation (8.1.43), we approximate the higher order derivative term by Chebyshev wavelets series as

$$\frac{\partial^\beta u_{r+1}}{\partial x^\beta} = \Psi^T(x) C^{r+1} \Psi(t). \tag{8.1.45}$$

Apply the fractional integral operator I_x^β on equation (8.1.45) and utilize the boundary conditions, we obtain

$$u_{r+1}(x,t) = \Big(I_x^\beta \Psi^T(x) - x\big(I_{x=1}^\beta \Psi^T(x)\big)\Big) C^{r+1}\Psi(t) + x\Big(f_2(t) - f_1(t)\Big) + f_1(t). \tag{8.1.46}$$

Use Equations (8.1.45) and (8.1.46) in Equation (8.1.43), we obtain

$$\begin{aligned} \frac{\partial^\alpha u_{r+1}}{\partial t^\alpha} = \Big(- a\Psi^T(x) - b u_r^{b-1}(I_x^\beta \Psi^T(x)) + bx u_r^{b-1}(I_{x=1}^\beta \Psi^T(x))\Big) C^{r+1}\Psi(t) \\ + \Psi^T(x) S^{r+1} \Psi(t), \end{aligned} \tag{8.1.47}$$

where

$$S^{r+1} = (\Psi^T)^{-1}\Big(- b u_r^{b-1}\big(x(f_2(t) - f_1(t)) + f_1(t)\big) + f(x,t) + u_r^b(b-1)\Big)(\Psi(t))^{-1}.$$

Apply fractional integral operator I_t^α to (8.1.47) and use the initial condition to obtain

$$\begin{aligned} u(x,t) = \Big(- a\Psi^T(x) - b u_r^{b-1}(I_x^\beta \Psi^T(x)) + bx u_r^{b-1}(I_{x=1}^\beta \Psi^T(x))\Big) C^{r+1}(I_t^\alpha \Psi(t)) \\ + \Psi^T(x) S^{r+1}(I_t^\alpha \Psi(t)) + t g_2(x) + g_1(x). \end{aligned} \tag{8.1.48}$$

From equation (8.1.46) and (8.1.48)

$$\Big(I_x^{\beta}\Psi^T(x) - x\big(I_{x=1}^{\beta}\Psi^T(x)\big)\Big)C^{r+1}\Psi(t) - \Big(- a\Psi^T(x) - bu_r^{b-1}(I_x^{\beta}\Psi^T(x)) + bxu_r^{b-1}(I_{x=1}^{\beta}\Psi^T(x))\Big)$$
$$C^{r+1}(I_t^{\alpha}\Psi(t)) + x\Big(f_2(t) - f_1(t)\Big) + f_1(t) - \Psi^T(x)S^{r+1}(I_t^{\alpha}\Psi(t)) - tg_2(x) - g_1(x) = 0, \tag{8.1.49}$$

or

$$(G^{r+1})^{-1}\Big(I_x^{\beta}\Psi^T(x) - x\big(I_{x=1}^{\beta}\Psi^T(x)\big)\Big)C^{r+1} - (G^{r+1})^{-1}C^{r+1}(I_t^{\alpha}\Psi(t))(\Psi(t))^{-1}$$
$$+(G^{r+1})^{-1}F^{r+1}(\Psi(t))^{-1} = 0, \tag{8.1.50}$$

where

$$G^{r+1} = \Big(- a\Psi^T(x) - bu_r^{b-1}(I_x^{\beta}\Psi^T(x)) + bxu_r^{b-1}(I_{x=1}^{\beta}\Psi^T(x))\Big)$$

and

$$F^{r+1} = x\Big(f_2(t) - f_1(t)\Big) + f_1(t) - \Psi^T(x)S^{r+1}(I_t^{\alpha}\Psi(t)) - tg_2(x) - g_1(x).$$

Equation (8.1.50) is the Sylvester equation. we get C^{r+1} at (r+1)th iteration from Equation (8.1.50) and substituting C^{r+1} in Equation (8.1.46) or (8.1.48), to get solution $u(x,t)$ at $(r+1)th$ iteration at the collocation points.

Example: Consider the following fractional Klein–Gordon equation,

$$\tfrac{\partial^{\alpha}u}{\partial t^{\alpha}} - \tfrac{\partial^{\beta}u}{\partial x^{\beta}} + u^2 = -x\cos(t) + x^2\cos^2(t),\ 1 < \alpha \leq 2,\ 1 < \beta \leq 2, \tag{8.1.51}$$

subject to the initial and boundary conditions
$u(x,0) = x,\ u_t(x,0) = 0,$
$u(0,t) = 0,\ u(1,t) = \cos(t).$
The exact solution, when $\alpha = 2,\ \beta = 2$, is given by [19]

$$u(x,t) = x\cos(t).$$

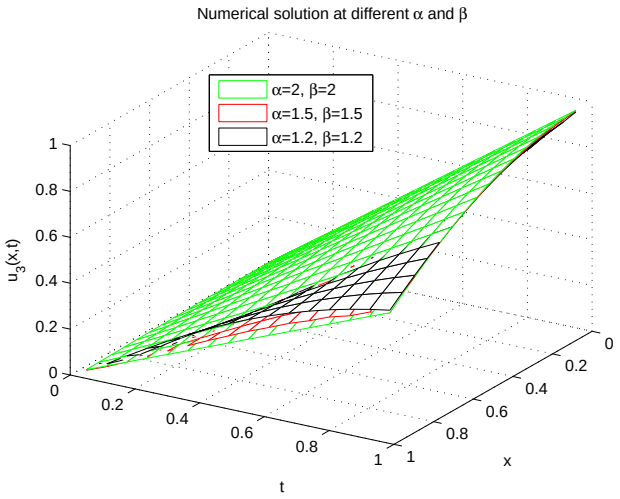

Figure 8.8: Solutions by the method at $k = 4,\ M = 2,$ and at different α and β.

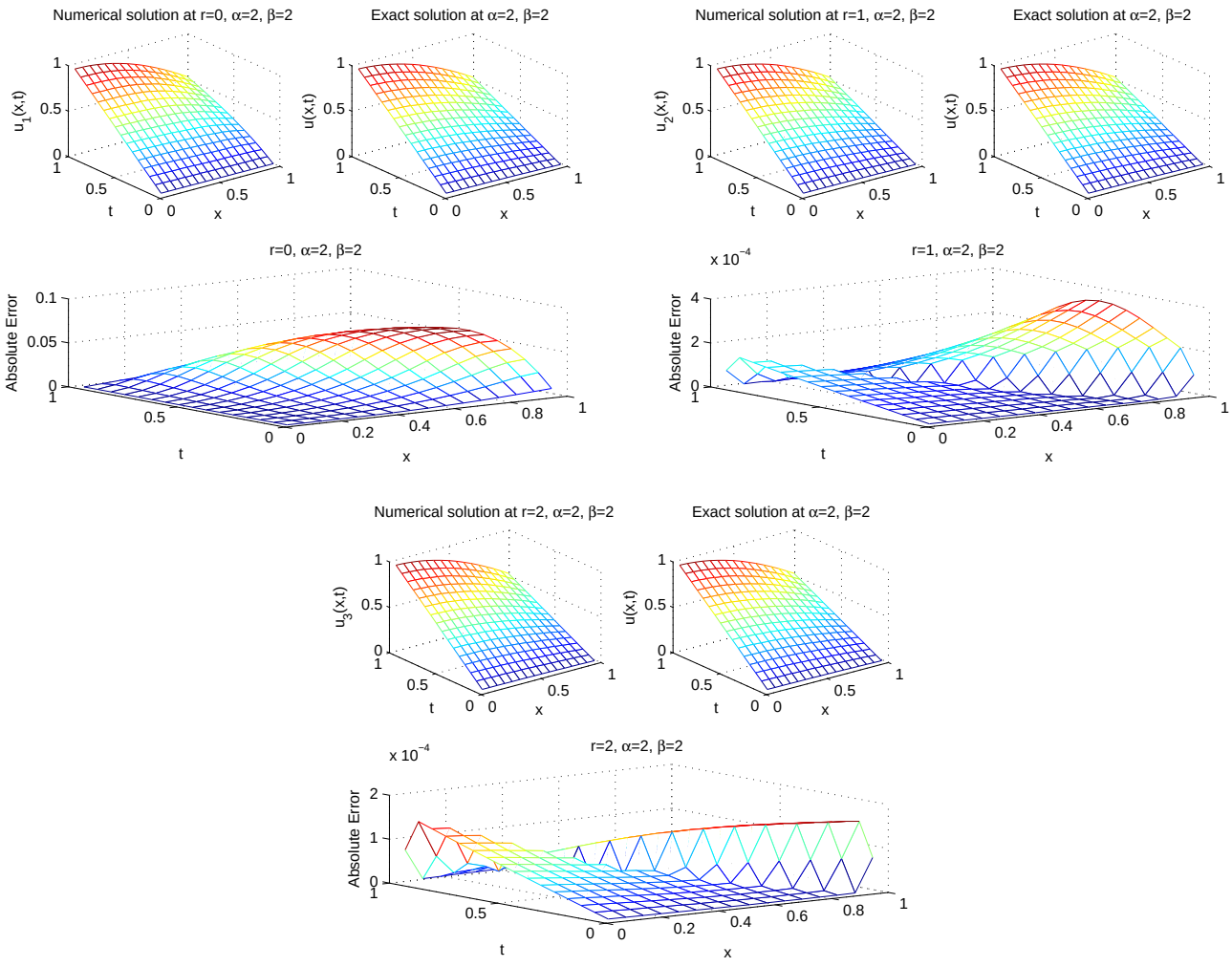

Figure 8.9: Comparison of exact solution at $\alpha = 2,\ \beta = 2$ and solutions by the Chebyshev wavelet quasilinearization technique at $k = 4,\ M = 2,\ \alpha = 2,\ \beta = 2$ and for different iterations r.

Figure 8.8 shows that solution by the method for fractional differential equation converge to the solution of integer differential equation while $\alpha,\ \beta$ approaches to 2. At $\alpha = 2$ and $\beta = 2$, solution by the method converge to the exact solution when iteration r is increased, as in Figure 8.9.

8.1.4 Convergence of the Chebyshev Wavelet Quasilinearization Method

We derive an error estimate of the Chebyshev wavelet quasilinearization approximations to an arbitrary unknown function.

Theorem: Let $r,\ k,\ M\ \to \infty$, then the series solution (8.1.3) converges to $y(x)$.

Proof: Let $L^2[0,1)$ be the Hilbert space and $\psi_{n,m}$ forms a basis of $L^2[0,1)$. Let us consider

$$y_{r+1}(x) \approx \sum_{n=1}^{2^{k-1}} \sum_{m=0}^{M-1} c_{nm}^{r+1} \psi_{n,m}(x), \tag{8.1.52}$$

where $c_{nm}^{r+1} = \langle y_{r+1}(x), \psi_{n,m}(x) \rangle$. Let $S_{k,M}^{r+1}$ be a sequence of partial sums of $c_{nm}^{r+1}\psi_{n,m}(x)$, we prove that $S_{k,M}^{r+1}$ is a Cauchy sequence in Hilbert space $L^2[0,1)$ and then we show that $S_{k,M}^{r+1}$ converges to $y_{r+1}(x)$, when $k, M \to \infty$.

We show that $S_{k,M}^{r+1}$ is a Cauchy sequence. Let $S_{\hat{k},\hat{M}}^{r+1}$ be arbitrary sums of $c_{nm}^{r+1}\psi_{n,m}(x)$ with $k > \hat{k},\ M > \hat{M}$.

$$\begin{aligned}
\|S_{k,M}^{r+1} - S_{\hat{k},\hat{M}}^{r+1}\|^2 &= \| \sum_{n=1}^{2^{k-1}} \sum_{m=0}^{M-1} c_{nm}^{r+1}\psi_{n,m}(x) - \sum_{n=1}^{2^{\hat{k}-1}} \sum_{m=0}^{\hat{M}-1} c_{nm}^{r+1}\psi_{n,m}(x)\|^2, \\
&= \| \sum_{n=2^{\hat{k}-1}+1}^{2^{k-1}} \sum_{m=\hat{M}}^{M-1} c_{nm}^{r+1}\psi_{n,m}^{\lambda}(x)\|^2, \\
&= \langle \sum_{n=2^{\hat{k}-1}+1}^{2^{k-1}} \sum_{m=\hat{M}}^{M-1} c_{nm}^{r+1}\psi_{n,m}(x), \sum_{i=2^{\hat{k}-1}+1}^{2^{k-1}} \sum_{j=\hat{M}}^{M-1} c_{ij}^{r+1}\psi_{i,j}(x)\rangle, \\
&= \sum_{n=2^{\hat{k}-1}+1}^{2^{k-1}} \sum_{m=\hat{M}}^{M-1} \sum_{i=2^{\hat{k}-1}+1}^{2^{k-1}} \sum_{j=\hat{M}}^{M-1} c_{nm}^{r+1}\overline{c}_{ij}^{r+1}\langle \psi_{n,m}(x), \psi_{i,j}(x)\rangle, \\
&= \sum_{n=2^{\hat{k}-1}+1}^{2^{k-1}} \sum_{m=\hat{M}}^{M-1} |c_{nm}^{r+1}|^2.
\end{aligned} \tag{8.1.53}$$

From the Bessel's inequality, we have $\sum_{n=1}^{\infty}\sum_{m=0}^{\infty} |c_{nm}^{r+1}|^2$ is convergent and hence

$$\|S_{k,M}^{r+1} - S_{\hat{k},\hat{M}}^{r+1}\|^2 \to 0 \text{ as } , k, M, \hat{k}, \hat{M} \to \infty.$$

This implies that $S_{k,M}^{r+1}$ is a Cauchy sequence and it converges to, say, $u_{r+1}(x) \in L^2[0,1)$. We need to show that $u_{r+1}(x) = y_{r+1}(x)$,

$$\begin{aligned}
\langle u_{r+1}(x) - y_{r+1}(x), \psi_{n,m}(x)\rangle &= \langle u_{r+1}(x), \psi_{n,m}(x)\rangle - \langle y_{r+1}(x), \psi_{n,m}(x)\rangle, \\
&= \lim_{k,M\to\infty} \langle S_{k,M}^{r+1}, \psi_{n,m}(x)\rangle - c_{nm}^{r+1}, \\
&= c_{nm}^{r+1} - c_{nm}^{r+1}, \\
&= 0.
\end{aligned} \tag{8.1.54}$$

Hence $\sum_{n=1}^{2^{k-1}}\sum_{m=0}^{M-1} c_{nm}^{r+1}\psi_{n,m}(x)$ converges to $y_{r+1}(x)$ as $k, M \to \infty$. Now we show that $y_{r+1}(x)$ converges to $y(x)$ as $r \to \infty$.

According to the convergence of quasilinearization technique, as given in subsection 3.1.1, we have

$$\max_x |y_{r+1} - y_r| \le \frac{b^2 \frac{k}{8}}{1 - \frac{b^2 m}{4}} (\max_x(|y_r - y_{r-1}|)^2, \tag{8.1.55}$$

where $b,\ k$ and m are positive finite constants and are given in [7]. From (8.1.55), we conclude that $y_{r+1}(x) \to y(x)$ as $r \to \infty$, if there is convergence at all.

8.1.5 Conclusion

Each iteration of quasilinearization technique gives linear differential equation in $y_{r+1}(x)$ which is solved to get $y_{r+1}(x)$ by Chebyshev wavelets operational matrix method. According to convergence analysis of method, $\sum_{n=1}^{2^{k-1}} \sum_{m=0}^{M-1} c_{nm}^{r+1} \psi_{n,m}(x)$ converges faster to $y_{r+1}(x)$ if we consider the higher level of resolution k or higher order Chebyshev polynomials M or higher both M and k i.e., we get more accurate results while increasing k and M, and at the same time quasilinearization technique works i.e., given an initial approximation $y_0(x)$, we get solution $y_1(x)$ of linear differential equation by Chebyshev wavelets method, at next iteration we get $y_2(x)$ and so on. Since quasilinearization technique is second order accurate so it gives rapid convergence.

We have constructed the Chebyshev wavelets operational matrices, $\mathbf{\Psi}_{\hat{m}\times\hat{m}}$, the Chebyshev wavelets operational matrix of fractional order integration, $\mathbf{P}^{\alpha}_{\hat{m}\times\hat{m}}$, and another Chebyshev wavelets operational matrix of fractional order integration, $\mathbf{K}^{\mathbf{f},\alpha}_{\hat{\mathbf{m}}\times\hat{\mathbf{m}}}$, which is used for solving boundary value problems. These operational matrices are used to reduce the fractional differential equation to a system of algebraic equations.

It is shown that Chebyshev wavelet quasilinearization technique gives good results when applied to different fractional nonlinear ordinary and partial differential equations. We get more accurate results while increasing k or M or both, and Figures 8.2, 8.4, 8.5, 8.7 and 8.9 show that approximate solution converge to the exact solution and absolute error decreases while increasing iterations r, as promised in convergence analysis. The solution of the fractional order differential equation converge to the solution of integer order differential equation as in Figure 8.1, 8.3, 8.6 and 8.8. The results obtained from Chebyshev wavelet quasilinearization technique are in good agreement with exact solutions. Different type of non-linearities can easily be handled by the Chebyshev wavelet quasilinearization technique.

8.2 Legendre Wavelet Quasilinearization Technique for Nonlinear Fractional Differential Equations

Legendre wavelet method without using the operational matrices have widely been used for solving ordinary/fractional, initial and boundary value problems [56, 61, 132]. This approach leads to complicated calculations. The Legendre wavelet operational matrix method [108, 110] got less attention but gives fast calculations.

In this section, we combine the Legendre operational matrix wavelet method and quasilinearization technique, which we named as the Legendre wavelet - quasilinearization technique, to solve the nonlinear fractional differential equations. According to the technique, we first use the quasilinearization technique to discretize the fractional nonlinear differential equation and then apply the Legendre wavelet method for the solution of discretized fractional differential equation. To the best

of our knowledge , Legendre wavelets never combined with quasilinearization technique.

8.2.1 Legendre Wavelets

The Legendre polynomials, $L_m(x)$, of order m are defined on the interval $[-1, 1]$ and given by the following recurrence formulae,

$$L_0(x) = 1, \quad L_1(x) = x, L_{m+1}(x) = \frac{2m+1}{m+1} x L_m(x) - \frac{m}{m+1} L_{m-1}(x), \quad m = 1, 2, 3, \cdots .$$

The Legendre wavelets are defined on interval $[0, 1)$ by

$$\psi_{n,m}(x) = \begin{cases} (m + \frac{1}{2})^{\frac{1}{2}} 2^{\frac{k}{2}} L_m(2^k x - \hat{n}), & \frac{\hat{n}-1}{2^k} \leq x < \frac{\hat{n}+1}{2^k}, \\ 0, & elsewhere, \end{cases}$$

where $k = 2, 3, \cdots$, is the level of resolution, $n = 1, 2, 3, \cdots, 2^{k-1}$, $\hat{n} = 2n - 1$, is the translation parameter, $m = 0, 1, 2, \cdots, M - 1$ is the order of the Legendre polynomials, $M > 0$.

Function approximations and construction of operational matrices, procedure of implementation to fractional nonlinear ordinary differential equation and convergence analysis of Legendre wavelet quasilinearization method are same as Chebyshev wavelet quasilinearization method and are given in subsections 8.1.1, 8.1.2 and 8.1.4 respectively.

8.2.2 Numerical Solution of Nonlinear Fractional Differential Equations

We solve nonlinear differential equations of fractional order by the Legendre wavelet - quasilinearization technique and compare the results with other numerical schemes and exact solution.

Example 1: Consider the general fractional Riccati differential equation

$$^cD^\alpha y(x) = Q(x)y(x) + R(x)y^2(x) + P(x), \ x \geq 0, \ 0 < \alpha \leq 1, \tag{8.2.1}$$

subject to the initial conditions $y(0) = y_0$.

Apply the quasilinearization technique to equation (8.2.1), to obtain

$$^cD^\alpha y_{r+1}(x) - (Q(x) + 2R(x)y_r(x))y_{r+1}(x) = P(x) - R(x)y_r^2(x), \ x \geq 0, \ 0 < \alpha \leq 1, \tag{8.2.2}$$

with the initial condition $y_{r+1}(0) = y_0$.

Apply the Legendre wavelet method to equation (8.2.2), the Legendre wavelet approximation of higher order derivative is

$$^cD^\alpha y_{r+1}(x) = \sum_{n=1}^{2^{k-1}} \sum_{m=0}^{M-1} a_{nm} \psi_{n,m}(x) = \mathbf{a}^T \mathbf{\Psi}(x). \tag{8.2.3}$$

Lower order derivatives are obtained by integrating equation (8.2.3) and use the initial conditions, we get

$$y_{r+1}(x) \quad = \quad \sum_{n=1}^{2^{k-1}} \sum_{m=0}^{M-1} a_{nm} I^{\alpha} \psi_{n,m}(x) + y_0 = \mathbf{a}^T \mathbf{P}^{\alpha}_{\hat{m} \times \hat{m}} \mathbf{\Psi}(x) + y_0. \tag{8.2.4}$$

Substitute equations (8.2.3) and (8.2.4) in (8.2.2), we obtain

$$\begin{aligned} \sum_{n=1}^{2^{k-1}} \sum_{m=0}^{M-1} a_{nm} [\psi_{n,m}(x) - (Q(x) + 2R(x) y_r(x)) I^{\alpha} \psi_{n,m}(x)] \\ = P(x) - R(x) y_r^2(x) + (Q(x) + 2R(x) y_r(x)) y_0. \end{aligned} \tag{8.2.5}$$

In particular, take $Q(x) = -2x^4,\ R(x) = x^3,\ P(x) = x^5 + 1$ and $y_0 = 0$, equation (8.2.5) becomes

$$\sum_{n=1}^{2^{k-1}} \sum_{m=0}^{M-1} a_{nm} [\psi_{n,m}(x) - (-2x^4 + 2x^3 y_r(x)) I^{\alpha} \psi_{n,m}(x)] = x^5 + 1 - x^3 y_r^2(x), \tag{8.2.6}$$

with the initial approximation $y_0(x) = 0$.

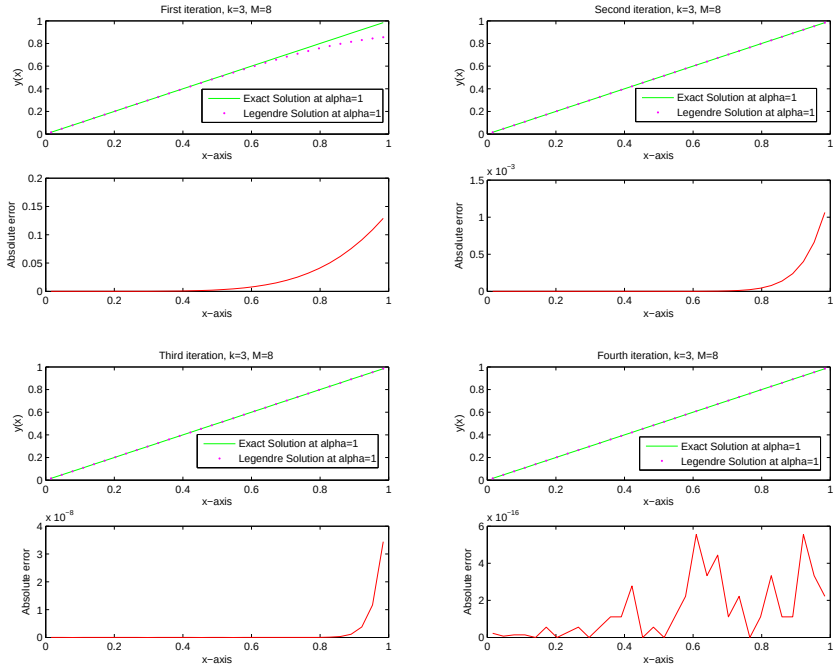

Figure 8.10: Comparison of exact solution and solution by the Legendre wavelet - quasilinearization technique at $k = 3,\ M = 8$ and for different iterations.

t	E_{ADM} [107]	E_{LWM}
0.2	1.137979×10^{-14}	5.551115×10^{-17}
0.4	7.456530×10^{-10}	1.665335×10^{-16}
0.6	4.897381×10^{-7}	2.220446×10^{-16}
0.8	4.879991×10^{-5}	2.220446×10^{-16}
0.9	3.202668×10^{-4}	4.440892×10^{-16}

Table 8.2: Comparison of the Legendre wavelets - quasilinearization technique (at 4^{th} iteration when $k = 7,\ M = 8$) with Adomian decomposition method [107] and exact solution for $\alpha = 1$.

We fix the order of the differential equation (8.2.1), $\alpha = 1$, and $k = 3,\ M = 8$. The graph in Figure 8.10 shows that the exact solution and approximate solution by the Legendre wavelet - quasilinearization technique at 4^{th} iteration. The absolute error reduces with increasing iterations.

For $k = 7$ and $M = 8$, Table 8.2 contains the results obtained by the Legendre wavelet - quasilinearization technique at 4^{th} iteration with solution by Adomian decomposition method and exact solution. For this problem the Legendre wavelet - quasilinearization technique gives significantly accurate results as compared to the Adomian decomposition method.

Example 2: Consider the fractional nonlinear singular initial value problem,

$$ {}^{c}D^{\alpha}y(x) + \tfrac{2}{x}y'(x) - 6y(x) = 4y\ln y,\ x \geq 0,\ 1 < \alpha \leq 2, \tag{8.2.7} $$

subject to the initial conditions $y(0) = 1,\ y'(0) = 0$.
The exact solution, when $\alpha = 2$, is [126]: $y(x) = e^{x^2}$.
Apply the quasilinearization technique to equation (8.2.7), we obtain

$$ {}^{c}D^{\alpha}y_{r+1}(x) + \tfrac{2}{x}y'_{r+1}(x) - (10 + 4\ln y_r(x))y_{r+1}(x) = -4y_r(x),\ x \geq 0,\ 1 < \alpha \leq 2, \tag{8.2.8} $$

with the initial conditions $y_{r+1}(0) = 1,\ y'_{r+1}(0) = 0$.
Apply the Legendre wavelet method to equation (8.2.8), we get

$$ \begin{aligned} \sum_{n=1}^{2^{k-1}} \sum_{m=0}^{M-1} a_{nm}[\psi_{n,m}(x) + \tfrac{2}{x}I^{\alpha-1}\psi_{n,m}(x) - (10 + 4\ln y_r(x))I^{\alpha}\psi_{n,m}(x)] \\ = -4y_r(x) + (10 + 4\ln y_r(x)). \end{aligned} \tag{8.2.9} $$

with the initial approximations $y_0(x) = 1,\ y'_0(x) = 0$.

t	$k=2,\ M=3$	$k=4,\ M=5$	$k=6,\ M=7$	$k=7,\ M=9$
0.2	2.997×10^{-3}	6.018×10^{-5}	1.918×10^{-6}	2.901×10^{-7}
0.4	4.092×10^{-3}	9.012×10^{-5}	2.873×10^{-6}	4.344×10^{-7}
0.6	7.440×10^{-3}	1.640×10^{-4}	5.209×10^{-6}	7.729×10^{-7}
0.8	1.676×10^{-2}	3.387×10^{-4}	9.817×10^{-6}	6.275×10^{-7}

Table 8.3: Absolute error for different values of k and M, at 2^{nd} iteration, $\alpha=2$.

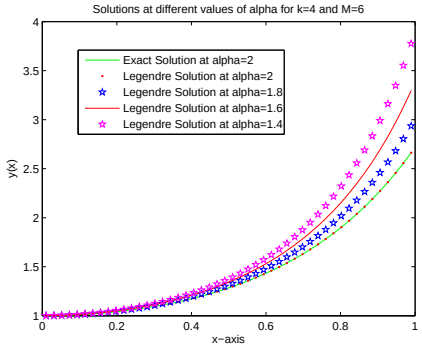

Figure 8.11: Solutions by the Legendre wavelet - quasilinearization technique at 2^{nd} iteration by using $k=4,\ M=6$, for different values of α.

Comparison of exact solution and approximate solution by the Legendre wavelet - quasilinearization technique at 2^{nd} iteration is shown in Table 8.3. We get more accurate results while increasing both k and M. Solution at 2^{nd} iteration, with $k=4$, $M=6$ and at different values of α is shown in Figure 8.11 along with exact solution at $\alpha=2$. We observe that the approximate solutions converge to the exact solution, when α approaches to 2.

Example 3: Consider the following α^{th} order fractional Van der Pol oscillator problem

$$ {}^{c}D^{\alpha}y(x)+\frac{dy}{dx}+y(x)+y^{2}(x)\frac{dy}{dx}=2\cos(x)-\cos^{3}(x),\ 1<\alpha\leq 2, \tag{8.2.10}$$

subject to the initial conditions $y(0)=0$, $y'(0)=1$. The exact solution, when $\alpha=2$, is [8], $y(x)=\sin(x)$.

Quasilinearization technique to equation (8.2.10) leads to

$$\begin{aligned} {}^{c}D^{\alpha}y_{r+1}(x)+(1+2y_{r}(x)y'_{r}(x))y_{r+1}(x)+(1+y_{r}^{2}(x))y'_{r+1}(x)\\ =2y_{r}^{2}(x)y'_{r}(x)+2\cos(x)-\cos^{3}(x),\ 1<\alpha\leq 2, \end{aligned} \tag{8.2.11}$$

with the initial conditions $y_{r+1}(0)=0$, $y'_{r+1}(0)=1$.

Consider the Legendre wavelet approximation and use the initial conditions, we get

$$\begin{aligned} {}^{c}D^{\alpha}y(x) &= \sum_{n=1}^{2^{k-1}}\sum_{m=0}^{M-1} a_{nm}\psi_{n,m}(x), \\ y(x) &= \sum_{n=1}^{2^{k-1}}\sum_{m=0}^{M-1} a_{nm}I^{\alpha}\psi_{n,m}(x) + x, \\ y'(x) &= \sum_{n=1}^{2^{k-1}}\sum_{m=0}^{M-1} a_{nm}I^{\alpha-1}\psi_{n,m}(x) + 1. \end{aligned} \tag{8.2.12}$$

Substitute equations (8.2.12) in (8.2.11), we obtain

$$\begin{aligned} &\sum_{n=1}^{2^{k-1}}\sum_{m=0}^{M-1} a_{nm}[\psi_{n,m}(x) + (1+y_r^2(x))I^{\alpha-1}\psi_{n,m}(x) + (1+2y_r'(x)y_r(x))I^{\alpha}\psi_{n,m}(x)] \\ &\qquad = 2y_r^2(x)y_r'(x) - (1+y_r^2(x)) - x(1+2y_r'(x)y_r(x)) + 2\cos(x) - \cos^3(x). \end{aligned} \tag{8.2.13}$$

with the initial approximations $y_0(x) = 0$, $y_0'(x) = 1$.

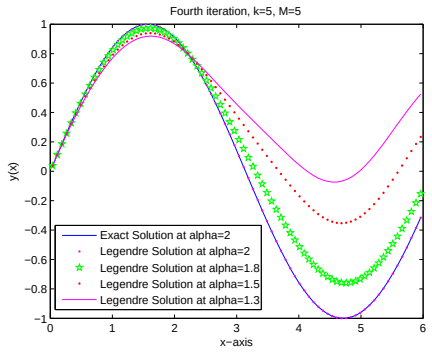

Figure 8.12: Solutions by the Legendre wavelet - quasilinearization technique at 4^{th} iteration by using $k = 5,\ M = 5$, for different values of α

	$k=7,\ M=7$	$k=8,\ M=8$	$k=9,\ M=9$			
x	y_{LWM}	y_{LWM}	y_{LWM}	y_{VIM} [9]	y_{HPM} [9]	y_{EXACT}
0.2	0.1986692194	0.1986693095	0.1986693266	0.1986676148	0.1986692604	0.1986693308
0.4	0.3894181493	0.3894183054	0.3894183350	0.3893138342	0.3894101010	0.3894183423
0.6	0.5646422331	0.5646424274	0.5646424643	0.563525292	0.5645175388	0.5646424734
0.8	0.7173558385	0.7173560426	0.7173560814	0.7115469778	0.7165444751	0.7173560909
0.9	0.7833266633	0.7833268627	0.7833269006	0.7720563532	0.7816179472	0.7833269096

Table 8.4: Solution ($\alpha = 2$) by the Legendre wavelet - quasilinearization technique at 3^{rd} iteration and different values of $k,\ M$ compared with homotopy perturbation method [9], variational iteration method [9] and exact solution.

The primary purpose of *Example* 3 is to show the applicability of Legendre wavelet - quasilinearization method on large domain, as shown in Figure 8.12. We fix the solutions at fourth iteration by taking $k = 5,\ M = 5$, and $0 \leq x \leq 6$. Exact solution at $\alpha = 2$ is also plotted and Figure 8.12 shows that the Legendre solution converges to the exact solution, when α approaches to 2. From the numerical results in Table 8.4, it is clear that the approximate solution by Legendre wavelet - quasilinearization technique are close to exact solutions and becomes more close to exact solution while increasing k and M, when $\alpha = 2$, and also more accurate as compared to variational iteration method [9] and homotopy perturbation method [9].

Example 4: Consider the fractional nonlinear oscillator equation

$$ {}^{c}D^{\alpha}y(x) + \omega^2 y(x) = \lambda y^m(x),\ 0 \leq x \leq 1,\ 1 < \alpha \leq 2, \tag{8.2.14} $$

subject to the boundary conditions $y(0) = 0,\ y(1) = A,\ \ A > 0$, where m is a positive integer and λ is a positive real number.

Apply the quasilinearization technique to equation (8.2.14), we get

$$ {}^{c}D^{\alpha}y_{r+1}(x) + (\omega^2 - m\lambda y_r^{m-1}(x))y_{r+1}(x) = (1-m)\lambda y_r^m(x),\ 0 \leq x \leq 1,\ 1 < \alpha \leq 2, \tag{8.2.15} $$

with the boundary conditions $y_{r+1}(0) = 0,\ y_{r+1}(1) = A$.

Apply the Legendre wavelet method to equation (8.2.15), we obtain

$$ \begin{aligned} &\sum_{n=1}^{2^{k-1}} \sum_{m=0}^{M-1} a_{nm}[\psi_{n,m}(x) - (\omega^2 - m\lambda y_r^{m-1}(x))I^{\alpha}\psi_{n,m}(x) - x(\omega^2 - m\lambda y_r^{m-1}(x)) \\ &\quad (\tfrac{1}{\Gamma(\alpha)} \int_0^1 (1-s)^{\alpha-1}\psi_{n,m}(s)ds)] = (1-m)\lambda y_r^m(x) - Ax(\omega^2 - m\lambda y_r^{m-1}(x)), \end{aligned} \tag{8.2.16} $$

with the initial approximation $y_0(x) = 0$.

To verify the validity of the approximation (8.2.16), we consider a Duffing oscillator, $m = 3$, with the parameters $\omega^2 = \frac{5}{4}$ and $\lambda = \frac{1}{2}$, which has exact solution [119]: $y(x) = sn(x|\frac{1}{4})$, and $A = sn(1|\frac{1}{4})$, where sn is the Jacobi elliptic function.

	$k=7, M=11$				
	$\alpha=1.5$	$\alpha=1.8$	$\alpha=2$		
x	y_{LWM}	y_{LWM}	y_{LWM}	y_{ADM} [119]	y_{EXACT}
0.1	0.113145	0.104671	0.099792	0.0996758	0.099792
0.3	0.323190	0.305949	0.294466	0.294127	0.294466
0.5	0.503727	0.487739	0.475084	0.474580	0.475083
0.7	0.652792	0.643492	0.634295	0.633792	0.634293
0.9	0.772571	0.770284	0.767087	0.766860	0.767085

Table 8.5: Comparison of solutions by the Legendre wavelet - quasilinearization technique at 3^{rd} iteration, $k=7$, $M=11$, and Adomian decomposition method.

Solution at different values of α by the Legendre wavelet - quasilinearization technique at 3^{rd} iteration is shown in Table 8.5, by fixing $k=7$ and $M=11$. The results by developed method along with exact solution and solution by Adomian decomposition method at $\alpha=2$, is shown in Table 8.5. Method gives better results than the Adomian decomposition method.

Example 5: Consider the following fractional nonlinear differential equation

$$ {}^{c}D^{\alpha}y(x)+a(x)y'^{2}(x)+b(x)y(x)y'(x)=f(x),\ 0\le x\le 1,\ 1<\alpha\le 2, \tag{8.2.17} $$

subject to the boundary conditions $y(0)=0,\ y(1)=1$. The exact solution of equation (8.2.17) depends on its order, which is $y(x)=x^{\alpha}$.

Apply the quasilinearization technique to equation (8.2.17), to obtain

$$ \begin{aligned} &{}^{c}D^{\alpha}y(x)+b(x)y'_r(x)y_{r+1}(x)+(2a(x)y'_r(x)+b(x)y_r(x))y'_{r+1}(x)\\ &\quad=f(x)+a(x)y'^{2}_r(x)+b(x)y_r(x)y'_r(x),\ 0\le x\le 1,\ 1<\alpha\le 2, \end{aligned} \tag{8.2.18} $$

with the boundary conditions $y_{r+1}(0)=0,\ y_{r+1}(1)=1$.

Apply the Legendre wavelet method to equation (8.2.18), we get

$$ \begin{aligned} &\sum_{n=1}^{2^{k-1}}\sum_{m=0}^{M-1}a_{nm}[\psi_{n,m}(x)+b(x)y'_r(x)I^{\alpha}\psi_{n,m}(x)-xb(x)y'_r(x)\\ &(\tfrac{1}{\Gamma(\alpha)}\int_0^1(1-s)^{\alpha-1}\psi_{n,m}(s)ds)+(2a(x)y'_r(x)+b(x)y_r(x))I^{\alpha-1}\psi_{n,m}(x)\\ &-(2a(x)y'_r(x)+b(x)y_r(x))(\tfrac{1}{\Gamma(\alpha)}\int_0^1(1-s)^{\alpha-1}\psi_{n,m}(s)ds)]=f(x)+a(x)y'^{2}_r(x)\\ &+b(x)y_r(x)y'_r(x)-xb(x)y'_r(x)-(2a(x)y'_r(x)+b(x)y_r(x)), \end{aligned} \tag{8.2.19} $$

with the initial approximation $y_0(x)=0,\ y'_0(x)=0$.

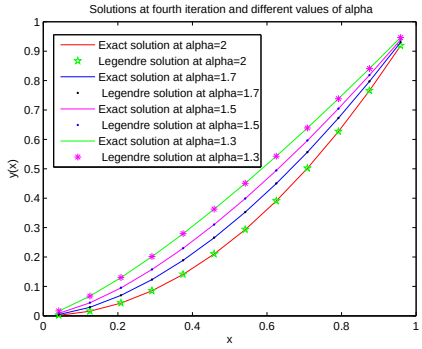

Figure 8.13: Exact solution and solution by the Legendre wavelet - quasilinearization technique at 4^{th} iteration, $k = 3$, $M = 3$, and at different values of α.

Since solution of the equation (8.2.17) depends on its order, Figure 8.13 shows that the exact solution and proposed solution at different values of α by fixing $k = 3$ and $M = 3$.

8.2.3 Conclusion

It is shown that the Legendre wavelet method with quasilinearization technique gives excellent results when applied to different fractional nonlinear initial and boundary value problems. Error by the Legendre wavelet - quasilinearization technique reduces while increasing iterations, as mentioned in Figure 8.10. The results obtained from the Legendre wavelet - quasilinearization technique are better from the results obtained by other methods and are in good agreement with exact solutions, as shown in Tables. Different type of non-linearities can easily be handled by the Legendre wavelet - quasilinearization technique.

Chapter 9

Gegenbauer Wavelets Operational Matrix Method for Fractional Differential Equations

In this chapter, we introduce a numerical method, named Gegenbauer wavelets method, which is derived from conventional Gegenbauer polynomials, for solving fractional initial and boundary value problems. The operational matrices are derived and utilized to reduce the fractional differential equation to a system of algebraic equations. We perform the convergence analysis for the Gegenbauer wavelets method. Numerical examples are provided to illustrate the efficiency and accuracy of the method.

Gegenbauer polynomials [38] or ultraspherical polynomials are orthogonal polynomials on the interval $[-1, 1]$ with respect to a certain weight function. They generalize the Legendre and Chebyshev polynomials. In the present work, we constructed the Gegenbauer wavelets by using the shifted Gegenbauer polynomials as their basis functions. The interval $[0, 1)$ is chosen to be the compact support of Gegenbauer wavelets. The purpose of introducing the Gegenbauer wavelets is to develop a numerical method for solving fractional differential equations. Boundary value problems are considerably more difficult to deal with than the initial value problems. Gegenbauer wavelets method for boundary value problems is more complicated than for initial value problems. We need more operational matrices for tackling the boundary conditions while solving boundary value problems.

9.1 Gegenbauer Polynomials and Gegenbauer Wavelets

The Gegenbauer polynomials [38], or ultra spherical harmonics polynomials, $C_m^{\lambda}(x)$, of order m are defined, for $\lambda > \frac{-1}{2}$, $m \in \mathbf{Z}^+$, on the interval $[-1, 1]$ and given by the following recurrence formulae,

$$C_0^{\lambda}(x) = 1, \quad C_1^{\lambda}(x) = 2\lambda x,$$

$$C^{\lambda}_{m+1}(x) = \frac{1}{m+1}(2(m+\lambda)xC^{\lambda}_{m}(x) - (m+2\lambda-1)C^{\lambda}_{m-1}(x)), \quad m = 1, 2, 3, \cdots .$$

The Gegenbauer polynomials are orthogonal on $[-1, 1]$ with respect to the weight function $(1-x^2)^{\lambda-\frac{1}{2}}$ as

$$\int_{-1}^{1}(1-x^2)^{\lambda-\frac{1}{2}}C^{\lambda}_{m}(x)C^{\lambda}_{n}(x)dx = L^{\lambda}_{m}\delta_{mn}, \quad \lambda > \frac{-1}{2},$$

where $L^{\lambda}_{m}(x) = \frac{\pi 2^{1-2\lambda}\Gamma(m+2\lambda)}{m!(m+\lambda)(\Gamma(\lambda))^2}$ is the normalizing factor and δ is the Kronecker delta function.

Gegenbauer polynomials generalize Legendre polynomials and Chebyshev polynomials. For $\lambda = 0$ and $\lambda = 1$, we get Chebyshev polynomials of first and second kind respectively and at $\lambda = \frac{1}{2}$ we get Legendre polynomial.

The Gegenbauer wavelets are defined on interval $[0, 1)$ by

$$\psi^{\lambda}_{n,m}(x) = \begin{cases} \frac{1}{\sqrt{L^{\lambda}_{m}}}2^{\frac{k}{2}}C^{\lambda}_{m}(2^k x - \hat{n}), & \frac{\hat{n}-1}{2^k} \leq x < \frac{\hat{n}+1}{2^k}, \\ 0, & elsewhere, \end{cases} \tag{9.1.1}$$

where $k = 1, 2, 3, \cdots$, is the level of resolution, $n = 1, 2, 3, \cdots, 2^{k-1}$, $\hat{n} = 2n - 1$, is the translation parameter, $m = 0, 1, 2, \cdots, M-1$ is the order of the Gegenbauer polynomials, $M > 0$. Corresponding to each $\lambda > \frac{-1}{2}$, we have a different family of wavelets i.e., when $\lambda = \frac{1}{2}$, we get Legendre wavelets [108], $\psi^{\frac{1}{2}}_{n,m}(x)$. Similarly for $\lambda = 0$ and $\lambda = 1$, we obtain the Chebyshev wavelet of first [77] and second kind [127], respectively. In the present work, we utilize the Gegenbauer wavelets at different values of $\lambda > \frac{-1}{2}$.

9.1.1 Function Approximations and Gegenbauer Wavelets Matrix

We can expand any function $f(x) \in L^2[0, 1)$ into truncated Gegenbauer wavelet series as ,

$$f(x) \approx \sum_{n=1}^{2^{k-1}}\sum_{m=0}^{M-1} a^{\lambda}_{nm}\psi^{\lambda}_{n,m}(x) = {\mathbf{a}^{\lambda}}^{T}\mathbf{\Psi}^{\lambda}(x), \tag{9.1.2}$$

where $\mathbf{a}^{\lambda}$ and Ψ^{λ} are $\hat{m} \times 1$, ($\hat{m} = 2^{k-1}M$), matrices, given by

$\mathbf{a}^{\lambda}$=$[a^{\lambda}_{10}, a^{\lambda}_{11}, \cdots, a^{\lambda}_{1M-1}, a^{\lambda}_{20}, a^{\lambda}_{21}, \cdots, a^{\lambda}_{2M-1}, \cdots, a^{\lambda}_{2^{k-1}0}, a^{\lambda}_{2^{k-1}1}, \cdots, a^{\lambda}_{2^{k-1}M-1}]^T$,

$\mathbf{\Psi}^{\lambda}(x) = [\psi^{\lambda}_{1,0}(x), \psi^{\lambda}_{1,1}(x), \cdots, \psi^{\lambda}_{1M-1}(x), \psi^{\lambda}_{2,0}(x), \psi^{\lambda}_{2,1}(x), \cdots, \psi^{\lambda}_{2,M-1}(x)$

$, \cdots, \psi^{\lambda}_{2^{k-1},0}(x), \psi^{\lambda}_{2^{k-1},1}(x), \cdots, \psi^{\lambda}_{2^{k-1},M-1}(x)]^T$.

The collocation points for the Gegenbauer wavelets are taken as $x_i = \frac{2i-1}{2^k M}$, $i = 1, 2, ..., 2^{k-1}M$. The Gegenbauer wavelet matrix ${\mathbf{\Psi}^{\lambda}}_{2^{k-1}M, 2^{k-1}M}$ is given as

$${\mathbf{\Psi}^{\lambda}}_{2^{k-1}M \times 2^{k-1}M} = [\mathbf{\Psi}^{\lambda}(\frac{1}{2^k M}), \mathbf{\Psi}^{\lambda}(\frac{3}{2^k M}), ..., \mathbf{\Psi}^{\lambda}(\frac{2^k M - 1}{2^k M})] \tag{9.1.3}$$

or

$$\boldsymbol{\Psi}^{\lambda}{}_{2^{k-1}M\times 2^{k-1}M} = \begin{bmatrix} \psi^{\lambda}_{1,0}(\frac{1}{2^kM}) & \psi^{\lambda}_{1,0}(\frac{3}{2^kM}) & \cdots & \psi^{\lambda}_{1,0}(\frac{2^kM-1}{2^kM}) \\ \psi^{\lambda}_{1,1}(\frac{1}{2^kM}) & \psi^{\lambda}_{1,1}(\frac{3}{2^kM}) & \cdots & \psi^{\lambda}_{1,1}(\frac{2^kM-1}{2^kM}) \\ \vdots & \vdots & \cdots & \vdots \\ \psi^{\lambda}_{1,M-1}(\frac{1}{2^kM}) & \psi^{\lambda}_{1,M-1}(\frac{3}{2^kM}) & \cdots & \psi^{\lambda}_{1,M-1}(\frac{2^kM-1}{2^kM}) \\ \psi^{\lambda}_{2,0}(\frac{1}{2^kM}) & \psi^{\lambda}_{2,0}(\frac{3}{2^kM}) & \cdots & \psi^{\lambda}_{2,0}(\frac{2^kM-1}{2^kM}) \\ \psi^{\lambda}_{2,1}(\frac{1}{2^kM}) & \psi^{\lambda}_{2,1}(\frac{3}{2^kM}) & \cdots & \psi^{\lambda}_{2,1}(\frac{2^kM-1}{2^kM}) \\ \vdots & \vdots & \cdots & \vdots \\ \psi^{\lambda}_{2,M-1}(\frac{1}{2^kM}) & \psi^{\lambda}_{2,M-1}(\frac{3}{2^kM}) & \cdots & \psi^{\lambda}_{2,M-1}(\frac{2^kM-1}{2^kM}) \\ \vdots & \vdots & \cdots & \vdots \\ \psi^{\lambda}_{2^{k-1},0}(\frac{1}{2^kM}) & \psi^{\lambda}_{2^{k-1},0}(\frac{3}{2^kM}) & \cdots & \psi^{\lambda}_{2^{k-1},0}(\frac{2^kM-1}{2^kM}) \\ \psi^{\lambda}_{2^{k-1},1}(\frac{1}{2^kM}) & \psi^{\lambda}_{2^{k-1},1}(\frac{3}{2^kM}) & \cdots & \psi^{\lambda}_{2^{k-1},1}(\frac{2^kM-1}{2^kM}) \\ \vdots & \vdots & \cdots & \vdots \\ \psi^{\lambda}_{2^{k-1},M-1}(\frac{1}{2^kM}) & \psi^{\lambda}_{2^{k-1},M-1}(\frac{3}{2^kM}) & \cdots & \psi^{\lambda}_{2^{k-1},M-1}(\frac{2^kM-1}{2^kM}) \end{bmatrix}$$

In particular, we fix $k = 2,\ M = 3$, we have $n = 1, 2$ and $m = 0, 1, 2$, the Gegenbauer wavelet matrix is given as

$$\boldsymbol{\Psi}^{\lambda}{}_{6\times 6} = \begin{bmatrix} \psi^{\lambda}_{1,0}(\frac{1}{12}) & \psi^{\lambda}_{1,0}(\frac{3}{12}) & \psi^{\lambda}_{1,0}(\frac{5}{12}) & \psi^{\lambda}_{1,0}(\frac{7}{12}) & \psi^{\lambda}_{1,0}(\frac{9}{12}) & \psi^{\lambda}_{1,0}(\frac{11}{12}) \\ \psi^{\lambda}_{2,0}(\frac{1}{12}) & \psi^{\lambda}_{2,0}(\frac{3}{12}) & \psi^{\lambda}_{2,0}(\frac{5}{12}) & \psi^{\lambda}_{2,0}(\frac{7}{12}) & \psi^{\lambda}_{2,0}(\frac{9}{12}) & \psi^{\lambda}_{2,0}(\frac{11}{12}) \\ \psi^{\lambda}_{1,1}(\frac{1}{12}) & \psi^{\lambda}_{1,1}(\frac{3}{12}) & \psi^{\lambda}_{1,1}(\frac{5}{12}) & \psi^{\lambda}_{1,1}(\frac{7}{12}) & \psi^{\lambda}_{1,1}(\frac{9}{12}) & \psi^{\lambda}_{1,1}(\frac{11}{12}) \\ \psi^{\lambda}_{2,1}(\frac{1}{12}) & \psi^{\lambda}_{2,1}(\frac{3}{12}) & \psi^{\lambda}_{2,1}(\frac{5}{12}) & \psi^{\lambda}_{2,1}(\frac{7}{12}) & \psi^{\lambda}_{2,1}(\frac{9}{12}) & \psi^{\lambda}_{2,1}(\frac{11}{12}) \\ \psi^{\lambda}_{1,2}(\frac{1}{12}) & \psi^{\lambda}_{1,2}(\frac{3}{12}) & \psi^{\lambda}_{1,2}(\frac{5}{12}) & \psi^{\lambda}_{1,2}(\frac{7}{12}) & \psi^{\lambda}_{1,2}(\frac{9}{12}) & \psi^{\lambda}_{1,2}(\frac{11}{12}) \\ \psi^{\lambda}_{2,2}(\frac{1}{12}) & \psi^{\lambda}_{2,2}(\frac{3}{12}) & \psi^{\lambda}_{2,2}(\frac{5}{12}) & \psi^{\lambda}_{2,2}(\frac{7}{12}) & \psi^{\lambda}_{2,2}(\frac{9}{12}) & \psi^{\lambda}_{2,2}(\frac{11}{12}) \end{bmatrix}$$

Compact support of the Gegenbauer wavelets is $[\frac{2n-2}{2^k}, \frac{2n}{2^k})$, when $n = 1$, support of $\psi^{\lambda}_{1,m}(x)$ is $[0, \frac{1}{2})$, so $\psi^{\lambda}_{1,0}(x), \psi^{\lambda}_{1,1}(x), \psi^{\lambda}_{1,2}(x)$ are zero at $x = \frac{7}{12}, \frac{9}{12}, \frac{11}{12}$. Similarly, for $n = 2$, support of $\psi^{\lambda}_{2,m}(x)$ is $[\frac{1}{2}, 1)$, this implies that $\psi^{\lambda}_{2,0}(x), \psi^{\lambda}_{2,1}(x), \psi^{\lambda}_{2,2}(x)$ are zero at $x = \frac{1}{12}, \frac{3}{12}, \frac{5}{12}$, we have

$$\boldsymbol{\Psi}^{\lambda}{}_{6\times 6} = \begin{bmatrix} \psi^{\lambda}_{1,0}(\frac{1}{12}) & \psi^{\lambda}_{1,0}(\frac{3}{12}) & \psi^{\lambda}_{1,0}(\frac{5}{12}) & 0 & 0 & 0 \\ 0 & 0 & 0 & \psi^{\lambda}_{2,0}(\frac{7}{12}) & \psi^{\lambda}_{2,0}(\frac{9}{12}) & \psi^{\lambda}_{2,0}(\frac{11}{12}) \\ \psi^{\lambda}_{1,1}(\frac{1}{12}) & \psi^{\lambda}_{1,1}(\frac{3}{12}) & \psi^{\lambda}_{1,1}(\frac{5}{12}) & 0 & 0 & 0 \\ 0 & 0 & 0 & \psi^{\lambda}_{2,1}(\frac{7}{12}) & \psi^{\lambda}_{2,1}(\frac{9}{12}) & \psi^{\lambda}_{2,1}(\frac{11}{12}) \\ \psi^{\lambda}_{1,2}(\frac{1}{12}) & \psi^{\lambda}_{1,2}(\frac{3}{12}) & \psi^{\lambda}_{1,2}(\frac{5}{12}) & 0 & 0 & 0 \\ 0 & 0 & 0 & \psi^{\lambda}_{2,2}(\frac{7}{12}) & \psi^{\lambda}_{2,2}(\frac{9}{12}) & \psi^{\lambda}_{2,2}(\frac{11}{12}) \end{bmatrix}$$

For fix value of λ, say $\lambda = 5$, we have

$$\mathbf{\Psi^5}_{6\times 6} = \begin{bmatrix} \frac{2}{\sqrt{L_0^5}}C_0^5(\frac{-2}{3}) & \frac{2}{\sqrt{L_0^5}}C_0^5(0) & \frac{2}{\sqrt{L_0^5}}C_0^5(\frac{2}{3}) & 0 & 0 & 0 \\ 0 & 0 & 0 & \frac{2}{\sqrt{L_0^5}}C_0^5(\frac{-2}{3}) & \frac{2}{\sqrt{L_0^5}}C_0^5(0) & \frac{2}{\sqrt{L_0^5}}C_0^5(\frac{2}{3}) \\ \frac{2}{\sqrt{L_1^5}}C_1^5(\frac{-2}{3}) & \frac{2}{\sqrt{L_1^5}}C_1^5(0) & \frac{2}{\sqrt{L_1^5}}C_1^5(\frac{2}{3}) & 0 & 0 & 0 \\ 0 & 0 & 0 & \frac{2}{\sqrt{L_1^5}}C_1^5(\frac{-2}{3}) & \frac{2}{\sqrt{L_1^5}}C_1^5(0) & \frac{2}{\sqrt{L_1^5}}C_1^5(\frac{2}{3}) \\ \frac{2}{\sqrt{L_2^5}}C_2^5(\frac{-2}{3}) & \frac{2}{\sqrt{L_2^5}}C_2^5(0) & \frac{2}{\sqrt{L_2^5}}C_2^5(\frac{2}{3}) & 0 & 0 & 0 \\ 0 & 0 & 0 & \frac{2}{\sqrt{L_2^5}}C_2^5(\frac{-2}{3}) & \frac{2}{\sqrt{L_2^5}}C_2^5(0) & \frac{2}{\sqrt{L_2^5}}C_2^5(\frac{2}{3}) \end{bmatrix}$$

or

$$\Psi^5_{6\times 6} = \begin{pmatrix} 2.2746 & 2.2746 & 2.2746 & 0 & 0 & 0 \\ 0 & 0 & 0 & 2.2746 & 2.2746 & 2.2746 \\ -5.2530 & 0 & 5.2530 & 0 & 0 & 0 \\ 0 & 0 & 0 & -5.2530 & 0 & 5.2530 \\ 7.8628 & -1.8145 & 7.8628 & 0 & 0 & 0 \\ 0 & 0 & 0 & 7.8628 & -1.8145 & 7.8628 \end{pmatrix}.$$

Similarly, we get different Gegenbauer wavelet matrices for different value of λ.

9.1.2 The Gegenbauer Wavelets Operational Matrix of Fractional Order Integration

For simplicity, we write (9.1.2) as

$$f(x) \approx \sum_{i=1}^{\hat{m}} a_i^\lambda \psi_i^\lambda(x) = {\mathbf{a}^\lambda}^T \Psi^\lambda(x), \tag{9.1.4}$$

where $a_i^\lambda = a_{m,n}^\lambda$, $\psi_i^\lambda = \psi_{m,n}^\lambda(x)$. The index i is determined by the equation $i = M(n-1)+m+1$ and $\hat{m} = 2^{k-1}M$. Also, $\mathbf{a}^\lambda = [a_1^\lambda, a_2^\lambda, \cdots, a_{\hat{m}}^\lambda]^T$, $\mathbf{\Psi}^\lambda(x) = [\psi_1^\lambda(x), \psi_2^\lambda(x), \cdots, \psi_{\hat{m}}^\lambda(x)]^T$.
An arbitrary function $f \in L_2[0,1)$, can be expanded into block-pulse functions [68] as

$$f(x) \approx \sum_{i=0}^{\hat{m}-1} f_i b_i(x) = \mathbf{f}^T \mathbf{B}(x),$$

where f_i are the coefficients of the block-pulse function. The Gegenbauer wavelets can be expanded into $m-$set of block-pulse Functions as

$$\mathbf{\Psi}^\lambda(x) = \mathbf{\Psi}^\lambda_{\hat{m}\times\hat{m}} \mathbf{B}(x). \tag{9.1.5}$$

The fractional integral of block-pulse function vector can be written as

$$(\mathcal{I}^\alpha \mathbf{B})(x) = \mathbf{F}^\alpha_{\hat{m}\times\hat{m}}\ \mathbf{B}(x), \tag{9.1.6}$$

where $\mathbf{F}^{\alpha}_{\hat{m}\times\hat{m}}$ is given in [68] with

$$\mathbf{P}^{\lambda,\alpha}_{\hat{m}\times\hat{m}} = \mathbf{\Psi}^{\lambda}_{\hat{m}\times\hat{m}}\mathbf{F}^{\alpha}(\mathbf{\Psi}^{\lambda}_{\hat{m}\times\hat{m}})^{-1}. \tag{9.1.7}$$

The Gegenbauer wavelets operational matrix of integration $\mathbf{P}^{\lambda,\alpha}_{\hat{m}\times\hat{m}}$ of fractional order α is constructed for different $\lambda > \frac{-1}{2}$ and are utilize for solving differential equations. In particular, for $k = 2$, $M = 3$, $\alpha = 1.25$, $\lambda = 5$, the Gegenbauer wavelet operational matrix of fractional order integration $\mathbf{P}^{5,\ 1.25}_{6\times6}$ is given by

$$\mathbf{P}^{5,\ 1.25}_{8\times8} = \begin{pmatrix} 0.1592 & 0.4581 & 0.0551 & 0.0189 & 0.0028 & -0.0017 \\ 0 & 0.1592 & 0 & 0.0551 & 0 & 0.0028 \\ -0.2462 & -0.0634 & -0.0278 & 0.0090 & 0.0247 & -0.0018 \\ 0 & -0.2462 & 0 & -0.0278 & 0 & 0.0247 \\ 0.3599 & 0.9284 & 0.0843 & 0.0406 & -0.0061 & -0.0041 \\ 0 & 0.3599 & 0 & 0.0843 & 0 & -0.0061 \end{pmatrix}$$

For $k = 2$, $M = 3$, $\alpha = 1.25$, $\lambda = 12$, we have

$$\mathbf{P}^{12,\ 1.25}_{6\times6} = \begin{pmatrix} 0.1580 & 0.4589 & 0.0374 & 0.0128 & 0.0014 & -0.0008 \\ 0 & 0.1580 & 0 & 0.0374 & 0 & 0.0014 \\ -0.3781 & -0.0922 & -0.0278 & 0.0090 & 0.0179 & -0.0013 \\ 0 & -0.3781 & 0 & -0.0278 & 0 & 0.0179 \\ 0.8748 & 2.2912 & 0.1490 & 0.0672 & -0.0049 & -0.0048 \\ 0 & 0.8748 & 0 & 0.1490 & 0 & -0.0049 \end{pmatrix}.$$

For different values of λ, we get different families of Gegenbauer wavelets matrices and their corresponding different operational matrices of fractional order integration. This phenomena makes calculations fast because the operational matrix $\mathbf{P}^{\lambda,\ \alpha}_{\hat{m}\times\hat{m}}$ contains many zero entries.

9.1.3 Operational Matrix of Fractional Order Integration for Boundary Value Problems

We drive another operational matrix of fractional integration to solve the fractional boundary value problems. Let $g(x) \in L_2[0, b]$ be a given function, $b > 0$, then

$$g(x)I^{\alpha}_{b}\psi^{\lambda}_{n,m}(x) = \frac{g(x)}{\Gamma(\alpha)}\int_0^b (b-s)^{\alpha-1}\psi^{\lambda}_{n,m}(s)ds. \tag{9.1.8}$$

Since the Gegenbauer wavelets are supported on the intervals $[\frac{(2n-2)b}{2^k}, \frac{2nb}{2^k})$, therefore

$$\begin{aligned} g(x)I^{\alpha}_{b}\psi^{\lambda}_{n,m}(x) &= \frac{g(x)2^{\frac{k}{2}}}{\sqrt{(L^{\lambda}_{m})}\Gamma(\alpha)}\int_{\frac{(2n-2)b}{2^k}}^{\frac{2nb}{2^k}} (b-s)^{\alpha-1}C^{\lambda}_{m}(2^k s - 2n + 1)ds, \\ &= g(x)V^{\lambda,\alpha,b}_{n,m}, \end{aligned} \tag{9.1.9}$$

where $V_{n,m}^{\lambda,\alpha,b} = \frac{2^{\frac{k}{2}}}{\sqrt{(L_m^\lambda)}\Gamma(\alpha)} \int\limits_{\frac{(2n-2)b}{2^k}}^{\frac{2nb}{2^k}} (b-s)^{\alpha-1} C_m^\lambda(2^k s - 2n + 1) ds.$

Expand the equation (9.1.9) at the collocation points, $x_i = \frac{2i-1}{2^k M}$, where $i = 1, 2, ..., 2^{k-1}M$, to obtain

$$\mathbf{Q}_{\hat{\mathbf{m}}\times\hat{\mathbf{m}}}^{\mathbf{g},\lambda,\alpha,\mathbf{b}} = \mathbf{V}_{\hat{\mathbf{m}}\times\mathbf{1}}^{\lambda,\alpha,\mathbf{b}} \mathbf{B}_{\mathbf{1}\times\hat{\mathbf{m}}}, \tag{9.1.10}$$

where $\mathbf{B}_{\mathbf{1}\times\hat{\mathbf{m}}} = [g(x_1), g(x_2), ..., g(x_{\hat{m}})]$,
$\mathbf{V}_{\hat{\mathbf{m}}\times\mathbf{1}}^{\lambda,\alpha,\mathbf{b}} = [V_{1,0}^{\lambda,\alpha,b}, V_{1,1}^{\lambda,\alpha,b}, \cdots, V_{1M-1}^{\lambda,\alpha,b}, V_{2,0}^{\lambda,\alpha,b}, V_{2,1}^{\lambda,\alpha,b}, \cdots, V_{2,M-1}^{\lambda,\alpha,b}, \cdots, V_{2^{k-1},0}^{\lambda,\alpha,b}, V_{2^{k-1},1}^{\lambda,\alpha,b}, \cdots, V_{2^{k-1},M-1}^{\lambda,\alpha,b}]^T$.

$$\mathbf{Q}_{\hat{\mathbf{m}},\hat{\mathbf{m}}}^{\mathbf{g},\lambda\times\alpha,\mathbf{b}} = \begin{bmatrix} V_{1,0}^{\lambda,\alpha,b} g(\frac{1}{2^k M}) & V_{1,0}^{\lambda,\alpha,b} g(\frac{3}{2^k M}) & \cdots & V_{1,0}^{\lambda,\alpha,b} g(\frac{2^k M-1}{2^k M}) \\ V_{1,1}^{\lambda,\alpha,b} g(\frac{1}{2^k M}) & V_{1,1}^{\lambda,\alpha,b} g(\frac{3}{2^k M}) & \cdots & V_{1,1}^{\lambda,\alpha,b} g(\frac{2^k M-1}{2^k M}) \\ \vdots & \vdots & \cdots & \vdots \\ V_{1,M-1}^{\lambda,\alpha,b} g(\frac{1}{2^k M}) & V_{1,M-1}^{\lambda,\alpha,b} g(\frac{3}{2^k M}) & \cdots & V_{1,M-1}^{\lambda,\alpha,b} g(\frac{2^k M-1}{2^k M}) \\ V_{2,0}^{\lambda,\alpha,b} g(\frac{1}{2^k M}) & V_{2,0}^{\lambda,\alpha,b} g(\frac{3}{2^k M}) & \cdots & V_{2,0}^{\lambda,\alpha,b} g(\frac{2^k M-1}{2^k M}) \\ V_{2,1}^{\lambda,\alpha,b} g(\frac{1}{2^k M}) & V_{2,1}^{\lambda,\alpha,b} g(\frac{3}{2^k M}) & \cdots & V_{2,1}^{\lambda,\alpha,b} g(\frac{2^k M-1}{2^k M}) \\ \vdots & \vdots & \cdots & \vdots \\ V_{2,M-1}^{\lambda,\alpha,b} g(\frac{1}{2^k M}) & V_{2,M-1}^{\lambda,\alpha,b} g(\frac{3}{2^k M}) & \cdots & V_{2,M-1}^{\lambda,\alpha,b} g(\frac{2^k M-1}{2^k M}) \\ \vdots & \vdots & \cdots & \vdots \\ V_{2^{k-1},0}^{\lambda,\alpha,b} g(\frac{1}{2^k M}) & V_{2^{k-1},0}^{\lambda,\alpha,b} g(\frac{3}{2^k M}) & \cdots & V_{2^{k-1},0}^{\lambda,\alpha,b} g(\frac{2^k M-1}{2^k M}) \\ V_{2^{k-1},1}^{\lambda,\alpha,b} g(\frac{1}{2^k M}) & V_{2^{k-1},1}^{\lambda,\alpha,b} g(\frac{3}{2^k M}) & \cdots & V_{2^{k-1},1}^{\lambda,\alpha,b} g(\frac{2^k M-1}{2^k M}) \\ \vdots & \vdots & \cdots & \vdots \\ V_{2^{k-1},M-1}^{\lambda,\alpha,b} g(\frac{1}{2^k M}) & V_{2^{k-1},M-1}^{\lambda,\alpha,b} g(\frac{3}{2^k M}) & \cdots & V_{2^{k-1},M-1}^{\lambda,\alpha,b} g(\frac{2^k M-1}{2^k M}) \end{bmatrix}.$$

In particular, for $\lambda = 7,\ k = 2,\ M = 3,\ \alpha = 1.5,\ b = 1,$ and $g(x) = x^2$, we have

$$\mathbf{Q}_{\mathbf{6}\times\mathbf{6}}^{\mathbf{g},\mathbf{7},\mathbf{1.5},\mathbf{1}} = \begin{bmatrix} V_{1,0}^{7,1.5,1} g(\frac{1}{12}) & V_{1,0}^{7,1.5,1} g(\frac{3}{12}) & V_{1,0}^{7,1.5,1} g(\frac{5}{12}) & V_{1,0}^{7,1.5,1} g(\frac{7}{12}) & V_{1,0}^{7,1.5,1} g(\frac{9}{12}) & V_{1,0}^{7,1.5,1} g(\frac{11}{12}) \\ V_{2,0}^{7,1.5,1} g(\frac{1}{12}) & V_{2,0}^{7,1.5,1} g(\frac{3}{12}) & V_{2,0}^{7,1.5,1} g(\frac{5}{12}) & V_{2,0}^{7,1.5,1} g(\frac{7}{12}) & V_{2,0}^{7,1.5,1} g(\frac{9}{12}) & V_{2,0}^{7,1.5,1} g(\frac{11}{12}) \\ V_{1,1}^{7,1.5,1} g(\frac{1}{12}) & V_{1,1}^{7,1.5,1} g(\frac{3}{12}) & V_{1,1}^{7,1.5,1} g(\frac{5}{12}) & V_{1,1}^{7,1.5,1} g(\frac{7}{12}) & V_{1,1}^{7,1.5,1} g(\frac{9}{12}) & V_{1,1}^{7,1.5,1} g(\frac{11}{12}) \\ V_{2,1}^{7,1.5,1} g(\frac{1}{12}) & V_{2,1}^{7,1.5,1} g(\frac{3}{12}) & V_{2,1}^{7,1.5,1} g(\frac{5}{12}) & V_{2,1}^{7,1.5,1} g(\frac{7}{12}) & V_{2,1}^{7,1.5,1} g(\frac{9}{12}) & V_{2,1}^{7,1.5,1} g(\frac{11}{12}) \\ V_{1,2}^{7,1.5,1} g(\frac{1}{12}) & V_{1,2}^{7,1.5,1} g(\frac{3}{12}) & V_{1,2}^{7,1.5,1} g(\frac{5}{12}) & V_{1,2}^{7,1.5,1} g(\frac{7}{12}) & V_{1,2}^{7,1.5,1} g(\frac{9}{12}) & V_{1,2}^{7,1.5,1} g(\frac{11}{12}) \\ V_{2,2}^{7,1.5,1} g(\frac{1}{12}) & V_{2,2}^{7,1.5,1} g(\frac{3}{12}) & V_{2,2}^{7,1.5,1} g(\frac{5}{12}) & V_{2,2}^{7,1.5,1} g(\frac{7}{12}) & V_{2,2}^{7,1.5,1} g(\frac{9}{12}) & V_{2,2}^{7,1.5,1} g(\frac{11}{12}) \end{bmatrix}$$

or

$$\mathbf{Q}_{\mathbf{6}\times\mathbf{6}}^{\mathbf{g},\mathbf{7},\mathbf{1.5},\mathbf{1}} = \begin{bmatrix} 0.0103 & 0.0924 & 0.2566 & 0.5029 & 0.8313 & 1.2419 \\ 0.0056 & 0.0505 & 0.1403 & 0.2750 & 0.4547 & 0.6792 \\ -0.0007 & -0.0059 & -0.0165 & -0.0324 & -0.0535 & -0.0799 \\ -0.0013 & -0.0115 & -0.0321 & -0.0629 & -0.1039 & -0.1552 \\ 0.0038 & 0.0341 & 0.0949 & 0.1859 & 0.3073 & 0.4591 \\ 0.0019 & 0.0174 & 0.0485 & 0.0950 & 0.1570 & 0.2345 \end{bmatrix}$$

9.2 Convergence of the Gegenbauer Wavelets Method

Let $2^{k-1},\ M\ \to \infty$, then the series solution (9.1.2) converges to $f(x)$.

Proof: Take the inner product of $f(x)$ and $\psi^{\lambda}_{n,m}(x)$ with respect to the weight function, we get

$$a^{\lambda}_{nm} = \langle f(x), \psi^{\lambda}_{n,m}(x)\rangle = \int_0^1 (1-x^2)^{\lambda-\frac{1}{2}} f(x)\psi^{\lambda}_{n,m}(x)dx$$

We introduce notations, $\hat{p} = 2^{k-1},\ p = 2^{d-1},\ \hat{q} = M$ and $q = N$, where k and d denotes the level of resolutions and, M and N represents the order of the Gegenbauer polynomials.

Let $S^{\lambda}_{\hat{p},\hat{q}}$ be a sequence of partial sums of $a^{\lambda}_{ij}\psi^{\lambda}_{i,j}(x)$, we prove that $S_{\hat{p},\hat{q}}$ is a Cauchy sequence in Hilbert space $L^2[0,1)$ and then we show that $S^{\lambda}_{\hat{p},\hat{q}}$ converges to $f(x)$, when $\hat{p},\hat{q} \to \infty$. First we show that $S^{\lambda}_{\hat{p},\hat{q}}$ is a Cauchy sequence. For this purpose, let $S^{\lambda}_{p,q}$ be arbitrary sums of $a^{\lambda}_{ij}\psi^{\lambda}_{i,j}(x)$ with $\hat{p} > p,\ \hat{q} > q$.

$$\begin{aligned}
\|S^{\lambda}_{\hat{p},\hat{q}} - S^{\lambda}_{p,q}\|^2 &= \|\sum_{i=p+1}^{\hat{p}}\sum_{j=q}^{\hat{q}-1} a^{\lambda}_{ij}\psi^{\lambda}_{i,j}(x)\|^2, \\
&= \langle \sum_{i=p+1}^{\hat{p}}\sum_{j=q}^{\hat{q}-1} a^{\lambda}_{ij}\psi^{\lambda}_{i,j}(x), \sum_{r=p+1}^{\hat{p}}\sum_{s=q}^{\hat{q}-1} a^{\lambda}_{rs}\psi^{\lambda}_{r,s}(x)\rangle, \\
&= \sum_{i=p+1}^{\hat{p}}\sum_{j=q}^{\hat{q}-1}\sum_{r=p+1}^{\hat{p}}\sum_{s=q}^{\hat{q}-1} a^{\lambda}_{ij}\overline{a}^{\lambda}_{rs}\langle\psi^{\lambda}_{i,j}(x), \psi^{\lambda}_{r,s}(x)\rangle, \\
&= \sum_{i=p+1}^{\hat{p}}\sum_{j=q}^{\hat{q}-1} |a^{\lambda}_{ij}|^2.
\end{aligned} \tag{9.2.1}$$

From the Bessel's inequality, we have $\sum_{i=1}^{\infty}\sum_{j=0}^{\infty} |a^{\lambda}_{ij}|^2$ is convergent and hence

$$\|S^{\lambda}_{\hat{p},\hat{q}} - S^{\lambda}_{p,q}\|^2 \to 0 \text{ as } \hat{p},\hat{q},p,q \to \infty.$$

This implies that $S^{\lambda}_{\hat{p},\hat{q}}$ is a Cauchy sequence and it converges to, say, $y(x) \in L^2[0,1)$. We need to show that $y(x) = f(x)$,

$$\begin{aligned}
\langle y(x) - f(x), \psi^{\lambda}_{i,j}(x)\rangle &= \langle y(x), \psi^{\lambda}_{i,j}(x)\rangle - \langle f(x), \psi^{\lambda}_{i,j}(x)\rangle, \\
&= \lim_{\hat{p},\hat{q}\to\infty} \langle S^{\lambda}_{\hat{p},\hat{q}}, \psi^{\lambda}_{i,j}(x)\rangle - a^{\lambda}_{ij}, \\
&= a^{\lambda}_{ij} - a^{\lambda}_{ij}, \\
&= 0.
\end{aligned} \tag{9.2.2}$$

Hence $\sum_{i=1}^{\hat{p}}\sum_{j=0}^{\hat{q}-1} a^{\lambda}_{ij}\psi^{\lambda}_{i,j}(x)$ converges to $f(x)$ as $\hat{p},\hat{q} \to \infty$.

9.3 Implementation and Examples

We describe the algorithm by working out few examples. We implement the Gegenbauer wavelets method to fractional initial as well as boundary value problems.

9.3.1 Initial Value Problems

Example 1. Consider the following Bagley Torvik equation

$$\begin{aligned} b_1^c D^2 y(x) + b_2^c D^{1.5} y(x) + b_3 y(x) = f(x),\ x \geq 0, \\ y(0) = 1,\ y'(0) = 1, \end{aligned} \tag{9.3.1}$$

where $f(x) = b_3(x+1)$, and the exact solution [108] is $y(x) = x+1$. Apply the Gegenbauer wavelet method to equation (9.3.1), we approximate the higher order term by the Gegenbauer wavelets series as

$$D^2 y(x) = \sum_{n=1}^{2^{k-1}} \sum_{m=0}^{M-1} a_{nm}^{\lambda} \psi_{n,m}^{\lambda}(x) = {\mathbf{a}^{\lambda}}^T \Psi^{\lambda}(x). \tag{9.3.2}$$

Lower order derivatives are obtained by integrating (9.3.2) and using the initial conditions

$$Dy(x) = \sum_{n=1}^{2^{k-1}} \sum_{m=0}^{M-1} a_{nm}^{\lambda} (I_x^1 \psi_{n,m}^{\lambda}(x)) + 1 = {\mathbf{a}^{\lambda}}^T \mathbf{P}^{\lambda,1} \Psi^{\lambda}(x) + 1, \tag{9.3.3}$$

$$y(x) = \sum_{n=1}^{2^{k-1}} \sum_{m=0}^{M-1} a_{nm}^{\lambda} (I_x^2 \psi_{n,m}^{\lambda}(x)) + x + 1 = {\mathbf{a}^{\lambda}}^T \mathbf{P}^{\lambda,2} \Psi^{\lambda}(x) + x + 1, \tag{9.3.4}$$

$$D^{1.5} y(x) = \sum_{n=1}^{2^{k-1}} \sum_{m=0}^{M-1} a_{nm}^{\lambda} (I_x^{0.5} \psi_{n,m}^{\lambda}(x)) = {\mathbf{a}^{\lambda}}^T \mathbf{P}^{\lambda,0.5} \Psi^{\lambda}(x). \tag{9.3.5}$$

Substitute (9.3.2), (9.3.4), and (9.3.5) in equation (9.3.1), we get

$$\begin{aligned} \sum_{n=1}^{2^{k-1}} \sum_{m=0}^{M-1} (b_1 a_{nm}^{\lambda} \psi_{n,m}^{\lambda}(x) + b_2 a_{nm}^{\lambda} (I_x^{0.5} \psi_{n,m}^{\lambda}(x)) + b_3 a_{nm}^{\lambda} (I_x^2 \psi_{n,m}^{\lambda}(x)) \\ = -b_3(1+x) + f(x),\ x \geq 0. \end{aligned} \tag{9.3.6}$$

Equation (9.3.6) at the collocation points, $x_i = \frac{2i-1}{2^k M}$, $i = 1, 2, \cdots, 2^{k-1}M$, and in vector notation, takes the following form by using equations (9.1.3) and (9.1.7)

$$\begin{gathered} {\mathbf{a}^{\lambda}}^T (b_1 \Psi_{\hat{m} \times \hat{m}}^{\lambda} + b_2 \mathbf{P}_{\hat{m} \times \hat{m}}^{\lambda,0.5} \Psi_{\hat{m} \times \hat{m}}^{\lambda} + b_3 \mathbf{P}_{\hat{m} \times \hat{m}}^{\lambda,2} \Psi_{\hat{m} \times \hat{m}}^{\lambda}) = F, \\ \text{or} \\ {\mathbf{a}^{\lambda}}^T U_{\hat{m} \times \hat{m}}^{\lambda} = F, \end{gathered} \tag{9.3.7}$$

where $F = \{-b_3(1+x_i) + f(x_i)\}_{i=1}^{2^{k-1}M}$ and $U_{\hat{m} \times \hat{m}}^{\lambda} = (b_1 \Psi_{\hat{m} \times \hat{m}}^{\lambda} + b_2 \mathbf{P}_{\hat{m} \times \hat{m}}^{\lambda,0.5} \Psi_{\hat{m} \times \hat{m}}^{\lambda} + b_3 \mathbf{P}_{\hat{m} \times \hat{m}}^{\lambda,2} \Psi_{\hat{m} \times \hat{m}}^{\lambda})$.

Consider $b_1 = b_2 = b_3 = 1$ and $\lambda = 17.5,\ k = 2,\ M = 4$, we get

$$U_{8\times 8}^{17.5} = \begin{pmatrix} 3.9117 & 4.6393 & 5.1779 & 5.6801 & 2.2699 & 2.0590 & 2.0610 & 2.1288 \\ 0 & 0 & 0 & 0 & 3.9117 & 4.6393 & 5.1779 & 5.6801 \\ -17.8455 & -9.2678 & 2.3847 & 15.8417 & 1.0869 & 0.1013 & -0.1984 & -0.3492 \\ 0 & 0 & 0 & 0 & -17.8455 & -9.2678 & 2.3847 & 15.8417 \\ 57.0389 & 14.3879 & 12.3357 & 65.5851 & 18.9272 & 16.3578 & 16.1898 & 16.6459 \\ 0 & 0 & 0 & 0 & 57.0389 & 14.3879 & 12.3357 & 65.5851 \\ -147.2366 & -25.9284 & -21.4612 & 128.2630 & 8.4966 & 0.8268 & -1.4405 & -2.5715 \\ 0 & 0 & 0 & 0 & -147.2366 & -25.9284 & -21.4612 & 128.2630 \end{pmatrix}$$

$$F = \begin{pmatrix} 0 & 0 & 0 & 0 & 0 & 0 & 0 & 0 \end{pmatrix}, \quad \mathbf{a}^{17.5^T} = \begin{pmatrix} 0 & 0 & 0 & 0 & 0 & 0 & 0 & 0 \end{pmatrix}.$$

Substitute $\mathbf{a}^{17.5^T}$ in equation (9.3.4) to obtain

$$y(x) = x + 1, \tag{9.3.8}$$

which is the exact solution.

Example 2. Consider the following fractional differential equation with variable coefficients

$$\begin{aligned} gD^2y(x) + b(x)^cD^\alpha y(x) + c(x)Dy(x) + e(x)^cD^\beta y(x) + k(x)y(x) = f(x), \\ 0 < \beta < 1, 1 < \alpha < 2, \\ y(0) = 2,\ y'(0) = 0, \end{aligned} \tag{9.3.9}$$

where g is a constant and

$f(x) = -g - \frac{b(x)}{\Gamma(3-\alpha)}x^{2-\alpha} - xc(x) - \frac{e(x)}{\Gamma(3-\beta)}x^{2-\beta} + k(x)(2 - \frac{1}{2}x^2)$, and the exact solution [39] is $y(x) = 2 - \frac{1}{2}x^2$.

Apply the Gegenbauer wavelets method to equation (9.3.9), we obtain

$$\begin{aligned} \mathbf{a}^{\lambda^T}(g\Psi_{\hat{m}\times\hat{m}}^\lambda + \mathbf{P}_{\hat{m}\times\hat{m}}^{\lambda,2-\alpha}\Psi_{\hat{m}\times\hat{m}}^\lambda B + \mathbf{P}_{\hat{m}\times\hat{m}}^{\lambda,1}\Psi_{\hat{m}\times\hat{m}}^\lambda C + \mathbf{P}_{\hat{m}\times\hat{m}}^{\lambda,2-\beta}\Psi_{\hat{m}\times\hat{m}}^\lambda E \\ + \mathbf{P}_{\hat{m}\times\hat{m}}^{\lambda,2}\Psi_{\hat{m}\times\hat{m}}^\lambda K) = L, \end{aligned} \tag{9.3.10}$$

and solution at the collocation points is given by

$$Y = \mathbf{a}^{\lambda^T}\mathbf{P}_{\hat{m}\times\hat{m}}^{\lambda,2}\Psi_{\hat{m}\times\hat{m}}^\lambda + 2, \tag{9.3.11}$$

where $L = [f(x_1) - 2k(x_1), f(x_2) - 2k(x_2), ..., f(x_{\hat{m}}) - 2k(x_{\hat{m}})],\ Y = [y(x_1, y(x_2), ..., y(x_{\hat{m}}))]$ and

B, C, E and K are the diagonal matrices and are given by

$$B = \begin{bmatrix} b(x_1) & 0 & \cdots & 0 \\ 0 & b(x_2) & \cdots & 0 \\ \vdots & \vdots & \ddots & \vdots \\ 0 & 0 & \cdots & b(x_{\hat{m}}) \end{bmatrix},\ C = \begin{bmatrix} c(x_1) & 0 & \cdots & 0 \\ 0 & c(x_2) & \cdots & 0 \\ \vdots & \vdots & \ddots & \vdots \\ 0 & 0 & \cdots & c(x_{\hat{m}}) \end{bmatrix}$$

$$E = \begin{bmatrix} e(x_1) & 0 & \cdots & 0 \\ 0 & e(x_2) & \cdots & 0 \\ \vdots & \vdots & \ddots & \vdots \\ 0 & 0 & \cdots & e(x_{\hat{m}}) \end{bmatrix}, \text{ and } K = \begin{bmatrix} k(x_1) & 0 & \cdots & 0 \\ 0 & k(x_2) & \cdots & 0 \\ \vdots & \vdots & \ddots & \vdots \\ 0 & 0 & \cdots & k(x_{\hat{m}}) \end{bmatrix}$$

where $x_i = \frac{2i-1}{2\hat{m}},\ i = 1, 2, ..., \hat{m}$, are collocation points.

We consider $g = 1,\ b(x) = \sqrt{x},\ c(x) = e^x,\ e(x) = x^{\frac{1}{4}},$ and $k(x) = x^{\frac{1}{5}}$. We fix $\alpha = 1.755,\ \beta = 0.333$ and plot the exact solution and solution by the Gegenbauer wavelets method at $k = 5,\ M = 11,\ \lambda = 30$, as shown in Figure 9.1, along with the absolute error. Table 9.1 shows that absolute error reduces while increasing k and M, as in convergence analysis.

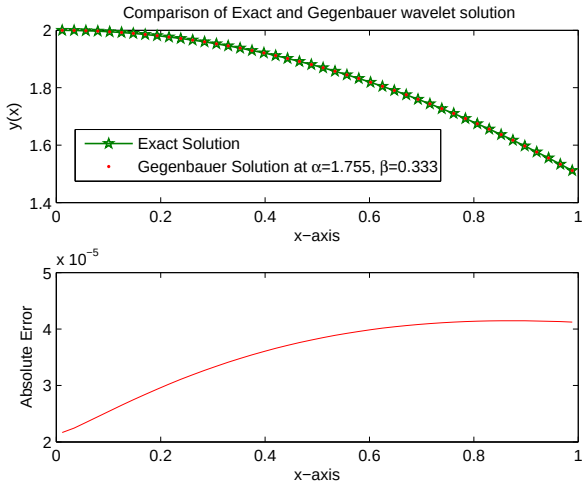

Figure 9.1: Exact solution and Solution by the Gegenbauer wavelet method by taking $k = 5$, $M = 11,\ \lambda = 30$, at $\beta = 0.333$ and $\alpha = 1.755$.

x	$k=2,\ M=3$	$k=4,\ M=5$	$k=6,\ M=7$	$k=7,\ M=9$
0.1	1.1894×10^{-3}	0.3059×10^{-4}	0.1174×10^{-5}	0.2017×10^{-6}
0.2	1.2516×10^{-3}	0.3553×10^{-4}	0.1496×10^{-5}	0.2709×10^{-6}
0.3	1.3127×10^{-3}	0.3969×10^{-4}	0.1767×10^{-5}	0.3289×10^{-6}
0.4	1.3649×10^{-3}	0.4304×10^{-4}	0.1989×10^{-5}	0.3765×10^{-6}
0.5	1.4015×10^{-3}	0.4563×10^{-4}	0.2164×10^{-5}	0.4145×10^{-6}
0.6	1.4233×10^{-3}	0.4753×10^{-4}	0.2298×10^{-5}	0.4439×10^{-6}
0.7	1.4333×10^{-3}	0.4883×10^{-4}	0.2396×10^{-5}	0.4656×10^{-6}
0.8	1.4331×10^{-3}	0.4960×10^{-4}	0.2462×10^{-5}	0.4806×10^{-6}
0.9	1.4242×10^{-3}	0.4993×10^{-4}	0.2501×10^{-5}	0.4901×10^{-6}
1.0	1.4079×10^{-3}	0.4991×10^{-4}	0.2517×10^{-5}	0.4948×10^{-6}

Table 9.1: Absolute error for different values of k and M, at $\lambda=7$ and $\alpha=1.8,\ \beta=0.7$.

9.3.2 Boundary Value Problems

Example 3. Consider the following fractional boundary value problem

$$\begin{aligned} {}^cD^{\alpha}y(x) = {}^c\,D^{\beta}y(x) + h(x),\ 1<\alpha\le 2,\ 0<\beta\le 1,\\ y(0)=0,\ y(1)=0, \end{aligned} \tag{9.3.12}$$

where $h(x)=-e^{x-1}-1$, and the exact solution [109] is known at $\alpha=2$ and $\beta=1$, $y(x)=x(1-e^{x-1})$.

Consider the Gegenbauer wavelet approximation of higher order derivative term in equation (9.3.12)

$${}^cD^{\alpha}y(x)=\sum_{n=1}^{2^{k-1}}\sum_{m=0}^{M-1}a^{\lambda}_{nm}\psi^{\lambda}_{n,m}(x). \tag{9.3.13}$$

Now to get the Gegenbauer wavelet series for lower order derivative terms we integrate equation (9.3.13) and use the boundary condition, to get

$$\begin{aligned} y(x)&=\sum_{n=1}^{2^{k-1}}\sum_{m=0}^{M-1}a^{\lambda}_{nm}(I^{\alpha}_x\psi^{\lambda}_{n,m}(x)-x(\tfrac{1}{\Gamma(\alpha)}\int_0^1(1-s)^{\alpha-1}\psi_{n,m}(s)ds)),\\ {}^cD^{\beta}y(x)&=\sum_{n=1}^{2^{k-1}}\sum_{m=0}^{M-1}a^{\lambda}_{nm}(I^{\alpha-\beta}_x\psi^{\lambda}_{n,m}(x)-\tfrac{\Gamma(2)}{\Gamma(2-\beta)}x^{1-\beta}(\tfrac{1}{\Gamma(\alpha)}\int_0^1(1-s)^{\alpha-1}\psi_{n,m}(s)ds)). \end{aligned} \tag{9.3.14}$$

Substitute the equations (9.3.13) and (9.3.14) in equation (9.3.12), we obtain

$$\sum_{n=1}^{2^{k-1}}\sum_{m=0}^{M-1}a^{\lambda}_{nm}(\psi^{\lambda}_{n,m}(x)-I^{\alpha-\beta}_x\psi^{\lambda}_{n,m}(x)+\tfrac{\Gamma(2)}{\Gamma(2-\beta)}x^{1-\beta}(\tfrac{1}{\Gamma(\alpha)}\int_0^1(1-s)^{\alpha-1}\psi_{n,m}(s)ds))=h(x). \tag{9.3.15}$$

Use equations (9.1.3), (9.1.7) and (9.1.10), we get

$$\mathbf{a}^{\lambda^T}(\Psi^{\lambda}_{\hat{m}\times\hat{m}} - \mathbf{P}^{\lambda,\alpha-\beta}_{\hat{m}\times\hat{m}}\Psi^{\lambda}_{\hat{m}\times\hat{m}} + \mathbf{Q}^{\mathbf{g},\lambda,\alpha,\mathbf{1}}_{\hat{\mathbf{m}}\times\hat{\mathbf{m}}}) = H, \tag{9.3.16}$$

and solution at the collocation points is given by

$$Y = \mathbf{a}^{\lambda^T}\mathbf{P}^{\lambda,\alpha}_{\hat{m}\times\hat{m}}\Psi^{\lambda}_{\hat{m}\times\hat{m}} - \mathbf{a}^{\lambda^T}\mathbf{Q}^{\mathbf{R},\lambda,\alpha,\mathbf{1}}_{\hat{\mathbf{m}}\times\hat{\mathbf{m}}}, \tag{9.3.17}$$

where $H = [h(x_1), h(x_2), ..., h(x_{\hat{m}})]$, and $g = \frac{\Gamma(2)}{\Gamma(2-\beta)}x^{1-\beta},\ R = x$.

Solve the equation (9.3.16) for $\mathbf{a}^{\lambda^T}$, and substitute it in (9.3.17) to get $y(x)$, at the collocation points. Choose $\lambda = 5,\ k = 10,\ M = 3$, the results obtained by the Gegenbauer wavelet method y_{GWM} is shown in Table 9.2 along with the absolute error E_{GWM}. It shows that Gegenbauer wavelet method provides better results as compared to homotopy perturbation method y_{HPM} [128] and Haar wavelet method y_{HAAR} [109]. We can get more accurate results while increasing k or M or both. According to the Figure 9.2, solution by the Gegenbauer wavelet method at different values of α converge to the exact solution, when α approaches to 2.

$\lambda = 5,\ k = 10,\ M = 3$ $\alpha = 2,\ \beta = 1$					
x	y_{HPM} [128]	y_{HAAR} [109]	y_{GWM}	y_{Exact}	E_{GWM}
0.1	0.05934820	0.05934300	0.05934302	0.05934303	1.58953244e-8
0.2	0.11014318	0.11013418	0.11013419	0.11013421	1.97211689e-8
0.3	0.15103441	0.15102438	0.15102438	0.15102441	2.46505651e-8
0.4	0.18048329	0.18047531	0.18047531	0.18047535	3.08917651e-8
0.5	0.19673826	0.19673463	0.19673463	0.19673467	3.86865598e-8
0.6	0.19780653	0.19780792	0.19780792	0.19780797	4.83152341e-8
0.7	0.18142196	0.18142718	0.18142719	0.18142725	6.01022115e-8
0.8	0.14500893	0.14501532	0.14501532	0.14501540	7.44224910e-8
0.9	0.08564186	0.08564623	0.08564623	0.08564632	9.17089691e-8

Table 9.2: Comparison of the Gegenbauer wavelet method with homotopy perturbation and Haar wavelet method.

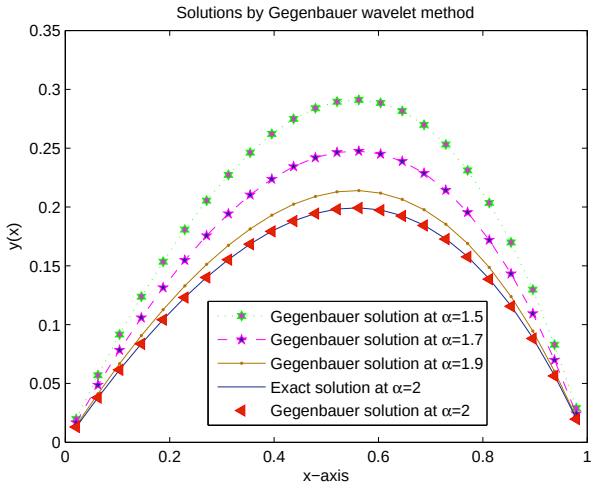

Figure 9.2: Solution by the Gegenbauer wavelet method by taking $k = 4$, $M = 3$, $\lambda = 5$, at $\beta = 1$ and different α

Example 4. Consider the following fractional boundary value problem with variable coefficients

$$\begin{aligned} {}^cD^{\alpha}y(x) + e(x)Dy(x) + b(x){}^cD^{\beta}y(x) + c(x)y(x) = f(x),\ 1 < \alpha \leq 2, 0 < \beta < 1, \\ y(0) = 0,\ y(1) = 0, \end{aligned} \tag{9.3.18}$$

where $f(x) = \Gamma(\alpha+1) - \frac{\Gamma(8)}{\Gamma(8-\beta)}x^{7-\alpha} + e(x)(\alpha x^{\alpha-1} - 7x^6) + b(x)(\frac{\Gamma(\alpha+1)}{\Gamma(\alpha-\beta+1)}x^{\alpha-\beta} - \frac{\Gamma(8)}{\Gamma(8-\beta)}x^{7-\beta}) + c(x)(x^{\alpha} - x^7)$, and the exact solution depends on the order of the equation (9.3.18), $y(x) = x^{\alpha} - x^7$. Apply the Gegenbauer wavelets method to equation (9.3.18), we get

$$\begin{aligned} \mathbf{a}^{\lambda T}(\Psi^{\lambda}_{\hat{m}\times\hat{m}} + \mathbf{P}^{\lambda,\alpha-1}_{\hat{m}\times\hat{m}}\Psi^{\lambda}_{\hat{m}\times\hat{m}}E + \mathbf{P}^{\lambda,\alpha-\beta}_{\hat{m}\times\hat{m}}\Psi^{\lambda}_{\hat{m}\times\hat{m}}B + \mathbf{P}^{\lambda,\alpha}_{\hat{m}\times\hat{m}}\Psi^{\lambda}_{\hat{m}\times\hat{m}}C \\ -\mathbf{Q}^{\mathbf{e},\lambda,\alpha,\mathbf{1}}_{\hat{\mathbf{m}}\times\hat{\mathbf{m}}} - \mathbf{Q}^{\mathbf{g},\lambda,\alpha,\mathbf{1}}_{\hat{\mathbf{m}}\times\hat{\mathbf{m}}} - \mathbf{Q}^{\mathbf{h},\lambda,\alpha,\mathbf{1}}_{\hat{\mathbf{m}}\times\hat{\mathbf{m}}}) = F, \end{aligned} \tag{9.3.19}$$

and solution at the collocation points is given by

$$Y = \mathbf{a}^{\lambda T}\mathbf{P}^{\lambda,\alpha}_{\hat{m}\times\hat{m}}\Psi^{\lambda}_{\hat{m}\times\hat{m}} - \mathbf{a}^{\lambda T}\mathbf{Q}^{\mathbf{R},\lambda,\alpha,\mathbf{1}}_{\hat{\mathbf{m}}\times\hat{\mathbf{m}}}, \tag{9.3.20}$$

where $F = [f(x_1), f(x_2), ..., f(x_{\hat{m}})]$, $Y = [y(x_1, y(x_2), ..., y(x_{\hat{m}}))]$, $e = e(x)$, $g = b(x)(\frac{\Gamma(2)}{\Gamma(2-\beta)}x^{1-\beta})$, $h = xc(x)$, $R = x$, and E, B and C are the diagonal matrices and are given by

$$E = \begin{bmatrix} e(x_1) & 0 & \cdots & 0 \\ 0 & e(x_2) & \cdots & 0 \\ \vdots & \vdots & \ddots & \vdots \\ 0 & 0 & \cdots & e(x_{\hat{m}}) \end{bmatrix},\ B = \begin{bmatrix} b(x_1) & 0 & \cdots & 0 \\ 0 & b(x_2) & \cdots & 0 \\ \vdots & \vdots & \ddots & \vdots \\ 0 & 0 & \cdots & b(x_{\hat{m}}) \end{bmatrix} \text{ and}$$

$$C = \begin{bmatrix} c(x_1) & 0 & \cdots & 0 \\ 0 & c(x_2) & \cdots & 0 \\ \vdots & \vdots & \ddots & \vdots \\ 0 & 0 & \cdots & c(x_{\hat{m}}) \end{bmatrix}$$

where $x_i = \frac{2i-1}{2\hat{m}},\ i = 1, 2, ..., \hat{m}$, are collocation points

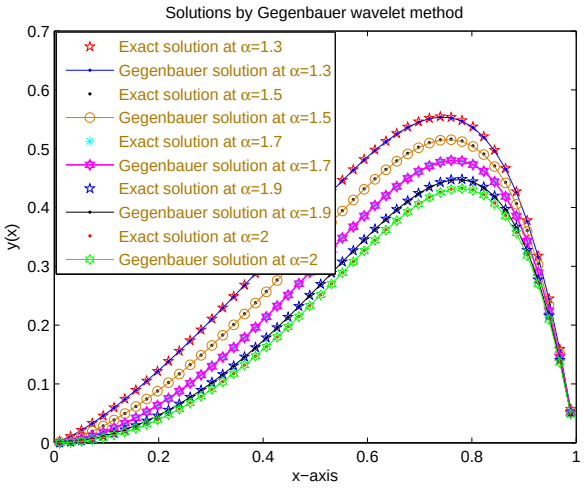

Figure 9.3: Solution by the Gegenbauer wavelet method by taking $k = 5,\ M = 3,\ \lambda = 15$, at $\beta = 0.5$ and different α

We consider $e(x) = \sin(x),\ b(x) = e^x,\ c(x) = x^2$ and fix the parameters $k = 5,\ M = 3,\ \lambda = 15$. Exact solutions and solutions by Gegenbauer wavelet method agrees at different values of α, and $\beta = 0.5$, as shown in Figure 9.3.

9.3.3 Conclusion

We have derived the Gegenbauer wavelets matrix, $\mathbf{\Psi}^{\lambda}{}_{2^{k-1}M,2^{k-1}M}$, the Gegenbauer wavelets operational matrix of fractional order integration, $\mathbf{P}^{\lambda,\alpha}_{\hat{m}\times\hat{m}}$, and another Gegenbauer wavelets operational matrix of fractional order integration, $\mathbf{Q}^{\mathbf{g},\lambda,\alpha,\mathbf{b}}_{\hat{\mathbf{m}}\times\hat{\mathbf{m}}}$, which is used for solving boundary value problems. These matrices are successfully utilized to solve the fractional initial and boundary value problems with constant or variable coefficients.

According to the Table 9.1, we get more accurate results while increasing k or M or both, as in convergence analysis. The solution of the fractional order differential equation converge to the solution of integer order differential equation as in Figure 9.2. Gegenbauer wavelets method is also compared with the other numerical methods. Gegenbauer wavelets method is more accurate than the homotopy perturbation method and Haar wavelet method, as shown in Table 9.2. Gegenbauer wavelet method is highly competitive in comparison with the classical methods.

Chapter 10

Methods for Solving Delay Differential Equations

A functional differential equation is one in which the rate of change of unknown function depends not only on the values of unknown function for the same time value but also on previous time values. The solution of delay differential equations not only require information of current state, but also requires some information about the previous state. Delay differential equations have numerous applications in mathematical modeling [14]: for example, physiological and pharmaceutical kinetics, chemical kinetics, the navigational control of ships and aircraft, population dynamics and infectious diseases.

Fractional delay differential equation is a generalization of the delay differential equation to arbitrary non-integer order. During the last decade, several papers have been devoted to the study of the numerical solution of fractional delay differential equations. For most of fractional order delay differential equations, exact solutions are not known. Therefore different numerical methods [87, 88, 124] have been developed and applied for providing approximate solutions.

The procedure of converting discrete delay differential equation to an ordinary differential equation is established by the method of steps [118]. It is easy to understand and use. In [41], the method of steps is utilize to solve linear and nonlinear discrete delay differential equation with different types of delay.

In this chapter, we introduced three approximate methods for solving delay differential equation. The methods are combinations of method of steps with radial basis function networks, Chebyshev wavelet method and Hermite wavelet method respectively. We discussed these three methods in this chapter.

10.1 Radial Basis Function Networks for Delay Differential Equation

For last decades, radial basis function collocation method is used for solving differential equations arising in mathematical problems. The radial basis functions is a mesh-free schemes, avoid grid generation and the domain of interest can be considered by a set of scattered data points [123]. The multiquadric radial basis functions [85] is very important and useful method for the numerical solution of ordinary and Partial Differential Equations. In [42, 43], radial basis function collocation method have been shown numerically and theoretically that it is very accurate even for a small number of collocation points.

In this section, combination of method of steps and radial basis function networks is used for solving delay differential equations. We transform the delay differential equation to an ordinary differential equation and then implement the radial basis function collocation method to find the solution of obtained ordinary differential equation. Total number of collocation points and radial basis functions are taken to be the same. Numerical examples are given to show the advantages of the technique over radial basis functions collocation method.

10.1.1 Radial Basis Function Networks

We can expand any function $f(x) \in L^2[a, b)$ into radial basis function networks as

$$f(x) \approx \sum_{j=0}^{M} w_j h_j(x), \tag{10.1.1}$$

where $M+1$ is the number of radial basis functions, w_j are the network weights, and x is the input. In the present work, we consider a multiquadrics radial basis function

$$h_j(x) = \sqrt{(x - d_j)^2 + b_j^2}$$

where $d_j{}'s$ are the centres of radial basis functions and $b_j{}'s$ are the widths of radial basis function. Large or small width of the radial basis function makes the response of a neuron flat or peak respectively. The width of the j^{th} radial basis function is chosen as [85]

$$b_j = \nu e_j$$

where $\nu > 0$ and e_j is the distance from the j^{th} center to the nearest center. Consider input points $\{x_j\}_{j=0}^{M}$, where $M+1$ is the total number of collocation points and we get desired outputs $\{y_j\}_{j=0}^{M}$ corresponding to the collocation points. The set of network weights $\{w_j\}_{j=0}^{M}$ can be found using the general linear least square methods.

10.1.2 Implementation of Radial Basis Function Collocation Method

Consider the following form of second order delay differential equation with discrete delay

$$\frac{d^2y}{dx^2} = f(x, y(x), y'(x), y(px-\tau), y'(px-\tau)),\ a \le x \le b, \tag{10.1.2}$$

subject to the initial conditions $y(a) = y_0$, $y'(a) = y'_0$, or boundary conditions $\alpha_1 y(a)+\beta_1 y'(a) = \gamma_1$, $\alpha_2 y(b) + \beta_2 y'(b) = \gamma_2$, where $p,\ y_0,\ y'_0,\ \alpha_1,\ \beta_1,\ \gamma_1,\ \alpha_2,\ \beta_2,$ and γ_2 are constants, f is a continuous linear or nonlinear function, $\tau(x, y(x))$ is delay and $px - \tau(x, y(x))$ is called delay argument.
We can approximate the solution of equation (10.1.2) by the radial basis function networks as

$$y(x) \simeq \sum_{j=0}^{M} w_j h_j(x). \tag{10.1.3}$$

In the delay equations, we also have to approximate the $y(px-\tau)$ in terms of the radial basis function series at delay time as

$$y(px-\tau) \simeq \sum_{j=0}^{M} w_j h_j(px-\tau). \tag{10.1.4}$$

Substituting equation (10.1.3), (10.1.4) in equation (10.1.2), we get the residual as

$$\begin{aligned}\sum_{j=0}^{M} w_j \tfrac{d^2}{dx^2} h_j(x) - f\big(x, \sum_{j=0}^{M} w_j h_j(x), \sum_{j=0}^{M} w_j h'_j(x), \sum_{j=0}^{M} w_j h_j(px-\tau),\\ \sum_{j=0}^{M} w_j h'_j(px-\tau)\big).\end{aligned} \tag{10.1.5}$$

Set the residual (10.1.5) equal to zero at the set of collocation points, x_i,

$$\begin{aligned}\sum_{j=0}^{M} w_j \tfrac{d^2}{dx^2} h_j(x_i) - f\big(x_i, \sum_{j=0}^{M} w_j h_j(x_i), \sum_{j=0}^{M} w_j h'_j(x_i), \sum_{j=0}^{M} w_j h_j(px_i-\tau),\\ \sum_{j=0}^{M} w_j h'_j(px_i-\tau)\big) = 0.\end{aligned} \tag{10.1.6}$$

We obtain $M-1$ equations from equation (10.1.6) by using collocation points x_i. There are $M+1$ unknowns, $\{w_j\}_{j=0}^{M}$, and $M-1$ equations. Two more equations obtain from the conditions of equation (10.1.2), that is

$$y(a) = y_0,\ \ \Rightarrow \sum_{j=0}^{M} w_j h_j(a) = y_0,$$

$$y'(a) = y'_0,\ \ \Rightarrow \sum_{j=0}^{M} w_j h'_j(a) = y'_0,$$

or

$$\alpha_1 y(a) + \beta_1 y'(a) = \gamma_1,\ \ \Rightarrow \alpha_1 \sum_{j=0}^{M} w_j h_j(a) + \beta_1 \sum_{j=0}^{M} w_j h'_j(a) = \gamma_1,$$

$$\alpha_2 y(b) + \beta_2 y'(b) = \gamma_2, \quad \Rightarrow \alpha_2 \sum_{j=0}^{M} w_j h_j(b) + \beta_2 \sum_{j=0}^{M} w_j h_j'(b) = \gamma_2.$$

Now we obtained $M+1$ equations either linear or nonlinear along with $M+1$ unknown coefficients w_j, which is solved by Newton iterative method to get w_j $'s$ and use it in (10.1.3) to get the approximate solution.

10.1.3 Implementation of the Method

The method of steps [41, 118] is used to transform the delay differential equations to ordinary differential equations on a given intervals. Consider the following delay differential equation with discrete delay

$$\begin{aligned} \tfrac{d^2y}{dx^2} = f(x, y(x), y'(x), y(px-\tau), y'(px-\tau)) \quad &, \ a \le x \le b, \\ y(x) = \phi(x) \quad &, \ -b \le x \le a. \end{aligned} \tag{10.1.7}$$

We solve problems in two steps. In first step, we transform the delay differential equation to ordinary differential equation by using method of steps and in second step, we implement the radial basis function collocation method, which is described in section 10.1.2, on resulting ordinary differential equation.

Step I: The solution $y(x)$ of delay differential equation (10.1.7) is known on $[-b, a]$, say $\phi(x)$, and call this solution $y_0(x)$, that is $y_0(px-\tau) = \phi(px-\tau)$.

Now the delay differential equation on $[a, b]$ takes the form

$$\tfrac{d^2y}{dx^2} = f(x, y(x), y'(x), y_0(px-\tau), y_0'(px-\tau)), \ a \le x \le b. \tag{10.1.8}$$

It is an ordinary differential equation with no delay term, because $y_0(px-\tau)$ and $y_0'(px-\tau)$ are known.

Step II: We solve this ordinary differential equation on $[a, b]$ by using the radial basis function collocation method and denote this solution as $y_1(x)$, which is defined on $[a, b]$.

Delay differential equation on $[b, 2b]$ becomes

$$\tfrac{d^2y}{dx^2} = f(x, y(x), y'(x), y_1(px-\tau), y_1'(px-\tau)), \ b \le x \le 2b, \tag{10.1.9}$$

which is again an ordinary differential equation and solve it by the radial basis function networks to get $y_2(x)$ on $[b, 2b]$. This procedure may be continued for subsequent intervals.

10.1.4 Numerical Solutions

In this section, we solve linear and nonlinear delay differential equations by using both the radial basis function collocation method and proposed method and compare the results with each other and exact solution. The collocation points are chosen to be the same as centers, $\{d_j\}_{j=0}^{M} = \{x_j\}_{j=0}^{M}$.

The width of the j^{th} radial basis function is $b_j = \nu e_j$, where $e_j = x_{j+1} - x_j$ and $\nu > 0$. We consider $\nu = 20,\ 100,\ 200$ and 200 in Examples 1, 2, 3 and 4 respectively.

Example 1. Consider the linear delay differential equation

$$\begin{aligned} \tfrac{dy}{dx} &= \tfrac{1}{2}e^{\frac{x}{2}}y(\tfrac{x}{2}) + \tfrac{1}{2}y(x), \quad 0 < x \leq 1, \\ y(x) &= e^x, \qquad\qquad x \leq 0. \end{aligned} \tag{10.1.10}$$

The exact solution is $y(x) = e^x$.

		$M = 8$			
x	y_{RBFN}	y_{PRO}	y_{exact}	E_{RBFN}	E_{PRO}
0.1	1.105170918075648	1.105170863740288	1.105170855606515	6.24691e-08	5.43354e-08
0.2	1.221402758160170	1.221402856590157	1.221402863666870	1.05507e-07	9.84300e-08
0.3	1.349858807576003	1.349858788968366	1.349858782042489	2.55335e-08	1.86076e-08
0.4	1.491824697641270	1.491824438669770	1.491824412174714	2.85467e-07	2.58971e-07
0.5	1.648721270700128	1.648721317398444	1.648721323561253	5.28611e-08	4.66983e-08
0.6	1.822118800390509	1.822119254967360	1.822119295929978	4.95539e-07	4.54577e-07
0.7	2.013752707470477	2.013752509582033	2.013752499151085	2.08319e-07	1.97888e-07
0.8	2.225540928492468	2.225540178147770	2.225540113992763	8.14500e-07	7.50345e-07
0.9	2.459603111156950	2.459604456196746	2.459604485114913	1.37396e-06	1.34504e-06
1.0	2.718281828459045	2.718271894779136	2.718271375842572	1.04526e-05	9.93368e-06

Table 10.1: Comparison of the radial basis function collocation method and proposed method at $M = 8$ with Exact solution.

The results obtained by the radial basis function collocation method, y_{RBFN}, and present method, y_{PRO}, at $M = 8$ are shown in Table 10.1 along with exact solution, y_{exact}, where E_{RBFN} and E_{PRO} represents the absolute error by radial basis function collocation method and present method respectively. Present method provides better results as compared to radial basis function collocation method.

For the problem (10.1.10), present and radial basis function collocation method takes 7 *seconds* and 9 *seconds* respectively. For this purpose, we use *Maple* 13, system with *Core Duo CPU* 2.00 GHz and RAM 2.50GB.

Example 2. Consider the first order system of delay differential equations

$$\begin{aligned} \tfrac{dy}{dx} &= y(x) - z(x) + y(\tfrac{x}{2}) - e^{\frac{x}{2}} + e^{-x} \quad , \quad 0 \leq x \leq 1 \\ \tfrac{dz}{dx} &= -y(x) - z(x) - z(\tfrac{x}{2}) + e^{\frac{-x}{2}} + e^{x} \quad , \\ y(x) &= e^x, \quad z(x) = e^{-x} \qquad\qquad , \ 0 \leq x, \end{aligned} \tag{10.1.11}$$

The exact solution is [104]

$$y(x) = e^x, \quad z(x) = e^{-x}. \tag{10.1.12}$$

			$M = 10$	
x	$E_{y_{RBFN}}$	$E_{y_{PRO}}$	$E_{z_{RBFN}}$	$E_{z_{PRO}}$
0.1	7.0409e-10	6.7479e-10	1.3130e-10	1.4285e-10
0.2	8.3987e-10	7.3608e-10	3.1837e-11	6.2746e-11
0.3	1.0038e-09	8.0754e-10	7.0113e-11	1.7884e-11
0.4	1.2073e-09	8.9950e-10	1.7321e-10	9.6736e-11
0.5	1.4572e-09	1.0152e-09	2.8226e-10	1.7684e-10
0.6	1.7335e-09	1.1309e-09	4.0698e-10	2.6622e-10
0.7	2.0876e-09	1.2945e-09	5.3670e-10	3.5221e-10
0.8	2.4927e-09	1.4730e-09	6.8998e-10	4.5102e-10
0.9	2.9569e-09	1.6682e-09	8.6674e-10	5.5985e-10
1.0	3.3129e-09	1.7036e-09	1.1344e-09	7.4364e-10

Table 10.2: Absolute errors by radial basis function networks $E_{y_{RBFN}}$, $E_{z_{RBFN}}$ and present method $E_{y_{PRO}}$, $E_{z_{PRO}}$ at $M = 10$.

The absolute error by the radial basis function collocation method and present method are given in Table 10.2. According to the results, proposed method is more accurate as compared to radial basis collocation method.

Present and radial basis function collocation method takes 85 *seconds* and 160 *seconds* respectively for solving system (10.1.11).

Example 3. Consider the delay differential equations with nonlinear delay function

$$\begin{array}{c} \frac{d^3y}{dx^3} = 2y^2(\frac{x}{2}) - 1 \quad , \ 0 \le x \le 1, \\ y(x) = \sin(x) \qquad , x \le 0, \end{array} \tag{10.1.13}$$

The exact solution is [105], $y(x) = \sin(x)$.

	$M=4$	$M=8$	$M=12$
x	E_{PRO}	E_{PRO}	E_{PRO}
0.1	4.83592e-08	4.81648e-12	8.87562e-19
0.2	1.75599e-06	2.32022e-11	7.60022e-19
0.3	1.75600e-05	6.06338e-12	7.35690e-18
0.4	7.95568e-05	8.69715e-12	4.81231e-20
0.5	2.49494e-04	2.09505e-10	1.97600e-17
0.6	6.27890e-04	1.35259e-10	1.32771e-17
0.7	1.36286e-03	6.19630e-10	2.59420e-18
0.8	2.65845e-03	4.02785e-09	8.29066e-17
0.9	4.78246e-03	4.63197e-08	6.46850e-16
1.0	8.07353e-03	2.28389e-07	6.32662e-14

Table 10.3: Absolute error by proposed method at different M.

Absolute error by present method at different values of M are shown in Table 10.3. According to the Table 10.3, we obtain more accurate results while increasing M.

Example 4. Consider the following nonlinear pantograph equation

$$\frac{d^2y}{dx^2} - \frac{8}{3}y'(\frac{x}{2})y(x) - 8x^2y(\frac{x}{2}) = \frac{-4}{3} - \frac{22}{3}x - 7x^2 - \frac{5}{3}x^3, \quad 0 \leq x \leq 1, \tag{10.1.14}$$

subject to the boundary conditions $y(0) = y(1) = 1$.

The exact solution is given by [1], $y(x) = 1 + x - x^3$.

	$M=12$	$M=15$	$M=20$	$M=25$
x	E_{PRO}	E_{PRO}	E_{PRO}	E_{PRO}
0.1	1.30716e-17	3.58196e-19	6.98392e-26	2.34956e-29
0.2	2.67614e-17	7.20286e-19	1.40681e-25	4.72857e-29
0.3	4.01346e-17	1.09121e-18	2.12345e-25	7.17179e-29
0.4	5.34373e-17	1.47850e-18	2.86677e-25	9.70581e-29
0.5	7.09090e-17	1.87855e-18	3.67347e-25	1.23424e-28
0.6	8.26400e-17	2.30394e-18	4.47129e-25	1.51001e-28
0.7	1.02193e-16	2.74542e-18	5.33450e-25	1.80139e-28
0.8	1.17716e-16	3.22784e-18	6.29137e-25	2.10847e-28
0.9	1.39402e-16	3.66054e-18	7.28024e-25	2.42230e-28

Table 10.4: Absolute error by present method at different M.

Table 10.4 shows that larger values of M gives more accurate results.

10.1.5 Conclusion

Linear and non linear delay differential equations can easily be handled by the method. It is shown that method provides better results as compared to the radial basis function collocation method and are in good agreement with exact solution, as shown in Table 10.1 and 10.2. We can get more accurate results while increasing M.

Present method is more efficient than the radial basis function collocation method, as given for Example 1 and 2. Efficiency of radial basis function collocation method further decreases in case of non linear delay differential equation.

10.2 Chebyshev Wavelet Method for Fractional Delay–Type Equations

Chebyshev polynomials method [120] is implemented for finding the numerical solution of the delay differential equations in which they utilize the shifted Chebyshev polynomials for solving the pantograph equations. Chebyshev wavelet method [133] are implemented for fractional nonlinear Fredholm integro-differential equations in which they used the second kind Chebyshev wavelet. In [127], Chebyshev wavelet method are used to solve the fractional differential equations.

In this section, we developed the shifted Chebyshev wavelets method for solving the linear and nonlinear fractional delay differential equations, fractional delay Volterra integro–differential equations and fractional system of delay differential equations. To the best of our knowledge, Chebyshev wavelets method have never been implemented for fractional delay equations. According to the development, we approximate the delay unknown functions by the Chebyshev wavelets series at delay time, which we call the delay Chebyshev wavelet series. We also proposed a technique by combining the method of steps and Chebyshev wavelets method for solving fractional delay differential equations. This technique converts the fractional delay differential equation on a given interval to an fractional differential equation without delay over that interval, by using the function defined on previous interval, and then apply the Chebyshev wavelet method on the obtained fractional non–delay differential equation to find the solution. Numerical examples are presented to demonstrate the benefits of computing with these approaches.

10.2.1 Chebyshev Wavelets

In the present work, we use the sifted Chebyshev polynomials on $[a, b]$, so the shifted Chebyshev nodes are

$$x_k = \frac{b-a}{2}\cos\Big(\frac{(2k+1)\pi}{2M}\Big) + \frac{a+b}{2},\ k = 0, 1, 2, ..., M-1,$$

where a and b are real numbers, $a < b$. The shifted Chebyshev polynomials $T_m(x)$, of order m are defined on the interval $[a, b]$ and given by the following recurrence formulae

$$T_0(x) = 1,\ \ T_1(x) = \frac{2x-(b+a)}{b-a},\ \ T_{m+1}(x) = 2\Big(\frac{2x-(b+a)}{b-a}\Big)T_m(x) - T_{m-1}(x),\ \ m = 1, 2, 3, \cdots.$$

The polynomials $T_m(x)$ are orthogonal with respect to the weight function $\frac{1}{\sqrt{1-\left(\frac{2x-(b+a)}{b-a}\right)^2}}$, that is

$$\int_a^b \frac{1}{\sqrt{1-\big(\frac{2x-(b+a)}{b-a}\big)^2}} T_m(x)T_n(x)dx = \begin{cases} 0, & m \neq n; \\ (\frac{b-a}{2})\pi, & m = n = 0; \\ (\frac{b-a}{4})\pi, & m = n \neq 0. \end{cases} \tag{10.2.1}$$

The discrete wavelets transform is defined as

$$\psi_{j,k}(x) = 2^{\frac{j}{2}}\psi(2^j x - k).$$

The set $\psi_{j,k}$ forms an orthogonal basis of $L_2(\mathbb{R})$. That is

$$\langle\ \psi_{j,k}(x), \psi_{l,m}(x)\rangle = \delta_{jl}\delta_{km}.$$

The Chebyshev wavelets are defined on interval $[a, b]$ by

$$\psi_{n,m}(x) = \begin{cases} 2^{\frac{k}{2}}\sqrt{\frac{4}{(b-a)\pi}}T_m(2^k x - \hat{n}), & a + (b-a)\frac{\hat{n}-1}{2^k} \leq x < a + (b-a)\frac{\hat{n}+1}{2^k}, \\ 0, & elsewhere, \end{cases}$$

where $k = 1, 2, 3, \cdots$, is the level of resolution, $n = 1, 2, 3, \cdots, 2^{k-1}$, $\hat{n} = 2n - 1$, is the translation parameter, $m = 1, 2, \cdots, M-1$ is the order of the Chebyshev polynomials, $M > 0$.

Function Approximations

We can expand any function $f(x) \in L^2[a, b)$ into truncated Chebyshev wavelet series as

$$f(x) \approx \sum_{n=1}^{2^{k-1}}\sum_{m=0}^{M-1} a_{nm}\psi_{n,m}(x) = \mathbf{a}^T\Psi(x), \tag{10.2.2}$$

where $\mathbf{a}$ and Ψ are $\hat{m} \times 1$ ($\hat{m} = 2^{k-1}M$) matrices, given by

$$\mathbf{a} = [a_{10}, a_{11}, \cdots, a_{1M-1}, a_{20}, a_{21}, \cdots, a_{2M-1}, \cdots, a_{2^{k-1}0}, a_{2^{k-1}1}, \cdots, a_{2^{k-1}M-1}]^T,$$
$$\mathbf{\Psi}(x) = [\psi_{1,0}(x), \psi_{1,1}(x), \cdots, \psi_{1M-1}(x), \psi_{2,0}(x), \psi_{2,1}(x), \cdots, \psi_{2,M-1}(x),$$
$$\cdots, \psi_{2^{k-1},0}(x), \psi_{2^{k-1},1}(x), \cdots, \psi_{2^{k-1},M-1}(x)]^T.$$

10.2.2 Convergence Analysis

Let $L^2([a,b])$ be a Hilbert space for which $\psi_{n,m}(x)$ form an orthonormal sequence in $L^2([a,b])$. Let $y(x) \in L^2([a,b])$, we have

$$y(x) \approx \sum_{n=1}^{2^{k-1}} \sum_{m=0}^{M-1} a_{nm}\psi_{n,m}(x), \tag{10.2.3}$$

where $a_{nm} = \langle y(x), \psi_{n,m}(x)\rangle$ is an inner product of $y(x)$ and $\psi_{n,m}(x)$. Equation (10.2.3) can be written as

$$y(x) \approx \sum_{n=1}^{2^{k-1}} \sum_{m=0}^{M-1} \langle y(x), \psi_{n,m}(x)\rangle \psi_{n,m}(x). \tag{10.2.4}$$

For simplicity, let $j = M(n-1)+m+1$, we can write (10.2.4) as

$$y(x) \approx \sum_{j=1}^{\hat{m}} \langle y(x), \psi_j(x)\rangle \psi_j(x) = \sum_{j=1}^{\hat{m}} a_j \psi_j(x) = \mathbf{a}^T \mathbf{\Psi}(x), \tag{10.2.5}$$

where $a_j = a_{mn},\ \psi_j(x) = \psi_{m,n}(x),\ \hat{m} = 2^{k-1}M$ and $\mathbf{a} = [a_1, a_2, ..., a_{\hat{m}}]^T$,
$\mathbf{\Psi}(x) = [\psi_1(x), \psi_2(x), ..., \psi_{\hat{m}}(x)]^T$. Convergence of Legendre wavelet method is analyzed in [122], where the authors have considered a particular case by choosing $k = 1$. Following the similar procedure, we get the convergence of the general orthogonal wavelet method for all level of resolution k.

Since $\hat{m} = 2^{k-1}M$ and method converges if $\hat{m} \to \infty$ i.e., when we use higher order Chebyshev polynomials $M-1$, or use large level of resolution k, or use both higher M and k, we get more accurate results.

10.2.3 Procedure for Implementation

Consider the following form of α^{th} order fractional nonlinear delay equation with both discrete and continuous delay

$$\begin{aligned} {}^cD^{\alpha}y(x) = h(x) + f\big(y(x), y'(x), y(px-\tau), y'(px-\tau), \int_{px-\tau}^{x} h(x,s,y(s))ds\big), \\ a \le x \le b,\ 1 < \alpha \le 2, \end{aligned} \tag{10.2.6}$$

subject to the initial conditions $y(a) = y_0,\ y'(a) = y_0'$, where $h(x)$ is a source function and f is a continuous linear or nonlinear function. Also $y_0,\ y_0', p$, are constants, $\tau(x, y(x))$ is delay, $px - \tau(x, y(x))$ is called delay argument and $y(px - \tau(x, y(x)))$ is the solution of the delay term. The delay $\tau(x, y(x))$ is called constant delay, time dependent delay and state dependent delay if the delay $\tau(x, y(x))$ is constant, function of time x, and function of time x and $y(x)$ respectively.

We can approximate the solution of equation (10.2.6) by the Chebyshev wavelet method as

$$y(x) \approx \sum_{n=1}^{2^{k-1}} \sum_{m=0}^{M-1} a_{nm}\psi_{n,m}(x). \tag{10.2.7}$$

In the delay equations, we also have to approximate $y(px-\tau)$ in terms of the Chebyshev wavelet series at delay time as

$$y(px-\tau) \approx \sum_{n=1}^{2^{k-1}} \sum_{m=0}^{M-1} a_{nm}\psi_{n,m}(px-\tau). \tag{10.2.8}$$

We call this series as the delay Chebyshev wavelet series. Substituting equation (10.2.7), (10.2.8) in equation (10.2.6), we get the residual as

$$\begin{aligned}&\sum_{n=1}^{2^{k-1}} \sum_{m=0}^{M-1} a_{nm}\ {}^{c}D^{\alpha}\psi_{n,m}(x) - h(x) - f\Big(\sum_{n=1}^{2^{k-1}} \sum_{m=0}^{M-1} a_{nm}\psi_{n,m}(x), \sum_{n=1}^{2^{k-1}} \sum_{m=0}^{M-1} a_{nm}\psi'_{n,m}(x),\\ &\sum_{n=1}^{2^{k-1}} \sum_{m=0}^{M-1} a_{nm}\psi_{n,m}(px-\tau), \sum_{n=1}^{2^{k-1}} \sum_{m=0}^{M-1} a_{nm}\psi'_{n,m}(px-\tau),\\ &\int_{px-\tau}^{x} h(x,s, \sum_{n=1}^{2^{k-1}} \sum_{m=0}^{M-1} a_{nm}\psi_{n,m}(s))ds\Big).\end{aligned} \tag{10.2.9}$$

Set the residual (10.2.9) equal to zero at the set of Chebyshev nodes, x_i,

$$\begin{aligned}&\sum_{n=1}^{2^{k-1}} \sum_{m=0}^{M-1} a_{nm}\ {}^{c}D^{\alpha}\psi_{n,m}(x_i) - h(x_i) - f\Big(\sum_{n=1}^{2^{k-1}} \sum_{m=0}^{M-1} a_{nm}\psi_{n,m}(x_i), \sum_{n=1}^{2^{k-1}} \sum_{m=0}^{M-1} a_{nm}\psi'_{n,m}(x_i),\\ &\sum_{n=1}^{2^{k-1}} \sum_{m=0}^{M-1} a_{nm}\psi_{n,m}(px_i-\tau), \sum_{n=1}^{2^{k-1}} \sum_{m=0}^{M-1} a_{nm}\psi'_{n,m}(px_i-\tau),\\ &\int_{px_i-\tau}^{x_i} h(x,s, \sum_{n=1}^{2^{k-1}} \sum_{m=0}^{M-1} a_{nm}\psi_{n,m}(s))ds\Big) = 0.\end{aligned} \tag{10.2.10}$$

We obtain $2^{k-1}M-d$ equations, where d is the number of conditions of the delay equation. According to equation (10.2.6), two conditions are given ($d=2$) so we get $2^{k-1}M-2$ equations from equation (10.2.10) by using chebyshev nodes x_i. Two more equations obtain from the conditions of equation (10.2.6), that is

$$\begin{aligned} y(a) = y_0 \quad &\Rightarrow \sum_{n=1}^{2^{k-1}} \sum_{m=0}^{M-1} a_{nm}\psi_{n,m}(0) = y_0,\\ y'(a) = y'_0 \quad &\Rightarrow \sum_{n=1}^{2^{k-1}} \sum_{m=0}^{M-1} a_{nm}\psi'_{n,m}(0) = y'_0.\end{aligned}$$

We obtained $2^{k-1}M$ equations either linear or nonlinear along with $2^{k-1}M$ unknown coefficients a_{nm}, which is solved by Newton iterative method to get $a_{nm}{}'s$ and use it in (10.2.7) to get the approximate solution.

10.2.4 Numerical Solutions

In this section, we solve linear and nonlinear delay differential and Volterra integro-differential equations of fractional order by the Chebyshev wavelet method, for $k=1$ and at different M, and compare the results with exact solution. Through this work we use Caputo derivatives.

The term y_{CWM} represent the solution by Chebyshev wavelets method, y_{exact} represent the exact solution and E_{CWM} represents their absolute error.

Nonlinear Delayed Fractional Differential Equations

Example 1. Consider the following nonlinear fractional pantograph equation

$$^{c}D^{\alpha}y(x) - \tfrac{8}{3}y'(\tfrac{x}{2})y(x) - 8x^2y(\tfrac{x}{2}) = \tfrac{-4}{3} - \tfrac{22}{3}x - 7x^2 - \tfrac{5}{3}x^3, \quad 0 \leq x \leq 1, \ 1 < \alpha \leq 2, \qquad (10.2.11)$$

subject to the boundary conditions $y(0) = y(1) = 1$. The exact solution, when $\alpha = 2$, is given by [1], $y(x) = 1 + x - x^3$.

The results obtained by the Chebyshev wavelets method by taking $k = 1$, $M = 5$, is shown in Figure 10.1 and Table 10.5. Figure 10.1 shows that solution by the Chebyshev wavelet method approaches to exact solution, when α approaches to 2. Table 10.5 indicates that results obtained from the Chebyshev wavelets method are more close to exact solution.

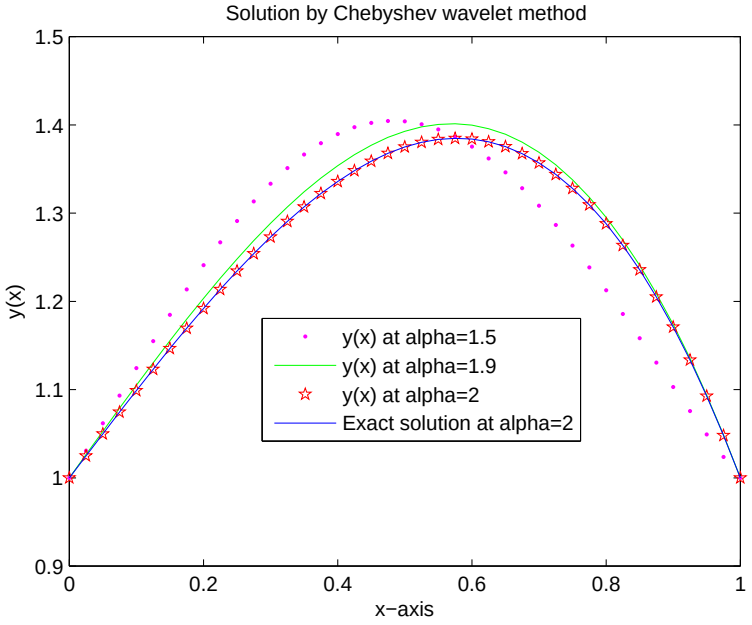

Figure 10.1: Solutions by the Chebyshev wavelet method at different α, $M = 5$ and exact solutions at $\alpha = 2$.

$\alpha = 2$		$M = 5$	
x	y_{CWM}	y_{exact}	E_{CWM}
0.0	1.000	1.000	3.0e-100
0.1	1.099	1.099	0.0e+00
0.2	1.192	1.192	0.0e+00
0.3	1.273	1.273	0.0e+00
0.4	1.336	1.336	0.0e+00
0.5	1.375	1.375	0.0e+00
0.6	1.384	1.384	0.0e+00
0.7	1.357	1.357	0.0e+00
0.8	1.288	1.288	0.0e+00
0.9	1.171	1.171	1.0e-99
1.0	1.000	1.000	9.0e-100

Table 10.5: Comparison of the solution by Chebyshev wavelets method at $M = 5$, with Exact solution at $\alpha = 2$.

Fractional Volterra Delay Integro-Differential Equations

Example 2. Consider the fractional Volterra delay integro-differential equations for which only a continuously distributed delay is presented

$$\begin{aligned} {}^{c}D^{\alpha}y(x) &= e^{-2}y(x) + 2\int_{x-1}^{x} e^{s-x}y(s)ds \quad , \quad x \geq 0,\ 0 < \alpha \leq 1, \\ y(x) &= e^{x} \qquad\qquad\qquad\qquad\qquad , x \leq 0, \end{aligned} \tag{10.2.12}$$

The exact solution, when $\alpha = 1$, is given by [106], $y(x) = e^{x}$.

Figure 10.2 shows that approximate solution at different α converge to the exact solution at $\alpha = 1$, when α approaches to 1. According to the Table 10.6, we take $k = 1$ and absolute error goes down while increasing M.

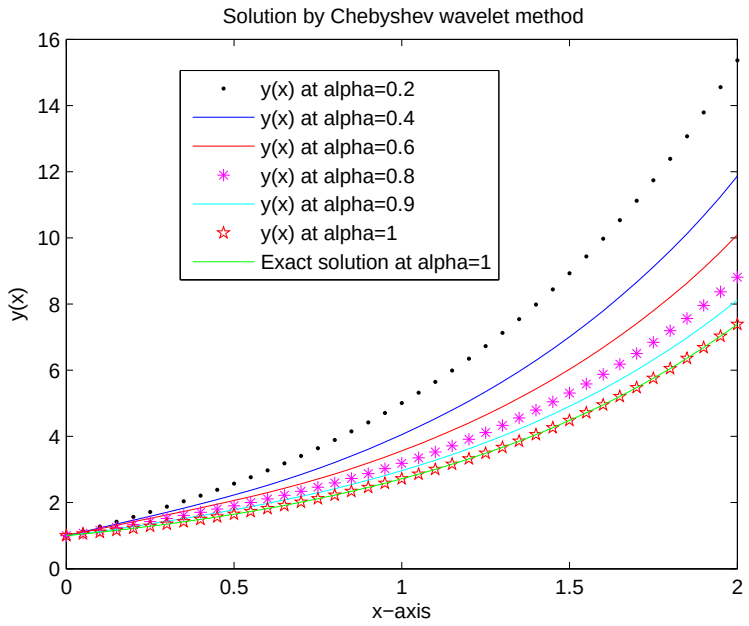

Figure 10.2: Solution by the Chebyshev wavelet method at different α, $M = 10$ and exact solution at $\alpha = 1$.

$\alpha = 1$	$M = 10$	$M = 20$	$M = 30$	$M = 40$	$M = 50$
x	E_{CWM}	E_{CWM}	E_{CWM}	E_{CWM}	E_{CWM}
0.0	0.00000e+00	0.00000e+00	0.00000e+00	0.00000e+00	0.00000e+00
0.2	3.53755e-07	1.92910e-15	1.47443e-25	9.33233e-32	1.20200e-39
0.4	4.82617e-07	3.88233e-15	1.00623e-23	6.58330e-32	1.37272e-39
0.6	5.41694e-07	5.06443e-15	1.71088e-23	3.89809e-32	1.38842e-39
0.8	6.31832e-07	6.02721e-15	2.10738e-23	3.80014e-32	1.58040e-39
1.0	7.64294e-07	7.22217e-15	2.48458e-23	5.03183e-32	1.93476e-39
1.2	9.35777e-07	8.78809e-15	2.98929e-23	6.52316e-32	2.38860e-39
1.4	1.15049e-06	1.07466e-14	3.64803e-23	8.06468e-32	2.92845e-39
1.6	1.40205e-06	1.31386e-14	4.46346e-23	9.81924e-32	3.57680e-39
1.8	1.71333e-06	1.60509e-14	5.45593e-23	1.19590e-31	4.36647e-39
2.0	2.04433e-06	1.96036e-14	6.66430e-23	1.45971e-31	5.33218e-39

Table 10.6: Absolute error at different M.

Example 3. Consider the fractional Volterra delay integro-differential equations with both discretely and continuously distributed delays

$$
\begin{aligned}
{}^{c}D^{\alpha}y(x) &= y(x-1) + \int_{x-1}^{x} y(s)ds \quad , \quad x \geq 0,\ 0 < \alpha \leq 1, \\
y(x) &= e^{x} \qquad\qquad\qquad\qquad , x \leq 0,
\end{aligned}
\tag{10.2.13}
$$

The exact solution, when $\alpha = 1$, is [106], $y(x) = e^{x}$.

Solution obtained by Chebyshev wavelets method at different values of α is shown in Figure 10.3, along with exact solution at $\alpha = 1$. We also compared the approximate solution with exact solution at $\alpha = 1$, by using the absolute error as shown in Table 10.7.

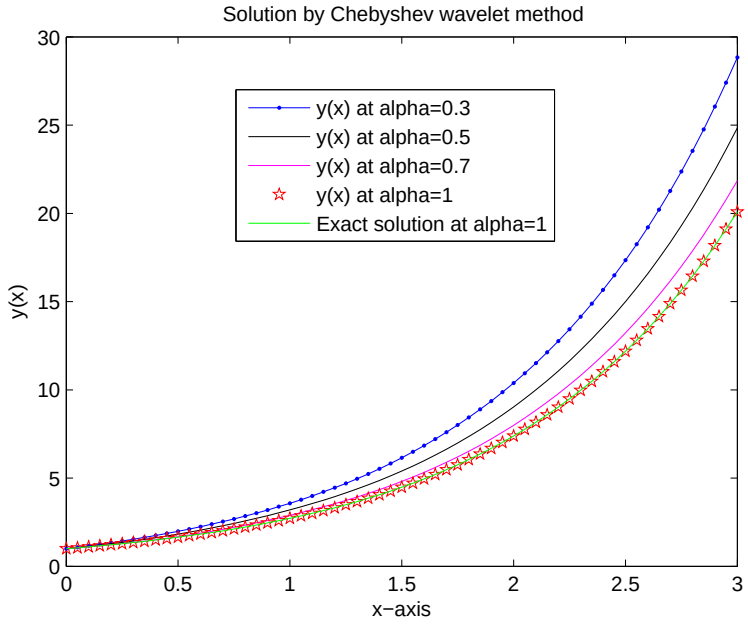

Figure 10.3: Solution by the Chebyshev wavelet method at different α, $M = 12$ and exact solution at $\alpha = 1$ is also shown.

$\alpha = 1$	$M = 10$	$M = 20$	$M = 30$	$M = 40$	$M = 50$
x	E_{CWM}	E_{CWM}	E_{CWM}	E_{CWM}	E_{CWM}
0.0	0.00000e+00	0.00000e+00	0.00000e+00	0.00000e+00	0.00000e+00
0.3	5.81674e-06	5.65937e-13	1.08285e-19	1.64100e-26	2.36835e-33
0.6	1.46019e-05	2.12560e-13	1.02644e-19	1.86827e-26	2.96658e-33
0.9	1.90008e-05	7.14313e-14	8.48984e-20	1.78400e-26	3.00450e-33
1.2	2.25328e-05	3.72624e-14	1.19050e-19	2.36895e-26	3.90696e-33
1.5	3.02529e-05	2.25379e-13	1.83171e-19	3.48261e-26	5.63686e-33
1.8	4.20864e-05	2.93035e-13	2.50886e-19	4.78519e-26	7.75561e-33
2.1	5.66581e-05	3.23038e-13	3.30574e-19	6.36598e-26	1.03595e-32
2.4	7.65962e-05	4.23074e-13	4.42834e-19	8.53715e-26	1.38990e-32
2.7	1.03032e-04	5.96889e-13	6.00172e-19	1.15477e-25	1.87850e-32
3.0	1.44809e-04	8.17098e-13	8.12080e-19	1.56158e-25	2.53965e-32

Table 10.7: Absolute error at different M.

Example 4. Consider the following fractional nonlinear integro–differential equation with proportional delay in kernel

$$\begin{aligned} {}^cD^{\alpha}y(x) + (\tfrac{x}{2} - 2)y(x) - 2\int_0^x y(\tfrac{s}{2})^2 ds = 1 \quad &, \ x \geq 0, \ 0 < \alpha \leq 1, \\ y(x) = xe^x \quad &, \ x \leq 0. \end{aligned} \tag{10.2.14}$$

Considering $\alpha = 1$ and substituting $x = 0$ in equation (10.2.14), we get $y'(0) = 1$. By taking derivative of (10.2.14), we obtain the pantograph equation

$$\begin{aligned} {}^cD^{\alpha+1}y(x) + (\tfrac{x}{2} - 2)y'(x) + \tfrac{1}{2}y(x) - 2y(\tfrac{x}{2})^2 = 0 \quad &, \ x \geq 0, \\ y(x) = xe^x \quad &, \ x \leq 0, \end{aligned} \tag{10.2.15}$$

with the initial conditions $y(0) = 0, \ y'(0) = 1$. The exact solution, when $\alpha = 1$, is given in [1], $y(x) = xe^x$.

Solution by the Chebyshev wavelet method at different α, $M = 6$ and exact solution at $\alpha = 1$ is shown in Figure 10.4. Table 10.8 compares the exact solution and solution by Chebyshev wavelet method at $\alpha = 1$ and $M = 7$.

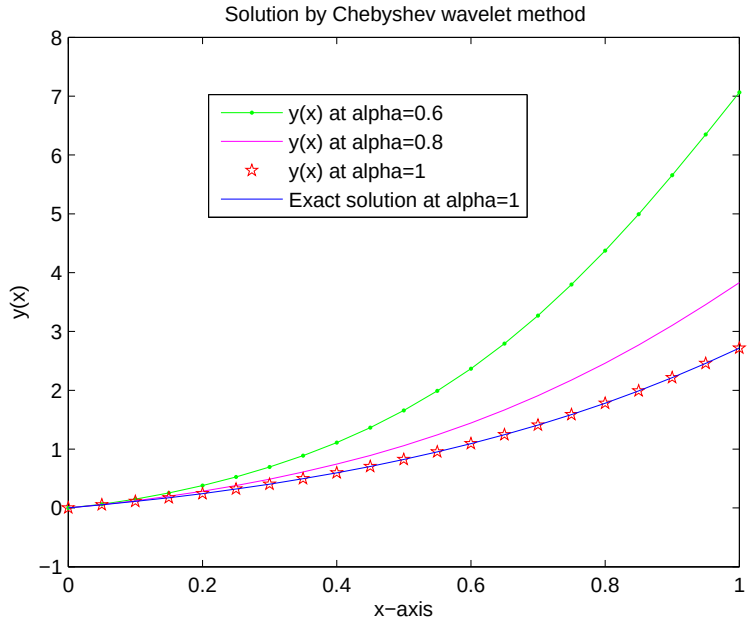

Figure 10.4: Solution by the Chebyshev wavelet method at different α, $M = 6$ and exact solution at $\alpha = 1$.

$\alpha = 1$		$M = 7$	
x	y_{exact}	y_{CWM}	E_{CWM}
0.0	0.000000000000000	0.000000000000000	5.47880e-32
0.1	0.110517091807565	0.110517060483851	3.13237e-08
0.2	0.244280551632034	0.244280466993502	8.46385e-08
0.3	0.404957642272801	0.404957652876706	1.06039e-08
0.4	0.596729879056508	0.596729933166477	5.41100e-08
0.5	0.824360635350064	0.824360416827363	2.18523e-07
0.6	1.093271280234305	1.093270782690551	4.97544e-07
0.7	1.409626895229334	1.409626919077817	2.38485e-08
0.8	1.780432742793974	1.780433427114300	6.84320e-07
0.9	2.213642800041255	2.213636987730133	5.81231e-06
1.0	2.718281828459045	2.718238592350892	4.32361e-05

Table 10.8: Comparison of exact solution and solution by Chebyshev wavelet method at $\alpha = 1$ and $M = 7$.

System of Fractional Order Delay Differential Equations

Example 5. Consider the fractional order system of delay differential equations

$$\begin{aligned} {}^cD^{\alpha}y(x) &= y(x) - z(x) + y(\tfrac{x}{2}) - e^{\frac{x}{2}} + e^{-x} \quad , \ 0 < \alpha \leq 1, \ \ 0 \leq x \leq 1, \\ {}^cD^{\alpha}z(x) &= -y(x) - z(x) - z(\tfrac{x}{2}) + e^{\frac{-x}{2}} + e^{x} \quad , \\ y(x) &= e^{x}, \quad z(x) = e^{-x}, \qquad\qquad 0 \leq x, \end{aligned} \tag{10.2.16}$$

The exact solution, when $\alpha = 1$, is [104]

$$y(x) = e^{x}, \quad z(x) = e^{-x}. \tag{10.2.17}$$

Figure 10.5 shows the solutions by Chebyshev wavelets method at different α. The approximate solutions approaches to exact solution, when α approaches 1. Exact solutions and solutions by Chebyshev wavelet method at $\alpha = 1$ and $M = 15$ is shown in Table 10.9, along with the absolute errors, $E_{y_{CWM}}$ and $E_{z_{CWM}}$.

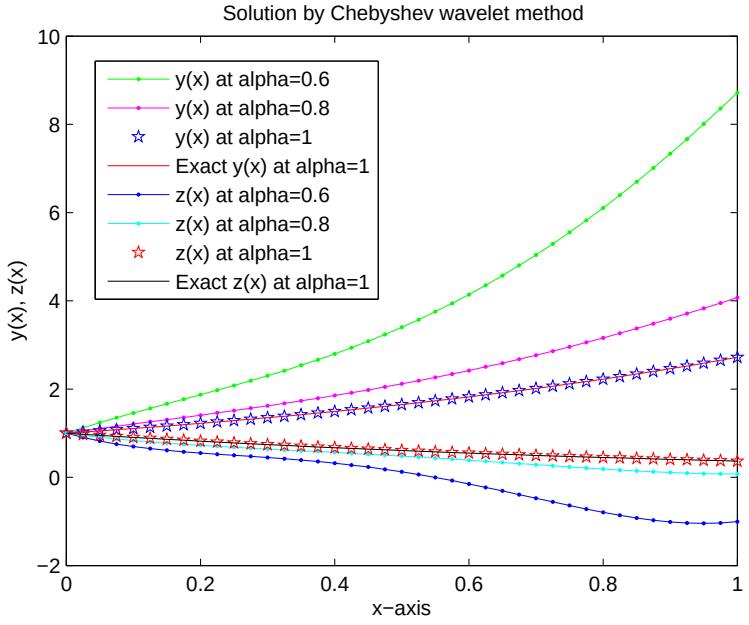

Figure 10.5: Solutions by the Chebyshev wavelet method at different α, $M = 5$ and exact solutions at $\alpha = 1$.

$\alpha = 1$				$M = 15$		
x	y_{CWM}	y_{exact}	$E_{y_{CWM}}$	z_{CWM}	z_{exact}	$E_{z_{CWM}}$
0.0	1.0000	1.0000	0.0000e+00	1.0000	1.0000	1.0000e-99
0.1	1.1052	1.1052	3.4579e-22	0.9048	0.9048	1.2852e-22
0.2	1.2214	1.2214	1.0407e-21	0.8187	0.8187	4.1707e-22
0.3	1.3499	1.3499	1.6882e-21	0.7408	0.7408	6.3206e-22
0.4	1.4918	1.4918	1.6656e-21	0.6703	0.6703	6.8670e-22
0.5	1.6487	1.6487	2.4307e-21	0.6065	0.6065	9.9268e-22
0.6	1.8221	1.8221	2.4914e-21	0.5488	0.5488	1.0176e-21
0.7	2.0138	2.0138	3.8977e-21	0.4966	0.4966	1.3803e-21
0.8	2.2255	2.2255	4.0018e-21	0.4493	0.4493	1.5151e-21
0.9	2.4596	2.4596	1.3108e-21	0.4066	0.4066	5.7753e-22
1.0	2.7183	2.7183	9.2257e-20	0.3679	0.3679	3.3664e-20

Table 10.9: Comparison of Exact solution and solution by Chebyshev wavelet method at $\alpha = 1$ and $M = 15$.

10.2.5 Procedure for Implementation of Proposed Method

The method of steps [118] is the simplest method for converting delay differential equations to ordinary differential equations on a given intervals. Consider the following fractional nonlinear delay differential equation with discrete delay

$$\begin{aligned} {}^cD^{\alpha}y(x) = h(x) + f(y(x), y'(x), y(px-\tau), y'(px-\tau)), \quad & a \le x \le b,\ 1 < \alpha \le 2, \\ y(x) = \phi(x), \quad & -b \le x \le a. \end{aligned} \tag{10.2.18}$$

Method consists of two steps, in first step we convert the fractional delay differential equation to fractional non–delay differential equation by method of steps and in second step, we apply the Chebyshev wavelet method on resulting fractional non–delay differential equation by using the procedure which is described in section 10.2.3.

Step I: In the fractional delay differential equation the solution $y(x)$ is known on $[-b, a]$, say $\phi(x)$, and call this solution $y_0(x)$, that is $y_0(px-\tau) = \phi(px-\tau)$, which is known.

Now the fractional delay differential equation on $[a, b]$ takes the form

$${}^cD^{\alpha}y(x) = h(x) + f(y(x), y'(x), y_0(px-\tau), y_0'(px-\tau)),\ a \le x \le b,\ 1 < \alpha \le 2, \tag{10.2.19}$$

subject to the initial conditions $y(a) = \phi(a)$, $y'(a) = \phi'(a)$.

It is an fractional non–delay differential equation because $y_0(px-\tau)$ and $y_0'(px-\tau)$ are known.

Step II: We solve this fractional non–delay differential equation on $[a, b]$ by using the Chebyshev wavelet method and denote this solution as $y_1(x)$, which is defined on $[a, b]$.

Delay differential equation on $[b, 2b]$ becomes

$$ {}^{c}D^{\alpha}y(x) = h(x) + f(y(x), y'(x), y_1(px-\tau), y_1'(px-\tau)),\ b \le x \le 2b,\ 1 < \alpha \le 2, \tag{10.2.20} $$

subject to the initial conditions $y(b) = \phi(b)$, $y'(b) = \phi'(b)$.
which is again an fractional non–delay differential equation and solve it by the Chebyshev wavelet method to get $y_2(x)$ on $[b, 2b]$. This procedure may be continued for subsequent intervals.

10.2.6 Numerical Solutions

In this section, we solve fractional nonlinear delay differential equations with discrete delays by the present method and compare the results with exact solution, solution by Legendre wavelet methods and Chebyshev wavelet method.

Example 6. Consider the following fractional nonlinear delay differential equations

$$ \begin{aligned} {}^{c}D^{\alpha}y(x) &= 1 - 2y^2(\tfrac{x}{2}) \quad ,\ 0 < \alpha \le 1,\ \ 0 < x \le 1 \\ y(x) &= \sin(x), \qquad\qquad 0 \le x, \end{aligned} \tag{10.2.21} $$

The exact solution, when $\alpha = 1$, is [56], $y(x) = \sin(x)$.

Figure 10.6 shows that present solution converges to the exact solution when α approaches to 1. According to the Table 10.10, present method y_{pro} provides better results as compared to Legendre wavelet method y_{LWM}. In present method, we use low resolution level, $k = 1$, but still we get more accurate results as compared to Legendre wavelet method for $k = 2$.

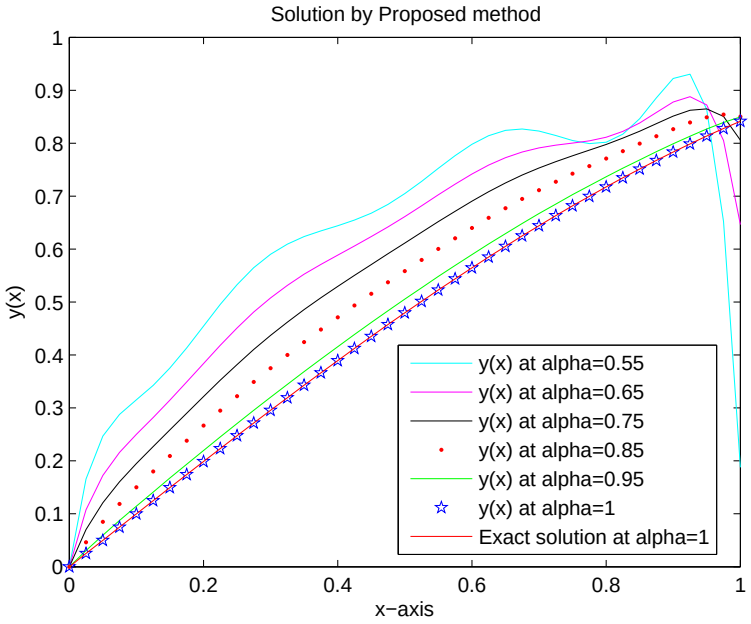

Figure 10.6: Solutions by the present method at different α, $M = 9,\ k = 1$ and exact solutions at $\alpha = 1$.

$\alpha = 1$				
x	y_{LWM}	y_{pro}	y_{exact}	E_{abs}
0.000	0.000000000	0.000000000	0.000000000	1.23452e-22
0.125	0.124674731	0.124674733	0.124674733	1.70708e-12
0.250	0.247403957	0.247403959	0.247403959	2.47323e-12
0.375	0.366272527	0.366272529	0.366272529	9.36426e-12
0.500	0.479425537	0.479425539	0.479425538	1.78774e-11
0.625	0.585097271	0.585097273	0.585097272	1.88843e-11
0.750	0.681638759	0.681638760	0.681638760	3.04277e-12
0.875	0.767543501	0.767543502	0.767543502	1.64433e-12
1.000	0.841470984	0.841470984	0.841470984	4.51086e-10

Table 10.10: Comparison between exact solution, Legendre wavelet method [56] for $M = 9,\ k = 2$, and present method for $M = 9,\ k = 1$.

Example 7. Consider the fractional delay differential equations with nonlinear delay function,

$$
\begin{aligned}
{}^{c}D^{\alpha}y(x) &= 2y^2(\tfrac{x}{2}) - 1 \quad , \ 2 < \alpha \leq 3, \quad 0 \leq x \leq 1, \\
y(x) &= \sin(x) \qquad\quad , x \leq 0,
\end{aligned}
\tag{10.2.22}
$$

The exact solution, when $\alpha = 3$, is [105], $y(x) = \sin(x)$.

By fixing $k = 1$ and $M = 20$, we plot the solutions by method at different values of α and exact solution at $\alpha = 3$ on large interval, as shown in Figure 10.7. Comparison of exact solution y_{exact} and approximate solution y_{pro} at $\alpha = 3$, $M = 50$ and $k = 1$, is shown in Table 10.11.

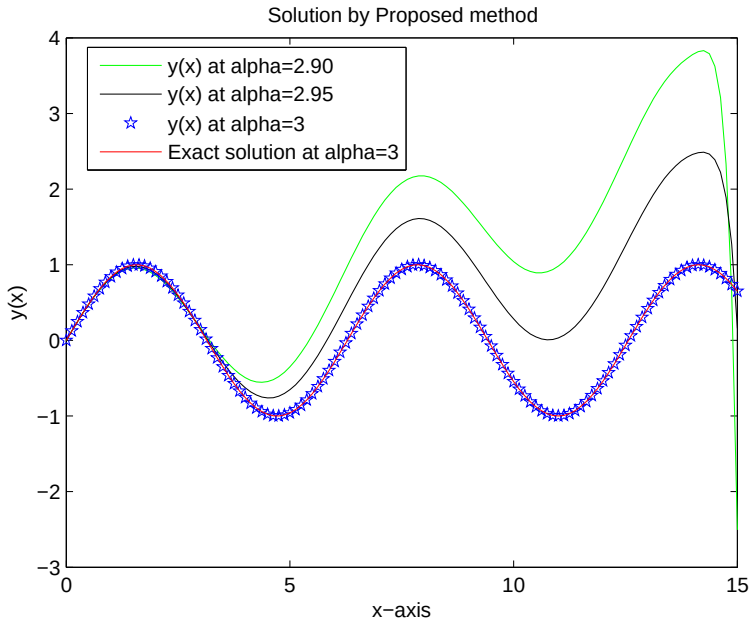

Figure 10.7: Solutions by the present method at different α, $M = 20$, $k = 1$ and exact solutions at $\alpha = 3$.

$\alpha = 3$			
x	y_{pro}	y_{exact}	E_{abs}
0.000	0.0000000	0.0000000	1.25843e-214
0.125	0.1246747	0.1246747	3.13235e-96
0.250	0.2474040	0.2474040	2.02963e-95
0.375	0.3662725	0.3662725	3.72562e-95
0.500	0.4794255	0.4794255	6.40642e-95
0.625	0.5850973	0.5850973	9.34377e-95
0.750	0.6816388	0.6816388	4.01299e-95
0.875	0.7675435	0.7675435	6.11317e-94
1.000	0.8414710	0.8414710	1.00063e-89

Table 10.11: Solution by present method for $M = 50,\ k = 1$.

Comparison of Chebyshev Wavelet Method and Present Method

In this example, we compare the Chebyshev wavelet method and proposed method.

Example 8. Consider the fractional nonlinear pantograph equation

$$ {}^{c}D^{\alpha}y(x) + (y'(\tfrac{x}{2}))^2 - \tfrac{1}{4}y(\tfrac{x}{2}) - \tfrac{1}{4}y(x) = 0, \quad 0 \leq x \leq 1,\ 1 < \alpha \leq 2, \tag{10.2.23} $$

subject to the initial conditions $y(0) = y'(0) = 1$. The exact solution, when $\alpha = 2$, is [1], $y(x) = e^x$.

For $\alpha = 2$, $k = 1$ and $M = 7$, Table 10.12 contains the exact solution y_{exact}, solution obtained by the Chebyshev wavelet method y_{CWM} and present method y_{pro}. E_{CWM} and E_{pro} represents absolute error by Chebyshev wavelet method and present method respectively. It indicates that the present method provides significantly accurate results as compared to Chebyshev wavelet method. Also present method take less computational time as compared to the Chebyshev wavelet method. For the problem (10.2.23), present and Chebyshev wavelet method takes 1.44 *seconds* and 8.09 *seconds* respectively.

For this purpose, we use $Maple$ 13 in system with $Core\ Duo\ CPU$ 2.00 GHz and RAM 2.50GB.

$\alpha = 2$		$M = 7$			
x	y_{pro}	y_{CWM}	y_{exact}	E_{CWM}	E_{pro}
0.0	1.000000000000000	1.000000000000000	1.000000000000000	0.00000e+00	0.00000e+00
0.1	1.105170917987022	1.105170918075648	1.105170918046593	2.90544e-11	8.86261e-11
0.2	1.221402760355470	1.221402758160170	1.221402758178371	1.82008e-11	2.19530e-09
0.3	1.349858805809554	1.349858807576003	1.349858806748101	8.27902e-10	1.76645e-09
0.4	1.491824680504743	1.491824697641270	1.491824678359615	1.92817e-08	1.71365e-08
0.5	1.648721270700128	1.648721270700128	1.648721078676698	1.92023e-07	2.09532e-192
0.6	1.822118901602975	1.822118800390509	1.822117704955597	1.09543e-06	1.01212e-07
0.7	2.013752782405488	2.013752707470477	2.013748284301158	4.42317e-06	7.49350e-08
0.8	2.225539717513771	2.225540928492468	2.225526749646569	1.41788e-05	1.21098e-06
0.9	2.459596083968986	2.459603111156950	2.459564553456737	3.85577e-05	7.02719e-06
1.0	2.718257075060718	2.718281828459045	2.718189119155270	9.27093e-05	2.47534e-05

Table 10.12: Comparison of the Chebyshev wavelets method and present method, by fixing $M = 7$, $k = 1$, and $\alpha = 2$.

10.2.7 Conclusion

It is shown that the Chebyshev wavelet method gives good results when applied to different linear and nonlinear fractional delay differential equation, fractional delay Volterra integro–differential equations and fractional system of delay differential equation and are in good agreement with exact solutions. According to the convergence analysis, error by the Chebyshev wavelet method reduces while increasing M, as shown in Tables 10.6 and 10.7. Tables 10.5 - 10.9 shows the comparison of exact solution and solution by the Chebyshev wavelets method. According to the comparison, we conclude that Chebyshev wavelets method is a suitable technique for solving fractional delay–type equations.

The solution of the fractional order delay equation converge to the solution of integer order delay equation as shown in Figures.

Proposed technique gives more accurate results as compared to the Legendre wavelet method and are in good agreement with exact solution, as shown in Table 10.10. Solution by present technique converges to the exact solution at higher M as in Table 10.11. According to the Table 10.12, Chebyshev wavelet method gives more accurate results at $x = 0$ to $x = 0.3$ and less accurate results at $x = 0.4$ to $x = 1.0$ as compared to the present method.

Present method is more efficient than the Chebyshev wavelet method. It is a more powerful technique for solving fractional delay differential equation as compared to the Chebyshev wavelet method.

10.3 Hermite Wavelet Method for Fractional Delay Differential Equations

Hermite wavelet method [2] is implemented for finding the numerical solution of the boundary value problems and compare the obtained solutions with exact solution. In [121], authors utilized the physicists Hermite wavelet method for solving linear singular differential equations. According to our information, Hermite wavelet method has not been implemented for delay differential equations.

In this section, we combine method of steps with Hermite wavelet method for solving the fractional delay differential equations. We also implement the Hermite wavelet method for solving fractional delay differential equation, as describe in *Example* 6, which were not implemented before. Shifted Chebyshev nodes are used as the collocation points. Several numerical examples are solved to show the applicability of the proposed method (Hermite step method). Comparison of solutions by these two methods, proposed method and Hermite wavelet method, with each other and with exact solution are also presented.

10.3.1 Hermite Wavelets

The Hermite polynomials $H_m(x)$, of order m are defined on the interval $[-\infty, \infty]$ and given by the following recurrence formulae,

$$H_0(x) = 1, \quad H_1(x) = 2x, \quad H_{m+1}(x) = 2xH_m(x) - 2mH_{m-1}(x), \quad m = 1, 2, 3, \cdots .$$

The polynomials $H_m(x)$ are orthogonal with respect to the weight function e^{-x^2}, that is

$$\int_{-\infty}^{\infty} e^{-x^2} H_m(x) H_n(x) dx = \begin{cases} 0, & m \neq n; \\ n! 2^n \sqrt{\pi}, & m = n. \end{cases} \tag{10.3.1}$$

The Hermite wavelets are defined on interval $[0, 1)$ by

$$\psi_{n,m}(x) = \begin{cases} 2^{\frac{k}{2}} \sqrt{\frac{1}{n! 2^n \sqrt{\pi}}} H_m(2^k x - \hat{n}), & \frac{\hat{n}-1}{2^k} \leq x < \frac{\hat{n}+1}{2^k}, \\ 0, & elsewhere, \end{cases}$$

where $k = 1, 2, 3, \cdots$, is the level of resolution, $n = 1, 2, 3, \cdots, 2^{k-1}$, $\hat{n} = 2n - 1$, is the translation parameter, $m = 1, 2, \cdots, M - 1$ is the order of the Hermite polynomials, $M > 0$.

10.3.2 Convergence Analysis

Function approximations and convergence analysis of Hermite wavelet method are same as for Chebyshev wavelet method and are given in subsection 10.2.1 and 10.2.2 respectively.

10.3.3 Procedure for Implementation of Hermite Step Method

The method of steps [118] is used to convert the discrete delay differential equations to non-delay differential equations on a given intervals. Consider the following fractional delay differential equation with discrete delay

$$\begin{aligned} {}^cD^{\alpha}y(x) = g(x) + f(y(x), y'(x), y(qx-\tau), y'(qx-\tau)) \quad &, \ a \le x \le b, \ 1 < \alpha \le 2, \\ y(x) = \phi(x), \qquad\qquad\qquad\qquad\qquad\qquad &-b \le x \le a. \end{aligned} \tag{10.3.2}$$

where $g(x)$ is a source function and f is a continuous linear or nonlinear function. Also q is constant, τ is delay and $qx-\tau$ is called delay argument. The delay $\tau(x, y(x))$ is called constant delay, time dependent delay and state dependent delay if the delay $\tau(x, y(x))$ is constant, function of time x, and function of time x and $y(x)$ respectively.

Hermite step method consists of two methods, method of steps and Hermite wavelet method. We first implement the method of steps to the fractional delay differential equation (10.3.2) and get the fractional non–delay differential equation by utilizing initial function, $\phi(x)$, and then we utilize the Hermite wavelet method for solving the obtained fractional non–delay differential equation.

Method of Steps: In the fractional delay differential equation the solution $y(x)$ is known on $[-b, a]$, say $\phi(x)$, and call this solution $y_0(x)$, that is $y_0(qx-\tau) = \phi(qx-\tau)$, which is known. Now the fractional delay differential equation on $[a, b]$ takes the form

$${}^cD^{\alpha}y(x) = g(x) + f(y(x), y'(x), y_0(qx-\tau), y_0'(qx-\tau)), \ a \le x \le b, \ 1 < \alpha \le 2, \tag{10.3.3}$$

subject to the initial conditions $y(a) = \phi(a)$, $y'(a) = \phi'(a)$.

It is an fractional non–delay differential equation because $y_0(qx-\tau)$ and $y_0'(qx-\tau)$ are known.

Hermite Wavelet Method for Fractional Non Delay Differential Equation: We solve the obtained fractional non–delay differential equation (10.3.3) on $[a, b]$ by using the Hermite wavelet method. The procedure for implementation of Hermite wavelet method for fractional differential equation is as follows:

Step 1: Approximate the unknown function $y(x)$ of equation (10.3.3) by the Hermite wavelet method as

$$y(x) \simeq \sum_{n=1}^{2^{k-1}} \sum_{m=0}^{M-1} a_{nm}\psi_{n,m}(x). \tag{10.3.4}$$

Step 2: Substituting equation (10.3.4) in equation (10.3.3) to get the residual

$$\begin{aligned} \sum_{n=1}^{2^{k-1}} \sum_{m=0}^{M-1} a_{nm}^c D^{\alpha}\psi_{n,m}(x) = g(x) + f\Big(&\sum_{n=1}^{2^{k-1}} \sum_{m=0}^{M-1} a_{nm}\psi_{n,m}(x), \sum_{n=1}^{2^{k-1}} \sum_{m=0}^{M-1} a_{nm}\psi'_{n,m}(x), \\ &y_0(qx-\tau), y_0'(qx-\tau)\Big). \end{aligned} \tag{10.3.5}$$

Step 3: Set the residual (10.3.5) equal to zero at the set of Chebyshev nodes, $x_i = \frac{b-a}{2}\cos(\frac{(2i+1)\pi}{2^k M}) +$

$\frac{a+b}{2}$, $i = 0, 1, 2, ..., M-1$, on interval $[a, b]$.

$$\sum_{n=1}^{2^{k-1}} \sum_{m=0}^{M-1} a_{nm}^{c} D^{\alpha} \psi_{n,m}(x_i) - g(x_i) - f\Big(\sum_{n=1}^{2^{k-1}} \sum_{m=0}^{M-1} a_{nm} \psi_{n,m}(x_i), \sum_{n=1}^{2^{k-1}} \sum_{m=0}^{M-1} a_{nm} \psi'_{n,m}(x_i), y_0(qx_i - \tau), y'_0(qx_i - \tau) \Big) = 0. \tag{10.3.6}$$

We obtain $2^{k-1}M - p$ equations, where p is the number of conditions of the delay equation. Two conditions are given ($p = 2$) so we get $2^{k-1}M-2$ equations from equation (10.3.6) by using Chebyshev nodes x_i. Two more equations obtain from the conditions of equation (10.3.2), that is

$$y(a) = \phi(a) \quad \Rightarrow \sum_{n=1}^{2^{k-1}} \sum_{m=0}^{M-1} a_{nm} \psi_{n,m}(a) = \phi(a),$$

$$y'(a) = \phi'(a) \quad \Rightarrow \sum_{n=1}^{2^{k-1}} \sum_{m=0}^{M-1} a_{nm} \psi'_{n,m}(a) = \phi'(a).$$

We obtained $2^{k-1}M$ equations either linear or nonlinear along with $2^{k-1}M$ unknown coefficients a_{nm}, which is solved by Newton iterative method to get $a_{nm}{}'s$ and use it in (10.3.4) to get the approximate solution. Denote the obtained solution as $y_1(x)$, which is defined on $[a, b]$.
Continue the procedure for the subsequent interval, delay differential equation on $[b, 2b]$ becomes

$${}^{c}D^{\alpha} y(x) = h(x) + f(y(x), y'(x), y_1(qx - \tau), y'_1(qx - \tau)),\ b \le x \le 2b,\ 1 < \alpha \le 2, \tag{10.3.7}$$

subject to the initial conditions $y(b) = y_1(b)$, $y'(b) = y'_1(b)$.
Which is again an fractional non–delay differential equation and solve it by the Hermite wavelet method to get $y_2(x)$ on $[b, 2b]$. This procedure may be continued for subsequent intervals.

10.3.4 Numerical Solutions

In this Section, we utilize the Hermite step method for finding the numerical solution of linear and nonlinear fractional delay differential equations. The notations y_{pro}, y_{exact} and E_{abs} represents the solution by Hermite step method, exact solution and their absolute error respectively. We use the results up to 100 decimal places. Through this work we use Caputo derivatives.

Linear Delayed Fractional Differential Equations

Example 1. Consider the fractional delay differential equation

$${}^{c}D^{\alpha} y(x) + y(x) - y(x - \tau) = \tfrac{2}{\Gamma(3-\alpha)} x^{2-\alpha} - \tfrac{1}{\Gamma(2-\alpha)} x^{1-\alpha} + 2\tau x - \tau^2 - \tau, \quad x > 0,\ 0 < \alpha < 1, \quad y(x) = 0,\ x \le 0. \tag{10.3.8}$$

The exact solution [124], when $\alpha = 1$, is $y(x) = x^2 - x$.

The results obtained by the Hermite step method, by taking $\alpha = 0.5,\ k = 1,\ M = 3$, and $\tau = 0.01e^{-x}$, is shown in Figure 10.8 along with the exact solution. Table 10.13 indicates that results obtained from the Hermite step method are more close to exact solution and better than the method [124]. E_{abs} and Err represents the absolute error by Hermite step method and method [124], respectively.

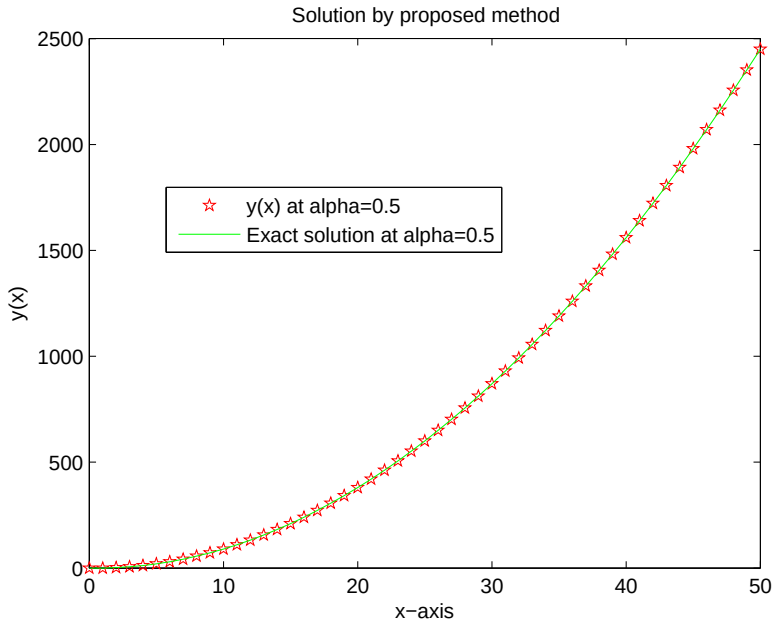

Figure 10.8: Solutions by the Hermite step method, $\tau = 0.01e^{-x}$, and exact solutions, at $\alpha = 0.5$.

	$\tau = 0.1,\ \alpha = 0.2$		$\tau = 0.01e^{-x},\ \alpha = 0.9$		$\tau = 0.01e^{-x},\ \alpha = 0.2$	
x	E_{abs}	Err [124]	E_{abs}	Err [124]	E_{abs}	Err [124]
5	1.9e-97	0.0062	4.0000e-98	0.0010	2.7e-97	0.0074
10	2.7e-97	0.0134	1.1000e-97	4.7115e-4	4.0e-97	0.0082
50	3.0e-96	0.0690	0.0000e+00	7.0303e-4	5.0e-96	0.0052

Table 10.13: Comparison of the solution by Hermite step method at $M = 3$, with exact solution and method [124].

Example 2. Consider the following fractional delay differential equation

$$ {}^{c}D^{\alpha}y(x) = -y(x) - y(x-0.3) + e^{-x+0.3},\ \ 0 \le x \le 1,\ 2 < \alpha \le 3, \tag{10.3.9} $$

subject to the initial conditions $y(0) = 1,\ y'(0) = -1,$ and $y''(0) = 1$. The exact solution, when

$\alpha = 1$, is $y(x) = e^{-x}$.

The data in Table 10.14 shows that this method provides more accurate results as compared to Adomian decomposition method [36]. These results are obtained by fixing $M = 25$ and $k = 1$, at $\alpha = 3$. Solution by the Hermite step method at different values of α are shown in Figure 10.9, which shows that solutions by Hermite step method at different α converges to the exact solution at $\alpha = 3$, when α approaches to 3.

x	y_{pro}	y_{exact}	E_{abs}	E_{ADM} [36]
0.0	1.000000000000000	1.000000000000000	0.00e+00	8.52e-14
0.2	0.818730753077982	0.818730753077982	9.12e-42	3.83e-14
0.4	0.670320046035639	0.670320046035639	6.90e-41	1.68e-13
0.6	0.548811636094026	0.548811636094026	2.38e-40	6.00e-14
0.8	0.449328964117222	0.449328964117222	6.01e-41	6.66e-15
1.0	0.367879441171442	0.367879441171442	3.58e-36	4.57e-14

Table 10.14: Comparison of the solution by Hermite step method, $M = 25$, with exact solution and Adomian decomposition method [36], at $\alpha = 3$.

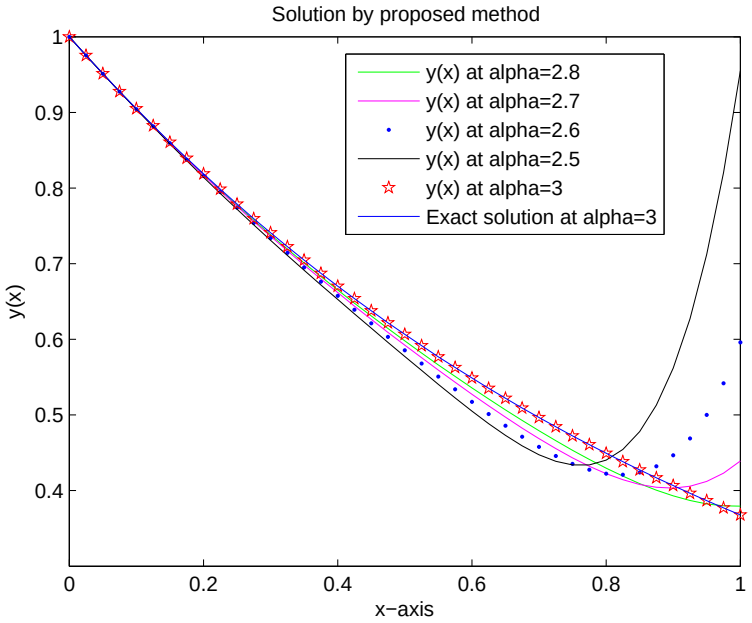

Figure 10.9: Solutions by the Hermite step method at different α, $M = 7$, $k = 1$, and exact solution at $\alpha = 3$.

Example 3. Consider the fractional pantograph equation,

$$
\begin{aligned}
{}^{c}D^{\alpha}y(x) &= \tfrac{1}{2}e^{\frac{x}{2}}y(\tfrac{x}{2}) + \tfrac{1}{2}y(x) \quad , \ 0 < \alpha \leq 1, \quad 0 \leq x \leq 1, \\
y(0) &= 1.
\end{aligned}
\tag{10.3.10}
$$

The exact solution, when $\alpha = 1$, is $y(x) = e^x$.

By fixing $k = 1$ and $M = 4$, we plot the solutions by Hermite step method at different values of α and exact solution at $\alpha = 1$, as shown in Figure 10.10. It shows that present solution approaches to the exact solution while α approaches to 1.

Comparison of present solution y_{pro} at $\alpha = 1$, $M = 30$ and $k = 1$, with Adomian decomposition method [36] and the spline function technique [37], is shown in Table 10.15. The notations E_{abs}, E_{ADM} and E_{spline} represents the absolute error by Hermite step method, Adomian decomposition method and the spline function technique respectively. We can get more accurate results while increasing M.

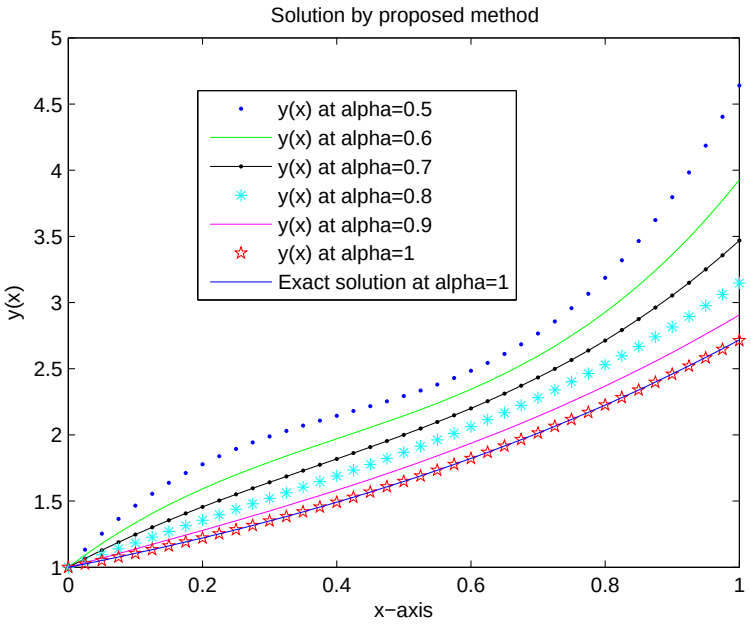

Figure 10.10: Solutions by the Hermite step method at different α, $M = 4$, $k = 1$ and exact solutions at $\alpha = 1$.

$\alpha = 1$					
x	y_{pro}	y_{exact}	E_{abs}	E_{ADM} [36]	E_{spline} [37]
0.2	1.221402758160170	1.221402758160170	1.96519e-51	0.00	3.10e-15
0.4	1.491824697641270	1.491824697641270	2.51474e-51	2.22e-16	7.54e-15
0.6	1.822118800390509	1.822118800390509	2.56283e-51	2.22e-16	1.39e-14
0.8	2.225540928492468	2.225540928492468	1.03409e-50	1.33e-15	2.13e-14
1.0	2.718281828459045	2.718281828459045	8.81662e-49	4.88e-15	3.19e-14

Table 10.15: Solution by present method for $M = 30,\ k = 1$.

Example 4. Consider the following fractional neutral functional differential equation with proportional delay

$$
\begin{gathered}
{}^{c}D^{\alpha}y(x) = -y(x) + 0.1y(0.8x) + 0.5{}^{c}D^{\alpha}y(0.8x) + (0.32x - 0.5)e^{-0.8x} + e^{-x}, \quad x \geq 0,\ 0 < \alpha \leq 1, \\
y(0) = 0,
\end{gathered}
\tag{10.3.11}
$$

which has the exact solution, when $\alpha = 1$, is xe^{x}.

We implement the method by fixing $k = 1,\ M = 5$, at different values of α, the results are shown in Figure 10.11 along with the exact solution at $\alpha = 1$. Table 10.16 shows that present method gives more accurate results as compared to the spectral shifted Legendre-Gauss collocation (SLC) method [12], the reproducing kernel Hilbert space method ($RKHSM$) [79] and a Runge-Kutta-type (RKT) method [125].

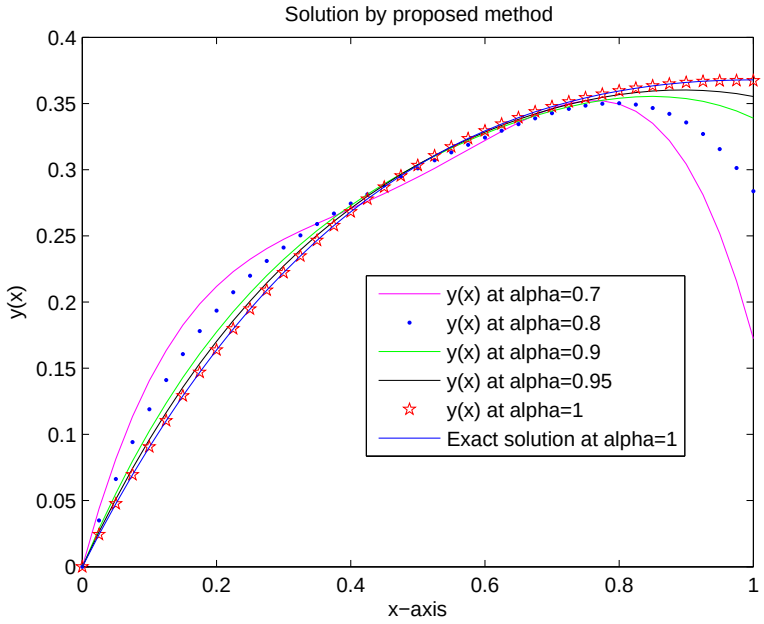

Figure 10.11: Solution by the present method at different α, $M = 5$ and exact solution at $\alpha = 1$.

$\alpha = 1$				$M = 17$
x	*SLC method* [12]	*RKHSM* [79]	*RKT method* [125]	E_{abs}
0.1	4.27e-17	1.42e-4	8.68e-4	1.23e-24
0.2	2.70e-17	1.17e-4	1.49e-3	3.41e-25
0.3	5.94e-17	9.45e-4	1.90e-3	1.74e-24
0.4	8.01e-17	7.59e-4	2.16e-3	2.79e-24
0.5	8.27e-17	6.03e-4	2.28e-3	3.33e-24
0.6	1.95e-16	4.73e-4	2.31e-3	3.94e-24
0.7	1.56e-16	3.64e-4	2.27e-3	3.56e-24
0.8	8.80e-17	2.75e-4	2.17e-3	2.35e-25
0.9	1.03e-16	2.03e-4	2.03e-3	1.02e-23
1.0	1.23e-16	1.43e-4	1.86e-3	1.58e-22

Table 10.16: Absolute errors using Hermite step method at $\alpha = 1$ and $M = 17$.

Nonlinear Delayed Fractional Differential Equations

Example 5. Consider the fractional nonlinear delay differential equation

$$ {}^{c}D^{\alpha}y(x) = 1 - 2y^2(\tfrac{x}{2}), \quad 0 \leq x \leq 1, \ 1 < \alpha \leq 2, \tag{10.3.12} $$

subject to the initial conditions, $y(0) = 1$, $y'(0) = 0$. The exact solution [66], when $\alpha = 2$, is $y(x) = \cos(x)$.

Solutions by present method at different values of α is plotted in Figure 10.12, which shows that present solution is converges to the exact solution when α approaches to 2. According to the Table 10.17, absolute error reduces while increasing M.

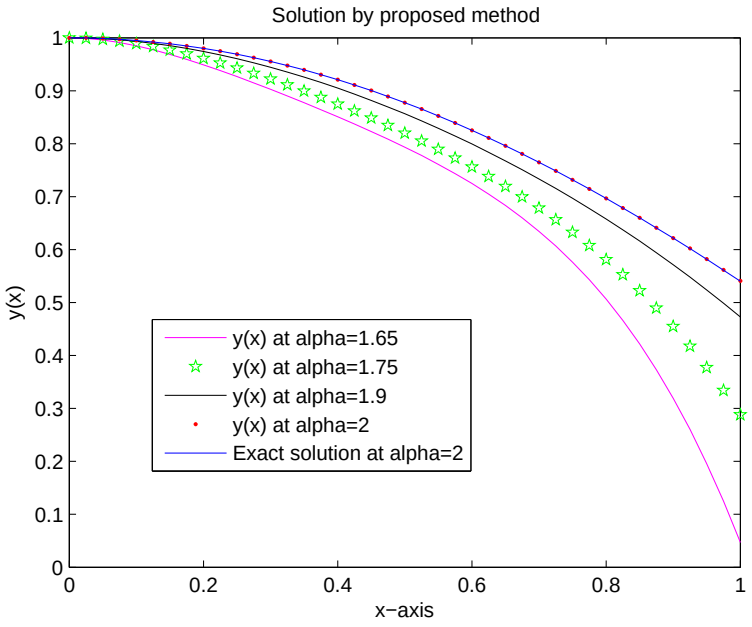

Figure 10.12: Solution by the Hermite step method at different α, $M = 5$ and exact solution at $\alpha = 2$.

$\alpha = 2$	$M = 15$	$M = 25$	$M = 30$	$M = 40$
x	E_{abs}	E_{abs}	E_{abs}	E_{abs}
0.1	2.17077e-23	1.96989e-42	8.02964e-52	5.46682e-60
0.2	4.49566e-23	2.28499e-42	7.79780e-52	1.52681e-59
0.3	1.67001e-22	6.26291e-42	1.42878e-51	1.57732e-59
0.4	3.60801e-23	2.25484e-41	2.38398e-51	5.49810e-60
0.5	2.87200e-22	2.25484e-41	4.19542e-51	1.09577e-58
0.6	4.60073e-24	7.94684e-41	6.75256e-51	9.58443e-59
0.7	4.89152e-22	1.18456e-40	1.12211e-50	3.69647e-57
0.8	1.23582e-21	1.36081e-40	1.58769e-50	1.69940e-55
0.9	5.88496e-21	4.92247e-40	5.35881e-50	5.29603e-54
1.0	5.30153e-19	1.25319e-37	1.99293e-47	3.70755e-53

Table 10.17: Absolute errors by using present method at different M and $\alpha = 2$.

Comparison of Hermite Step Method and Hermite Wavelet Method

Example 6. Consider the fractional nonlinear neutral delay differential equation ,

$$ {}^{c}D^{\alpha}y(x) = \tfrac{1}{2}y(x) + \tfrac{1}{2}y(\tfrac{x}{2})\,{}^{c}D^{\alpha}y(\tfrac{x}{2}), \quad x \geq 0,\ 0 < \alpha \leq 1, \tag{10.3.13} $$

subject to the initial conditions, $y(0) = 1$. The exact solution [67] , when $\alpha = 1$, is $y(x) = e^{x}$.

Hermite Wavelet Method for Fractional Delay Differential Equation

We can approximate the solution of equation (10.3.13) by the Hermite wavelet method as

$$ y(x) \simeq \sum_{n=1}^{2^{k-1}} \sum_{m=0}^{M-1} a_{nm}\psi_{n,m}(x). \tag{10.3.14} $$

In the delay equations, we also have to approximate the delay unknown function $y(\frac{x}{2})$ in terms of the Hermite wavelet series at delay time as

$$ y(\tfrac{x}{2}) \simeq \sum_{n=1}^{2^{k-1}} \sum_{m=0}^{M-1} a_{nm}\psi_{n,m}(\tfrac{x}{2}). \tag{10.3.15} $$

We call this series as the delay Hermite wavelet series. Substituting equation (10.3.14), (10.3.15) in equation (10.3.13), we get the residual as

$$ \begin{aligned} \sum_{n=1}^{2^{k-1}} \sum_{m=0}^{M-1} a^{c}_{nm} D^{\alpha}\psi_{n,m}(x) &= \tfrac{1}{2} \sum_{n=1}^{2^{k-1}} \sum_{m=0}^{M-1} a_{nm}\psi_{n,m}(x) \\ +\tfrac{1}{2} \sum_{n=1}^{2^{k-1}} \sum_{m=0}^{M-1} a_{nm}\psi_{n,m}(\tfrac{x}{2}) &\Big(\sum_{n=1}^{2^{k-1}} \sum_{m=0}^{M-1} a^{c}_{nm} D^{\alpha}\psi_{n,m}(\tfrac{x}{2}) \Big). \end{aligned} \tag{10.3.16} $$

Set the residual (10.3.16) equal to zero at the set of Chebyshev nodes, $x_i = \frac{1}{2}\cos(\frac{(2i+1)\pi}{2^k M}) + \frac{1}{2},\ k = 0, 1, 2, ..., M-1$, on interval $[0, 1]$, we get

$$\begin{aligned} &\sum_{n=1}^{2^{k-1}} \sum_{m=0}^{M-1} a^c_{nm} D^\alpha \psi_{n,m}(x_i) - \tfrac{1}{2} \sum_{n=1}^{2^{k-1}} \sum_{m=0}^{M-1} a_{nm} \psi_{n,m}(x_i) \\ &-\tfrac{1}{2} \sum_{n=1}^{2^{k-1}} \sum_{m=0}^{M-1} a_{nm} \psi_{n,m}(\tfrac{x_i}{2}) \Big(\sum_{n=1}^{2^{k-1}} \sum_{m=0}^{M-1} a^c_{nm} D^\alpha \psi_{n,m}(\tfrac{x_i}{2}) \Big) = 0. \end{aligned} \tag{10.3.17}$$

We get $2^{k-1}M-1$ equations from equation (10.3.17) by using chebyshev nodes x_i. One more equation obtain from the condition of equation (10.3.13), that is

$$y(0) = 1 \quad \Rightarrow \sum_{n=1}^{2^{k-1}} \sum_{m=0}^{M-1} a_{nm} \psi_{n,m}(0) = 1,$$

We obtained $2^{k-1}M$ nonlinear equations along with $2^{k-1}M$ unknown coefficients a_{nm}, which is solved by Newton iterative method to get $a_{nm}{}'s$ and use it in (10.3.14) to get the approximate solution by Hermite wavelet method.

We fix $M = 9,\ k = 1$ and implement the Hermite wavelet and Hermite step method to (10.3.13). The results are shown in Table 10.18 along with the absolute errors. According to the Table 10.18, Hermite wavelet and Hermite step method gives good results that is, for some points Hermite step method is more accurate as compared to Hermite wavelet method and vice versa.

For the problem (10.3.13), run time of present method and Hermite wavelet method are 1.21 and 26.21 seconds respectively. Hermite step method is more efficient than the Hermite wavelet method. y_{HWM} and E_{HWM} represents the solution by Hermite wavelet method and their absolute error, respectively.

For this purpose, we use $Maple$ 13 in system with $Core\ Duo\ CPU$ 2.00 GHz and RAM 2.50GB

$\alpha = 1$					
x	y_{HWM}	y_{pro}	y_{exact}	E_{HWM}	E_{pro}
0.0	1.0000000000	1.0000000000	1.0000000000	0.00000e+00	0.00000e+00
0.1	1.1051709181	1.1051709181	1.1051709181	1.33288e-11	5.37737e-12
0.2	1.2214027582	1.2214027581	1.2214027582	3.93123e-12	1.14859e-11
0.3	1.3498588076	1.3498588076	1.3498588076	2.83949e-11	2.13830e-11
0.4	1.4918246977	1.4918246976	1.4918246976	1.26536e-11	6.30257e-12
0.5	1.6487212707	1.6487212707	1.6487212707	8.42958e-12	3.08447e-11
0.6	1.8221188004	1.8221188004	1.8221188004	5.79353e-11	1.57380e-11
0.7	2.0137527076	2.0137527075	2.0137527075	8.92374e-11	4.32148e-11
0.8	2.2255409285	2.2255409284	2.2255409285	3.39446e-11	6.08108e-11
0.9	2.4596031112	2.4596031112	2.4596031112	6.71791e-11	6.72473e-11
1.0	2.7182818276	2.7182818276	2.7182818285	8.41911e-10	8.35594e-10

Table 10.18: Comparison of present and Hermite wavelet method $M = 9,\ k = 1$.

10.3.5 Conclusion

It is shown that method gives excellent results when applied to different fractional linear and non-linear delay differential equations. The results obtained from the Hermite step method are more accurate and better than the results obtained from other methods, as shown in Tables 10.13-10.16. The solution of the fractional delay differential equation converge to the solution of integer delay differential equation, as shown in Figures 10.9-10.12. According to the convergence analysis, error by the present method reduces while increasing M, as shown in Tables 10.17. Table 10.18 indicates that both Hermite wavelet method and present method gives good results. Hermite step method is more efficient than the Hermite wavelet method.

Chapter 11

Summary

Most of the numerical methods are not adequate to handle the fractional nonlinear differential equations, which necessitates the deriving of new approximation techniques for fractional nonlinear differential equations. The major objective of this thesis is to develop new numerical methods and their supporting analysis for solving fractional nonlinear differential equations. A series of six published papers and seven manuscripts has been presented on the solution of fractional nonlinear ordinary differential equations, fractional nonlinear partial differential equations, and linear and nonlinear fractional delay differential equation. We have included these papers and manuscripts in Chapters 2 to 10 and are summarized as follows:

In Chapter 1 we have provided a brief introduction of fractional calculus, quasilinearization technique and wavelet analysis. The non−uniform Haar wavelet matrix, operational matrix of fractional integration and operational matrix of fractional integration for boundary value problems are constructed in Chapter 2 and utilized for solving fractional initial and boundary value problems over non−uniform nodes. The obtained solutions by non−uniform Haar wavelet method are better than the uniform Haar wavelet method.

The principle objective of considering the non uniform nodes for the Haar wavelets is to deal with the solution of problems for which solution behave abruptly on some part of the domain, that is, it is smooth on some part of domain and suddenly have abrupt changes. The present method can handle these types of problems with reasonable accuracy. We have constructed the subintervals by keeping in view the behavior of the problem's solution.

A numerical technique, Haar wavelet quasilinearization technique, is developed by using both uniform and non−uniform Haar wavelet operational matrix method in conjunction with quasilinearization technique, as given in Chapter 3. Method of implementation is investigated and utilized for solving fractional nonlinear initial and boundary value problems. Convergence analysis of the method has also presented. The obtained solutions are more accurate and efficient than the solution obtained by other numerical methods. More accurate results are obtained by increasing iteration of method. It is observed that solution of the fractional order, α, differential equation converge to the

solution of integer order differential equation when α approaches to the integer value.

In Chapter 4 we developed Haar wavelet quasilinearization technique for heat convection–radiation and fractional oscillation equations. Haar wavelet quasilinearization technique gave stable and sufficiently accurate results when applied to heat convection–radiation equations as compared to generalized approximation method, homotopy perturbation method and variational iteration method. We also developed Haar wavelet quasilinearization technique for forced and force-free duffing-Van der Pol oscillator equation and higher order oscillation equation. The method provides good results as compared to homotopy perturbation method, variational iteration method, decomposition method and generalized differential quadrature rule method. The results are in good agreement with exact solutions or forth order Runge–Kutta method.

Haar wavelet quasilinearization technique has been extended, in Chapter 5, for fractional nonlinear partial differential equations. Procedure of implementation of the method for general fractional nonlinear partial differential equation has been introduced. Convergence analysis of Haar wavelet quasilinearization technique for function of two variables has also been investigated. It has been observed that method gives more accurate results while increasing level of resolution or iteration of the method or both. We considered the fractional generalized Berger–Fisher equation, fractional Klein Gordon equations and fractional Bergers equation to show the applicability of the method. Our results are more accurate than the reduced differential transform method, variational iteration method and homotopy perturbation method.

In Chapter 6, a numerical method for fractional nonlinear differential equation by utilizing Haar wavelet operational matrix method and Picard technique has been discussed. Convergence of the method is discussed in details. The method is applied on fractional nonlinear initial and boundary value problems. We considered fractional nonlinear Bratu type equation, duffing equation and Lane–Emden type equation as test problems. Graphical results show that solution of fractional order equation converge to the solution of integer order equation when fractional order value approaches to integer value, and it is also observed that solution becomes more accurate by increasing iteration of the method.

In Chapter 7 combination of wavelet Galerkin method and quasilinearization technique is implemented for solving nonlinear boundary value problems. Daubechies scaling functions are used as Galerkin basis. We have successfully derived the expression for computing the two term connection coefficients as shown in section 7.2 and appendix. These connection coefficients are used in wavelet Galerkin quasilinearization technique for solving nonlinear boundary value problems. The description of implementation for the method has given in section 7.3. Comparison analysis with other numerical methods has also been presented for the sake of accuracy and efficiency of the present method.

The two solution methods for fractional nonlinear differential equations are presented in Chapter 8. One of them is Chebyshev wavelet quasilinearization technique and the other method is Legendre

wavelet quasilinearization technique. The wavelet matrix, operational matrix of fractional integration for initial and boundary value problems are constructed and utilized for solving fractional nonlinear ordinary differential equations. Chebyshev wavelet quasilinearization technique is also extended for fractional nonlinear partial differential equations. The procedure of implementation of Chebyshev wavelet quasilinearization and Legendre wavelet quasilinearization are same and are described for fractional nonlinear duffing oscillator with damping effect, fractional nonlinear Lane Emden initial and boundary value problem, general fractional Riccati equation, fractional nonlinear oscillator equations, fractional Bergers differential equation and fractional Klein Gordon equation. Convergence analysis of the methods is presented which shows that approximate solution converges to the exact solution while increasing level of resolution or order of polynomials or iteration of the methods or all. Comparison of Legendre wavelet quasilinearization technique is carried out with Adomian decomposition method, variational iteration method and homotopy perturbation method. It has been observed that method provides more accurate and stable results. The graphical analysis shows that solution of the fractional order differential equations converge to the solution of integer order differential equations and absolute error decreases while increasing iteration of the methods.

In Chapter 9 we introduced a new numerical method, Gegenbauer wavelets operational matrix method, for solving fractional differential equation. We derived Gegenbauer wavelet matrix, Gegenbauer wavelet operational matrix of fractional integration and Gegenbauer wavelet operational matrix of fractional integration for boundary value problems and utilized for solving fractional linear differential equations. Implementation is carried out on different problems and convergence analysis is also investigated. Comparison of the method with Haar wavelet method and homotopy perturbation method shows that our results are more accurate.

In Chapter 10, three numerical methods are presented for delay differential equations. The first method is the combination of radial basis function networks and method of steps. The procedure of implementation of radial basis function collocation method and proposed method are presented and utilized for the solution of different linear and nonlinear delay differential equations. Comparison of these two methods is presented which shows that present method is more efficient than the radial basis function collocation method. In section 10.2, we developed the Chebyshev wavelets method for solving the linear and nonlinear fractional delay differential equations, fractional delay Volterra integro–differential equations and fractional system of delay differential equations. We also introduced a technique by combining Chebyshev wavelet method and method of steps for solving fractional delay differential equations. Comparison of our method and Chebyshev wavelet method is presented which shows that our method is more efficient than the Chebyshev wavelet method. The procedure of implementation and convergence analysis are also given. Another method which we developed in Chapter 10 is the combination of Hermite wavelet method and method of steps. Comparison of method with Hermite wavelet method, Adomian decomposition method, the spline function technique, spectral shifted Legendre-Gauss collocation method, reproducing kernel Hilbert

space method and Runge-Kutta-type method are presented. The method is more efficient than the Hermite wavelet method at least for the tested problem.

Wavelets quasilinearization technique can be extended for fractional nonlinear partial differential equations, and Gegenbauer wavelet quasilinearization technique can be developed for fractional nonlinear differential equations.

Appendix

Two Term Connection Coefficients

We construct the two term connection coefficients at different level of resolution j, for different Daubechies wavelets, by using MATLAB program.

	$j=0,\ N=6$	$j=1,\ N=6$	$j=2,\ N=6$
$\Omega_{-4}^{0,2}$	5.357142857141826e-003	2.142857142857320e-002	8.571428571428662e-002
$\Omega_{-3}^{0,2}$	1.142857142857159e-001	4.571428571428521e-001	1.828571428571418e+000
$\Omega_{-2}^{0,2}$	-8.761904761904875e-001	-3.504761904761875e+000	-1.401904761904759e+001
$\Omega_{-1}^{0,2}$	3.390476190476216e+000	1.356190476190466e+001	5.424761904761887e+001
$\Omega_{0}^{0,2}$	-5.267857142857139e+000	-2.107142857142841e+001	-8.428571428571381e+001
$\Omega_{1}^{0,2}$	3.390476190476166e+000	1.356190476190468e+001	5.424761904761871e+001
$\Omega_{2}^{0,2}$	-8.761904761904648e-001	-3.504761904761882e+000	-1.401904761904751e+001
$\Omega_{3}^{0,2}$	1.142857142857137e-001	4.571428571428545e-001	1.828571428571419e+000
$\Omega_{4}^{0,2}$	5.357142857143558e-003	2.142857142857155e-002	8.571428571428807e-002

Table 1: Two term connection at $N=6,\ d_1=0,\ d_2=2$ and different j

	$j=3,\ N=6$	$j=4,\ N=6$	$j=5,\ N=6$
$\Omega_{-4}^{0,2}$	3.428571428571458e-001	1.371428571428649e+000	5.485714285714518e+000
$\Omega_{-3}^{0,2}$	7.314285714285692e+000	2.925714285714256e+001	1.170285714285708e+002
$\Omega_{-2}^{0,2}$	-5.607619047619031e+001	-2.243047619047600e+002	-8.972190476190496e+002
$\Omega_{-1}^{0,2}$	2.169904761904755e+002	8.679619047618978e+002	3.471847619047619e+003
$\Omega_{0}^{0,2}$	-3.371428571428556e+002	-1.348571428571417e+003	-5.394285714285691e+003
$\Omega_{1}^{0,2}$	2.169904761904752e+002	8.679619047618978e+002	3.471847619047593e+003
$\Omega_{2}^{0,2}$	-5.607619047619014e+001	-2.243047619047599e+002	-8.972190476190377e+002
$\Omega_{3}^{0,2}$	7.314285714285687e+000	2.925714285714264e+001	1.170285714285707e+002
$\Omega_{4}^{0,2}$	3.428571428571566e-001	1.371428571428608e+000	5.485714285714590e+000

Table 2: Two term connection at $N=6,\ d_1=0,\ d_2=2$ and different j

	$j=6,\ N=6$	$j=7,\ N=6$	$j=8,\ N=6$
$\Omega_{-4}^{0,2}$	2.194285714285784e+001	8.777142857143053e+001	3.510857142857163e+002
$\Omega_{-3}^{0,2}$	4.681142857142830e+002	1.872457142857140e+003	7.489828571428539e+003
$\Omega_{-2}^{0,2}$	-3.588876190476193e+003	-1.435550476190475e+004	-5.742201904761879e+004
$\Omega_{-1}^{0,2}$	1.388739047619045e+004	5.554956190476182e+004	2.221982476190466e+005
$\Omega_{0}^{0,2}$	-2.157714285714270e+004	-8.630857142857112e+004	-3.452342857142838e+005
$\Omega_{1}^{0,2}$	1.388739047619032e+004	5.554956190476169e+004	2.221982476190463e+005
$\Omega_{2}^{0,2}$	-3.588876190476136e+003	-1.435550476190469e+004	-5.742201904761864e+004
$\Omega_{3}^{0,2}$	4.681142857142813e+002	1.872457142857137e+003	7.489828571428535e+003
$\Omega_{4}^{0,2}$	2.194285714285805e+001	8.777142857143291e+001	3.510857142857182e+002

Table 3: Two term connection at $N=6,\ d_1=0,\ d_2=2$ and different j

	$j=9,\ N=6$	$j=10,\ N=6$	$j=11,\ N=6$
$\Omega_{-4}^{0,2}$	1.404342857142891e+003	5.617371428571553e+003	2.246948571428641e+004
$\Omega_{-3}^{0,2}$	2.995931428571427e+004	1.198372571428564e+005	4.793490285714245e+005
$\Omega_{-2}^{0,2}$	-2.296880761904784e+005	-9.187523047618968e+005	-3.675009219047597e+006
$\Omega_{-1}^{0,2}$	8.887929904761952e+005	3.555171961904737e+006	1.422068784761896e+007
$\Omega_{0}^{0,2}$	-1.380937142857141e+006	-5.523748571428541e+006	-2.209499428571414e+007
$\Omega_{1}^{0,2}$	8.887929904761834e+005	3.555171961904749e+006	1.422068784761895e+007
$\Omega_{2}^{0,2}$	-2.296880761904731e+005	-9.187523047619022e+005	-3.675009219047592e+006
$\Omega_{3}^{0,2}$	2.995931428571412e+004	1.198372571428568e+005	4.793490285714257e+005
$\Omega_{4}^{0,2}$	1.404342857142966e+003	5.617371428571412e+003	2.246948571428614e+004

Table 4: Two term connection at $N=6,\ d_1=0,\ d_2=2$ and different j

	$j=0,\ N=8$	$j=1,\ N=8$	$j=2,\ N=8$
$\Omega_{-6}^{0,2}$	1.592164927486754e-005	6.368659709865587e-005	2.547463883897427e-004
$\Omega_{-5}^{0,2}$	-1.630376885702075e-003	-6.521507542809107e-003	-2.608603017123232e-002
$\Omega_{-4}^{0,2}$	-1.057272777801076e-002	-4.229091111203748e-002	-1.691636444481578e-001
$\Omega_{-3}^{0,2}$	1.509728996160295e-001	6.038915984641060e-001	2.415566393856457e+000
$\Omega_{-2}^{0,2}$	-6.978691043580259e-001	-2.791476417432023e+000	-1.116590566972836e+001
$\Omega_{-1}^{0,2}$	2.642070208104647e+000	1.056828083241845e+001	4.227312332967440e+001
$\Omega_{0}^{0,2}$	-4.165973640696393e+000	-1.666389456278559e+001	-6.665557825114267e+001
$\Omega_{1}^{0,2}$	2.642070208104588e+000	1.056828083241853e+001	4.227312332967385e+001
$\Omega_{2}^{0,2}$	-6.978691043579955e-001	-2.791476417432061e+000	-1.116590566972809e+001
$\Omega_{3}^{0,2}$	1.509728996160251e-001	6.038915984641088e-001	2.415566393856425e+000
$\Omega_{4}^{0,2}$	-1.057272777800908e-002	-4.229091111203711e-002	-1.691636444481482e-001
$\Omega_{5}^{0,2}$	-1.630376885702051e-003	-6.521507542809029e-003	-2.608603017123440e-002
$\Omega_{6}^{0,2}$	1.592164927491819e-005	6.368659709770528e-005	2.547463883940679e-004

Table 5: Two term connection at $N=8,\ d_1=0,\ d_2=2$ and different j

	$j=3,\ N=8$	$j=4,\ N=8$	$j=5,\ N=8$
$\Omega^{0,2}_{-6}$	1.018985553571927e-003	4.075942214264236e-003	1.630376885708006e-002
$\Omega^{0,2}_{-5}$	-1.043441206849605e-001	-4.173764827397488e-001	-1.669505930959118e+000
$\Omega^{0,2}_{-4}$	-6.766545777925135e-001	-2.706618311170434e+000	-1.082647324468204e+001
$\Omega^{0,2}_{-3}$	9.662265575425584e+000	3.864906230170310e+001	1.545962492068136e+002
$\Omega^{0,2}_{-2}$	-4.466362267891171e+001	-1.786544907156519e+002	-7.146179628626170e+002
$\Omega^{0,2}_{-1}$	1.690924933186943e+002	6.763699732747868e+002	2.705479893099166e+003
$\Omega^{0,2}_{0}$	-2.666223130045711e+002	-1.066489252018283e+003	-4.265957008073134e+003
$\Omega^{0,2}_{1}$	1.690924933186991e+002	6.763699732747851e+002	2.705479893099126e+003
$\Omega^{0,2}_{2}$	-4.466362267891412e+001	-1.786544907156511e+002	-7.146179628625968e+002
$\Omega^{0,2}_{3}$	9.662265575425868e+000	3.864906230170296e+001	1.545962492068111e+002
$\Omega^{0,2}_{4}$	-6.766545777926012e-001	-2.706618311170378e+000	-1.082647324468142e+001
$\Omega^{0,2}_{5}$	-1.043441206849559e-001	-4.173764827397630e-001	-1.669505930958990e+000
$\Omega^{0,2}_{6}$	1.018985553548858e-003	4.075942214262211e-003	1.630376885715088e-002

Table 6: Two term connection at $N=8,\ d_1=0,\ d_2=2$ and different j

	$j=6,\ N=8$	$j=7,\ N=8$	$j=8,\ N=8$
$\Omega^{0,2}_{-6}$	6.521507542830642e-002	2.608603017129146e-001	1.043441206855564e+000
$\Omega^{0,2}_{-5}$	-6.678023723836140e+000	-2.671209489534182e+001	-1.068483795813761e+002
$\Omega^{0,2}_{-4}$	-4.330589297872758e+001	-1.732235719149116e+002	-6.928942876596633e+002
$\Omega^{0,2}_{-3}$	6.183849968272513e+002	2.473539987308997e+003	9.894159949236040e+003
$\Omega^{0,2}_{-2}$	-2.858471851450443e+003	-1.143388740580170e+004	-4.573554962320728e+004
$\Omega^{0,2}_{-1}$	1.082191957239662e+004	4.328767828958627e+004	1.731507131583458e+005
$\Omega^{0,2}_{0}$	-1.706382803229253e+004	-6.825531212917001e+004	-2.730212485166792e+005
$\Omega^{0,2}_{1}$	1.082191957239654e+004	4.328767828958623e+004	1.731507131583431e+005
$\Omega^{0,2}_{2}$	-2.858471851450408e+003	-1.143388740580167e+004	-4.573554962320595e+004
$\Omega^{0,2}_{3}$	6.183849968272465e+002	2.473539987308988e+003	9.894159949235864e+003
$\Omega^{0,2}_{4}$	-4.330589297872614e+001	-1.732235719149057e+002	-6.928942876596170e+002
$\Omega^{0,2}_{5}$	-6.678023723836182e+000	-2.671209489534469e+001	-1.068483795813737e+002
$\Omega^{0,2}_{6}$	6.521507542837254e-002	2.608603017125445e-001	1.043441206858962e+000

Table 7: Two term connection at $N=8,\ d_1=0,\ d_2=2$ and different j

	$j=9,\ N=8$	$j=10,\ N=8$	$j=11,\ N=8$
$\Omega_{-6}^{0,2}$	4.173764827425225e+000	1.669505930971174e+001	6.678023723861125e+001
$\Omega_{-5}^{0,2}$	-4.273935183255965e+002	-1.709574073302103e+003	-6.838296293208365e+003
$\Omega_{-4}^{0,2}$	-2.771577150638221e+003	-1.108630860255392e+004	-4.434523441021765e+004
$\Omega_{-3}^{0,2}$	3.957663979694332e+004	1.583065591877754e+005	6.332262367511063e+005
$\Omega_{-2}^{0,2}$	-1.829421984928236e+005	-7.317687939713063e+005	-2.927075175885267e+006
$\Omega_{-1}^{0,2}$	6.926028526333740e+005	2.770411410533518e+006	1.108164564213415e+007
$\Omega_{0}^{0,2}$	-1.092084994066722e+006	-4.368339976266882e+006	-1.747335990506750e+007
$\Omega_{1}^{0,2}$	6.926028526333884e+005	2.770411410533526e+006	1.108164564213399e+007
$\Omega_{2}^{0,2}$	-1.829421984928308e+005	-7.317687939713104e+005	-2.927075175885189e+006
$\Omega_{3}^{0,2}$	3.957663979694424e+004	1.583065591877755e+005	6.332262367510970e+005
$\Omega_{4}^{0,2}$	-2.771577150638528e+003	-1.108630860255384e+004	-4.434523441021545e+004
$\Omega_{5}^{0,2}$	-4.273935183255515e+002	-1.709574073302138e+003	-6.838296293208033e+003
$\Omega_{6}^{0,2}$	4.173764827361305e+000	1.669505930957055e+001	6.678023723903364e+001

Table 8: Two term connection at $N=8,\ d_1=0,\ d_2=2$ and different j

	$j=0,\ N=10$	$j=1,\ N=10$	$j=2,\ N=10$
$\Omega_{-8}^{0,2}$	3.538762372724263e-009	1.415503991870649e-008	5.662015979006055e-008
$\Omega_{-7}^{0,2}$	1.656544135415504e-006	6.626176543753997e-006	2.650470617655871e-005
$\Omega_{-6}^{0,2}$	3.671453838941836e-004	1.468581535579231e-003	5.874326142311675e-003
$\Omega_{-5}^{0,2}$	7.946205571441002e-004	3.178482228576603e-003	1.271392891430086e-002
$\Omega_{-4}^{0,2}$	-2.990798043764482e-002	-1.196319217506301e-001	-4.785276870025282e-001
$\Omega_{-3}^{0,2}$	1.809535500933656e-001	7.238142003736265e-001	2.895256801494564e+000
$\Omega_{-2}^{0,2}$	-6.495021899805745e-001	-2.598008759923048e+000	-1.039203503969259e+001
$\Omega_{-1}^{0,2}$	2.414790351192434e+000	9.659161404771346e+000	3.863664561908612e+001
$\Omega_{0}^{0,2}$	-3.834994313783372e+000	-1.533997725513428e+001	-6.135990902053714e+001
$\Omega_{1}^{0,2}$	2.414790351193088e+000	9.659161404771760e+000	3.863664561908625e+001
$\Omega_{2}^{0,2}$	-6.495021899809332e-001	-2.598008759923271e+000	-1.039203503969266e+001
$\Omega_{3}^{0,2}$	1.809535500934332e-001	7.238142003736624e-001	2.895256801494574e+000
$\Omega_{4}^{0,2}$	-2.990798043766519e-002	-1.196319217506370e-001	-4.785276870025272e-001
$\Omega_{5}^{0,2}$	7.946205571434909e-004	3.178482228574532e-003	1.271392891429838e-002
$\Omega_{6}^{0,2}$	3.671453838939398e-004	1.468581535577375e-003	5.874326142312047e-003
$\Omega_{7}^{0,2}$	1.656544135440499e-006	6.626176543772582e-006	2.650470617638380e-005
$\Omega_{8}^{0,2}$	3.538759177639483e-009	1.415503921834577e-008	5.662016104188667e-008

Table 9: Two term connection at $N=10,\ d_1=0,\ d_2=2$ and different j

	$j=3,\ N=10$	$j=4,\ N=10$	$j=5,\ N=10$
$\Omega_{-8}^{0,2}$	2.264806438372176e-007	9.059225398626676e-007	3.623690337895192e-006
$\Omega_{-7}^{0,2}$	1.060188247094546e-004	4.240752987948207e-004	1.696301195479521e-003
$\Omega_{-6}^{0,2}$	2.349730456924624e-002	9.398921827703768e-002	3.759568731075404e-001
$\Omega_{-5}^{0,2}$	5.085571565716359e-002	2.034228626290972e-001	8.136914505139112e-001
$\Omega_{-4}^{0,2}$	-1.914110748010074e+000	-7.656442992040458e+000	-3.062577196816142e+001
$\Omega_{-3}^{0,2}$	1.158102720597830e+001	4.632410882391194e+001	1.852964352956579e+002
$\Omega_{-2}^{0,2}$	-4.156814015877082e+001	-1.662725606350729e+002	-6.650902425403700e+002
$\Omega_{-1}^{0,2}$	1.545465824763454e+002	6.181863299053630e+002	2.472745319621593e+003
$\Omega_{0}^{0,2}$	-2.454396360821485e+002	-9.817585443285968e+002	-3.927034177314373e+003
$\Omega_{1}^{0,2}$	1.545465824763442e+002	6.181863299053988e+002	2.472745319621433e+003
$\Omega_{2}^{0,2}$	-4.156814015877019e+001	-1.662725606350923e+002	-6.650902425402835e+002
$\Omega_{3}^{0,2}$	1.158102720597821e+001	4.632410882391496e+001	1.852964352956441e+002
$\Omega_{4}^{0,2}$	-1.914110748010080e+000	-7.656442992040895e+000	-3.062577196815917e+001
$\Omega_{5}^{0,2}$	5.085571565719506e-002	2.034228626287706e-001	8.136914505151182e-001
$\Omega_{6}^{0,2}$	2.349730456924411e-002	9.398921827694688e-002	3.759568731079856e-001
$\Omega_{7}^{0,2}$	1.060188247070593e-004	4.240752987864339e-004	1.696301195438063e-003
$\Omega_{8}^{0,2}$	2.264806433832283e-007	9.059225265746785e-007	3.623690487151188e-006

Table 10: Two term connection at $N=10,\ d_1=0,\ d_2=2$ and different j

	$j=6,\ N=10$	$j=7,\ N=10$	$j=8,\ N=10$
$\Omega_{-8}^{0,2}$	1.449476095478013e-005	5.797904425998113e-005	2.319161855334121e-004
$\Omega_{-7}^{0,2}$	6.785204780689570e-003	2.714081912618476e-002	1.085632764907711e-001
$\Omega_{-6}^{0,2}$	1.503827492434704e+000	6.015309969721770e+000	2.406123987898113e+001
$\Omega_{-5}^{0,2}$	3.254765802062957e+000	1.301906320824141e+001	5.207625283291282e+001
$\Omega_{-4}^{0,2}$	-1.225030878726426e+002	-4.900123514905859e+002	-1.960049405962209e+003
$\Omega_{-3}^{0,2}$	7.411857411825775e+002	2.964742964730459e+003	1.185897185892127e+004
$\Omega_{-2}^{0,2}$	-2.660360970161092e+003	-1.064144388064541e+004	-4.256577552257807e+004
$\Omega_{-1}^{0,2}$	9.890981278485660e+003	3.956392511394458e+004	1.582557004557715e+005
$\Omega_{0}^{0,2}$	-1.570813670925753e+004	-6.283254683703004e+004	-2.513301873481197e+005
$\Omega_{1}^{0,2}$	9.890981278486488e+003	3.956392511394397e+004	1.582557004557820e+005
$\Omega_{2}^{0,2}$	-2.660360970161541e+003	-1.064144388064509e+004	-4.256577552258379e+004
$\Omega_{3}^{0,2}$	7.411857411826508e+002	2.964742964730407e+003	1.185897185892225e+004
$\Omega_{4}^{0,2}$	-1.225030878726577e+002	-4.900123514905757e+002	-1.960049405962483e+003
$\Omega_{5}^{0,2}$	3.254765802060289e+000	1.301906320824192e+001	5.207625283296589e+001
$\Omega_{6}^{0,2}$	1.503827492430988e+000	6.015309969726228e+000	2.406123987889844e+001
$\Omega_{7}^{0,2}$	6.785204780497495e-003	2.714081912528849e-002	1.085632764891305e-001
$\Omega_{8}^{0,2}$	1.449476001059264e-005	5.797904514574883e-005	2.319161639579069e-004

Table 11: Two term connection at $N=10,\ d_1=0,\ d_2=2$ and different j

	$j=9,\ N=10$	$j=10,\ N=10$	$j=11,\ N=10$
$\Omega_{-8}^{0,2}$	9.276646904372849e-004	3.710658850163947e-003	1.484263561211925e-002
$\Omega_{-7}^{0,2}$	4.342531059812703e-001	1.737012424094660e+000	6.948049696175408e+000
$\Omega_{-6}^{0,2}$	9.624495951573638e+001	3.849798380619461e+002	1.539919352248286e+003
$\Omega_{-5}^{0,2}$	2.083050113320538e+002	8.332200453272749e+002	3.332880181307076e+003
$\Omega_{-4}^{0,2}$	-7.840197623849253e+003	-3.136079049539793e+004	-1.254431619815909e+005
$\Omega_{-3}^{0,2}$	4.743588743568555e+004	1.897435497427526e+005	7.589741989710131e+005
$\Omega_{-2}^{0,2}$	-1.702631020903137e+005	-6.810524083613269e+005	-2.724209633445335e+006
$\Omega_{-1}^{0,2}$	6.330228018230894e+005	2.532091207292494e+006	1.012836482917001e+007
$\Omega_{0}^{0,2}$	-1.005320749392482e+006	-4.021282997569930e+006	-1.608513199027968e+007
$\Omega_{1}^{0,2}$	6.330228018231288e+005	2.532091207292382e+006	1.012836482916944e+007
$\Omega_{2}^{0,2}$	-1.702631020903350e+005	-6.810524083612668e+005	-2.724209633445025e+006
$\Omega_{3}^{0,2}$	4.743588743568901e+004	1.897435497427429e+005	7.589741989709628e+005
$\Omega_{4}^{0,2}$	-7.840197623849910e+003	-3.136079049539589e+004	-1.254431619815815e+005
$\Omega_{5}^{0,2}$	2.083050113318606e+002	8.332200453274910e+002	3.332880181310069e+003
$\Omega_{6}^{0,2}$	9.624495951559901e+001	3.849798380626097e+002	1.539919352250294e+003
$\Omega_{7}^{0,2}$	4.342531059587488e-001	1.737012424069827e+000	6.948049696444462e+000
$\Omega_{8}^{0,2}$	9.276646604721024e-004	3.710658979601785e-003	1.484263606959022e-002

Table 12: Two term connection at $N=10,\ d_1=0,\ d_2=2$ and different j

	$j=0,\ N=12$	$j=1,\ N=12$	$j=2,\ N=12$
$\Omega^{0,2}_{-10}$	-1.264097876724598e-011	-5.056507963203803e-011	-2.022556636237721e-010
$\Omega^{0,2}_{-9}$	2.629981104154165e-008	1.051992439199124e-007	4.207969757357792e-007
$\Omega^{0,2}_{-8}$	-3.466086046077293e-006	-1.386434418283787e-005	-5.545737674116930e-005
$\Omega^{0,2}_{-7}$	-5.436337907645785e-005	-2.174535163049358e-004	-8.698140652207401e-004
$\Omega^{0,2}_{-6}$	-6.569629078445609e-005	-2.627851631397719e-004	-1.051140652547745e-003
$\Omega^{0,2}_{-5}$	6.478061041939686e-003	2.591224416775302e-002	1.036489766710306e-001
$\Omega^{0,2}_{-4}$	-4.936161063950125e-002	-1.974464425580035e-001	-7.897857702320411e-001
$\Omega^{0,2}_{-3}$	2.049054694327311e-001	8.196218777309501e-001	3.278487510923756e+000
$\Omega^{0,2}_{-2}$	-6.307332429629734e-001	-2.522932971852045e+000	-1.009173188740778e+001
$\Omega^{0,2}_{-1}$	2.311866563670177e+000	9.247466254681022e+000	3.698986501872334e+001
$\Omega^{0,2}_{0}$	-3.686063482147259e+000	-1.474425392858916e+001	-5.897701571435668e+001
$\Omega^{0,2}_{1}$	2.311866563670155e+000	9.247466254680465e+000	3.698986501872263e+001
$\Omega^{0,2}_{2}$	-6.307332429629595e-001	-2.522932971851724e+000	-1.009173188740734e+001
$\Omega^{0,2}_{3}$	2.049054694327266e-001	8.196218777308840e-001	3.278487510923633e+000
$\Omega^{0,2}_{4}$	-4.936161063949909e-002	-1.974464425579911e-001	-7.897857702319906e-001
$\Omega^{0,2}_{5}$	6.478061041939042e-003	2.591224416775772e-002	1.036489766710283e-001
$\Omega^{0,2}_{6}$	-6.569629078481492e-005	-2.627851631390393e-004	-1.051140652556928e-003
$\Omega^{0,2}_{7}$	-5.436337907630618e-005	-2.174535163050178e-004	-8.698140652209454e-004
$\Omega^{0,2}_{8}$	-3.466086045782824e-006	-1.386434418290632e-005	-5.545737673255587e-005
$\Omega^{0,2}_{9}$	2.629981098109758e-008	1.051992439770264e-007	4.207969755590383e-007
$\Omega^{0,2}_{10}$	-1.264109848372647e-011	-5.056394558717779e-011	-2.022561442652375e-010

Table 13: Two term connection at $N=12,\ d_1=0,\ d_2=2$ and different j

	$j=3,\ N=12$	$j=4,\ N=12$	$j=5,\ N=12$
$\Omega^{0,2}_{-10}$	-8.090370440306238e-010	-3.235921798249199e-009	-1.294449946187273e-008
$\Omega^{0,2}_{-9}$	1.683187899282874e-006	6.732751659830736e-006	2.693100639211662e-005
$\Omega^{0,2}_{-8}$	-2.218295069247718e-004	-8.873180281702858e-004	-3.549272110902696e-003
$\Omega^{0,2}_{-7}$	-3.479256260885189e-003	-1.391702504349056e-002	-5.566810017416912e-002
$\Omega^{0,2}_{-6}$	-4.204562610165038e-003	-1.681825044122728e-002	-6.727300176309307e-002
$\Omega^{0,2}_{-5}$	4.145959066840249e-001	1.658383626737518e+000	6.633534506945009e+000
$\Omega^{0,2}_{-4}$	-3.159143080927814e+000	-1.263657232371543e+001	-5.054628929484694e+001
$\Omega^{0,2}_{-3}$	1.311395004369412e+001	5.245580017478679e+001	2.098232006991118e+002
$\Omega^{0,2}_{-2}$	-4.036692754962765e+001	-1.614677101985510e+002	-6.458708407940686e+002
$\Omega^{0,2}_{-1}$	1.479594600748868e+002	5.918378402996212e+002	2.367351361198232e+003
$\Omega^{0,2}_{0}$	-2.359080628574246e+002	-9.436322514297131e+002	-3.774529005718785e+003
$\Omega^{0,2}_{1}$	1.479594600748943e+002	5.918378402995226e+002	2.367351361198261e+003
$\Omega^{0,2}_{2}$	-4.036692754963201e+001	-1.614677101984934e+002	-6.458708407940849e+002
$\Omega^{0,2}_{3}$	1.311395004369506e+001	5.245580017477295e+001	2.098232006991148e+002
$\Omega^{0,2}_{4}$	-3.159143080928074e+000	-1.263657232371056e+001	-5.054628929484770e+001
$\Omega^{0,2}_{5}$	4.145959066840644e-001	1.658383626736738e+000	6.633534506945354e+000
$\Omega^{0,2}_{6}$	-4.204562610220666e-003	-1.681825044093799e-002	-6.727300176362197e-002
$\Omega^{0,2}_{7}$	-3.479256260887767e-003	-1.391702504349444e-002	-5.566810017416796e-002
$\Omega^{0,2}_{8}$	-2.218295069311091e-004	-8.873180276715695e-004	-3.549272110864563e-003
$\Omega^{0,2}_{9}$	1.683187898198771e-006	6.732751658693551e-006	2.693100643916897e-005
$\Omega^{0,2}_{10}$	-8.090318943597590e-010	-3.236047377047866e-009	-1.294447589830267e-008

Table 14: Two term connection at $N=12,\ d_1=0,\ d_2=2$ and different j

	$j=6,\ N=12$	$j=7,\ N=12$	$j=8,\ N=12$
$\Omega^{0,2}_{-10}$	-5.177798005768146e-008	-2.071134660283070e-007	-8.284647747797681e-007
$\Omega^{0,2}_{-9}$	1.077240255634689e-004	4.308961018884622e-004	1.723584407706808e-003
$\Omega^{0,2}_{-8}$	-1.419708844297557e-002	-5.678835376430962e-002	-2.271534150343634e-001
$\Omega^{0,2}_{-7}$	-2.226724006964358e-001	-8.906896027893919e-001	-3.562758411151697e+000
$\Omega^{0,2}_{-6}$	-2.690920070539038e-001	-1.076368028218255e+000	-4.305472112864513e+000
$\Omega^{0,2}_{-5}$	2.653413802778020e+001	1.061365521111146e+002	4.245462084443969e+002
$\Omega^{0,2}_{-4}$	-2.021851571793860e+002	-8.087406287175115e+002	-3.234962514869842e+003
$\Omega^{0,2}_{-3}$	8.392928027964472e+002	3.357171211185718e+003	1.342868484474241e+004
$\Omega^{0,2}_{-2}$	-2.583483363176286e+003	-1.033393345270493e+004	-4.133573381081803e+004
$\Omega^{0,2}_{-1}$	9.469405444792965e+003	3.787762177917145e+004	1.515104871166828e+005
$\Omega^{0,2}_{0}$	-1.509811602287520e+004	-6.039246409150057e+004	-2.415698563660018e+005
$\Omega^{0,2}_{1}$	9.469405444793052e+003	3.787762177917239e+004	1.515104871166920e+005
$\Omega^{0,2}_{2}$	-2.583483363176337e+003	-1.033393345270549e+004	-4.133573381082342e+004
$\Omega^{0,2}_{3}$	8.392928027964599e+002	3.357171211185867e+003	1.342868484474377e+004
$\Omega^{0,2}_{4}$	-2.021851571793910e+002	-8.087406287175722e+002	-3.234962514870345e+003
$\Omega^{0,2}_{5}$	2.653413802778164e+001	1.061365521111244e+002	4.245462084444683e+002
$\Omega^{0,2}_{6}$	-2.690920070542778e-001	-1.076368028217790e+000	-4.305472112865718e+000
$\Omega^{0,2}_{7}$	-2.226724006966231e-001	-8.906896027867058e-001	-3.562758411148717e+000
$\Omega^{0,2}_{8}$	-1.419708844339636e-002	-5.678835377427147e-002	-2.271534150964587e-001
$\Omega^{0,2}_{9}$	1.077240255873366e-004	4.308961019825347e-004	1.723584405719999e-003
$\Omega^{0,2}_{10}$	-5.177775730313133e-008	-2.071113334110827e-007	-8.284509886632400e-007

Table 15: Two term connection at $N=12,\ d_1=0,\ d_2=2$ and different j

	$j=9,\ N=12$	$j=10,\ N=12$	$j=11,\ N=12$
$\Omega^{0,2}_{-10}$	-3.313762787046124e-006	-1.325499511088505e-005	-5.302076941954415e-005
$\Omega^{0,2}_{-9}$	6.894337644103972e-003	2.757735060343232e-002	1.103094022302312e-001
$\Omega^{0,2}_{-8}$	-9.086136604628754e-001	-3.634454641732330e+000	-1.453781856576694e+001
$\Omega^{0,2}_{-7}$	-1.425103364457279e+001	-5.700413457830712e+001	-2.280165383133559e+002
$\Omega^{0,2}_{-6}$	-1.722188845141308e+001	-6.888755380609204e+001	-2.755502152214489e+002
$\Omega^{0,2}_{-5}$	1.698184833778097e+003	6.792739335112789e+003	2.717095734044612e+004
$\Omega^{0,2}_{-4}$	-1.293985005948137e+004	-5.175940023792531e+004	-2.070376009516870e+005
$\Omega^{0,2}_{-3}$	5.371473937897389e+004	2.148589575158954e+005	8.594358300635415e+005
$\Omega^{0,2}_{-2}$	-1.653429352432863e+005	-6.613717409731468e+005	-2.645486963892423e+006
$\Omega^{0,2}_{-1}$	6.060419484667570e+005	2.424167793867029e+006	9.696671175467806e+006
$\Omega^{0,2}_{0}$	-9.662794254640138e+005	-3.865117701856049e+006	-1.546047080742411e+007
$\Omega^{0,2}_{1}$	6.060419484667510e+005	2.424167793866993e+006	9.696671175468177e+006
$\Omega^{0,2}_{2}$	-1.653429352432826e+005	-6.613717409731258e+005	-2.645486963892637e+006
$\Omega^{0,2}_{3}$	5.371473937897281e+004	2.148589575158902e+005	8.594358300635886e+005
$\Omega^{0,2}_{4}$	-1.293985005948089e+004	-5.175940023792341e+004	-2.070376009517003e+005
$\Omega^{0,2}_{5}$	1.698184833778067e+003	6.792739335112339e+003	2.717095734044764e+004
$\Omega^{0,2}_{6}$	-1.722188845149549e+001	-6.888755380590808e+001	-2.755502152236020e+002
$\Omega^{0,2}_{7}$	-1.425103364457827e+001	-5.700413457832755e+001	-2.280165383135506e+002
$\Omega^{0,2}_{8}$	-9.086136603797715e-001	-3.634454641532466e+000	-1.453781856625087e+001
$\Omega^{0,2}_{9}$	6.894337652143804e-003	2.757735061252992e-002	1.103094020768655e-001
$\Omega^{0,2}_{10}$	-3.313774710144577e-006	-1.325508314812706e-005	-5.302055374571969e-005

Table 16: Two term connection at $N=12,\ d_1=0,\ d_2=2$ and different j

	$j=0,\ N=14$	$j=1,\ N=14$	$j=2,\ N=14$
$\Omega^{0,2}_{-12}$	2.003462875478288e-014	7.618350316625926e-014	2.858820963466460e-013
$\Omega^{0,2}_{-11}$	1.634254355550330e-010	6.537017486924693e-010	2.614810929834814e-009
$\Omega^{0,2}_{-10}$	2.065484709089308e-009	8.261941195446524e-009	3.304777456916617e-008
$\Omega^{0,2}_{-9}$	1.486183289949873e-006	5.944733159288970e-006	2.377893264002077e-005
$\Omega^{0,2}_{-8}$	1.401115549807462e-006	5.604462200919528e-006	2.241784880570807e-005
$\Omega^{0,2}_{-7}$	4.156644098757038e-005	1.662657639545149e-004	6.650630557927202e-004
$\Omega^{0,2}_{-6}$	-1.605235464468504e-003	-6.420941857888948e-003	-2.568376743163273e-002
$\Omega^{0,2}_{-5}$	1.396368919026623e-002	5.585475676107586e-002	2.234190270444499e-001
$\Omega^{0,2}_{-4}$	-6.705236229077559e-002	-2.682094491631042e-001	-1.072837796652847e+000
$\Omega^{0,2}_{-3}$	2.233591022278455e-001	8.934364089113975e-001	3.573745635646781e+000
$\Omega^{0,2}_{-2}$	-6.214976746649311e-001	-2.485990698659797e+000	-9.943962794643531e+000
$\Omega^{0,2}_{-1}$	2.255045788050212e+000	9.020183152201167e+000	3.608073260881296e+001
$\Omega^{0,2}_{0}$	-3.604515526034094e+000	-1.441806210413690e+001	-5.767224841655087e+001
$\Omega^{0,2}_{1}$	2.255045788050778e+000	9.020183152203455e+000	3.608073260880956e+001
$\Omega^{0,2}_{2}$	-6.214976746652678e-001	-2.485990698661171e+000	-9.943962794641442e+000
$\Omega^{0,2}_{3}$	2.233591022279253e-001	8.934364089117365e-001	3.573745635646189e+000
$\Omega^{0,2}_{4}$	-6.705236229079710e-002	-2.682094491631991e-001	-1.072837796652589e+000
$\Omega^{0,2}_{5}$	1.396368919027134e-002	5.585475676108752e-002	2.234190270443578e-001
$\Omega^{0,2}_{6}$	-1.605235464477370e-003	-6.420941857909641e-003	-2.568376743161370e-002
$\Omega^{0,2}_{7}$	4.156644098906695e-005	1.662657639562138e-004	6.650630558251257e-004
$\Omega^{0,2}_{8}$	1.401115550250582e-006	5.604462200952607e-006	2.241784880614045e-005
$\Omega^{0,2}_{9}$	1.486183289837643e-006	5.944733159309059e-006	2.377893263959070e-005
$\Omega^{0,2}_{10}$	2.065485192623341e-009	8.261940622026800e-009	3.304776483630680e-008
$\Omega^{0,2}_{11}$	1.634254269376621e-010	6.537017414408330e-010	2.614810865017833e-009
$\Omega^{0,2}_{12}$	1.777667872026136e-014	7.096607082343888e-014	2.876951548315236e-013

Table 17: Two term connection at $N=14,\ d_1=0,\ d_2=2$ and different j

	$j=3,\ N=14$	$j=4,\ N=14$	$j=5,\ N=14$
$\Omega^{0,2}_{-12}$	1.154082450048948e-012	4.577769708109114e-012	1.834192269131837e-011
$\Omega^{0,2}_{-11}$	1.045922654362139e-008	4.183695686175578e-008	1.673477785825097e-007
$\Omega^{0,2}_{-10}$	1.321911088563116e-007	5.287640484921418e-007	2.115056337805130e-006
$\Omega^{0,2}_{-9}$	9.511573054315589e-005	3.804629222214576e-004	1.521851688849178e-003
$\Omega^{0,2}_{-8}$	8.967139525743209e-005	3.586855811944848e-004	1.434742325069759e-003
$\Omega^{0,2}_{-7}$	2.660252223318906e-003	1.064100889327469e-002	4.256403557314682e-002
$\Omega^{0,2}_{-6}$	-1.027350697264921e-001	-4.109402789059906e-001	-1.643761115623913e+000
$\Omega^{0,2}_{-5}$	8.936761081774594e-001	3.574704432708721e+000	1.429881773083465e+001
$\Omega^{0,2}_{-4}$	-4.291351186609631e+000	-1.716540474644068e+001	-6.866161898575710e+001
$\Omega^{0,2}_{-3}$	1.429498254258224e+001	5.717993017034102e+001	2.287197206813462e+002
$\Omega^{0,2}_{-2}$	-3.977585117855665e+001	-1.591034047142773e+002	-6.364136188570444e+002
$\Omega^{0,2}_{-1}$	1.443229304352213e+002	5.772917217409739e+002	2.309166886963776e+003
$\Omega^{0,2}_{0}$	-2.306889936661977e+002	-9.227559746648044e+002	-3.691023898659174e+003
$\Omega^{0,2}_{1}$	1.443229304352618e+002	5.772917217409738e+002	2.309166886963963e+003
$\Omega^{0,2}_{2}$	-3.977585117858114e+001	-1.591034047142778e+002	-6.364136188571611e+002
$\Omega^{0,2}_{3}$	1.429498254258853e+001	5.717993017034251e+001	2.287197206813821e+002
$\Omega^{0,2}_{4}$	-4.291351186611410e+000	-1.716540474644241e+001	-6.866161898577295e+001
$\Omega^{0,2}_{5}$	8.936761081774295e-001	3.574704432709711e+000	1.429881773083878e+001
$\Omega^{0,2}_{6}$	-1.027350697265636e-001	-4.109402789059335e-001	-1.643761115623996e+000
$\Omega^{0,2}_{7}$	2.660252223299098e-003	1.064100889320341e-002	4.256403557277424e-002
$\Omega^{0,2}_{8}$	8.967139521364732e-005	3.586855808967927e-004	1.434742323553625e-003
$\Omega^{0,2}_{9}$	9.511573054646635e-005	3.804629222224450e-004	1.521851688826565e-003
$\Omega^{0,2}_{10}$	1.321910506251359e-007	5.287642447179209e-007	2.115056935526588e-006
$\Omega^{0,2}_{11}$	1.045922682805499e-008	4.183695492490508e-008	1.673477861419150e-007
$\Omega^{0,2}_{12}$	1.136419647863200e-012	4.605273840114645e-012	1.836439044732966e-011

Table 18: Two term connection at $N=14,\ d_1=0,\ d_2=2$ and different j

	$j=6,\ N=14$	$j=7,\ N=14$	$j=8,\ N=14$
$\Omega^{0,2}_{-12}$	7.343895836829572e-011	2.936802453332225e-010	1.175793956651511e-009
$\Omega^{0,2}_{-11}$	6.693921970241139e-007	2.677565768408699e-006	1.071026613620596e-005
$\Omega^{0,2}_{-10}$	8.460223699413345e-006	3.384090091004247e-005	1.353636072980174e-004
$\Omega^{0,2}_{-9}$	6.087406756037182e-003	2.434962702215654e-002	9.739850809027002e-002
$\Omega^{0,2}_{-8}$	5.738969292708812e-003	2.295587719035902e-002	9.182350873920780e-002
$\Omega^{0,2}_{-7}$	1.702561422902897e-001	6.810245691671077e-001	2.724098276660951e+000
$\Omega^{0,2}_{-6}$	-6.575044462493648e+000	-2.630017784997982e+001	-1.052007113999123e+002
$\Omega^{0,2}_{-5}$	5.719527092334836e+001	2.287810836933717e+002	9.151243347735485e+002
$\Omega^{0,2}_{-4}$	-2.746464759431456e+002	-1.098585903772256e+003	-4.394343615089313e+003
$\Omega^{0,2}_{-3}$	9.148788827257300e+002	3.659515530901930e+003	1.463806212360844e+004
$\Omega^{0,2}_{-2}$	-2.545654475429403e+003	-1.018261790171407e+004	-4.073047160685860e+004
$\Omega^{0,2}_{-1}$	9.236667547857247e+003	3.694667019142275e+004	1.477866807656956e+005
$\Omega^{0,2}_{0}$	-1.476409559463712e+004	-5.905638237854715e+004	-2.362255295141910e+005
$\Omega^{0,2}_{1}$	9.236667547854233e+003	3.694667019142155e+004	1.477866807656845e+005
$\Omega^{0,2}_{2}$	-2.545654475427582e+003	-1.018261790171337e+004	-4.073047160685201e+004
$\Omega^{0,2}_{3}$	9.148788827252663e+002	3.659515530901813e+003	1.463806212360692e+004
$\Omega^{0,2}_{4}$	-2.746464759430191e+002	-1.098585903772284e+003	-4.394343615089056e+003
$\Omega^{0,2}_{5}$	5.719527092335471e+001	2.287810836934194e+002	9.151243347736851e+002
$\Omega^{0,2}_{6}$	-6.575044462488378e+000	-2.630017784997643e+001	-1.052007113998908e+002
$\Omega^{0,2}_{7}$	1.702561422913951e-001	6.810245691654139e-001	2.724098276660222e+000
$\Omega^{0,2}_{8}$	5.738969294964641e-003	2.295587717712905e-002	9.182350870757253e-002
$\Omega^{0,2}_{9}$	6.087406756104002e-003	2.434962702255506e-002	9.739850809182690e-002
$\Omega^{0,2}_{10}$	8.460228615856428e-006	3.384091193019296e-005	1.353636486489300e-004
$\Omega^{0,2}_{11}$	6.693921807045750e-007	2.677565370708196e-006	1.071026410582643e-005
$\Omega^{0,2}_{12}$	7.480789131216059e-011	2.953386307471755e-010	1.183922637664226e-009

Table 19: Two term connection at $N=14,\ d_1=0,\ d_2=2$ and different j

	$j=9,\ N=14$	$j=10,\ N=14$	$j=11,\ N=14$
$\Omega^{0,2}_{-12}$	4.695620124341847e-009	1.885291117920846e-008	7.519061383690603e-008
$\Omega^{0,2}_{-11}$	4.284106490153028e-005	1.713640117304137e-004	6.854569144629773e-004
$\Omega^{0,2}_{-10}$	5.414543635458626e-004	2.165818547071371e-003	8.663270441031195e-003
$\Omega^{0,2}_{-9}$	3.895940323715649e-001	1.558376129322234e+000	6.233504517948456e+000
$\Omega^{0,2}_{-8}$	3.672940349639070e-001	1.469176140297406e+000	5.876704559668548e+000
$\Omega^{0,2}_{-7}$	1.089639310664806e+001	4.358557242690666e+001	1.743422897063438e+002
$\Omega^{0,2}_{-6}$	-4.208028455996761e+002	-1.683211382398976e+003	-6.732845529594937e+003
$\Omega^{0,2}_{-5}$	3.660497339094018e+003	1.464198935637764e+004	5.856795742550541e+004
$\Omega^{0,2}_{-4}$	-1.757737446035789e+004	-7.030949784141364e+004	-2.812379913657155e+005
$\Omega^{0,2}_{-3}$	5.855224849443671e+004	2.342089939776810e+005	9.368359759109465e+005
$\Omega^{0,2}_{-2}$	-1.629218864274463e+005	-6.516875457095336e+005	-2.606750182838986e+006
$\Omega^{0,2}_{-1}$	5.911467230628029e+005	2.364586892250772e+006	9.458347569004558e+006
$\Omega^{0,2}_{0}$	-9.449021180567668e+005	-3.779608472226996e+006	-1.511843388890816e+007
$\Omega^{0,2}_{1}$	5.911467230627207e+005	2.364586892251235e+006	9.458347569003698e+006
$\Omega^{0,2}_{2}$	-1.629218864273970e+005	-6.516875457098145e+005	-2.606750182838473e+006
$\Omega^{0,2}_{3}$	5.855224849442493e+004	2.342089939777558e+005	9.368359759108279e+005
$\Omega^{0,2}_{4}$	-1.757737446035539e+004	-7.030949784143725e+004	-2.812379913656950e+005
$\Omega^{0,2}_{5}$	3.660497339094717e+003	1.464198935637901e+004	5.856795742551587e+004
$\Omega^{0,2}_{6}$	-4.208028455994950e+002	-1.683211382399622e+003	-6.732845529592935e+003
$\Omega^{0,2}_{7}$	1.089639310664794e+001	4.358557242651029e+001	1.743422897063545e+002
$\Omega^{0,2}_{8}$	3.672940348553743e-001	1.469176139264744e+000	5.876704557400261e+000
$\Omega^{0,2}_{9}$	3.895940323723735e-001	1.558376129313524e+000	6.233504517937830e+000
$\Omega^{0,2}_{10}$	5.414546042618743e-004	2.165818228533662e-003	8.663273622172268e-003
$\Omega^{0,2}_{11}$	4.284106484763625e-005	1.713640441711847e-004	6.854569232499823e-004
$\Omega^{0,2}_{12}$	4.747546607506164e-009	1.869653425815363e-008	7.578033373943364e-008

Table 20: Two term connection at $N=14,\ d_1=0,\ d_2=2$ and different j

	$j=0,\ N=16$	$j=1,\ N=16$	$j=2,\ N=16$
$\Omega^{0,2}_{-14}$	-1.148024275421403e-015	9.259482049878509e-017	1.423856581191772e-015
$\Omega^{0,2}_{-13}$	2.709917921565594e-013	1.083063162907301e-012	4.332294476795473e-012
$\Omega^{0,2}_{-12}$	-5.813834711638026e-011	-2.325549267994774e-010	-9.302198506703989e-010
$\Omega^{0,2}_{-11}$	-1.058570541219077e-008	-4.234282226909658e-008	-1.693712895251933e-007
$\Omega^{0,2}_{-10}$	-3.723076306330369e-007	-1.489230520877817e-006	-5.956922090640851e-006
$\Omega^{0,2}_{-9}$	2.090423495448280e-006	8.361693980982877e-006	3.344677592465187e-005
$\Omega^{0,2}_{-8}$	-2.398228524608487e-005	-9.592914097935484e-005	-3.837165639121684e-004
$\Omega^{0,2}_{-7}$	4.516792028712516e-004	1.806716811499788e-003	7.226867246003963e-003
$\Omega^{0,2}_{-6}$	-4.097656893425651e-003	-1.639062757370445e-002	-6.556251029481604e-002
$\Omega^{0,2}_{-5}$	2.207029188483285e-002	8.828116753928755e-002	3.531246701571179e-001
$\Omega^{0,2}_{-4}$	-8.226639997426313e-002	-3.290655998968139e-001	-1.316262399587235e+000
$\Omega^{0,2}_{-3}$	2.371780582155096e-001	9.487122328614122e-001	3.794848931445703e+000
$\Omega^{0,2}_{-2}$	-6.156141465574054e-001	-2.462456586227665e+000	-9.849826344910953e+000
$\Omega^{0,2}_{-1}$	2.219146593891828e+000	8.876586375563809e+000	3.550634550225573e+001
$\Omega^{0,2}_{0}$	-3.553692289913436e+000	-1.421476915965254e+001	-5.685907663861011e+001
$\Omega^{0,2}_{1}$	2.219146593890713e+000	8.876586375564839e+000	3.550634550225886e+001
$\Omega^{0,2}_{2}$	-6.156141465566998e-001	-2.462456586228314e+000	-9.849826344912939e+000
$\Omega^{0,2}_{3}$	2.371780582152939e-001	9.487122328616032e-001	3.794848931446319e+000
$\Omega^{0,2}_{4}$	-8.226639997418213e-002	-3.290655998968780e-001	-1.316262399587475e+000
$\Omega^{0,2}_{5}$	2.207029188481781e-002	8.828116753929494e-002	3.531246701571725e-001
$\Omega^{0,2}_{6}$	-4.097656893423902e-003	-1.639062757370759e-002	-6.556251029482763e-002
$\Omega^{0,2}_{7}$	4.516792028764111e-004	1.806716811498624e-003	7.226867245996593e-003
$\Omega^{0,2}_{8}$	-2.398228524510812e-005	-9.592914098033821e-005	-3.837165639207784e-004
$\Omega^{0,2}_{9}$	2.090423495429467e-006	8.361693981091696e-006	3.344677592417852e-005
$\Omega^{0,2}_{10}$	-3.723076303519969e-007	-1.489230521936113e-006	-5.956922087642646e-006
$\Omega^{0,2}_{11}$	-1.058570538606602e-008	-4.234282230700323e-008	-1.693712891459849e-007
$\Omega^{0,2}_{12}$	-5.813861165777252e-011	-2.325552130724581e-010	-9.302216554492291e-010
$\Omega^{0,2}_{13}$	2.710265897197415e-013	1.083047560804446e-012	4.332824906909346e-012
$\Omega^{0,2}_{14}$	2.354102626208739e-016	-1.428257943608805e-016	-1.073286815161846e-015

Table 21: Two term connection at $N=16,\ d_1=0,\ d_2=2$ and different j

	$j=3,\ N=16$	$j=4,\ N=16$	$j=5,\ N=16$
$\Omega^{0,2}_{-14}$	-6.430865232832079e-015	1.897813205243266e-014	-1.421520082319231e-014
$\Omega^{0,2}_{-13}$	1.733011347277772e-011	6.932382510470170e-011	2.772514675785338e-010
$\Omega^{0,2}_{-12}$	-3.720875252483431e-009	-1.488353836402891e-008	-5.953444351341502e-008
$\Omega^{0,2}_{-11}$	-6.774851549268767e-007	-2.709940618597296e-006	-1.083976250349363e-005
$\Omega^{0,2}_{-10}$	-2.382768837599288e-005	-9.531075357703401e-005	-3.812430128467083e-004
$\Omega^{0,2}_{-9}$	1.337871036988788e-004	5.351484147965492e-004	2.140593659131520e-003
$\Omega^{0,2}_{-8}$	-1.534866255634000e-003	-6.139465022574630e-003	-2.455786009083434e-002
$\Omega^{0,2}_{-7}$	2.890746898397288e-002	1.156298759360733e-001	4.625195037439536e-001
$\Omega^{0,2}_{-6}$	-2.622500411792560e-001	-1.049000164717136e+000	-4.196000658870219e+000
$\Omega^{0,2}_{-5}$	1.412498680628531e+000	5.649994722513906e+000	2.259997889006128e+001
$\Omega^{0,2}_{-4}$	-5.265049598349354e+000	-2.106019839339830e+001	-8.424079357359062e+001
$\Omega^{0,2}_{-3}$	1.517939572578404e+001	6.071758290314003e+001	2.428703316125345e+002
$\Omega^{0,2}_{-2}$	-3.939930537964776e+001	-1.575972215186051e+002	-6.303888860743228e+002
$\Omega^{0,2}_{-1}$	1.420253820090306e+002	5.681015280361482e+002	2.272406112144414e+003
$\Omega^{0,2}_{0}$	-2.274363065544447e+002	-9.097452262177873e+002	-3.638980904871088e+003
$\Omega^{0,2}_{1}$	1.420253820090329e+002	5.681015280361170e+002	2.272406112144568e+003
$\Omega^{0,2}_{2}$	-3.939930537964922e+001	-1.575972215185858e+002	-6.303888860744203e+002
$\Omega^{0,2}_{3}$	1.517939572578460e+001	6.071758290313523e+001	2.428703316125626e+002
$\Omega^{0,2}_{4}$	-5.265049598349678e+000	-2.106019839339759e+001	-8.424079357359798e+001
$\Omega^{0,2}_{5}$	1.412498680628661e+000	5.649994722514461e+000	2.259997889005910e+001
$\Omega^{0,2}_{6}$	-2.622500411792894e-001	-1.049000164717085e+000	-4.196000658868997e+000
$\Omega^{0,2}_{7}$	2.890746898399916e-002	1.156298759360413e-001	4.625195037438571e-001
$\Omega^{0,2}_{8}$	-1.534866255685811e-003	-6.139465022738140e-003	-2.455786009098188e-002
$\Omega^{0,2}_{9}$	1.337871036980203e-004	5.351484148009024e-004	2.140593659174635e-003
$\Omega^{0,2}_{10}$	-2.382768835027504e-005	-9.531075340004174e-005	-3.812430136155573e-004
$\Omega^{0,2}_{11}$	-6.774851551344431e-007	-2.709940616914608e-006	-1.083976250707321e-005
$\Omega^{0,2}_{12}$	-3.720883006473321e-009	-1.488352700342403e-008	-5.953416982463951e-008
$\Omega^{0,2}_{13}$	1.733114870963507e-011	6.933016894667235e-011	2.772693901509178e-010
$\Omega^{0,2}_{14}$	-9.863396946603916e-017	3.929253139294437e-015	-3.462184090075471e-014

Table 22: Two term connection at $N=16,\ d_1=0,\ d_2=2$ and different j

	$j=6,\ N=16$	$j=7,\ N=16$	$j=8,\ N=16$
$\Omega^{0,2}_{-14}$	-2.643303228421481e-013	-2.214815803650501e-013	-1.104271249411186e-012
$\Omega^{0,2}_{-13}$	1.109179004604097e-009	4.436836856803815e-009	1.774416780106512e-008
$\Omega^{0,2}_{-12}$	-2.381359513091238e-007	-9.525463495315582e-007	-3.810194604444282e-006
$\Omega^{0,2}_{-11}$	-4.335904993721131e-005	-1.734361998399463e-004	-6.937448008868793e-004
$\Omega^{0,2}_{-10}$	-1.524972051988884e-003	-6.099888213422666e-003	-2.439955285757138e-002
$\Omega^{0,2}_{-9}$	8.562374636624036e-003	3.424949854722228e-002	1.369979941849385e-001
$\Omega^{0,2}_{-8}$	-9.823144036782526e-002	-3.929257614609567e-001	-1.571703045789018e+000
$\Omega^{0,2}_{-7}$	1.850078014975232e+000	7.400312059904473e+000	2.960124823961027e+001
$\Omega^{0,2}_{-6}$	-1.678400263547242e+001	-6.713601054189937e+001	-2.685440421676483e+002
$\Omega^{0,2}_{-5}$	9.039991556024404e+001	3.615996622409519e+002	1.446398648963774e+003
$\Omega^{0,2}_{-4}$	-3.369631742943917e+002	-1.347852697177512e+003	-5.391410788709776e+003
$\Omega^{0,2}_{-3}$	9.714813264502061e+002	3.885925305800781e+003	1.554370122320259e+004
$\Omega^{0,2}_{-2}$	-2.521555544297473e+003	-1.008622217718989e+004	-4.034488870875826e+004
$\Omega^{0,2}_{-1}$	9.089624448577923e+003	3.635849779431179e+004	1.454339911772456e+005
$\Omega^{0,2}_{0}$	-1.455592361948433e+004	-5.822369447793745e+004	-2.328947779117510e+005
$\Omega^{0,2}_{1}$	9.089624448577995e+003	3.635849779431208e+004	1.454339911772511e+005
$\Omega^{0,2}_{2}$	-2.521555544297512e+003	-1.008622217719007e+004	-4.034488870876178e+004
$\Omega^{0,2}_{3}$	9.714813264502005e+002	3.885925305800811e+003	1.554370122320371e+004
$\Omega^{0,2}_{4}$	-3.369631742943744e+002	-1.347852697177499e+003	-5.391410788710167e+003
$\Omega^{0,2}_{5}$	9.039991556023291e+001	3.615996622409337e+002	1.446398648963758e+003
$\Omega^{0,2}_{6}$	-1.678400263547400e+001	-6.713601054189819e+001	-2.685440421675962e+002
$\Omega^{0,2}_{7}$	1.850078014975881e+000	7.400312059904264e+000	2.960124823960967e+001
$\Omega^{0,2}_{8}$	-9.823144036392971e-002	-3.929257614552836e-001	-1.571703045824285e+000
$\Omega^{0,2}_{9}$	8.562374636688602e-003	3.424949854686245e-002	1.369979941875777e-001
$\Omega^{0,2}_{10}$	-1.524972054454305e-003	-6.099888217548274e-003	-2.439955287258221e-002
$\Omega^{0,2}_{11}$	-4.335904994497258e-005	-1.734361998786672e-004	-6.937447998477694e-004
$\Omega^{0,2}_{12}$	-2.381364777395823e-007	-9.525460875436087e-007	-3.810184513151683e-006
$\Omega^{0,2}_{13}$	1.109239707299676e-009	4.436563873418627e-009	1.774757790238731e-008
$\Omega^{0,2}_{14}$	-1.019233313044627e-013	-2.405024925524931e-014	-2.790263323189326e-012

Table 23: Two term connection at $N=16,\ d_1=0,\ d_2=2$ and different j

	$j=9,\ N=16$	$j=10,\ N=16$	$j=11,\ N=16$
$\Omega^{0,2}_{-14}$	7.551037005846955e-012	-2.920170671107247e-011	-1.290348394267641e-010
$\Omega^{0,2}_{-13}$	7.098787147611045e-008	2.839180552136943e-007	1.135726982016560e-006
$\Omega^{0,2}_{-12}$	-1.524075800899198e-005	-6.096313414043894e-005	-2.438515059316123e-004
$\Omega^{0,2}_{-11}$	-2.774979195702157e-003	-1.109991679168744e-002	-4.439966710182935e-002
$\Omega^{0,2}_{-10}$	-9.759821155684499e-002	-3.903928455658621e-001	-1.561571382373987e+000
$\Omega^{0,2}_{-9}$	5.479919767425753e-001	2.191967907017031e+000	8.767871627843451e+000
$\Omega^{0,2}_{-8}$	-6.286812183180321e+000	-2.514724873288658e+001	-1.005889949340979e+002
$\Omega^{0,2}_{-7}$	1.184049929584994e+002	4.736199718337545e+002	1.894479887334948e+003
$\Omega^{0,2}_{-6}$	-1.074176168670433e+003	-4.296704674682432e+003	-1.718681869872476e+004
$\Omega^{0,2}_{-5}$	5.785594595854648e+003	2.314237838342118e+004	9.256951353368387e+004
$\Omega^{0,2}_{-4}$	-2.156564315483984e+004	-8.626257261935688e+004	-3.450502904774413e+005
$\Omega^{0,2}_{-3}$	6.217480489281385e+004	2.486992195712398e+005	9.947968782849874e+005
$\Omega^{0,2}_{-2}$	-1.613795548350452e+005	-6.455182193401243e+005	-2.582072877360562e+006
$\Omega^{0,2}_{-1}$	5.817359647090040e+005	2.326943858835907e+006	9.307775435343744e+006
$\Omega^{0,2}_{0}$	-9.315791116470114e+005	-3.726316446587991e+006	-1.490526578635202e+007
$\Omega^{0,2}_{1}$	5.817359647089910e+005	2.326943858836005e+006	9.307775435343994e+006
$\Omega^{0,2}_{2}$	-1.613795548350372e+005	-6.455182193401873e+005	-2.582072877360716e+006
$\Omega^{0,2}_{3}$	6.217480489281201e+004	2.486992195712584e+005	9.947968782850248e+005
$\Omega^{0,2}_{4}$	-2.156564315483968e+004	-8.626257261936225e+004	-3.450502904774463e+005
$\Omega^{0,2}_{5}$	5.785594595854924e+003	2.314237838342007e+004	9.256951353368003e+004
$\Omega^{0,2}_{6}$	-1.074176168670345e+003	-4.296704674681576e+003	-1.718681869872648e+004
$\Omega^{0,2}_{7}$	1.184049929584814e+002	4.736199718337445e+002	1.894479887335277e+003
$\Omega^{0,2}_{8}$	-6.286812183284223e+000	-2.514724873312776e+001	-1.005889949326440e+002
$\Omega^{0,2}_{9}$	5.479919767545959e-001	2.191967906991213e+000	8.767871627961164e+000
$\Omega^{0,2}_{10}$	-9.759821147940240e-002	-3.903928459566537e-001	-1.561571383746130e+000
$\Omega^{0,2}_{11}$	-2.774979194170024e-003	-1.109991679492958e-002	-4.439966718504985e-002
$\Omega^{0,2}_{12}$	-1.524073472109326e-005	-6.096293772827238e-005	-2.438518747931637e-004
$\Omega^{0,2}_{13}$	7.098790053280857e-008	2.839094051733652e-007	1.135756450302380e-006
$\Omega^{0,2}_{14}$	1.177418225985876e-012	-1.559153055245662e-011	-5.949704395952573e-011

Table 24: Two term connection at $N=16,\ d_1=0,\ d_2=2$ and different j

	$j=0,\ N=6$	$j=1,\ N=6$	$j=2,\ N=6$
$\Omega_{-4}^{0,1}$	-3.424657534244847e-004	-6.849315068494171e-004	-1.369863013698808e-003
$\Omega_{-3}^{0,1}$	-1.461187214611888e-002	-2.922374429223750e-002	-5.844748858447520e-002
$\Omega_{-2}^{0,1}$	1.452054794520550e-001	2.904109589041092e-001	5.808219178082186e-001
$\Omega_{-1}^{0,1}$	-7.452054794520550e-001	-1.490410958904109e+000	-2.980821917808222e+000
$\Omega_{0}^{0,1}$	-2.580266458986246e-015	1.269579863612015e-015	1.170252996448804e-014
$\Omega_{1}^{0,1}$	7.452054794520563e-001	1.490410958904108e+000	2.980821917808211e+000
$\Omega_{2}^{0,1}$	-1.452054794520550e-001	-2.904109589041092e-001	-5.808219178082179e-001
$\Omega_{3}^{0,1}$	1.461187214611873e-002	2.922374429223722e-002	5.844748858447472e-002
$\Omega_{4}^{0,1}$	3.424657534247128e-004	6.849315068494664e-004	1.369863013698641e-003

Table 25: Two term connection at $N=6,\ d_1=0,\ d_2=1$ and different j

	$j=3,\ N=6$	$j=4,\ N=6$	$j=5,\ N=6$
$\Omega_{-4}^{0,1}$	-2.739726027397891e-003	-5.479452054795143e-003	-1.095890410959065e-002
$\Omega_{-3}^{0,1}$	-1.168949771689486e-001	-2.337899543379004e-001	-4.675799086757952e-001
$\Omega_{-2}^{0,1}$	1.161643835616436e+000	2.323287671232873e+000	4.646575342465741e+000
$\Omega_{-1}^{0,1}$	-5.961643835616424e+000	-1.192328767123287e+001	-2.384657534246569e+001
$\Omega_{0}^{0,1}$	-1.499004750799484e-014	2.227680767978787e-014	-5.179881449458651e-014
$\Omega_{1}^{0,1}$	5.961643835616441e+000	1.192328767123285e+001	2.384657534246574e+001
$\Omega_{2}^{0,1}$	-1.161643835616437e+000	-2.323287671232870e+000	-4.646575342465746e+000
$\Omega_{3}^{0,1}$	1.168949771689510e-001	2.337899543378956e-001	4.675799086758059e-001
$\Omega_{4}^{0,1}$	2.739726027397371e-003	5.479452054797154e-003	1.095890410958777e-002

Table 26: Two term connection at $N=6,\ d_1=0,\ d_2=1$ and different j

	$j=6,\ N=6$	$j=7,\ N=6$	$j=8,\ N=6$
$\Omega_{-4}^{0,1}$	-2.191780821917990e-002	-4.383561643836622e-002	-8.767123287674131e-002
$\Omega_{-3}^{0,1}$	-9.351598173516031e-001	-1.870319634703213e+000	-3.740639269406386e+000
$\Omega_{-2}^{0,1}$	9.293150684931502e+000	1.858630136986300e+001	3.717260273972597e+001
$\Omega_{-1}^{0,1}$	-4.769315068493156e+001	-9.538630136986313e+001	-1.907726027397260e+002
$\Omega_{0}^{0,1}$	1.400247505457093e-013	3.523867193710038e-013	1.842622247494781e-013
$\Omega_{1}^{0,1}$	4.769315068493143e+001	9.538630136986282e+001	1.907726027397259e+002
$\Omega_{2}^{0,1}$	-9.293150684931497e+000	-1.858630136986299e+001	-3.717260273972601e+001
$\Omega_{3}^{0,1}$	9.351598173516045e-001	1.870319634703193e+000	3.740639269406429e+000
$\Omega_{4}^{0,1}$	2.191780821917412e-002	4.383561643835246e-002	8.767123287669129e-002

Table 27: Two term connection at $N=6,\ d_1=0,\ d_2=1$ and different j

	$j=9,\ N=6$	$j=10,\ N=6$	$j=11,\ N=6$
$\Omega_{-4}^{0,1}$	-1.753424657534592e-001	-3.506849315068540e-001	-7.013698630137928e-001
$\Omega_{-3}^{0,1}$	-7.481278538812837e+000	-1.496255707762563e+001	-2.992511415525104e+001
$\Omega_{-2}^{0,1}$	7.434520547945201e+001	1.486904109589039e+002	2.973808219178075e+002
$\Omega_{-1}^{0,1}$	-3.815452054794526e+002	-7.630904109589034e+002	-1.526180821917806e+003
$\Omega_{0}^{0,1}$	1.577602130184808e-012	2.530817623787548e-013	1.386710361021475e-012
$\Omega_{1}^{0,1}$	3.815452054794512e+002	7.630904109589035e+002	1.526180821917805e+003
$\Omega_{2}^{0,1}$	-7.434520547945193e+001	-1.486904109589038e+002	-2.973808219178076e+002
$\Omega_{3}^{0,1}$	7.481278538812731e+000	1.496255707762548e+001	2.992511415525115e+001
$\Omega_{4}^{0,1}$	1.753424657534483e-001	3.506849315069668e-001	7.013698630137033e-001

Table 28: Two term connection at $N=6,\ d_1=0,\ d_2=1$ and different j

	$j=0,\ N=8$	$j=1,\ N=8$	$j=2,\ N=8$
$\Omega_{-6}^{0,1}$	-8.408505370743570e-007	-1.681701074185182e-006	-3.363402148587037e-006
$\Omega_{-5}^{0,1}$	1.722061900053109e-004	3.444123800106526e-004	6.888247600212938e-004
$\Omega_{-4}^{0,1}$	2.224049670722979e-003	4.448099341445886e-003	8.896198682891706e-003
$\Omega_{-3}^{0,1}$	-3.358020705103609e-002	-6.716041410207226e-002	-1.343208282041450e-001
$\Omega_{-2}^{0,1}$	1.919989707989422e-001	3.839979415978848e-001	7.679958831957694e-001
$\Omega_{-1}^{0,1}$	-7.930095049744685e-001	-1.586019009948939e+000	-3.172038019897884e+000
$\Omega_{0}^{0,1}$	-5.526808655122328e-015	-9.499709280070580e-015	-2.882319835704930e-015
$\Omega_{1}^{0,1}$	7.930095049744733e-001	1.586019009948947e+000	3.172038019897884e+000
$\Omega_{2}^{0,1}$	-1.919989707989423e-001	-3.839979415978851e-001	-7.679958831957692e-001
$\Omega_{3}^{0,1}$	3.358020705103645e-002	6.716041410207291e-002	1.343208282041452e-001
$\Omega_{4}^{0,1}$	-2.224049670722941e-003	-4.448099341445797e-003	-8.896198682891706e-003
$\Omega_{5}^{0,1}$	-1.722061900050692e-004	-3.444123800105677e-004	-6.888247600212200e-004
$\Omega_{6}^{0,1}$	8.408505370934272e-007	1.681701074416322e-006	3.363402148683573e-006

Table 29: Two term connection at $N=8,\ d_1=0,\ d_2=1$ and different j

	$j=3,\ N=8$	$j=4,\ N=8$	$j=5,\ N=8$
$\Omega_{-6}^{0,1}$	-6.726804297145255e-006	-1.345360859426572e-005	-2.690721718865060e-005
$\Omega_{-5}^{0,1}$	1.377649520042688e-003	2.755299040085112e-003	5.510598080170548e-003
$\Omega_{-4}^{0,1}$	1.779239736578324e-002	3.558479473156773e-002	7.116958946313103e-002
$\Omega_{-3}^{0,1}$	-2.686416564082901e-001	-5.372833128165802e-001	-1.074566625633161e+000
$\Omega_{-2}^{0,1}$	1.535991766391540e+000	3.071983532783081e+000	6.143967065566161e+000
$\Omega_{-1}^{0,1}$	-6.344076039795772e+000	-1.268815207959155e+001	-2.537630415918313e+001
$\Omega_{0}^{0,1}$	-3.680793296229343e-015	9.973476745655034e-015	4.244684391948051e-014
$\Omega_{1}^{0,1}$	6.344076039795776e+000	1.268815207959154e+001	2.537630415918308e+001
$\Omega_{2}^{0,1}$	-1.535991766391540e+000	-3.071983532783079e+000	-6.143967065566161e+000
$\Omega_{3}^{0,1}$	2.686416564082905e-001	5.372833128165800e-001	1.074566625633159e+000
$\Omega_{4}^{0,1}$	-1.779239736578353e-002	-3.558479473156664e-002	-7.116958946313297e-002
$\Omega_{5}^{0,1}$	-1.377649520042484e-003	-2.755299040084932e-003	-5.510598080170267e-003
$\Omega_{6}^{0,1}$	6.726804297206082e-006	1.345360859416071e-005	2.690721718766981e-005

Table 30: Two term connection at $N=8,\ d_1=0,\ d_2=1$ and different j

	$j=6,\ N=8$	$j=7,\ N=8$	$j=8,\ N=8$
$\Omega_{-6}^{0,1}$	-5.381443437637813e-005	-1.076288687547044e-004	-2.152577375128900e-004
$\Omega_{-5}^{0,1}$	1.102119616034110e-002	2.204239232067915e-002	4.408478464136526e-002
$\Omega_{-4}^{0,1}$	1.423391789262624e-001	2.846783578525270e-001	5.693567157050568e-001
$\Omega_{-3}^{0,1}$	-2.149133251266320e+000	-4.298266502532643e+000	-8.596533005065291e+000
$\Omega_{-2}^{0,1}$	1.228793413113231e+001	2.457586826226461e+001	4.915173652452928e+001
$\Omega_{-1}^{0,1}$	-5.075260831836621e+001	-1.015052166367323e+002	-2.030104332734649e+002
$\Omega_{0}^{0,1}$	9.279286054895763e-014	4.780816005404218e-014	1.111912956398615e-013
$\Omega_{1}^{0,1}$	5.075260831836612e+001	1.015052166367323e+002	2.030104332734646e+002
$\Omega_{2}^{0,1}$	-1.228793413113231e+001	-2.457586826226463e+001	-4.915173652452927e+001
$\Omega_{3}^{0,1}$	2.149133251266317e+000	4.298266502532641e+000	8.596533005065284e+000
$\Omega_{4}^{0,1}$	-1.423391789262668e-001	-2.846783578525379e-001	-5.693567157050737e-001
$\Omega_{5}^{0,1}$	-1.102119616033992e-002	-2.204239232067903e-002	-4.408478464136004e-002
$\Omega_{6}^{0,1}$	5.381443437562496e-005	1.076288687544133e-004	2.152577375080155e-004

Table 31: Two term connection at $N=8,\ d_1=0,\ d_2=1$ and different j

	$j=9,\ N=8$	$j=10,\ N=8$	$j=11,\ N=8$
$\Omega_{-6}^{0,1}$	-4.305154750201835e-004	-8.610309500378567e-004	-1.722061900081141e-003
$\Omega_{-5}^{0,1}$	8.816956928271635e-002	1.763391385654493e-001	3.526782771308876e-001
$\Omega_{-4}^{0,1}$	1.138713431410138e+000	2.277426862820325e+000	4.554853725640538e+000
$\Omega_{-3}^{0,1}$	-1.719306601013058e+001	-3.438613202026111e+001	-6.877226404052226e+001
$\Omega_{-2}^{0,1}$	9.830347304905857e+001	1.966069460981170e+002	3.932138921962338e+002
$\Omega_{-1}^{0,1}$	-4.060208665469297e+002	-8.120417330938581e+002	-1.624083466187717e+003
$\Omega_{0}^{0,1}$	4.865058701158801e-013	-5.284185955124391e-013	-4.225487654003048e-013
$\Omega_{1}^{0,1}$	4.060208665469291e+002	8.120417330938589e+002	1.624083466187717e+003
$\Omega_{2}^{0,1}$	-9.830347304905855e+001	-1.966069460981170e+002	-3.932138921962340e+002
$\Omega_{3}^{0,1}$	1.719306601013055e+001	3.438613202026117e+001	6.877226404052229e+001
$\Omega_{4}^{0,1}$	-1.138713431410146e+000	-2.277426862820293e+000	-4.554853725640611e+000
$\Omega_{5}^{0,1}$	-8.816956928271781e-002	-1.763391385654292e-001	-3.526782771308567e-001
$\Omega_{6}^{0,1}$	4.305154750139888e-004	8.610309500521470e-004	1.722061900075186e-003

Table 32: Two term connection at $N=8,\ d_1=0,\ d_2=1$ and different j

	$j=0,\ N=10$	$j=1,\ N=10$	$j=2,\ N=10$
$\Omega_{-8}^{0,1}$	-2.696049513624955e-010	-5.392095888751848e-010	-1.078419669048528e-009
$\Omega_{-7}^{0,1}$	-2.524117113307028e-007	-5.048234227969769e-007	-1.009646845024442e-006
$\Omega_{-6}^{0,1}$	-5.404730164465636e-005	-1.080946032895173e-004	-2.161892065789329e-004
$\Omega_{-5}^{0,1}$	-2.392358200238082e-004	-4.784716400478805e-004	-9.569432800979131e-004
$\Omega_{-4}^{0,1}$	7.461396365775579e-003	1.492279273155188e-002	2.984558546310373e-002
$\Omega_{-3}^{0,1}$	-5.335257193267418e-002	-1.067051438653493e-001	-2.134102877307007e-001
$\Omega_{-2}^{0,1}$	2.288201870669558e-001	4.576403741339125e-001	9.152807482678232e-001
$\Omega_{-1}^{0,1}$	-8.259060118501859e-001	-1.651812023700376e+000	-3.303624047400773e+000
$\Omega_{0}^{0,1}$	2.062032995977524e-017	5.850954037754273e-015	8.066416953436720e-014
$\Omega_{1}^{0,1}$	8.259060118501861e-001	1.651812023700371e+000	3.303624047400705e+000
$\Omega_{2}^{0,1}$	-2.288201870669560e-001	-4.576403741339123e-001	-9.152807482678218e-001
$\Omega_{3}^{0,1}$	5.335257193267442e-002	1.067051438653487e-001	2.134102877306953e-001
$\Omega_{4}^{0,1}$	-7.461396365775853e-003	-1.492279273155184e-002	-2.984558546310492e-002
$\Omega_{5}^{0,1}$	2.392358200238775e-004	4.784716400478782e-004	9.569432800953953e-004
$\Omega_{6}^{0,1}$	5.404730164482921e-005	1.080946032895151e-004	2.161892065788593e-004
$\Omega_{7}^{0,1}$	2.524117111385085e-007	5.048234223693013e-007	1.009646845229118e-006
$\Omega_{8}^{0,1}$	2.696049654842978e-010	5.392097896509548e-010	1.078418667938476e-009

Table 33: Two term connection at $N=10,\ d_1=0,\ d_2=1$ and different j

	$j=3,\ N=10$	$j=4,\ N=10$	$j=5,\ N=10$
$\Omega_{-8}^{0,1}$	-2.156839029812038e-009	-4.313677415298035e-009	-8.627349408720405e-009
$\Omega_{-7}^{0,1}$	-2.019293690395968e-006	-4.038587381290359e-006	-8.077174763059951e-006
$\Omega_{-6}^{0,1}$	-4.323784131592555e-004	-8.647568263171378e-004	-1.729513652633565e-003
$\Omega_{-5}^{0,1}$	-1.913886560191572e-003	-3.827773120383501e-003	-7.655546240751445e-003
$\Omega_{-4}^{0,1}$	5.969117092620609e-002	1.193823418524131e-001	2.387646837048335e-001
$\Omega_{-3}^{0,1}$	-4.268205754614011e-001	-8.536411509227972e-001	-1.707282301845568e+000
$\Omega_{-2}^{0,1}$	1.830561496535652e+000	3.661122993071298e+000	7.322245986142621e+000
$\Omega_{-1}^{0,1}$	-6.607248094801546e+000	-1.321449618960303e+001	-2.642899237920577e+001
$\Omega_{0}^{0,1}$	1.158374177605779e-013	1.400922789672790e-013	-6.967185323646469e-013
$\Omega_{1}^{0,1}$	6.607248094801447e+000	1.321449618960292e+001	2.642899237920634e+001
$\Omega_{2}^{0,1}$	-1.830561496535649e+000	-3.661122993071294e+000	-7.322245986142624e+000
$\Omega_{3}^{0,1}$	4.268205754613932e-001	8.536411509227873e-001	1.707282301845611e+000
$\Omega_{4}^{0,1}$	-5.969117092620942e-002	-1.193823418524172e-001	-2.387646837048184e-001
$\Omega_{5}^{0,1}$	1.913886560191089e-003	3.827773120382484e-003	7.655546240766035e-003
$\Omega_{6}^{0,1}$	4.323784131572361e-004	8.647568263167217e-004	1.729513652635492e-003
$\Omega_{7}^{0,1}$	2.019293691413277e-006	4.038587377894723e-006	8.077174763077405e-006
$\Omega_{8}^{0,1}$	2.156836913690272e-009	4.313677054838900e-009	8.627358455766487e-009

Table 34: Two term connection at $N=10,\ d_1=0,\ d_2=1$ and different j

	$j=6,\ N=10$	$j=7,\ N=10$	$j=8,\ N=10$
$\Omega^{0,1}_{-8}$	-1.725471494132981e-008	-3.450942913576917e-008	-6.901885040700357e-008
$\Omega^{0,1}_{-7}$	-1.615434952040001e-005	-3.230869904435612e-005	-6.461739809218302e-005
$\Omega^{0,1}_{-6}$	-3.459027305265731e-003	-6.918054610522556e-003	-1.383610922105838e-002
$\Omega^{0,1}_{-5}$	-1.531109248155757e-002	-3.062218496312441e-002	-6.124436992622660e-002
$\Omega^{0,1}_{-4}$	4.775293674096536e-001	9.550587348193060e-001	1.910117469638619e+000
$\Omega^{0,1}_{-3}$	-3.414564603691221e+000	-6.829129207382422e+000	-1.365825841476485e+001
$\Omega^{0,1}_{-2}$	1.464449197228521e+001	2.928898394457037e+001	5.857796788914070e+001
$\Omega^{0,1}_{-1}$	-5.285798475841255e+001	-1.057159695168249e+002	-2.114319390336496e+002
$\Omega^{0,1}_{0}$	1.467212498638750e-012	2.879800469857873e-012	5.664922102075400e-012
$\Omega^{0,1}_{1}$	5.285798475841135e+001	1.057159695168225e+002	2.114319390336450e+002
$\Omega^{0,1}_{2}$	-1.464449197228518e+001	-2.928898394457032e+001	-5.857796788914061e+001
$\Omega^{0,1}_{3}$	3.414564603691130e+000	6.829129207382251e+000	1.365825841476447e+001
$\Omega^{0,1}_{4}$	-4.775293674096900e-001	-9.550587348193730e-001	-1.910117469638723e+000
$\Omega^{0,1}_{5}$	1.531109248153117e-002	3.062218496305587e-002	6.124436992611188e-002
$\Omega^{0,1}_{6}$	3.459027305261825e-003	6.918054610532298e-003	1.383610922103628e-002
$\Omega^{0,1}_{7}$	1.615434951564792e-005	3.230869902348481e-005	6.461739807311245e-005
$\Omega^{0,1}_{8}$	1.725469700276301e-008	3.450939927728653e-008	6.901879574515332e-008

Table 35: Two term connection at $N=10,\ d_1=0,\ d_2=1$ and different j

	$j=9,\ N=10$	$j=10,\ N=10$	$j=11,\ N=10$
$\Omega^{0,1}_{-8}$	-1.380375917867597e-007	-2.760752722587007e-007	-5.521507381460003e-007
$\Omega^{0,1}_{-7}$	-1.292347962219340e-004	-2.584695923951555e-004	-5.169391846133784e-004
$\Omega^{0,1}_{-6}$	-2.767221844206842e-002	-5.534443688417550e-002	-1.106888737682619e-001
$\Omega^{0,1}_{-5}$	-1.224887398521174e-001	-2.449774797046592e-001	-4.899549594103688e-001
$\Omega^{0,1}_{-4}$	3.820234939277341e+000	7.640469878554662e+000	1.528093975710940e+001
$\Omega^{0,1}_{-3}$	-2.731651682952901e+001	-5.463303365905875e+001	-1.092660673181187e+002
$\Omega^{0,1}_{-2}$	1.171559357782817e+002	2.343118715565631e+002	4.686237431131259e+002
$\Omega^{0,1}_{-1}$	-4.228638780672918e+002	-8.457277561345908e+002	-1.691455512269195e+003
$\Omega^{0,1}_{0}$	-1.067978662149538e-011	9.987827418797017e-013	3.655008755470717e-011
$\Omega^{0,1}_{1}$	4.228638780673005e+002	8.457277561345904e+002	1.691455512269164e+003
$\Omega^{0,1}_{2}$	-1.171559357782819e+002	-2.343118715565630e+002	-4.686237431131252e+002
$\Omega^{0,1}_{3}$	2.731651682952976e+001	5.463303365905870e+001	1.092660673181163e+002
$\Omega^{0,1}_{4}$	-3.820234939277085e+000	-7.640469878554626e+000	-1.528093975710974e+001
$\Omega^{0,1}_{5}$	1.224887398522411e-001	2.449774797045203e-001	4.899549594089175e-001
$\Omega^{0,1}_{6}$	2.767221844211033e-002	5.534443688436032e-002	1.106888737682778e-001
$\Omega^{0,1}_{7}$	1.292347963974198e-004	2.584695921032656e-004	5.169391849517267e-004
$\Omega^{0,1}_{8}$	1.380376417130166e-007	2.760754130758060e-007	5.521502103934498e-007

Table 36: Two term connection at $N=10,\ d_1=0,\ d_2=1$ and different j

	$j=0,\ N=12$	$j=1,\ N=12$	$j=2,\ N=12$
$\Omega_{-10}^{0,1}$	6.968102061150500e-013	1.393671723150309e-012	2.787685940467265e-012
$\Omega_{-9}^{0,1}$	-2.899666654226089e-009	-5.799333367477154e-009	-1.159866734500792e-008
$\Omega_{-8}^{0,1}$	4.206912046409758e-007	8.413824091421626e-007	1.682764817486590e-006
$\Omega_{-7}^{0,1}$	1.202657519585258e-005	2.405315039148907e-005	4.810630078300360e-005
$\Omega_{-6}^{0,1}$	4.296891570946732e-006	8.593783141464923e-006	1.718756628401881e-005
$\Omega_{-5}^{0,1}$	-1.588561543475901e-003	-3.177123086951281e-003	-6.354246173903122e-003
$\Omega_{-4}^{0,1}$	1.454551104199443e-002	2.909102208398829e-002	5.818204416797410e-002
$\Omega_{-3}^{0,1}$	-7.244058999766312e-002	-1.448811799953269e-001	-2.897623599906539e-001
$\Omega_{-2}^{0,1}$	2.585529441414751e-001	5.171058882829496e-001	1.034211776565901e+000
$\Omega_{-1}^{0,1}$	-8.501366615559489e-001	-1.700273323111905e+000	-3.400546646223837e+000
$\Omega_{0}^{0,1}$	-1.771531943484048e-014	-9.397701065441274e-015	3.189910223544962e-014
$\Omega_{1}^{0,1}$	8.501366615559639e-001	1.700273323111913e+000	3.400546646223813e+000
$\Omega_{2}^{0,1}$	-2.585529441414753e-001	-5.171058882829498e-001	-1.034211776565901e+000
$\Omega_{3}^{0,1}$	7.244058999766427e-002	1.448811799953273e-001	2.897623599906528e-001
$\Omega_{4}^{0,1}$	-1.454551104199388e-002	-2.909102208398797e-002	-5.818204416797575e-002
$\Omega_{5}^{0,1}$	1.588561543476083e-003	3.177123086951924e-003	6.354246173902477e-003
$\Omega_{6}^{0,1}$	-4.296891570917664e-006	-8.593783141911318e-006	-1.718756628367386e-005
$\Omega_{7}^{0,1}$	-1.202657519569253e-005	-2.405315039116234e-005	-4.810630078303700e-005
$\Omega_{8}^{0,1}$	-4.206912045171942e-007	-8.413824091943564e-007	-1.682764818798538e-006
$\Omega_{9}^{0,1}$	2.899666853418460e-009	5.799333632051729e-009	1.159866819379381e-008
$\Omega_{10}^{0,1}$	-6.968413855754819e-013	-1.393485636746043e-012	-2.788339218165746e-012

Table 37: Two term connection at $N=12,\ d_1=0,\ d_2=1$ and different j

	$j=3,\ N=12$	$j=4,\ N=12$	$j=5,\ N=12$
$\Omega^{0,1}_{-10}$	5.574496614888726e-012	1.115377020866846e-011	2.229965654981504e-011
$\Omega^{0,1}_{-9}$	-2.319733439946490e-008	-4.639466614937414e-008	-9.278934078712447e-008
$\Omega^{0,1}_{-8}$	3.365529637182767e-006	6.731059270956813e-006	1.346211854493656e-005
$\Omega^{0,1}_{-7}$	9.621260156601985e-005	1.924252031329031e-004	3.848504062630691e-004
$\Omega^{0,1}_{-6}$	3.437513256763476e-005	6.875026512463018e-005	1.375005302649743e-004
$\Omega^{0,1}_{-5}$	-1.270849234780765e-002	-2.541698469559886e-002	-5.083396939123046e-002
$\Omega^{0,1}_{-4}$	1.163640883359540e-001	2.327281766718988e-001	4.654563533438043e-001
$\Omega^{0,1}_{-3}$	-5.795247199813072e-001	-1.159049439962619e+000	-2.318098879925254e+000
$\Omega^{0,1}_{-2}$	2.068423553131800e+000	4.136847106263601e+000	8.273694212527209e+000
$\Omega^{0,1}_{-1}$	-6.801093292447624e+000	-1.360218658489527e+001	-2.720437316979078e+001
$\Omega^{0,1}_{0}$	-5.461996944086902e-014	1.466671462891199e-014	4.963300421700580e-013
$\Omega^{0,1}_{1}$	6.801093292447667e+000	1.360218658489525e+001	2.720437316979038e+001
$\Omega^{0,1}_{2}$	-2.068423553131800e+000	-4.136847106263594e+000	-8.273694212527195e+000
$\Omega^{0,1}_{3}$	5.795247199813085e-001	1.159049439962612e+000	2.318098879925202e+000
$\Omega^{0,1}_{4}$	-1.163640883359506e-001	-2.327281766719060e-001	-4.654563533437987e-001
$\Omega^{0,1}_{5}$	1.270849234780771e-002	2.541698469561734e-002	5.083396939121575e-002
$\Omega^{0,1}_{6}$	-3.437513256813831e-005	-6.875026513607995e-005	-1.375005302733390e-004
$\Omega^{0,1}_{7}$	-9.621260156592389e-005	-1.924252031338556e-004	-3.848504062644134e-004
$\Omega^{0,1}_{8}$	-3.365529635703508e-006	-6.731059272749183e-006	-1.346211854686139e-005
$\Omega^{0,1}_{9}$	2.319733460260197e-008	4.639466953672927e-008	9.278934499315327e-008
$\Omega^{0,1}_{10}$	-5.574606906675431e-012	-1.114879845632270e-011	-2.230719155450397e-011

Table 38: Two term connection at $N=12,\ d_1=0,\ d_2=1$ and different j

	$j=6,\ N=12$	$j=7,\ N=12$	$j=8,\ N=12$
$\Omega^{0,1}_{-10}$	4.460008150691497e-011	8.920383068978271e-011	1.784329365885219e-010
$\Omega^{0,1}_{-9}$	-1.855786659603524e-007	-3.711573577727717e-007	-7.423146935987642e-007
$\Omega^{0,1}_{-8}$	2.692423710000159e-005	5.384847419676242e-005	1.076969482921150e-004
$\Omega^{0,1}_{-7}$	7.697008125308266e-004	1.539401625053768e-003	3.078803250119820e-003
$\Omega^{0,1}_{-6}$	2.750010605172746e-004	5.500021210559334e-004	1.100004242122891e-003
$\Omega^{0,1}_{-5}$	-1.016679387824381e-001	-2.033358775648997e-001	-4.066717551297090e-001
$\Omega^{0,1}_{-4}$	9.309127066876437e-001	1.861825413375254e+000	3.723650826750292e+000
$\Omega^{0,1}_{-3}$	-4.636197759850479e+000	-9.272395519700977e+000	-1.854479103940188e+001
$\Omega^{0,1}_{-2}$	1.654738842505443e+001	3.309477685010887e+001	6.618955370021767e+001
$\Omega^{0,1}_{-1}$	-5.440874633958098e+001	-1.088174926791625e+002	-2.176349853583258e+002
$\Omega^{0,1}_{0}$	-4.609897213739054e-013	3.334560305993533e-013	2.464027161411541e-012
$\Omega^{0,1}_{1}$	5.440874633958133e+001	1.088174926791623e+002	2.176349853583238e+002
$\Omega^{0,1}_{2}$	-1.654738842505442e+001	-3.309477685010883e+001	-6.618955370021763e+001
$\Omega^{0,1}_{3}$	4.636197759850483e+000	9.272395519700886e+000	1.854479103940177e+001
$\Omega^{0,1}_{4}$	-9.309127066876174e-001	-1.861825413375198e+000	-3.723650826750481e+000
$\Omega^{0,1}_{5}$	1.016679387824613e-001	2.033358775648949e-001	4.066717551297869e-001
$\Omega^{0,1}_{6}$	-2.750010605372147e-004	-5.500021210920076e-004	-1.100004242165326e-003
$\Omega^{0,1}_{7}$	-7.697008125266731e-004	-1.539401625054399e-003	-3.078803250114857e-003
$\Omega^{0,1}_{8}$	-2.692423709323072e-005	-5.384847417592798e-005	-1.076969483767874e-004
$\Omega^{0,1}_{9}$	1.855786799154870e-007	3.711573633341429e-007	7.423147046276602e-007
$\Omega^{0,1}_{10}$	-4.459832786581782e-011	-8.920883463672624e-011	-1.784077643256998e-010

Table 39: Two term connection at $N=12,\ d_1=0,\ d_2=1$ and different j

	$j=9,\ N=12$	$j=10,\ N=12$	$j=11,\ N=12$
$\Omega_{-10}^{0,1}$	3.568814269824286e-010	7.135319054928643e-010	1.427296812279246e-009
$\Omega_{-9}^{0,1}$	-1.484629371143922e-006	-2.969258755612068e-006	-5.938517219001792e-006
$\Omega_{-8}^{0,1}$	2.153938965916432e-004	4.307877936993525e-004	8.615755868619370e-004
$\Omega_{-7}^{0,1}$	6.157606500207510e-003	1.231521300040246e-002	2.463042600080800e-002
$\Omega_{-6}^{0,1}$	2.200008484260971e-003	4.400016968362715e-003	8.800033936989898e-003
$\Omega_{-5}^{0,1}$	-8.133435102593426e-001	-1.626687020519306e+000	-3.253374041037593e+000
$\Omega_{-4}^{0,1}$	7.447301653500555e+000	1.489460330700241e+001	2.978920661400355e+001
$\Omega_{-3}^{0,1}$	-3.708958207880362e+001	-7.417916415760794e+001	-1.483583283152139e+002
$\Omega_{-2}^{0,1}$	1.323791074004353e+002	2.647582148008706e+002	5.295164296017404e+002
$\Omega_{-1}^{0,1}$	-4.352699707166504e+002	-8.705399414332979e+002	-1.741079882866586e+003
$\Omega_{0}^{0,1}$	1.645519158080046e-012	-3.221807682988138e-013	-2.510523739197342e-011
$\Omega_{1}^{0,1}$	4.352699707166489e+002	8.705399414332977e+002	1.741079882866605e+003
$\Omega_{2}^{0,1}$	-1.323791074004353e+002	-2.647582148008703e+002	-5.295164296017406e+002
$\Omega_{3}^{0,1}$	3.708958207880366e+001	7.417916415760755e+001	1.483583283152157e+002
$\Omega_{4}^{0,1}$	-7.447301653500960e+000	-1.489460330700204e+001	-2.978920661400361e+001
$\Omega_{5}^{0,1}$	8.133435102596023e-001	1.626687020519325e+000	3.253374041038964e+000
$\Omega_{6}^{0,1}$	-2.200008484321742e-003	-4.400016968558922e-003	-8.800033937259269e-003
$\Omega_{7}^{0,1}$	-6.157606500213888e-003	-1.231521300043118e-002	-2.463042600080695e-002
$\Omega_{8}^{0,1}$	-2.153938967247599e-004	-4.307877935254872e-004	-8.615755867573784e-004
$\Omega_{9}^{0,1}$	1.484629352077567e-006	2.969258773936342e-006	5.938517437145822e-006
$\Omega_{10}^{0,1}$	-3.567758616121751e-010	-7.135402283443558e-010	-1.426911748340083e-009

Table 40: Two term connection at $N=12,\ d_1=0,\ d_2=1$ and different j

	$j=0,\ N=14$	$j=1,\ N=14$	$j=2,\ N=14$
$\Omega^{0,1}_{-12}$	-9.093659201960153e-016	-1.020387742027126e-015	-2.551015341973991e-015
$\Omega^{0,1}_{-11}$	-1.203524319370248e-011	-2.407048567855346e-011	-4.814096829924245e-011
$\Omega^{0,1}_{-10}$	4.183055991508054e-010	8.366108141446448e-010	1.673221402103675e-009
$\Omega^{0,1}_{-9}$	-2.187113034221992e-007	-4.374226069287557e-007	-8.748452136645133e-007
$\Omega^{0,1}_{-8}$	-1.650167921185091e-006	-3.300335841844315e-006	-6.600671684218315e-006
$\Omega^{0,1}_{-7}$	4.236394680075738e-006	8.472789359913194e-006	1.694557871999972e-005
$\Omega^{0,1}_{-6}$	3.373440477639545e-004	6.746880955295991e-004	1.349376191057733e-003
$\Omega^{0,1}_{-5}$	-3.881454657631967e-003	-7.762909315264846e-003	-1.552581863053076e-002
$\Omega^{0,1}_{-4}$	2.268741101466512e-002	4.537482202933121e-002	9.074964405866265e-002
$\Omega^{0,1}_{-3}$	-9.018906621784878e-002	-1.803781324356944e-001	-3.607562648713963e-001
$\Omega^{0,1}_{-2}$	2.829650945261911e-001	5.659301890523817e-001	1.131860378104769e+000
$\Omega^{0,1}_{-1}$	-8.687439145242527e-001	-1.737487829048478e+000	-3.474975658097025e+000
$\Omega^{0,1}_{0}$	2.005960347975370e-014	-2.973839019641094e-014	7.652339070044165e-014
$\Omega^{0,1}_{1}$	8.687439145242358e-001	1.737487829048503e+000	3.474975658096962e+000
$\Omega^{0,1}_{2}$	-2.829650945261905e-001	-5.659301890523829e-001	-1.131860378104767e+000
$\Omega^{0,1}_{3}$	9.018906621784691e-002	1.803781324356978e-001	3.607562648713885e-001
$\Omega^{0,1}_{4}$	-2.268741101466551e-002	-4.537482202933151e-002	-9.074964405866125e-002
$\Omega^{0,1}_{5}$	3.881454657632025e-003	7.762909315264959e-003	1.552581863052757e-002
$\Omega^{0,1}_{6}$	-3.373440477645093e-004	-6.746880955281301e-004	-1.349376191058470e-003
$\Omega^{0,1}_{7}$	-4.236394680128265e-006	-8.472789360337551e-006	-1.694557872047109e-005
$\Omega^{0,1}_{8}$	1.650167921071844e-006	3.300335842200119e-006	6.600671684459459e-006
$\Omega^{0,1}_{9}$	2.187113032721298e-007	4.374226067335177e-007	8.748452132468603e-007
$\Omega^{0,1}_{10}$	-4.183055328314662e-010	-8.366109180119963e-010	-1.673222139639658e-009
$\Omega^{0,1}_{11}$	1.203530502022236e-011	2.407089322991096e-011	4.814053106038553e-011
$\Omega^{0,1}_{12}$	6.216532372502836e-016	1.500071897102762e-015	2.397264247450226e-015

Table 41: Two term connection at $N=14,\ d_1=0,\ d_2=1$ and different j

	$j=3,\ N=14$	$j=4,\ N=14$	$j=5,\ N=14$
$\Omega^{0,1}_{-12}$	-4.634393850498429e-015	-1.275690082076888e-014	-2.116636953714351e-014
$\Omega^{0,1}_{-11}$	-9.628226205861661e-011	-1.925632265438996e-010	-3.851300647795375e-010
$\Omega^{0,1}_{-10}$	3.346442942232174e-009	6.692892046182721e-009	1.338578119764802e-008
$\Omega^{0,1}_{-9}$	-1.749690427233403e-006	-3.499380852263309e-006	-6.998761705061007e-006
$\Omega^{0,1}_{-8}$	-1.320134336970431e-005	-2.640268673680747e-005	-5.280537347197350e-005
$\Omega^{0,1}_{-7}$	3.389115744115972e-005	6.778231488009504e-005	1.355646297624779e-004
$\Omega^{0,1}_{-6}$	2.698752382116903e-003	5.397504764224951e-003	1.079500952845710e-002
$\Omega^{0,1}_{-5}$	-3.105163726106119e-002	-6.210327452209935e-002	-1.242065490442127e-001
$\Omega^{0,1}_{-4}$	1.814992881173229e-001	3.629985762346430e-001	7.259971524692958e-001
$\Omega^{0,1}_{-3}$	-7.215125297427840e-001	-1.443025059485557e+000	-2.886050118971105e+000
$\Omega^{0,1}_{-2}$	2.263720756209526e+000	4.527441512419062e+000	9.054883024838109e+000
$\Omega^{0,1}_{-1}$	-6.949951316193983e+000	-1.389990263238783e+001	-2.779980526477555e+001
$\Omega^{0,1}_{0}$	6.209924764424032e-014	-2.939119803428816e-013	-6.767588055021938e-013
$\Omega^{0,1}_{1}$	6.949951316193931e+000	1.389990263238807e+001	2.779980526477612e+001
$\Omega^{0,1}_{2}$	-2.263720756209525e+000	-4.527441512419071e+000	-9.054883024838128e+000
$\Omega^{0,1}_{3}$	7.215125297427795e-001	1.443025059485587e+000	2.886050118971174e+000
$\Omega^{0,1}_{4}$	-1.814992881173232e-001	-3.629985762346500e-001	-7.259971524693020e-001
$\Omega^{0,1}_{5}$	3.105163726105801e-002	6.210327452211609e-002	1.242065490442382e-001
$\Omega^{0,1}_{6}$	-2.698752382116729e-003	-5.397504764223376e-003	-1.079500952844862e-002
$\Omega^{0,1}_{7}$	-3.389115744072425e-005	-6.778231488274878e-005	-1.355646297638668e-004
$\Omega^{0,1}_{8}$	1.320134336897328e-005	2.640268673823597e-005	5.280537347562757e-005
$\Omega^{0,1}_{9}$	1.749690427097165e-006	3.499380853899855e-006	6.998761706025780e-006
$\Omega^{0,1}_{10}$	-3.346444661503256e-009	-6.692889344397132e-009	-1.338577485534072e-008
$\Omega^{0,1}_{11}$	9.628382240067928e-011	1.925673023215563e-010	3.851335644982122e-010
$\Omega^{0,1}_{12}$	3.881789440223672e-015	1.189439841358159e-014	2.332122565200561e-014

Table 42: Two term connection at $N=14,\ d_1=0,\ d_2=1$ and different j

	$j=6,\ N=14$	$j=7,\ N=14$	$j=8,\ N=14$
$\Omega^{0,1}_{-12}$	-4.740267026698519e-014	-7.377985437513795e-014	-1.920298904016830e-013
$\Omega^{0,1}_{-11}$	-7.702610922270493e-010	-1.540510797212152e-009	-3.081028045139360e-009
$\Omega^{0,1}_{-10}$	2.677156188673411e-008	5.354309856249868e-008	1.070861451494485e-007
$\Omega^{0,1}_{-9}$	-1.399752340719014e-005	-2.799504682799360e-005	-5.599009365591120e-005
$\Omega^{0,1}_{-8}$	-1.056107469693313e-004	-2.112214939263439e-004	-4.224429877623725e-004
$\Omega^{0,1}_{-7}$	2.711292595184406e-004	5.422585190553425e-004	1.084517038093828e-003
$\Omega^{0,1}_{-6}$	2.159001905689903e-002	4.318003811387313e-002	8.636007622762833e-002
$\Omega^{0,1}_{-5}$	-2.484130980884254e-001	-4.968261961769300e-001	-9.936523923540052e-001
$\Omega^{0,1}_{-4}$	1.451994304938539e+000	2.903988609877130e+000	5.807977219754516e+000
$\Omega^{0,1}_{-3}$	-5.772100237942301e+000	-1.154420047588450e+001	-2.308840095176944e+001
$\Omega^{0,1}_{-2}$	1.810976604967623e+001	3.621953209935248e+001	7.243906419870515e+001
$\Omega^{0,1}_{-1}$	-5.559961052955217e+001	-1.111992210591036e+002	-2.223984421182091e+002
$\Omega^{0,1}_{0}$	1.195036562868803e-012	3.039221158569714e-013	4.438520263020029e-012
$\Omega^{0,1}_{1}$	5.559961052955116e+001	1.111992210591034e+002	2.223984421182053e+002
$\Omega^{0,1}_{2}$	-1.810976604967620e+001	-3.621953209935249e+001	-7.243906419870497e+001
$\Omega^{0,1}_{3}$	5.772100237942218e+000	1.154420047588454e+001	2.308840095176888e+001
$\Omega^{0,1}_{4}$	-1.451994304938594e+000	-2.903988609877191e+000	-5.807977219754376e+000
$\Omega^{0,1}_{5}$	2.484130980884350e-001	4.968261961769322e-001	9.936523923538364e-001
$\Omega^{0,1}_{6}$	-2.159001905691777e-002	-4.318003811385076e-002	-8.636007622776364e-002
$\Omega^{0,1}_{7}$	-2.711292595279895e-004	-5.422585190506353e-004	-1.084517038096656e-003
$\Omega^{0,1}_{8}$	1.056107469473008e-004	2.112214939008694e-004	4.224429877954504e-004
$\Omega^{0,1}_{9}$	1.399752340820121e-005	2.799504682332806e-005	5.599009364876137e-005
$\Omega^{0,1}_{10}$	-2.677156118693736e-008	-5.354309903464176e-008	-1.070862210031373e-007
$\Omega^{0,1}_{11}$	7.702656236172596e-010	1.540520990903657e-009	3.081068854621338e-009
$\Omega^{0,1}_{12}$	3.819578254630561e-014	7.680456331597872e-014	1.153192069429565e-013

Table 43: Two term connection at $N=14,\ d_1=0,\ d_2=1$ and different j

	$j=9,\ N=14$	$j=10,\ N=14$	$j=11,\ N=14$
$\Omega^{0,1}_{-12}$	-2.961957373655074e-013	-5.665348886591096e-013	-1.106219387048709e-012
$\Omega^{0,1}_{-11}$	-6.162108213913547e-009	-1.232414961043282e-008	-2.464826547194698e-008
$\Omega^{0,1}_{-10}$	2.141725216565016e-007	4.283449037625223e-007	8.566893365188916e-007
$\Omega^{0,1}_{-9}$	-1.119801873477969e-004	-2.239603747008321e-004	-4.479207495077898e-004
$\Omega^{0,1}_{-8}$	-8.448859756784086e-004	-1.689771951007886e-003	-3.379543902178116e-003
$\Omega^{0,1}_{-7}$	2.169034076295395e-003	4.338068152456392e-003	8.676136304799487e-003
$\Omega^{0,1}_{-6}$	1.727201524554215e-001	3.454403049109827e-001	6.908806098221395e-001
$\Omega^{0,1}_{-5}$	-1.987304784707517e+000	-3.974609569415280e+000	-7.949219138831976e+000
$\Omega^{0,1}_{-4}$	1.161595443950855e+001	2.323190887901782e+001	4.646381775803556e+001
$\Omega^{0,1}_{-3}$	-4.617680190353773e+001	-9.235360380707556e+001	-1.847072076141525e+002
$\Omega^{0,1}_{-2}$	1.448781283974098e+002	2.897562567948206e+002	5.795125135896407e+002
$\Omega^{0,1}_{-1}$	-4.447968842364112e+002	-8.895937684728199e+002	-1.779187536945656e+003
$\Omega^{0,1}_{0}$	-6.589283301769666e-012	-2.633744732637104e-011	-8.734767812061007e-012
$\Omega^{0,1}_{1}$	4.447968842364168e+002	8.895937684728417e+002	1.779187536945663e+003
$\Omega^{0,1}_{2}$	-1.448781283974101e+002	-2.897562567948214e+002	-5.795125135896412e+002
$\Omega^{0,1}_{3}$	4.617680190353849e+001	9.235360380707790e+001	1.847072076141538e+002
$\Omega^{0,1}_{4}$	-1.161595443950874e+001	-2.323190887901765e+001	-4.646381775803512e+001
$\Omega^{0,1}_{5}$	1.987304784707826e+000	3.974609569415967e+000	7.949219138831019e+000
$\Omega^{0,1}_{6}$	-1.727201524553275e-001	-3.454403049107459e-001	-6.908806098214101e-001
$\Omega^{0,1}_{7}$	-2.169034076207619e-003	-4.338068152350534e-003	-8.676136304735779e-003
$\Omega^{0,1}_{8}$	8.448859756362829e-004	1.689771951243437e-003	3.379543902361922e-003
$\Omega^{0,1}_{9}$	1.119801873023748e-004	2.239603746223188e-004	4.479207491312973e-004
$\Omega^{0,1}_{10}$	-2.141723675509842e-007	-4.283445810923666e-007	-8.566892999628293e-007
$\Omega^{0,1}_{11}$	6.162081031867288e-009	1.232406013731403e-008	2.464787863842850e-008
$\Omega^{0,1}_{12}$	3.415405258983562e-013	7.004616800332815e-013	1.527614622082337e-012

Table 44: Two term connection at $N=14,\ d_1=0,\ d_2=1$ and different j

	$j=0,\ N=16$	$j=1,\ N=16$	$j=2,\ N=16$
$\Omega^{0,1}_{-14}$	1.371660846034882e-016	1.133483965033230e-016	-2.130366470392521e-016
$\Omega^{0,1}_{-13}$	-1.240034252708606e-014	-2.457974331317060e-014	-4.938996778206259e-014
$\Omega^{0,1}_{-12}$	7.256004215050857e-013	1.450131252903530e-012	2.901120904542585e-012
$\Omega^{0,1}_{-11}$	9.697184738032619e-010	1.939437143482114e-009	3.878873940094430e-009
$\Omega^{0,1}_{-10}$	7.207948211956484e-008	1.441589643357304e-007	2.883179298632430e-007
$\Omega^{0,1}_{-9}$	-3.993810461589868e-008	-7.987620954705709e-008	-1.597524183894186e-007
$\Omega^{0,1}_{-8}$	-2.451992114549783e-007	-4.903984215036264e-007	-9.807968448259236e-007
$\Omega^{0,1}_{-7}$	-7.667706908354899e-005	-1.533541381669490e-004	-3.067082763353312e-004
$\Omega^{0,1}_{-6}$	1.031530213376507e-003	2.063060426751026e-003	4.126120853502637e-003
$\Omega^{0,1}_{-5}$	-6.958379116451669e-003	-1.391675823290300e-002	-2.783351646580214e-002
$\Omega^{0,1}_{-4}$	3.129014783948015e-002	6.258029567896263e-002	1.251605913579195e-001
$\Omega^{0,1}_{-3}$	-1.063640682894436e-001	-2.127281365788876e-001	-4.254562731577741e-001
$\Omega^{0,1}_{-2}$	3.032593514765940e-001	6.065187029531854e-001	1.213037405906374e+000
$\Omega^{0,1}_{-1}$	-8.834460460908277e-001	-1.766892092181637e+000	-3.533784184363293e+000
$\Omega^{0,1}_{0}$	-6.141045325830091e-015	-2.173764897400916e-014	-2.919326713291232e-014
$\Omega^{0,1}_{1}$	8.834460460908328e-001	1.766892092181655e+000	3.533784184363318e+000
$\Omega^{0,1}_{2}$	-3.032593514765954e-001	-6.065187029531846e-001	-1.213037405906375e+000
$\Omega^{0,1}_{3}$	1.063640682894451e-001	2.127281365788875e-001	4.254562731577785e-001
$\Omega^{0,1}_{4}$	-3.129014783948039e-002	-6.258029567895888e-002	-1.251605913579206e-001
$\Omega^{0,1}_{5}$	6.958379116450659e-003	1.391675823290129e-002	2.783351646580255e-002
$\Omega^{0,1}_{6}$	-1.031530213375280e-003	-2.063060426751547e-003	-4.126120853501163e-003
$\Omega^{0,1}_{7}$	7.667706908376750e-005	1.533541381684657e-004	3.067082763355221e-004
$\Omega^{0,1}_{8}$	2.451992111417998e-007	4.903984223680227e-007	9.807968443807015e-007
$\Omega^{0,1}_{9}$	3.993810457513655e-008	7.987620936162933e-008	1.597524182475894e-007
$\Omega^{0,1}_{10}$	-7.207948244957361e-008	-1.441589647392887e-007	-2.883179294000416e-007
$\Omega^{0,1}_{11}$	-9.697183764183109e-010	-1.939436993065447e-009	-3.878874306853540e-009
$\Omega^{0,1}_{12}$	-7.252036768650327e-013	-1.450590496349511e-012	-2.900530948295082e-012
$\Omega^{0,1}_{13}$	1.245476607713937e-014	2.478474487639414e-014	4.970056025386812e-014
$\Omega^{0,1}_{14}$	2.338325297269043e-019	4.340955735116002e-016	1.394726838992659e-016

Table 45: Two term connection at $N=16,\ d_1=0,\ d_2=1$ and different j

	$j=3,\ N=16$	$j=4,\ N=16$	$j=5,\ N=16$
$\Omega^{0,1}_{-14}$	4.456425147727763e-016	4.071930963747828e-017	-4.905382952480158e-015
$\Omega^{0,1}_{-13}$	-9.936133300288921e-014	-1.958557848380791e-013	-3.965817534169358e-013
$\Omega^{0,1}_{-12}$	5.800895798305475e-012	1.160874689025285e-011	2.321191708632698e-011
$\Omega^{0,1}_{-11}$	7.757748228388976e-009	1.551549641219591e-008	3.103099517772754e-008
$\Omega^{0,1}_{-10}$	5.766358586405585e-007	1.153271713489912e-006	2.306543440627997e-006
$\Omega^{0,1}_{-9}$	-3.195048367552289e-007	-6.390096744884248e-007	-1.278019351718962e-006
$\Omega^{0,1}_{-8}$	-1.961593689677080e-006	-3.923187382453329e-006	-7.846374757335848e-006
$\Omega^{0,1}_{-7}$	-6.134165526697048e-004	-1.226833105338093e-003	-2.453666210694881e-003
$\Omega^{0,1}_{-6}$	8.252241707001827e-003	1.650448341402558e-002	3.300896682803101e-002
$\Omega^{0,1}_{-5}$	-5.566703293160744e-002	-1.113340658632279e-001	-2.226681317264104e-001
$\Omega^{0,1}_{-4}$	2.503211827158423e-001	5.006423654316798e-001	1.001284730863339e+000
$\Omega^{0,1}_{-3}$	-8.509125463155630e-001	-1.701825092631093e+000	-3.403650185262193e+000
$\Omega^{0,1}_{-2}$	2.426074811812756e+000	4.852149623625479e+000	9.704299247251006e+000
$\Omega^{0,1}_{-1}$	-7.067568368726693e+000	-1.413513673745321e+001	-2.827027347490648e+001
$\Omega^{0,1}_{0}$	1.590394891935833e-013	4.244146351305575e-014	-5.340752145707917e-014
$\Omega^{0,1}_{1}$	7.067568368726561e+000	1.413513673745318e+001	2.827027347490654e+001
$\Omega^{0,1}_{2}$	-2.426074811812753e+000	-4.852149623625492e+000	-9.704299247251017e+000
$\Omega^{0,1}_{3}$	8.509125463155473e-001	1.701825092631100e+000	3.403650185262225e+000
$\Omega^{0,1}_{4}$	-2.503211827158426e-001	-5.006423654316798e-001	-1.001284730863375e+000
$\Omega^{0,1}_{5}$	5.566703293160476e-002	1.113340658632123e-001	2.226681317264377e-001
$\Omega^{0,1}_{6}$	-8.252241707005054e-003	-1.650448341401015e-002	-3.300896682802081e-002
$\Omega^{0,1}_{7}$	6.134165526692924e-004	1.226833105341155e-003	2.453666210675792e-003
$\Omega^{0,1}_{8}$	1.961593688931446e-006	3.923187379354861e-006	7.846374758709446e-006
$\Omega^{0,1}_{9}$	3.195048363214557e-007	6.390096727237132e-007	1.278019346592530e-006
$\Omega^{0,1}_{10}$	-5.766358595324536e-007	-1.153271718125744e-006	-2.306543433502799e-006
$\Omega^{0,1}_{11}$	-7.757747885972653e-009	-1.551549507651747e-008	-3.103099040685187e-008
$\Omega^{0,1}_{12}$	-5.802059917564717e-012	-1.160431673477888e-011	-2.320739172021296e-011
$\Omega^{0,1}_{13}$	9.847580104602041e-014	1.967964397493907e-013	3.920085518983520e-013
$\Omega^{0,1}_{14}$	-1.058414478057531e-016	1.104672208571300e-015	7.257992675575480e-019

Table 46: Two term connection at $N=16,\ d_1=0,\ d_2=1$ and different j

	$j=6,\ N=16$	$j=7,\ N=16$	$j=8,\ N=16$
$\Omega^{0,1}_{-14}$	-5.932417784836436e-015	-1.499822907383957e-014	-1.937580872204892e-014
$\Omega^{0,1}_{-13}$	-8.012823561025362e-013	-1.586654636810487e-012	-3.181992667795546e-012
$\Omega^{0,1}_{-12}$	4.641544242118252e-011	9.284300303185449e-011	1.857386100799850e-010
$\Omega^{0,1}_{-11}$	6.206197901497031e-008	1.241239676795707e-007	2.482479271917831e-007
$\Omega^{0,1}_{-10}$	4.613086888010296e-006	9.226173753048421e-006	1.845234751884255e-005
$\Omega^{0,1}_{-9}$	-2.556038689907971e-006	-5.112077384534750e-006	-1.022415478867391e-005
$\Omega^{0,1}_{-8}$	-1.569274950422817e-005	-3.138549900628333e-005	-6.277099812611156e-005
$\Omega^{0,1}_{-7}$	-4.907332421384718e-003	-9.814664842762199e-003	-1.962932968550942e-002
$\Omega^{0,1}_{-6}$	6.601793365601165e-002	1.320358673120900e-001	2.640717346243023e-001
$\Omega^{0,1}_{-5}$	-4.453362634527944e-001	-8.906725269056537e-001	-1.781345053811329e+000
$\Omega^{0,1}_{-4}$	2.002569461726710e+000	4.005138923453441e+000	8.010277846906657e+000
$\Omega^{0,1}_{-3}$	-6.807300370524421e+000	-1.361460074104876e+001	-2.722920148209741e+001
$\Omega^{0,1}_{-2}$	1.940859849450202e+001	3.881719698900398e+001	7.763439397800791e+001
$\Omega^{0,1}_{-1}$	-5.654054694981279e+001	-1.130810938996251e+002	-2.261621877992514e+002
$\Omega^{0,1}_{0}$	-2.872215220973313e-013	-1.636092220497607e-012	-8.741080883325535e-013
$\Omega^{0,1}_{1}$	5.654054694981303e+001	1.130810938996265e+002	2.261621877992522e+002
$\Omega^{0,1}_{2}$	-1.940859849450201e+001	-3.881719698900403e+001	-7.763439397800812e+001
$\Omega^{0,1}_{3}$	6.807300370524452e+000	1.361460074104897e+001	2.722920148209783e+001
$\Omega^{0,1}_{4}$	-2.002569461726733e+000	-4.005138923453475e+000	-8.010277846906986e+000
$\Omega^{0,1}_{5}$	4.453362634528394e-001	8.906725269056922e-001	1.781345053811436e+000
$\Omega^{0,1}_{6}$	-6.601793365602066e-002	-1.320358673120267e-001	-2.640717346241151e-001
$\Omega^{0,1}_{7}$	4.907332421365074e-003	9.814664842727264e-003	1.962932968544405e-002
$\Omega^{0,1}_{8}$	1.569274950989726e-005	3.138549902511642e-005	6.277099802673462e-005
$\Omega^{0,1}_{9}$	2.556038692758237e-006	5.112077387701098e-006	1.022415477057711e-005
$\Omega^{0,1}_{10}$	-4.613086874180953e-006	-9.226173751882891e-006	-1.845234745940235e-005
$\Omega^{0,1}_{11}$	-6.206198502033239e-008	-1.241239662057077e-007	-2.482479399945051e-007
$\Omega^{0,1}_{12}$	-4.640997488026645e-011	-9.279784292097722e-011	-1.857022676458353e-010
$\Omega^{0,1}_{13}$	7.929161781643192e-013	1.550395057947863e-012	3.275361082523044e-012
$\Omega^{0,1}_{14}$	8.397387221597780e-016	1.832958627061042e-014	-5.483593223707976e-014

Table 47: Two term connection at $N=16,\ d_1=0,\ d_2=1$ and different j

	$j=9,\ N=16$	$j=10,\ N=16$	$j=11,\ N=16$
$\Omega^{0,1}_{-14}$	-1.454878540147583e-014	-1.955619903015936e-014	-1.312777998534403e-013
$\Omega^{0,1}_{-13}$	-6.363656145884063e-012	-1.265671571755959e-011	-2.547828675151841e-011
$\Omega^{0,1}_{-12}$	3.713417929492187e-010	7.428252783584298e-010	1.485453978375123e-009
$\Omega^{0,1}_{-11}$	4.964958444868848e-007	9.929917590440886e-007	1.985983453603970e-006
$\Omega^{0,1}_{-10}$	3.690469502166279e-005	7.380938966529265e-005	1.476187798889735e-004
$\Omega^{0,1}_{-9}$	-2.044830954226878e-005	-4.089661900921275e-005	-8.179323802680611e-005
$\Omega^{0,1}_{-8}$	-1.255419960425406e-004	-2.510839920803659e-004	-5.021679843410730e-004
$\Omega^{0,1}_{-7}$	-3.925865937095228e-002	-7.851731874181912e-002	-1.570346374840230e-001
$\Omega^{0,1}_{-6}$	5.281434692482463e-001	1.056286938497035e+000	2.112573876993201e+000
$\Omega^{0,1}_{-5}$	-3.562690107622669e+000	-7.125380215246239e+000	-1.425076043049083e+001
$\Omega^{0,1}_{-4}$	1.602055569381391e+001	3.204111138762822e+001	6.408222277525508e+001
$\Omega^{0,1}_{-3}$	-5.445840296419544e+001	-1.089168059283905e+002	-2.178336118567808e+002
$\Omega^{0,1}_{-2}$	1.552687879560164e+002	3.105375759120316e+002	6.210751518240635e+002
$\Omega^{0,1}_{-1}$	-4.523243755985028e+002	-9.046487511970025e+002	-1.809297502394008e+003
$\Omega^{0,1}_{0}$	-4.163910493792970e-012	-8.982106246393310e-012	-1.277439891854268e-011
$\Omega^{0,1}_{1}$	4.523243755985063e+002	9.046487511970097e+002	1.809297502394018e+003
$\Omega^{0,1}_{2}$	-1.552687879560165e+002	-3.105375759120320e+002	-6.210751518240641e+002
$\Omega^{0,1}_{3}$	5.445840296419587e+001	1.089168059283913e+002	2.178336118567825e+002
$\Omega^{0,1}_{4}$	-1.602055569381395e+001	-3.204111138762755e+001	-6.408222277525559e+001
$\Omega^{0,1}_{5}$	3.562690107622763e+000	7.125380215245345e+000	1.425076043049096e+001
$\Omega^{0,1}_{6}$	-5.281434692481560e-001	-1.056286938496408e+000	-2.112573876992644e+000
$\Omega^{0,1}_{7}$	3.925865937094103e-002	7.851731874203148e-002	1.570346374836081e-001
$\Omega^{0,1}_{8}$	1.255419960665890e-004	2.510839921286645e-004	5.021679842653965e-004
$\Omega^{0,1}_{9}$	2.044830953624548e-005	4.089661906975100e-005	8.179323830211168e-005
$\Omega^{0,1}_{10}$	-3.690469497088060e-005	-7.380938994742371e-005	-1.476187799702449e-004
$\Omega^{0,1}_{11}$	-4.964958952550113e-007	-9.929918547887168e-007	-1.985983686868240e-006
$\Omega^{0,1}_{12}$	-3.712611049031478e-010	-7.425463035847393e-010	-1.484874377051332e-009
$\Omega^{0,1}_{13}$	6.327211159595169e-012	1.266832535004749e-011	2.510338406939905e-011
$\Omega^{0,1}_{14}$	2.133638768475553e-014	9.030814883171042e-014	1.014789213891910e-013

Table 48: Two term connection at $N=16,\ d_1=0,\ d_2=1$ and different j

References

[1] N. Abazari and R. Abazari, Solution of nonlinear second-order pantograph equations via differential transformation method, *World Academy of Science, Engineering and Technology* 3 (2009) 10–26.

[2] A. Ali, M. A. Iqbal and S. T. Mohyud-Din, Hermite wavelets method for boundary value problems, *International Journal of Modern Applied Physics*, 3 (2013) 38–47.

[3] K. Amaratunga and J.R. Williams, Wavelet-Galerkin solution of boundary value problems, *Archives of Computational Methods in Engineering* 4 (1997) 243–285.

[4] E. Babolian and A. Shahsavaran, Numerical solution of nonlinear Fredholm integral equations of the second kind using Haar wavelets, *Journal of Computational and Applied Mathematics*, 225 (2009) 87–95.

[5] R. E. Bellman, Functional equations in the theory of dynamic programming, part II, nonlinear differential equations, *Proceedings of the National Academy of Science*, 41 (1955) 482–483.

[6] R. E. Bellman, Functional equations in the theory of dynamic programming, part V, positivity and quasilinearity, *Proceedings of the National Academy of Science*, 41 (1955) 743–746.

[7] R. E. Bellman and R. E. Kalaba, Quasilinearization and nonlinear boundary-value problems, *American Elsevier Publishing Company*, (1965).

[8] S. H. Behiry, H. Hashish, I. L. El-kalla and A. Elsaid, A new algorithm for the decomposition solution of nonlinear differential equations, *Acta Applicandae Mathematicae*, 54 (2007) 459–466.

[9] A. Barari, M. Omidvar, A. R. Ghotbi and D. D. Ganji, Application of homotopy perturbation method and variational iteration method to nonlinear oscillator differential equations, *Acta Applicandae Mathematicae*, 104 (2008) 161–171.

[10] J. Biazar and H. Aminikhah, Exact and numerical solutions for non- linear Burger's equation by VIM, *Mathematical and Computer Modelling*, 49 (2009) 1394–1400.

[11] J. Besora, Galerkin wavelet method for global waves in 1D, *Master Thesis, Royal Institute of Technology, Sweden*, (2004).

[12] A. H. Bhrawy, L. M. Assas, E. Tohidi and M. A. Alghamdi, A Legendre-Gauss collocation method for neutral functional-differential equations with proportional delays, *Advances in Difference Equations* , 63 (2013) 1–16.

[13] J. Biazar and H. Ghazvini, Exact solutions for nonlinear Burgers' equation by homotopy perturbation method, *Numerical Methods for Partial Differential Equations,* 25 (2008) 833–842.

[14] C. T. H. Baker, C. A. H. Paul and D. R. Wille, Issues in the numerical solution of evolutionary delay differential equations, *Advances in Computational Mathematics* 3 (1995) 171–196.

[15] C. Cattani, Haar wavelet spline, *Journal of Interdisciplinary Mathematics*, 4 (2001) 35–47.

[16] C. F. Chen and C. H. Hsiao, Haar wavelet method for solving lumped and distributed-parameter systems, *IEE Proceedings Control Theory & Applications*, 144 (1997).

[17] G. A. Cordshooli and A. R. Vahidi, Solutions of Duffing - Van der Pol equation using decomposition method, *Advanced Studies in Theoretical Physics*, 5 (2011) 121–129.

[18] H. Chen and H. Zhang, New multiple soliton solutions to the general Burgers–Fisher equation and the Kuramoto–Sivashinsky equation, *Chaos, Solitons and Fractals*, 19 (2004) 71–76.

[19] C. Chun and S. Abbasbandy, New application of variational iteration method for analytic treatment of nonlinear partial differential equations, *World Applied Sciences Journal*, 16 (2012) 1677–1681.

[20] M. Chen, C. Hwang and Y. Shih, The computation of wavelet-Galerkin approximation on a bounded interval, *International Journal of Numerical Methods in Engineering*, 39 (1996) 2921–2944.

[21] P. Chang and P. Piau, Simple procedure for the designation of Haar wavelet matrices for differential equations, *Proceedings of the International MultiConference of Engineers and Computer Scientists, Hong Kong*, 2 (2008) 19–21.

[22] I. Celik, Haar wavelet method for solving generalized Burgers–Huxley equation, *Arab Journal of Mathematical Sciences*, 18 (2012) 25–37.

[23] I. Celik, Haar wavelet approximation for magnetohydrodynamic flow equations, *Applied Mathematical Modelling*, 37 (2013) 3894–3902 .

[24] J.-F. Cheng and Y.-M. Chu, Solution to the linear fractional differential equation using Adomian decomposition method, *Mathematical Problems in Engineering*, (2011) Article ID 587068, 14 pages, doi:10.1155/2011/587068.

[25] M.-Q. Chen, C. Hwang and Y.-P. Shih, The computation of wavelet-Galerkin approximation on a bounded interval, *International Journal for Numerical Methods in Engineering* 39 (1996) 2921–2944.

[26] L. Debnath, Wavelet Transforms and their Applications, *Birkhauser*, Boston (2002).

[27] F. Dubeau, S. Elmejdani and R. Ksantini, Non-uniform Haar wavelets, *Applied Mathematics and Computation*, 159 (2004) 194–199.

[28] E. Deeba, S.A. Khuri and S. Xie, An algorithm for solving boundary value problems, *Journal of Computational Physics*, 159 (2000) 125–138.

[29] I. Daubechies, Orthonormal bases of compactly supported wavelets, *Communications on Pure and Applied Mathematics*, 41 (1988) 909–996.

[30] I. Daubechies, Ten lectures on wavelets, *SIAM: Philadelphia, PA*, 1992.

[31] L. U. Dianfeng, T. Ohyoshi and L. ZHU, Treatment of boundary condition in the application of wavelet–Galerkin method to a SH wave problem, *Akita University (Japan)*, (1996).

[32] J. V. Devi and C. Suseela, Quasilinearization for fractional differential equations, *Communications in Applied Analysis*, 12 (2008) 407–418.

[33] J. V. Devi, F.A. McRae and Z. Drici, Generalized quasilinearization for fractional differential equations, *Computers and Mathematics with Applications*, 59 (2010) 1057–1062.

[34] V. S. Erturk and S. Momani, Differential transform method for obtaining positive solutions for two- point nonlinear boundary value problems, *international journal mathematical manuscripts*, 1 (2007) 65–72.

[35] V. S. Erturk, S. Momani and Z. Odibat, Application of generalized differential transform method to multi-order fractional differential equations, *Communications in Nonlinear Science and Numerical Simulation*, 13 (2008) 1642–1654.

[36] D. J. Evans and K. R. Raslan, The Adomian decomposition method for solving delay differential equation, *International Journal of Computer Mathematics*, 82 (2005) 49–54.

[37] A. El-Safty, M. S. Salim and M. A. El-Khatib, Convergence of the spline function for delay dynamic system, *International Journal of Computer Mathematics*, 80 (2003) 509–518.

[38] K. T. Elgindy and K. A. Smith-Miles, Solving boundary value problems, integral, and integro-differential equations using Gegenbauer integration matrices, *Journal of Computational and Applied Mathematics*, 237 (2013) 307–325.

[39] A. E. M. El-Mesiry, A. M. A. El-Sayed and H. A. A. El-Saka, Numerical methods for multi-term fractional (arbitrary) orders differential equations, *Applied Mathematics and Computation* 160 (2005) 683–699.

[40] X. Feng, L. Mei and G. He, An efficient algorithm for solving Troesch's problem, *Applied Mathematics and Computation*, 189 (2007) 500–507.

[41] C. E. Falbo, Some elementary methods for solving functional differential equations, *http* : $//www.mathfile.net/hicstat\_FDE.pdf$.

[42] C. Franke and R. Schaback, Convergence order estimates of meshless collocation methods using radial basis functions, *Advances in Computational Mathematics*, 8 (1998) 381–399.

[43] C. Franke and R. Schaback, Solving partial differential equations by collocation using radial basis functions, *Applied Mathematics and Computation*, 93 (1998) 73–82.

[44] K. A. Gepreel, Adomian decomposition method to find the approximate solutions for the fractional PDEs, *WSEAS Transactions on Mathematics* 11 (2012) 636–643.

[45] M. Gorji-Bandpy, M. Azimi and M. Mostofi, Analytical Methods to a Generalized Duffing Oscillator, *Australian Journal of Basic and Applied Sciences*, 5 (2011) 788–796.

[46] H. P. W. Gottlieb, Velocity-dependent conservative nonlinear oscillators with exact harmonic solution, *Journal of Sound and Vibration*, 230 (2000) 323–333.

[47] D. D. Ganji and A. Sadighi, Application of Homotopy- perturbation and variational iteration methods to nonlinear heat transfer and porous media equations, *Journal of Computational and Applied Mathematics*, 207 (2007) 24–34.

[48] D. D. Ganji and A. Rajabi, Assessment of homotopyŰperturbation and perturbation methods in heat radiation equations, *International Communications in Heat and Mass Transfer*, 33 (2006) 391–400.

[49] M. Garg and L. Dewan, A numerical method for linear ordinary differential equatons using non-recursive Haar connection coefficients, *International Journal of Computational Science and Mathematics*, 2 (2010) 429–440.

[50] A. K. Gupta and S. Saha Ray, Wavelet methods for solving fractional order differential equations, *Mathematical Problems in Engineering*, Volume 2014, Article ID 140453, 11 pages http://dx.doi.org/10.1155/2014/140453.

[51] V. K. Garg and K. R. Rajagopal, Stagnation point flow of a non-Newtonian fluid, *Mechanics Research Communications* 17 (1990) 415–421.

[52] G. Hariharan and K. Kannan, An overview of Haar wavelet method for solving differential and integral equations, *World Applied Sciences Journal*, 23 (2013) 1–14.

[53] G. Hariharan, K. Kannan and K.R. Sharma, Haar wavelet method for solving Fisher's equation, *Applied Mathematics and Computation*, 211 (2009) 284–292 .

[54] G. Hariharan and K. Kannan, Haar wavelet method for solving some nonlinear parabolic equations, *Journal of Mathematical Chemistry*, 48 (2010) 1044–1061.

[55] F. Haq, Siraj-ul-Islam and I. Aziz, Numerical solution of singularly perturbed two-point boundary value problems using non-uniform Haar wavelets, *International Journal for Computational Methods in Engineering Science and Mechanics*, 12 (2011) 168–175.

[56] M. S. Hafshejani, S. K. Vanani and J. S. Hafshejani, Numerical solution of delay differential equations using Legendre wavelet method, *World Applied Sciences Journal*, 13 (2011) 27–33.

[57] M. H. Heydari, M. R. Hooshmandasl, F. M. M. Ghaini and M. Li, Chebyshev wavelets method for solution of nonlinear fractional integro–differential equations in a large interval, *Advances in Mathematical Physics*, Volume 2013, Article ID 482083, 12 pages http://dx.doi.org/10.1155/2013/482083.

[58] M.H. Heydari, M.R. Hooshmandasl and F.M. M. Ghaini, A new approach of the Chebyshev wavelets method for partial differential equations with boundary conditions of the telegraph type, *Applied Mathematical Modelling* 38 (2014) 1597–1606.

[59] J.-H. He , G.-C. Wu and F. Austin, The variational iteration method which should be followed, *Nonlinear Science Letters A*, 1 (2010) 01–30.

[60] S.H. Hosseinnia, A. Ranjbar and S. Momani, Using an enhanced homotopy perturbation method in fractional differential equations via deforming the linear part, *Computers & Mathematics with Applications*, 56 (2008) 3138–3149.

[61] H. Jafari, M. Soleymanivaraki and M. A. Firoozjaee, Legendre wavelets for solving fractional differential equations, *Journal of Applied Mathematics, Islamic Azad University of Lahijan*, 7 (2011) 65–70.

[62] R. A. Khan, Generalized approximation method for heat radiation equations, *Applied Mathematics and Computation*, 212 (2009) 287–295.

[63] A. Kimiaeifar, A.R. Saidi, G.H. Bagheri, M. Rahimpour and D.G. Domairry, Analytical solution for Van der PolŰDuffing oscillators, *Chaos, Solitons and Fractals* 42 (2009) 2660–2666.

[64] D. Kocacoban, A. B. Koc, A. Kurnaz and Y. Keskyn, A better approximation to the solution of Burger-Fisher equation, *Proceedings of the World Congress on Engineering, U.K*, 1 (2011) 6–8.

[65] O. Kiymaz, Variational iteration method for a class of nonlinear differential equations, *International Journal of Contemporary Mathematical Sciences*, 5 (2010) 1819–1826.

[66] F. Karakoç and H. Bereketoglu, Solutions of delay differential equations by using differential transform method, *International Journal of Computer Mathematics*, 86 (2009) 914–923.

[67] M. M. Khader and S. T. Mohamed, Numerical treatment for first order neutral delay differential equations using spline functions, *Engineering Mathematics Letters*, 1 (2012) 32–43.

[68] A. Kilicman and Z. A. A. Al Zhour, Kronecker operational matrices for fractional calculus and some applications, *Applied Mathethatics and Computation*, 187 (2007) 250–265.

[69] M. R.-Kouchi, A numerical solution of chebyshev and hermite equations by wavelet, *Applied Mathematical Sciences*, 6 (2012) 5349–5357.

[70] M. T. Kajani, A. H. Vencheh and M. Ghasemi, The Chebyshev wavelets operational matrix of integration and product operation matrix, *International Journal of Computer Mathematics*, 86 (2009) 1118–1125.

[71] Ü. Lepik, H. Hein, Haar wavelets with applications, *Mathematical Engineering*, (2014).

[72] Ü. Lepik, Solving integral and differential equations by the aid of non-uniform Haar wavelets, *Applied Mathematics and Computation* 198 (2008) 326–332.

[73] Ü. Lepik, Solving PDEs with the aid of two-dimensional Haar wavelets, *Computers & Mathematics with Applications* 61 (2011) 1873–1879.

[74] E. S. Lee, Quasilinearization and invariant imbedding, *Academic Press New York and London*, (1968).

[75] G. R. Liu and T. Y. Wu, Numerical solution for differential equations of duffing-type nonlinearity using the generalized differential quadrature rule, *Journal of Sound and vibration*, 237 (2000) 805–817.

[76] A. Latto, H.L. Resnikoff and E. Tenenbaum, The evaluation of connection coefficients of compactly supported wavelets, *Proc. French-USA Workshop on wavelets and turbulence*, Princeton University, June 1991, New York, Springer, 1994.

[77] Y. Li, Solving a nonlinear fractional differential equation using Chebyshev wavelets, *Communications in Nonlinear Science and Numerical Simulation*, 9 (2010) 2284–2292.

[78] X. Li , M. Xu and X. Jiang, Homotopy perturbation method to time-fractional diffusion equation with a moving boundary condition, *Applied Mathematics and Computation*, 208 (2009) 434–439.

[79] X. Lv and Y. Gao, The RKHSM for solving neutral functional- differential equations with proportional delays, *Mathematical Methods in the Applied Sciences* 36 (2013) 642–649.

[80] S. Mukherjee, B. Roy and S. Dutta, Solution of the Duffing–van der Pol oscillator equation by a differential transform method, *Physica Scripta*, 83 (2011) 1–4.

[81] C. A. Monje, Y. Q. Chen, B. M. Vinagre, D. Xue and V. Feliu, Fractional-order systems and controls, *Advances in Industrial Control, Springer*, 2010.

[82] V. B. Mandelzweig and F. Tabakin, Quasilinearization approach to nonlinear problems in physics with application to nonlinear ODEs, *Computer Physics Communications*, 141 (2001) 268–281.

[83] S. A. Malik, I. M. Qureshi, M. Zubair and I. Haq, Solution to force-free and forced duffing-Van der Pol oscillator using memetic computing, *Journal of Basic and Applied Scientific Research*, 2 (2012) 11136–11148.

[84] S. T. Mohyud-din, Solution of troesch's problem using He's polynomials, *Revista De La, Union Mathematica Argentina*, 52 (2011) 143–148.

[85] N. Mai-Duy, Solving high order ordinary differential equations with radial basis function networks, *International Journal for Numerical Methods in Engineering*, 62 (2005) 824–852.

[86] J.C. Mason and D.C. Handscomb, Chebyshev Polynomials, *A CRC Press Company, New York*, (2003).

[87] B. P. Moghaddam and Z. S. Mostaghim, A numerical method based on finite difference for solving fractional delay differential equations, *Journal of Taibah University for Science*, 7 (2013) 120–127.

[88] M.L. Morgado, N.J. Ford and P.M. Lima, Analysis and numerical methods for fractional differential equations with delay, *Journal of Computational and Applied Mathematics* 252 (2013) 159–168.

[89] S. Momani and Z. Odibat, Homotopy perturbation method for nonlinear partial differential equations of fractional order, *Physics Letters A*, 365 (2007) 345–350.

[90] Y. Molliq R, M.S.M. Noorani and I. Hashim, Variational iteration method for fractional heat- and wave–like equations, *Nonlinear Analysis: Real World Applications*, 10 (2009) 1854–1869.

[91] R. N. Mohapatra, K. Vajravelu and Y. Yin, An improved quasilinearization method for second order nonlinear boundary value problems, *Journal of Mathematical Analysis and Applications*, 214 (1997) 55–62.

[92] V. Mishra and Sabina, Wavelet Solutions of Parabolic Equations, *Matematika* 26 (2010) 61–69.

[93] V. Mishra and Sabina, Wavelet-Galerkin Solutions of Ordinary Differential Equations, *International Journal of Mathematical Analysis* 5 (2011) 407–424.

[94] Z. Odibat and S. Momani, Modified homotopy perturbation method: application to quadratic Riccati differential equation of fractional order, *Chaos, Solitons and fractals*, 36 (2008) 167–174.

[95] Z. Odibat, S. Momani and V. S. Erturk, Generalized differential transform method: application to differential equations of fractional order, *Applied Mathematics and Computation*, 197 (2008) 467–477.

[96] K. B. Oldham and J. Spanier, The fractional calculus, *Academic Press, New york and London*, (1974).

[97] R. Polikar, The story of wavelets, *http://users.rowan.edu/ polikar/RESEARCH/PUBLICATIONS/wavelet99.pdf.*

[98] I. Podlubny, Fractional differential equations, *Academic Press, New York, NY, USA,* (1999).

[99] S. Qian and J. Weiss, Wavelets and the numerical solution of boundary value problems, *Applied Mathematics Letters* 6 (1993) 47–52.

[100] D. P. Radunovic, Wavelets from math to practice, *Springer-Verlag, Berlin Heidelberg, Germany*, (2009).

[101] S.M. Roberts and J. S. Shipman, On the closed form solution of Troesch's problem, *Journal of Computational Physics*, 21 (1976) 191–304.

[102] M.M. Rashidi, D.D. Ganji and S. Dinarvand, Explicit analytical solutions of the generalized Burger and Burger–Fisher equations by homotopy perturbation method, *Numerical Methods for Partial Differential Equations*, 25 (2009) 409–417.

[103] J. M. Restrepo and G. K. Leaf, Inner product computations using periodized Daubechies wavelets, *International Journal for Numerical Methods in Engineering*, 40 (1997) 3557–3578.

[104] M. A. Ramadan , A. El-Sherbeiny and M. N. Sherif, Numerical solution of system of first-order delay differential equations using polynomial spline functions, *International Journal of Computer Mathematics*, 83 (2006) 925-937.

[105] Y. M. Rangkuti and M.S.M. Noorani, The exact solution of delay differential equations using coupling variational iteration with Taylor series and small term, *Bulletin of Mathematics*, 4 (2012) 1–15.

[106] F. A. Rihan , E. H.Doha, M. I.Hassan and N. M.Kamel, Numerical treatments for Volterra delay integro-differential equations, *Computational Methods in Applied Mathematics* 9 (2009) 292–308.

[107] T. R. Ramesh Rao, The use of Adomian decomposition method for solving generalised Riccati differential equations, *Proceedings of the 6th IMT-GT Conference on Mathematics, Statistics and its Applications*, (2010).

[108] M. Razzaghi and S. Yousefi, The Legendre wavelets operational matrix of integration, *International Journal of Systems Science*, 32 (2001) 495–502.

[109] M. Rehman and R. A. Khan, A numerical method for solving boundary value problems for fractional differential equations, *Applied Mathematical Modelling* 36 (2012) 894–907.

[110] M. Rehman and R. A. Khan, The Legendre wavelet method for solving fractional differential equations, *Communications in Nonlinear Science and Numerical Simulation*, 16 (2011) 4163–4173.

[111] B. Ross, A brief history and exposition of the fundamental theory of fractional calculus, *Springer Lecture Notes in Mathematics* 57 (1975) 1–36.

[112] S. S. Ray and R.K. Bera, An approximate solution of a nonlinear fractional differential equation by Adomian decomposition method, *Applied Mathematics and Computation*, 167 (2005) 561–571.

[113] A.K. Scheider, Implementation of wavelet Galerkin method for boundary value problems, *Master Thesis, Rochester Institute of Technology, New York*, (1998).

[114] U. Saeed and M. Rehman, Numerical solution of fractional differential equations by the non–uniform Haar wavelet, submitted.

[115] U. Saeed and M. Rehman, Haar wavelet–quasilinearization technique for fractional nonlinear differential equations, *Applied Mathematics and Computation*, 220 (2013) 630–648 .

[116] U. Saeed and M. Rehman, Assessment of Haar wavelet-quasilinearization technique in heat convection- radiation equations, *Applied Computational Intelligence and Soft Computing*, vol. 2014, Article ID 454231, 5 pages, 2014. doi:10.1155/2014/454231.

[117] H. Sajadi, D.D. Ganji, and Y. V. Shenas, Application of numerical and semi-analytical approach on Van der Pol Duffing oscillators, *Journal of Advanced Research in Mechanical Engineering*, 1 (2010) 136–141 .

[118] H. Smith, An introduction to delay differential equations with applications to the life sciences, *Dynamical Systems & Differential Equations*, (2011).

[119] N. T. Shawagfeh, Analytic approximate solution for a nonlinear oscillator equation, *Computers & Mathematics with Applications*, 31 (1996) 135–141.

[120] S. Sedaghat, Y. Ordokhani and M. Dehghan, Numerical solution of the delay differential equations of pantograph type via Chebyshev polynomials, *Communications in Nonlinear Science and Numerical Simulation*, 17 (2012) 4815–4830.

[121] M. Usman and S. T. Mohyud-Din, Physicists hermite wavelet method for singular differential equations, *International Journal of Advances in Applied Mathematics and Mechanics*, 1 (2013) 16–29.

[122] S. G. Venkatesh, S.K. Ayyaswamy and S. Raja Balachandar, The Legendre wavelet method for solving initial value problems of Bratu-type, *Computers and Mathematics with Applications*, 63 (2012) 1287–1295.

[123] S. K. Vanani, J. S. Hafshejani, F. Soleymani and M. Khan, Radial basis collocation method for the solution of differential–difference equations, *World Applied Sciences Journal*, 13 (2011) 2526–2530.

[124] Z. Wang, A numerical method for delayed fractional-order differential equations, *Journal of Applied Mathematics*, Volume 2013, Article ID 256071, 7 pages, http://dx.doi.org/10.1155/2013/256071.

[125] W. Wang, Y. Zhang and S. Li, Stability of continuous Runge-Kutta-type methods for nonlinear neutral delay-differential equations, *Applied Mathematical Modelling*, 33 (2009) 3319–3329.

[126] A. M. Wazwaz, A new method for solving singular initial value problems in the second-order ordinary differential equations, *Applied Mathematics and Computation*, 128 (2002) 45–57.

[127] Y. Wang and Q. Fan, The second kind Chebyshev wavelet method for solving fractional differential equations, *Applied Mathematics and Computation*, 218 (2012) 8592–8601.

[128] Y. Wang, H. Song and D. Li, Solving two-point boundary value problems using combined homotopy perturbation method and greens function method, *Applied Mathematics and Computation*, 212 (2009) 366–376.

[129] P. Wang and Y. Hou, Generalized quasilinearization for the system of fractional differential equations, *Journal of Function Spaces and Applications*, Volume 2013, Article ID 793263, 5 pages http://dx.doi.org/10.1155/2013/793263.

[130] J.L. Wu, A wavelet operational method for solving fractional partial differential equations numerically, *Applied Mathematics and Computation*, 214 (2009) 31–40.

[131] L. Wang, Y. Ma and Z. Meng, Haar wavelet method for solving fractional partial differential equations numerically, *Applied Mathematics and Computation*, 227 (2014) 66–76.

[132] S. A. Yousefi, Legendre wavelets method for solving differential equations of LaneŰEmden type, *Applied Mathematics and Computation*, 181 (2006) 1417–1422.

[133] L. Zhu and Q. Fan, Solving fractional nonlinear Fredholm integro-differential equations by the second kind Chebyshev wavelet, *Communications in Nonlinear Science and Numerical Simulation*, 17 (2012) 2333–2341.